Aluminium and group IV metals for polymerisation of lactide

Felix David Janeway

Submitted in accordance with the requirements for the degree of

Doctor of Philosophy

The University of Leeds

School of Chemistry

December 2015

The candidate confirms that the work submitted is his own, except where work which has formed part of jointly authored publications has been included. The contribution of the candidate and the other authors to this work has been explicitly indicated below. The candidate confirms that appropriate credit has been given within the thesis where reference has been made to the work of others.

This copy has been supplied on the understanding that it is copyright material and that no quotation from the thesis may be published without proper acknowledgement

0. CONTENTS

0.1. Table of Contents

0.2. Table of Figures

0.3. Table of Schemes

0.4. Table of Tables

0.5. Table of Compounds

0.6. List of abbreviations

Symbol	Definition
σ	Chemical shift
$[M]^+$	Molecular Ion
$\{^1H\}$	Nucleus decoupled from nucleus of interest
°C	Degrees Celcius
Å	Angstrom 1×10^{-10} m
ad	Apparent doublet
Ar	Aromatic
Ar	Aryl
as	Apparent singlet
bd	Broad doublet
bs	Broad singlet
DNA	Deoxyribonucleic acid
ES	Electrospray
et al.	and others
etc.	*et cetera*
g	Grams
HIV	Human Immunodeficiency Virus
HT-29	Colon adenocarcinoma cell line
Hz	Hertz
^iPr	Iso-propyl
^xJ	Spin-spin coupling constant over x bonds
J	Joules
K	Degrees Kelvin
kJ	Kilojoules

L	General ligand
m	Multiplet
m/z	Mass per charge ratio
Me	Methyl
ml	Millilitre
mol	Mole
MTT	3-(4,5-dimethylthiazol-2-yl)-2,5-diphenyltetrazolium bromide
Ph	Phenyl ring
ppm	Parts per million
q	Quartet
R	General group
s	Singlet
s	Second
^{s}BuO	*Sec*-butoxide
t	Triplet
^{t}Bu	*Tert*-butyl
UV	Ultra Violet
μg	Microgram

0.7. **Acknowledgements**

1. INTRODUCTION

1.1. Project Aims

The overall aim of this project is to broaden the understanding of the polymerisation of lactide to make poly(lactic acid).

The major uses of poly(lactic acid) are in the household, replacing petroplastics to make disposable items such as plastic bags. During this project, new catalysts for the polymerisation of lactide will be synthesised, with both electron poor and electron precise target molecules being identified in order to discover useful replacements for current catalysts.

Study of the mechanism of the polymerisation of lactide will be achieved by variation of the steric and electronic properties of the catalysts, as insights into the mechanism of the polymerisation may also give ideas as to how to better design viable industrial alternatives to those compounds already established.

Target molecules will be tested for their ability to polymerise lactide to discover motifs which are efficient at synthesising poly(lactic acid), as well as exploring those motifs which are traditionally avoided for polymerisation of lactide.

The nature of the polymers obtained will be investigated, and qualifications of what makes a useful polymer for industrial use defined. The project will investigate the possible products formed after polymerisation, and attempts will be made to exploit the structure of a catalyst to impart functionality into the polymer chain itself.

Some of the target molecules of this project are also expected to have anti-cancer properties, so their anti-cancer activity will be assessed *in vitro*, and polymers made using anti-cancer active catalysts will be tested for anti-cancer activity.

1.2. Polymers

1.2.1. Types of Polymer

A polymer is a long chain molecule consisting of repeating units joined by covalent bonds. The first synthetic polymer was Bakelite, discovered in 1907 by Leo Baekeland.[1] The polymer was synthesised by subjecting phenol and formaldehyde mixtures to high temperatures and pressures to form a large phenolic network of arene rings. Bakelite was a synthetic analogue of a shellac resin harvested from insects.

The invention of a synthetic method of preparing materials with the properties of plastics allowed for a rapid increase in production volume of synthetic materials, despite the high energetic cost of preparing the polymer. Since then, metal and radical catalysts have been used to greatly reduce

the amount of energy required to perform a polymerisation reaction and to control the nature of the polymer itself.

The synthesis of polymers necessitates covalent bonding of many molecules together. This process can be metal-mediated, radical or chemical, with each method allowing a different degree of control of the properties of the final polymer including chain length, degree of branching of the polymer chain and the arrangement of any chiral centres within the polymer.

Polymers commonly used today are separated into polymers synthesised by carrying out addition reactions - addition polymers, and those formed by chemical condensation reactions - condensation polymers.

Common addition polymers include those made by the addition of alkene molecules together - poly(ethene), poly(propylene), poly(vinyl chloride) and poly(trifluoroethene) (PTFE, Teflon).

Common condensation polymers include polymers with ester or amide repeating units. Examples of these polymers include Kevlar®, nylon and polyethylene terephthalate (PET).

1.2.2. History of Catalysed Polymerisation

The first organometallic polymerisation catalyst was discovered by Karl Ziegler and used to produce a stereoregular polymer by Giulio Natta. For this reason they were jointly awarded the Nobel Prize in 1963. The catalyst was prepared by performing a ligand exchange reaction with α-$TiCl_3$ and $[AlCl(Cp)_2]_2$.[2] Due to the nature of the cyclopentadienyl (Cp) ligands around the titanium coordination sphere, alkenes are restricted by which path they can approach and must coordinate with a certain geometry. In this way the tacticity of the resultant polymers can be controlled by varying the nature of the ligands surrounding the catalysing metal. These particular catalysts have been used to produce long chain polymers for industrial production of poly(ethene), poly(propylene), poly(acetylene) and several others with carefully controlled crystalline properties. [3-5]

One way to control the properties of a polymer is to carefully control the ratio of monomer, or source chemical, to catalyst in the mixture. This can limit the length of the chains formed. Desirable catalysts are ones which produce polymer mixtures where most of the chains are of similar length. A commonly used measure of similarity of length of a polymer is the PDI, the polydispersity index, however the recognised IUPAC terminology is simply "dispersity".[6] To calculate the dispersity the M_w (weight average molecular mass) is divided by the M_n (number average molecular mass). A polymer mixture that contains only one length of polymer chain would have a dispersity of 1. A mixture with a wide range of chain lengths would have a number larger than 1 with the most disperse mixtures usually having a dispersity around 2.

Another feature of a polymer is the position of any groups which are attached to the polymer but are not part of the primary backbone of the polymer.

Isotactic:
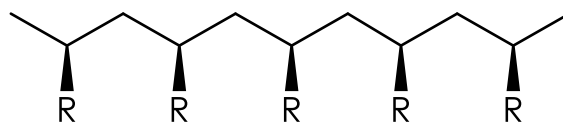
Figure 1.2-1 A representation of an isotactic polymer

In an isotactic polymer all ancillary, or 'R groups', are attached to the same face of the polymer. This is usually the resultant product of a polymerisation reaction using a Ziegler-Natta catalyst or other metal catalyst with significant steric bulk around the metal centre. These types of polymer tend to pack together more closely and form dense and rigid polymers than the other types of polymer.

Syndiotactic:
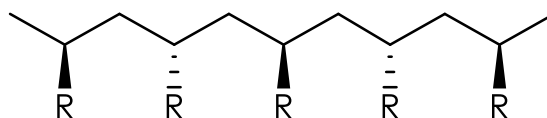
Figure 1.2-2 A representation of a syndiotactic polymer

Syndiotactic polymers have 'R groups' on alternating faces of the polymer chain. This type is also usually made by more complex organometallic catalysts. These chains will pack much less densely and will tend to be less crystalline.

Atactic:
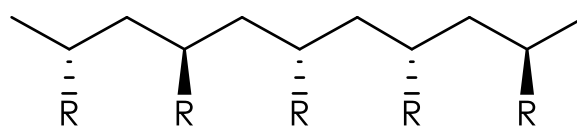
Figure 1.2-3 A representation of an atactic polymer

Atactic polymers have 'R groups' randomly dispersed across the faces. Due to their random nature these chains pack even less closely than syndiotactic polymers and tend to be much more amorphous. This leads to a more flexible polymer with a lower melting point. These types of polymers result from most radical polymerisations and polymerisations performed by catalysts without reasonable steric bulk or chiral ligands.

1.2.3. Catalysed Polymerisation Mechanisms

The mechanisms of many polymerisation reactions are not fully understood but the following have been proposed to explain the tacticity of the polymers they produce. Most of these mechanisms are based on alkyl insertion reactions.
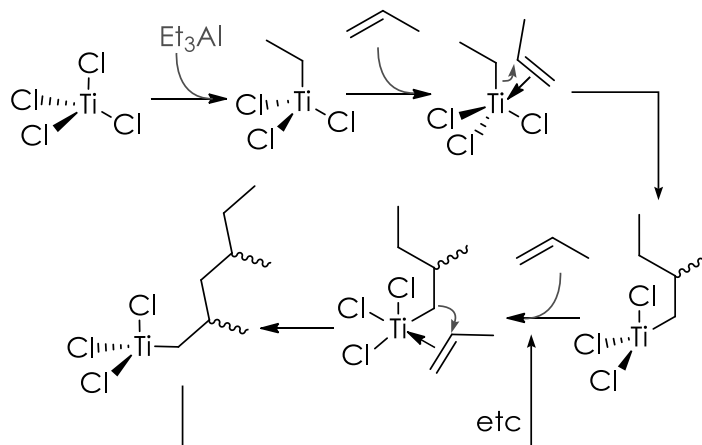
Figure 1.2-4 The Cossee-Arlman mechanism of a Ti polymerisation[7]

Figure 1.2-4 shows the coordination-insertion mechanism of propene, and addition polymer, at a titanium centre. As there is no restriction to the way the propene molecule approaches the metal centre in this complex the poly(propene) yielded by this catalyst has no 'R group' ordering and as such a random atactic polymer is yielded.

Isotactic polymer yielded
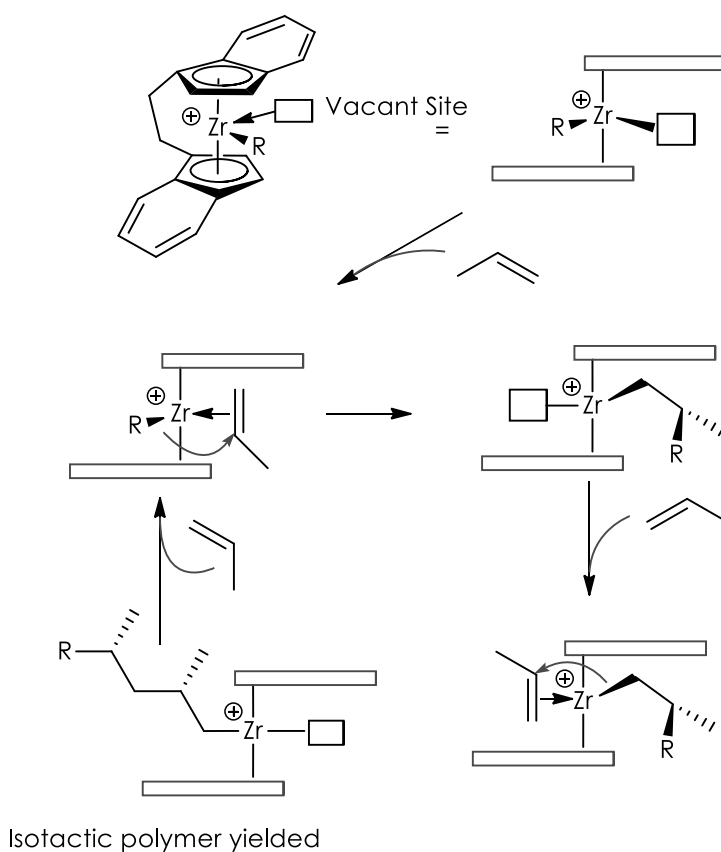
Figure 1.2-5 Mechanism of a metallocene polymerisation[8]

Figure 1.2-5 shows how catalyst design can be used to yield isotactic polymers. By using two tethered cyclopentadienyl ligands with bulky side groups the complex is shaped into a structure which dictates the orientation by which the propene coordiates to the zirconium centre and holds the propene in place during the alkyl insertion step.

1.2.4. Poly(lactic acid)
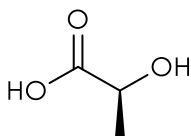
Figure 1.2-6 L-Lactic Acid Structure

Lactic acid is a biological acid which can be produced by fermentation industrially using *lactobacillus* bacteria on starch or dextrose sources such as corn, rice, wheat, sugar beets and sweet potatoes. This means that the product can be produced using a renewable material, rather than a petrochemical source. This makes it an excellent source material to be used in industrial procedures. The polymer produced is also compostable. The molecule has a chiral centre, but 99.5% of the raw lactic acid produced by fermentation is the L-isomer. Poly(lactic acid) (PLA) is a polyester based on lactic acid prepared by a condensation step to make a cyclic di-ester and then a ring-opening polymerisation step to make the polymer.
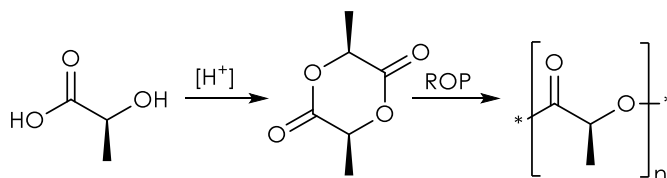
Figure 1.2-7 Polymerisation of Lactic Acid

This polymerisation process is an example of a living polymerisation and as such, chain length can be controlled by controlling the concentration of lactide in the reacting solution. Most research in this field has focussed on the synthesis of high molecular weight polymer chains suitable for use as an alternative plastic in the consumables market and in controlling the tacticity of the polymer to tune the required properties of the final polymer.

Many different metal sources have been used to catalyse the polymerisation of lactide. The ring-opening polymerisation can be crudely carried out with metal oxides or simple metal salts, with one recent paper reporting successful polymerisation of lactide using Pepto-Bismol, an over the counter dietary relief aid.[9]

While simple iron oxide has had some success with lactide polymerisation, much more complicated iron complexes have been synthesised and reported to initiate lactide polymerisation by Gibson *et al.*[10]
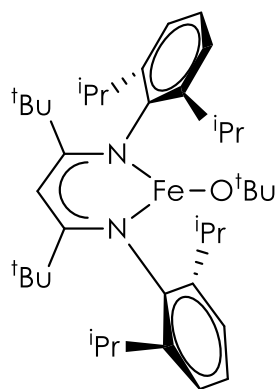
Figure 1.2-8 An iron alkoxide complex used for ROP of lactide

Other transition metal complexes reported to polymerise lactide include a dimeric zinc complex reported by Williams *et al*.[11]
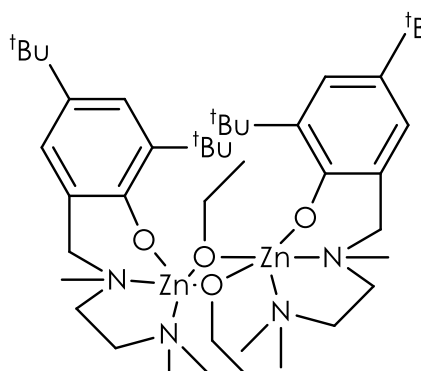
Figure 1.2-9 Zinc ethoxide dimer complex

While alkoxide groups are popular in catalysts for the ROP of lactide other ligands can be included which are displaced with an alcohol initiator before addition of lactide as in this yttrium complex also reported by Williams *et al*. whereby N(SiMe₃)₂ is displaced from the complex on activation.[12]
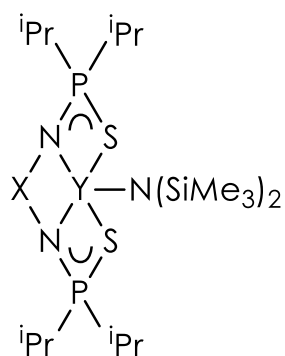
X = trans-1,2-cyclohexylene

Figure 1.2-10 Yttrium containing catalyst for ROP of lactide

Alkali metals have also been used to conduct ring-opening polymerisation reactions. Complicated structures based on lithium have been found to polymerise lactide rapidly at room temperature, though undergo a series of side reactions due to their basic nature which makes them inefficient as catalysts and the resulting mixture difficult to purify. [13]

More recent reports of very well defined polyamine-stabilised sodium complexes have been reported to polymerise 300 equivalents of lactide in CH_2Cl_2 at 25 °C in 5 minutes.[14]
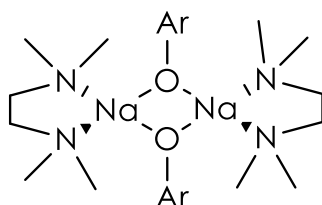
Figure 1.2-11 – Sodium polyamine aryloxide structures for polymerisation of lactide

Industrial polymerisation of lactide is performed using stannous octoate, which performs well in solution and dry-melt conditions, however concerns about tin oxide products leeching from the plastic into food and drinks contained within commercial plastics have stimulated research into less toxic metal catalysts for the production of poly(lactic acid).[15]
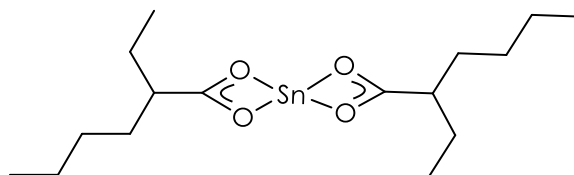
Figure 1.2-12 – Industrial stannous octoate catalyst for polymerisation of lactide

When used industrially stannous octoate requires an alcohol initiator in order to activate the complex towards polymerisation of lactide.[16]

1.2.5. Polymerisation of lactide in solution and dry melt conditions
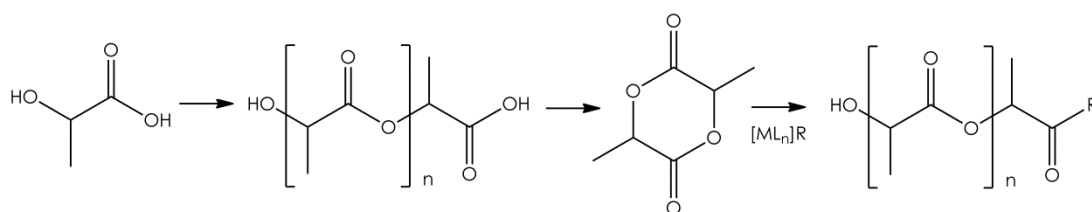
Figure 1.2-13 – Synthesis of poly(lactic acid) from raw lactic acid

There are two synthetic routes to poly(lactic acid), PLA. The first a direct method to catalyse a condensation reaction between lactic acid molecules. This method tends to yield polymers of low

molecular weight, i.e. less than 100,000 gmol[-1], as the catalyst is deactivated by the formation of water in the reaction.[17, 18] Another synthetic method is the ring-opening polymerisation of a dimer of lactic acid, lactide.
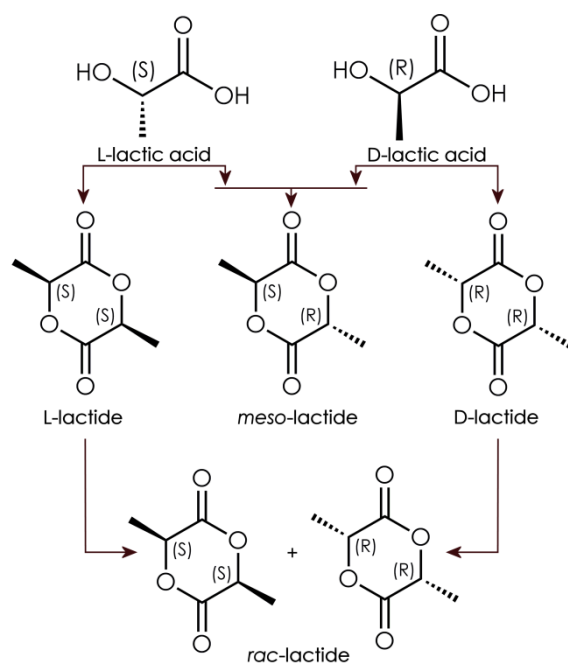
Figure 1.2-14 – Chiral enantiomers of lactic acid and their corresponding diastereomers of lactide

Lactide has two chiral carbon atoms in its structure, leading to several diasetreomers available for use in polymerisation reactions. (Figure 1.2-14) As lactic acid is sourced by fermentation of biomass a vast majority of the lactide produced industrially is L-lactide. However, D-lactide, *meso*-lactide and a racemic mixture of the two *RR* and *SS* enantiomers, *rac*-lactide, are also available.

Lactide is formed in a multi-step process by synthesising short oligomers of lactic acid, usually using a tin catalyst, then performing a cyclic deoligomerisation also using stannous salt.[19] The resulting cyclic diester is then able to undergo ring-opening polymerisation anhydrously, allowing the formation of polymers with much higher molecular weights and with narrower polydispersity indices. (Figure 1.2-13)

Polymerisations can be conducted in solution at various temperatures or under dry melt conditions where the lactide monomer is melted to act as a solvent. Lactide melts at 100 °C and therefore dry melt polymerisations tend to be carried out at temperatures exceeding 150 °C. The properties of the final plastic are dependent upon several factors; the length of the polymer, the polydispersity and the tacticity of the polymer. While these properties are dependent upon the action of the catalyst in the case of tacticity the chirality of the monomer is also important. The structure of isotactic poly(lactic acid) contains chiral carbons all with the same configuration, either R or S (Figure 1.2-15). As such the chain has a regular 3D shape and is able to pack closely with other chains. This increases the plastic's crystallinity, strength and melting point as well as increasing the

amount of time the polymer takes to degrade.[20] Isotactic polymers can only be synthesised using a diasteromer of lactide with both chiral carbons in the same S or R configuration, or using a catalyst capable of differentiating and catalysing the polymerisation of one diasteromer in a racemic mixture.
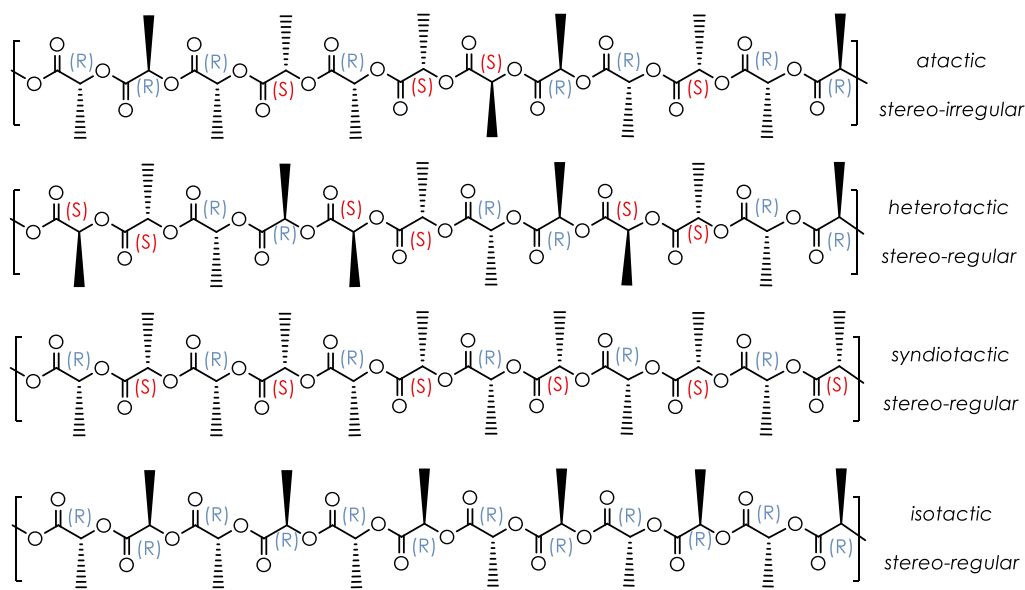
Figure 1.2-15 – Stereotacticity in chains of poly(lactic acid)

The tacticity of the final polymer is one property that a chemist may wish to control. They may also be interested in the colour of the polymer. The tacticity can vary properties of the polymer such as melting point, solubility and speed of breakdown of the plastic.[21a] The colour of the polymer is largely aesthetic, and can depend on the efficiency of the catalyst, as the reaction occurs the extra heat created must be dissipated or the polymer can easily burn as the monomer undergoes a series of thermolytic reactions. The ideal commercial polymer would be white so that the polymer can be coloured appropriately for the desired application.

1.2.6. Proposed ROP of lactide mechanism

In the case of lactide polymerisation the mechanism is unknown but could be based around the following steps.
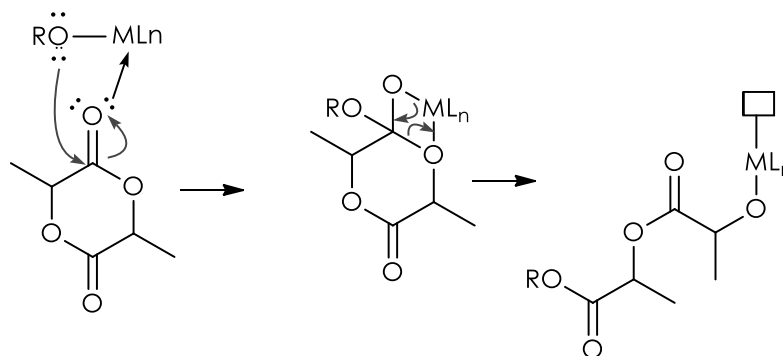
Figure 1.2-16 Possible Mechanism Of ROP of the Lactide Dimer

The carbonyl oxygen of the lactide coordinates to the metal centre via donation of a lone pair of electrons. This means that an active catalyst must have labile ligands capable of detaching from the centre and freeing up a coordination site. Dimers are ideal for this function as they can break apart into monomers yielding two metal centres each with a vacant binding site.

A pre-complexed alcohol initiating group inserts into the carbonyl double bond and allows the lactide ether oxygen to coordinate to the metal centre into the now vacant binding site.[21b]

The four membered transition state formed allows rearrangement and reforms the carbonyl double bond leaving the lactide ether oxygen complexed to the metal centre and ready to act as an initiating group for the next lactide molecule to complex.

1.2.7. Polymers for drug delivery

There has been interest in the literature in drug-delivery techniques using a wide variety of tailored nanoparticles as drug delivery matrices. Though there are many types of nanoparticle; non-metal, carbon allotropes, semiconducting metalloids and metal containing particles including magnetic particles, by far the most researched are ones made of polymeric materials. One way of forming a drug delivery system is to use water-soluble or degradable plastics in some combination of polyesters,[29-31] amides, urethanes,[[32, 33]] ethers, phosphorylcholines,[34] celluloses[35, 36] and more exotic cross-linked and unlinked block co-polymers to protect drugs from the aqueous environment of the blood plasma, control timed drug release,[37] and even tune drug release to chemical environments such as areas of specified pH[38] or temperature.[38, 39] This is achieved by forming chains of each of the monomers in a specific sequence in order to form domains of hydrophilic polymer, so-called 'blocks', and domains of hydrophobic polymer. These specifically designed polymers go on to form micelles, as the hydrophobic parts of the polymers form intermolecular attractions preferentially over interacting with an aqueous solvent, and *vice versa* in an organic

solvent. The results are structures such as spheres, rods or bi-layers of polymeric material providing an anhydrous area in which to store drugs protected from aqueous conditions. With careful design of the length and chemistry of the domains of the polymer it is possible to loosen the intermoleculear interactions in specific pH environments and allow targeted delivery of drugs to affected areas.

A more simple delivery matrix can be made by forming water soluble polymers or block co-polymers with hydroxyl or groups similarly amenable to condensation or addition reactions as terminals or side chains on the polymer. The number of hydroxyl groups on the chain can be controlled by regulating the stochiometry of the monomers used to make the polymers. These functional groups can then been used to covalently add drugs,[40, 41] fluorescent tags[42] and structural property modifiers[43] to the polymer to affect its properties *in vivo*. In this way small loadings of functional molecules can be loaded onto the plastic while retaining biodegradability.

1.3. **Cancer**

1.3.1. **Cancer**

'Cancer' is an umbrella term which covers a series of diseases caused by mutations in cells causing the cell to be unable to terminate. Cells which are unable to terminate are effectively immortal while there is supply of ATP and oxygen. The cells may also have other defects which make them no longer able to perform the specific task of the tissue. There are over 200 different types of cell in the human body, and so there are over 200 different types of cancer, ranging from cancers of specific organs or organ systems, isolated or 'alien' teratomas growing in tissues of different types to those in the tumour, or as a secondary result of another disease or virus such as Kaposi's sarcoma caused by human herpesvirus 8 and other HIV-related viruses.[22a]

The first step towards clinical use of an anti-cancer drug is to perform *in vitro* studies of the drug with isolated lines of human cancer cells. The efficacy of the drug *in vitro* gives some indication of its potential efficacy *in vivo* and so is a humane, comparatively inexpensive and high-throughput method of screening candidates for anti-cancer activity. The method is not without disadvantages, however, as *in vitro* methods are unable to model the responses of the whole organ system or tissue of a mammal might have to the drug. Using a single cell-focussed method does not model how the drug might be metabolised and converted within the body into an active drug, or deactivated by cells which are non-cancerous such as liver or kidney cells.[22b]

During cell line testing, human cancer cells are distributed evenly in a 96-well plate and different concentrations of drug are added to each lane of wells. The cells are allowed to incubate in a 3 day cycle. The fraction of cells alive after exposure to the drug is measured using the MTT-assay (Figure 1.3-1). Cells are exposed to a tetrazolium bromide salt which is yellow in colour. Wells containing cells which are alive will change colour to purple as the cells convert the tetrazolium salt into a purple coloured formazan.[23] The degree of conversion of the tetrazoium is studied using UV/visible spectroscopy and correlates with the fraction of cells alive in the wells.
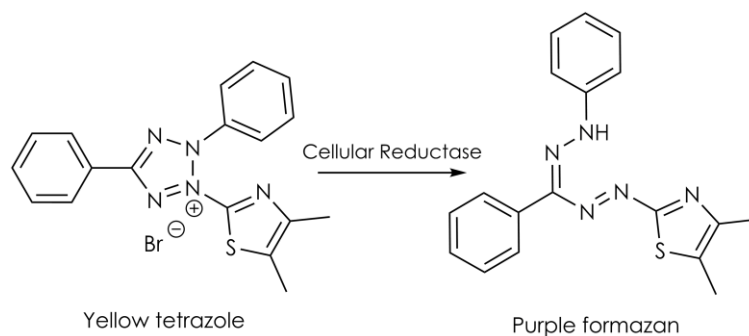
Figure 1.3-1 – MTT assay

The standard method to describe the activity of a cancer drug is to state the IC_{50} and compare this to the action of a *cis*-platin standard which is measured in parallel on the same batch of cells. The IC_{50} is the concentration of drug required to kill 50% of cells in a given medium. This standard allows us to assess drugs which do not reach 100% cell-death and will be used as a standard to compare efficacy of drugs in this work.

1.3.2. Titanium anti-cancer drugs

Budotitane (Figure 1.3-2) was discovered and reported by *Keppler et al* in 1986. [24] The drug was found to be a potent anti-cancer agent, undergoing Phase I trials for use in humans in 1983 and again in 1996. The first trial reported increased anti-cancer activity over *cis-platin* and lower observed toxicity.[25] The second study was conducted with 18 patients receiving doses between 180 mg/m^2 and 230 mg/m^2. The dose limiting side effect was found to be cardiac arrhythmia. Preliminary pharmacokinetic analysis found maximum concentrations of the drug in the bloodstream to be the same, within error, at both extremes of the dosages with values of 2.9 ± 1.2 µg and 2.2 ± 0.8 µg respectively.[26]
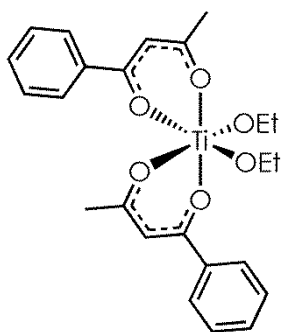
Figure 1.3-2 – Structure of Budotitane

During Phase I trials the drug was dispersed in a micellular formulation of glycerine polyethylene-glycolericinoleate and 1,2-propylene glycol with anhydrous ethanol in order to help stabilise the air and moisture sensitive drugs. The drug was found to have a fairly long half-life of 59.3 ± 12.1 hours and 78.7 ± 24 hours for the highest and lowest doses respectively.[27, 28] However, at this point clinical

trials were halted due to difficulties fully characterising the active species in the micellular formulation.

1.3.3. Cancer Specific Drug Delivery Systems

Cancer specific polymeric drugs and imaging agents have been developed, patented,[44] published[45] and reviewed.[46-48] Encapsulation of organic drugs such as doxorubicin,[49] paclitaxel[50] and plasmid DNA (Figure 1.3-3) has been investigated.[51] Several encapsulated metallodrugs have also been studied for their cytotoxic effect and use in medical imaging. The most focus has been on the well-defined Pt(II) species *cis*-platin[52, 53], and carboplatin[54], which have shown improved cytotoxicity against the free drug when delivered using dual membrane carbon nanotube morphologies and reduced cytotoxicity when using a herringbone morphology of carbon as the nanoparticle retains around 90% of the loaded drug. More recent developments have shown more improvements; Zhi *et al* have reported selective pH release of *cis*-platin using nanodiamond particles[55] and Shi *et al* have found that both *cis*-platin and *trans*-platin can be more active against breast and cervical cancers when bound to silica nanoparticles than the equivalent free drug.[56] Polymeric drug delivery matrices have received the most attention for metallodrugs and Phase I trials have begun for some *cis-platin* delivery systems.[57-59] *Cis-platin* has also been used as a co-drug in a synergistic medicine containing *cis-platin* and doxorubicin, the combination of which showed dramatic enhancements to the cytotoxicity of the drug mixture compared to the drugs separately.[60]
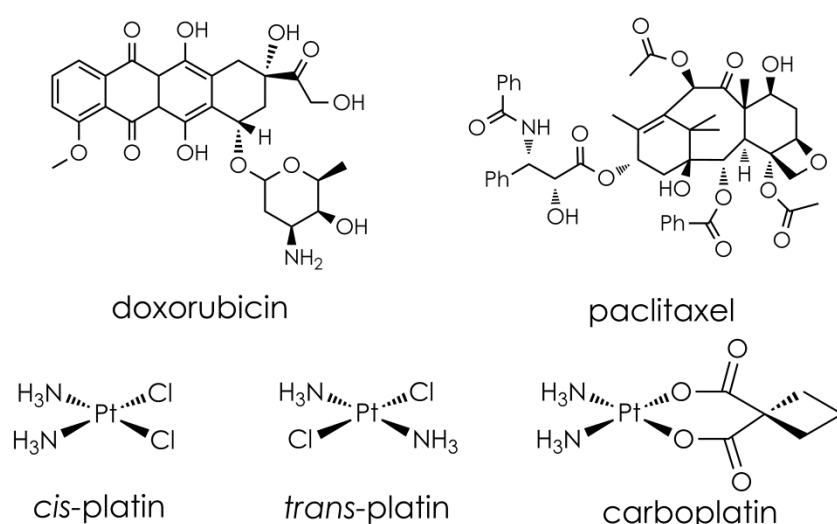
Figure 1.3-3 - Anti-cancer drugs of interest in nanoparticle delivery systems

There has also been interest in encapsulated Pt(IV) species, with the intention that the platinum will be reduced to the active Pt(II) species *in vivo*. In this way the Pt(IV) drug acts as a prodrug and also allows extra coordination sites for addition of targeting molecules.[61-65]

Other metals have also been studied for drug delivery. Magnetic Rh(II) complex nanoparticles have shown specific toxicity for cancerous breast cells over healthy breast cells.[66] A series of

ferrocenyl,[67, 68] Ru(III)[69] and Ni(II)[70] complexes have shown increased activity when delivered as micelles or in liposomes rather than as a free drug. There have also been reports of the use of chromium and ruthenium metal complexes with a nitrosyl ligand to act as a source of NO gas by irradiating cancer cells with UV or visible light to promote the release of NO in the cell and encourage apoptosis.[71-73]

Despite progress in the field there has only been one recent report of the use of titanium containing nanoparticles for treatment of cancer[74] and no reports in the literature of using micellular and nanoparticle techniques to overcome the problems inherent in delivery of Budotitane, and other titanium drugs based on the structure of Budotitane.

DFT calculations conducted by Šponer *et al* suggested that the identity of the active titanium species in the cell may be the same for all titanium complexes. The group found a correlation between the IC$_{50}$ of several titanocene drugs and the Gibb's energy of acid catalysed dissociation of the Cp ligands.[75] As the Gibb's free energy becomes more negative, the dissociation becomes more favourable and the compound becomes more cytotoxic. Šponer suggests, therefore, that the active species for all titanium drugs may be a maximally hydrolysed $[Ti(H_2O)_6]^{+4}$ species, as the activity of Budotitane is very similar to that of titanocene dichloride, despite the drugs having very different modes of coordination.[27]

1.4. Summary

Poly(lactic acid) is a medically and industrially useful polymer formed from lactide which can be synthesised by fermentation of waste plant materials. The feedstock for the plastic can be entirely synthesised without the use of petrol products and, as such, can be considered somewhat renewable. The polymer can be formed using direct condensation or by ring-opening polymerisation. While there are many examples of active catalysts for the ring-opening polymerisation of lactide, the mechanism of the polymerisation is still somewhat unknown, and this project seeks to add to the library of known active catalysts, quantify their ability to polymerise lactide, and seek structure-activity relationships where possible.

Cancer is an umbrella term describing a series of conditions caused by mutations of cells which causes those cells to malfunction. Some mutations of these cells prevent the cell from being able to perform apoptosis, a process by which a cell terminates, and so these 'faulty' cells continue to reproduce in the body. Medicinal attempts to deactivate cancerous cells focus on disrupting the DNA so that the cell is unable to replicate, form proteins necessary for its continued survival and this causes the cell to die. One method of disrupting the DNA within the cell is to add a Lewis acid which is able to form dative bonds with the nitrogen atoms in the nucleobases, and thus disrupt the double helix of the DNA. Titanium (IV) complexes are promising candidates for the treatment of cancer in patients, with one example of a titanium (IV) drug, Budotitane, having undergone Phase I and II trials in humans.[24] These trials were abandoned due to the difficulty in preparing a safe and suitable formulation of the drug. Recent developments in the production of polymer-based delivery systems

using a wide array of polymers suggests that polymer-based drug delivery systems might be of use for the delivery of titanium metallodrugs.[29-36] In order to prepare Ti(IV)-dispersed polymer preparations, the metal's ability to conduct the ring-opening polymerisation of lactide to form poly(lactic acid) could be exploited.

1.5. Chapter One References

1. Baekeland, L.H. On Soluble, Fusible, Resinous Condensation Products Of Phenols And Formaldehyde. *Journal Of Industrial & Engineering Chemistry*. 1909, **1**(8), pp.545-549.

2. Hill, A. *Organotransition Metal Chemistry*. 1 Ed. New York: Wiley-Interscience, 2002.

3. Pellecchia, C., Pappalardo, D., Oliva, L. And Zambelli, A. η^5-C$_5$Me$_5$TiMe$_3$-B(C$_6$F$_5$)$_3$: A True Ziegler-Natta Catalyst For The Syndiotactic-Specific Polymerization Of Styrene. *Journal Of The American Chemical Society*. 1995, **117**(24), pp.6593-6594.

4. Ishihara, N., Seimiya, T., Kuramoto, M. And Uoi, M. Crystalline Syndiotactic Polystyrene. *Macromolecules*. 1986, **19**(9), pp.2464-2465.

5. Coates, G.W., Hustad, P.D. And Reinartz, S. Catalysts For The Living Insertion Polymerization Of Alkenes: Access To New Polyolefin Architectures Using Ziegler–Natta Chemistry. *Angewandte Chemie International Edition*. 2002, **41**(13), pp.2236-2257.

6. Stepto, R.F.T. Dispersity In Polymer Science (IUPAC Recommendations 2009). *Pure And Applied Chemistry*. 2009, **81**(2), pp.351-353.

7. Allegra, G. Discussion On The Mechanism Of Polymerization Of α-Olefins With Ziegler-Natta Catalysts. *Die Makromolekulare Chemie*. 1971, **145**(1), pp.235-246.

8. Bochmann, M. *Organometallics 2*. Oxford: Oxford University Press, 1994.

9. Balasanthiran, V., Beilke, T.L. And Chisholm, M.H. Use Of Over The Counter Oral Relief Aids Or Dietary Supplements For The Ring-Opening Polymerization Of Lactide. *Dalton Transactions*. 2013, **42**(25), pp.9274-9278.

10. Gibson, V.C., Marshall, E.L., Navarro-Llobet, D., White, A.J.P. And Williams, D.J. A Well-Defined Iron(Ii) Alkoxide Initiator For The Controlled Polymerisation Of Lactide. *Journal Of The Chemical Society, Dalton Transactions*. 2002, (23), pp.4321-4322.

11. Williams, C.K., Breyfogle, L.E., Choi, S.K., Nam, W., Young, V.G., Hillmyer, M.A. And Tolman, W.B. A Highly Active Zinc Catalyst For The Controlled Polymerization Of Lactide. *Journal Of The American Chemical Society*. 2003, **125**(37), pp.11350-11359.

12. Hodgson, L.M., Platel, R.H., White, A.J.P. And Williams, C.K. A Series Of Bis(Thiophosphinic Amido)Yttrium Initiators For Lactide Ring-Opening Polymerization. *Macromolecules*. 2008, **41**(22), pp.8603-8607.

13. Ko, B.-T. And Lin, C.-C. Synthesis, Characterization, And Catalysis Of Mixed-Ligand Lithium Aggregates, Excellent Initiators For The Ring-Opening Polymerization Of L-Lactide. *Journal Of The American Chemical Society*. 2001, **123**(33), pp.7973-7977.

14. Calvo, B., Davidson, M.G. And García-Vivó, D. Polyamine-Stabilized Sodium Aryloxides: Simple Initiators For The Ring-Opening Polymerization Of Rac-Lactide. *Inorganic Chemistry*. 2011, **50**(8), pp.3589-3595.

15. Uhrich, K.E., Cannizzaro, S.M., Langer, R.S. And Shakesheff, K.M. Polymeric Systems For Controlled Drug Release. *Chemical Reviews*. 1999, **99**(11), pp.3181-3198.

16. Schindler, A., Hibionada, Y.M. And Pitt, C.G. Aliphatic Polyesters. III. Molecular Weight And Molecular Weight Distribution In Alcohol-Initiated Polymerizations Of ϵ-Caprolactone. *Journal Of Polymer Science: Polymer Chemistry Edition*. 1982, **20**(2), pp.319-326.

17. Moon, S.I. And Kimura, Y. Melt Polycondensation Of L-Lactic Acid To Poly(L-Lactic Acid) With Sn(II) Catalysts Combined With Various Metal Alkoxides. *Polymer International*. 2003, **52**(2), pp.299-303.

18. Konishi, S., Yokoi, T., Ochiai, B. And Endo, T. Effect Of Metal Triflates On Direct Polycondensation Of Lactic Acid. *Polymer Bulletin*. **64**(5), pp.435-443.

19. Upare, P.P., Hwang, Y.K., Chang, J.-S. And Hwang, D.W. Synthesis Of Lactide From Alkyl Lactate Via A Prepolymer Route. *Industrial & Engineering Chemistry Research*. **51**(13), pp.4837-4842.

20. Wisniewski, M., Borgne, A.L. And Spassky, N. Synthesis And Properties Of (D)- And (L)-Lactide Stereocopolymers Using The System Achiral Schiff's Base/Aluminium Methoxide As Initiator. *Macromolecular Chemistry And Physics*. 1997, **198**(4), pp.1227-1238.

21a. Tsuji, H., Kamo, S. And Horii, F. Solid-State ^{13}C NMR Analyses Of The Structures Of Crystallized And Quenched Poly(Lactide)S: Effects Of Crystallinity, Water Absorption, Hydrolytic Degradation, And Tacticity. *Polymer*. 2010, **51**(10), pp.2215-2220.

21b. Stephen, R., Sunoj, R.B. and Ghosh, P. 2011. A Computational Insight Into A Metal Mediated Pathway For The Ring-Opening Polymerization (ROP) Of Lactides By An Ionic {(NHC)$_2$Ag}+X- (X = halide) Type N-heterocyclic Carbene (NHC) Complex. Dalton Transactions. 40(39), pp.10156-10161.

22a. NHS-Choices. *Causes Of Kaposi's Sarcoma*. [Online]. 2013. [Accessed 01/03/2016]. Available From: Http://Www.Nhs.Uk/Conditions/Kaposis-Sarcoma/Pages/Causes.Aspx

22b. National Research Council (US) Committee On Methods Of Producing Monoclonal Antibodies. Monoclonal Antibody Production. Washington (DC): National Academies Press (US); 1999. 4, Summary Of Advantages And Disadvantages Of In Vitro And In Vivo Methods. Available From: Http://Www.Ncbi.Nlm.Nih.Gov/Books/NBK100200/

23. Cory, A.H., Owen, T.C., Barltrop, J.A. And Cory, J.G. Use Of An Aqueous Soluble Tetrazolium/Formazan Assay For Cell Growth Assays In Culture. Cancer Commun. 1991, **3**(7), pp.207-212.

24. Keppler K. B., S.D. Preclinical Evaluation Of Dichlorobis(1-Phenylbutane-1,3-Dionato)Titanium (IV) And Budotitane. Two Representatives Of The New Class Of Antitumor-Active Bis-Beta-Diketonato Metal Complexes *Arzneimittel-Forschung*. 1986, **36**(12), P.1822.

25.   Keller, H.J., Keppler, B. And Schmähl, D. Antitumor Activity Of *Cis*-Dihalogenobis(1-Phenyl-1,3-Butanedionato)Titanium(IV) Compounds. *Journal Of Cancer Research And Clinical Oncology.* 1983, **105**(1), pp.109-110.

26.   Schilling, T., Keppler, K.B., Heim, M.E., Niebch, G., Dietzfelbinger, H., Rastetter, J. And Hanauske, A.R. Clinical Phase I And Pharmacokinetic Trial Of The New Titanium Complex Budotitane. *Investigational New Drugs.* 1995, **13**(4), pp.327-332.

27.   Keppler, B.K., Friesen, C., Moritz, H.G., Vongerichten, H. And Vogel, E. Tumor-Inhibiting Bis(B-Diketonato) Metal Complexes. Budotitane, *Cis*-Diethoxybis(1-Phenylbutane-1,3-Dionato)Titanium(IV). In: *Bioinorganic Chemistry*.   Springer Berlin Heidelberg, 1991, pp.97-127.

28.   Clarke, M.J., Zhu, F. And Frasca, D.R. Non-Platinum Chemotherapeutic Metallopharmaceuticals. *Chem. Rev.* 1999, **99**(9), pp.2511-2534.

29.   Singh, S., Webster, D.C. And Singh, J. Thermosensitive Polymers: Synthesis, Characterization, And Delivery Of Proteins. *International Journal Of Pharmaceutics.* 2007, **341**(1-2), pp.68-77.

30.   Shah, N.M., Pool, M.D. And Metters, A.T. Influence Of Network Structure On The Degradation Of Photo-Cross-Linked PLA-B-PEG-B-PLA Hydrogels. *Biomacromolecules.* 2006, **7**(11), pp.3171-3177.

31.   Lee, W.-C., Li, Y.-C. And Chu, I.M. Amphiphilic Poly(D,L-Lactic Acid)/Poly(Ethylene Glycol)/Poly(D,L-Lactic Acid) Nanogels For Controlled Release Of Hydrophobic Drugs. *Macromolecular Bioscience.* 2006, **6**(10), pp.846-854.

32.   Kang, G.D., Cheon, S.H. And Song, S.C. Controlled Release Of Doxorubicin From Thermosensitive Poly(Organophosphazene) Hydrogels. *International Journal Of Pharmaceutics.* 2006, **319**(1-2), pp.29-36.

33.   Mequanint, K., Patel, A. And Bezuidenhout, D. Synthesis, Swelling Behavior, And Biocompatibility Of Novel Physically Cross-Linked Polyurethane-Block-Poly(Glycerol Methacrylate) Hydrogels. *Biomacromolecules.* 2006, **7**(3), pp.883-891.

34.   Ha, D., Lee, S., Chong, M., Lee, Y., Kim, S. And Park, Y. Preparation Of Thermo-Responsive And Injectable Hydrogels Based On Hyaluronic Acid And Poly(N-Isopropylacrylamide) And Their Drug Release Behaviors. *Macromolecular Research.* 2006, **14**(1), pp.87-93.

35.   Cai, T., Hu, Z., Ponder, B., St. John, J. And Moro, D. Synthesis And Study Of And Controlled Release From Nanoparticles And Their Networks Based On Functionalized Hydroxypropylcellulose. *Macromolecules.* 2003, **36**(17), pp.6559-6564.

36.   Uraki, Y., Imura, T., Kishimoto, T. And Ubukata, M. Body Temperature-Responsive Gels Derived From Hydroxypropylcellulose Bearing Lignin. *Carbohydrate Polymers.* 2004, **58**(2), pp.123-130.

37. Talukdar, M.M., Vinckier, I., Moldenaers, P. And Kinget, R. Rheological Characterization Of Xanthan Gum And Hydroxypropylmethyl Cellulose With Respect To Controlled-Release Drug Delivery. *Journal Of Pharmaceutical Sciences.* 1996, **85**(5), pp.537-540.

38. Determan, M.D., Cox, J.P. And Mallapragada, S.K. Drug Release From Ph-Responsive Thermogelling Pentablock Copolymers. *Journal Of Biomedical Materials Research Part A.* 2007, **81A**(2), pp.326-333.

39. Chen, P.C., Kohane, D.S., Park, Y.J., Bartlett, R.H., Langer, R. And Yang, V.C. Injectable Microparticle–Gel System For Prolonged And Localized Lidocaine Release. II. In Vivo Anesthetic Effects. *Journal Of Biomedical Materials Research Part A.* 2004, **70A**(3), pp.459-466.

40. Dernedde, J., Rausch, A., Weinhart, M., Enders, S., Tauber, R., Licha, K., Schirner, M., Zügel, U., Von Bonin, A. And Haag, R. Dendritic Polyglycerol Sulfates As Multivalent Inhibitors Of Inflammation. *Proceedings Of The National Academy Of Sciences.* 2010, **107**(46), pp.19679-19684.

41. Ray, W.C. And Grinstaff, M.W. Polycarbonate And Poly(Carbonate−Ester)S Synthesized From Biocompatible Building Blocks Of Glycerol And Lactic Acid. *Macromolecules.* 2003, **36**(10), pp.3557-3562.

42. Wolinsky, J.B., Ray, W.C., Colson, Y.L. And Grinstaff, M.W. Poly(Carbonate Ester)S Based On Units Of 6-Hydroxyhexanoic Acid And Glycerol. *Macromolecules.* 2007, **40**(20), pp.7065-7068.

43. Wolinsky, J.B., Yohe, S.T., Colson, Y.L. And Grinstaff, M.W. Functionalized Hydrophobic Poly(Glycerol-Co-E-Caprolactone) Depots For Controlled Drug Release. *Biomacromolecules.* 2012, **13**(2), pp.406-411.

44. Yamauchi, F. *Polymer And Fluorescence Probe Having The Polymer*. 2009. United States Patent Number US 20100022759 A1

45. Khemtong, C., Kessinger, C.W. And Gao, J. Polymeric Nanomedicine For Cancer MR Imaging And Drug Delivery. *Chemical Communications.* 2009, (24), pp.3497-3510.

46. Fau L. Y. , Prestwich, G.D. - Cancer-Targeted Polymeric Drugs. *Current Cancer Drug Targets.* 2002, **2**(3), pp.209-226.

47. Maldonado, C.R., Salassa, L., Gomez-Blanco, N. And Mareque-Rivas, J.C. Nano-Functionalization Of Metal Complexes For Molecular Imaging And Anticancer Therapy. *Coord. Chem. Rev.* **257**(19-20).

48. Paavola, A., Yliruusi, J., Kajimoto, Y., Kalso, E., Wahlström, T. And Rosenberg, P. Controlled Release Of Lidocaine From Injectable Gels And Efficacy In Rat Sciatic Nerve Block. *Pharmaceutical Research.* 1995, **12**(12), pp.1997-2002.

49. Yokoyama, M., Okano, T., Sakurai, Y., Ekimoto, H., Shibazaki, C. And Kataoka, K. Toxicity And Antitumor Activity Against Solid Tumors Of Micelle-Forming Polymeric

Anticancer Drug And Its Extremely Long Circulation In Blood. *Cancer Research*. 1991, **51**(12), pp.3229-3236.

50. Hamaguchi, T., Matsumura, Y., Suzuki, M., Shimizu, K., Goda, R., Nakamura, I., Nakatomi, I., Yokoyama, M., Kataoka, K. And Kakizoe, T. NK105, A Paclitaxel-Incorporating Micellar Nanoparticle Formulation, Can Extend In Vivo Antitumour Activity And Reduce The Neurotoxicity Of Paclitaxel. *Britishjjournal Of Cancer*. 2005, **92**(7), pp.1240-1246.

51. Akagi, D., Oba, M., Koyama, H., Nishiyama, N., Fukushima, S., Miyata, T., Nagawa, H. And Kataoka, K. Biocompatible Micellar Nanovectors Achieve Efficient Gene Transfer To Vascular Lesions Without Cytotoxicity And Thrombus Formation. *Gene Therapy* 2007, **14**(13), pp.1029-1038.

52. Nishiyama, N. And Kataoka, K. Preparation And Characterization Of Size-Controlled Polymeric Micelle Containing *Cis*-Dichlorodiammineplatinum(II) In The Core. *Journal Of Controlledrrelease : Official Journal Of The Controlled Release Society*. 2001, **74**(1-3), pp.83-94.

53. Tripisciano, C., Kraemer, K., Taylor, A. And Borowiak-Palen, E. Single-Wall Carbon Nanotubes Based Anticancer Drug Delivery System. *Chem. Phys. Lett.* 2009, **478**(4–6), pp.200-205.

54. Hampel, S., Kunze, D., Haase, D., Krämer, K., Rauschenbach, M., Ritschel, M., Leonhardt, A., Thomas, J., Oswald, S., Hoffmann, V. And Büchner, B. Carbon Nanotubes Filled With A Chemotherapeutic Agent: A Nanocarrier Mediates Inhibition Of Tumor Cell Growth. *Nanomedicine*. 2008, **3**(2), pp.175-182.

55. Guan, B., Zou, F. And Zhi, J. Nanodiamond As The Ph-Responsive Vehicle For An Anticancer Drug. *Small*. 2010, **6**(14), pp.1514-1519.

56. Gu, J., Su, S., Li, Y., He, Q., Zhong, J. And Shi, J. Surface Modification−Complexation Strategy For *Cis*-Platin Loading In Mesoporous Nanoparticles. *The Journal Of Physical Chemistry Letters*. 2010, **1**(24), pp.3446-3450.

57. Rademaker-Lakhai, J.M., Terret, C., Howell, S.B., Baud, C.M., De Boer, R.F., Pluim, D., Beijnen, J.H., Schellens, J.H.M. And Droz, J.-P. A Phase I And Pharmacological Study Of The Platinum Polymer AP5280 Given As An Intravenous Infusion Once Every 3 Weeks In Patients With Solid Tumors. *Clinical Cancer Research*. 2004, **10**(10), pp.3386-3395.

58. Campone, M., Rademaker-Lakhai, J.M., Bennouna, J., Howell, S.B., Nowotnik, D.P., Beijnen, J.H. And Schellens, J.H. Phase I And Pharmacokinetic Trial Of AP5346, A DACH-Platinum-Polymer Conjugate, Administered Weekly For Three Out Of Every 4 Weeks To Advanced Solid Tumor Patients. *Cancer Chemother Pharmacol*. 2007, **60**(4), pp.523-533.

59.   Malik, N., Evagorou, E.G. And Duncan, R. Dendrimer-Platinate: A Novel Approach To Cancer Chemotherapy. *Anti-Cancer Drugs*. 1999, **10**(8), pp.767-776.

60.   Lee, S.M., O'Halloran, T.V. And Nguyen, S.T. Polymer-Caged Nanobins For Synergistic *Cis*-Platin−Doxorubicin Combination Chemotherapy. *J. Am. Chem. Soc.* 2010, **132**(48), pp.17130-17138.

61.   Bednarski, P.J., Mackay, F.S. And Sadler, P.J. Photoactivatable Platinum Complexes. *Anticancer Agents Med Chem.* 2007, **7**(1), pp.75-93.

62.   Muller, P., Schroder, B., Parkinson, J.A., Kratochwil, N.A., Coxall, R.A., Parkin, A., Parsons, S. And Sadler, P.J. Nucleotide Cross-Linking Induced By Photoreactions Of Platinum(IV)-Azide Complexes. *Angew Chem Int Ed Engl.* 2003, **42**(3), pp.335-339.

63.   Barnes, K.R., Kutikov, A. And Lippard, S.J. Synthesis, Characterization, And Cytotoxicity Of A Series Of Estrogen-Tethered Platinum(IV) Complexes. *Chemistry & Biology*. 2004, **11**(4), pp.557-564.

64.   Mukhopadhyay, S., Barnés, C.M., Haskel, A., Short, S.M., Barnes, K.R. And Lippard, S.J. Conjugated Platinum(IV)−Peptide Complexes For Targeting Angiogenic Tumor Vasculature. *Bioconjugate Chemistry*. 2007, **19**(1), pp.39-49.

65.   Hall, M.D. And Hambley, T.W. Platinum(IV) Antitumour Compounds: Their Bioinorganic Chemistry. *Coord. Chem. Rev.* 2002, **232**(1–2), pp.49-67.

66.   Sinisterra, R.D., Shastri, V.P., Najjar, R. And Langer, R. Encapsulation And Release Of Rhodium(II) Citrate And Its Association Complex With Hydroxypropyl-Beta-Cyclodextrin From Biodegradable Polymer Microspheres. *J Pharm Sci.* 1999, **88**(5), pp.574-576.

67.   Allard, E., Passirani, C., Garcion, E., Pigeon, P., Vessières, A., Jaouen, G. And Benoit, J.-P. Lipid Nanocapsules Loaded With An Organometallic Tamoxifen Derivative As A Novel Drug-Carrier System For Experimental Malignant Gliomas. *Journal Of Controlled Release*. 2008, **130**(2), pp.146-153.

68.   Allard, E., Jarnet, D., Vessières, A., Vinchon-Petit, S., Jaouen, G., Benoit, J.-P. And Passirani, C. Local Delivery Of Ferrociphenol Lipid Nanocapsules Followed By External Radiotherapy As A Synergistic Treatment Against Intracranial 9L Glioma Xenograft. *Pharm Res.* 2010, **27**(1), pp.56-64.

69.   Mangiapia, G., D'Errico, G., Simeone, L., Irace, C., Radulescu, A., Di Pascale, A., Colonna, A., Montesarchio, D. And Paduano, L. Ruthenium-Based Complex Nanocarriers For Cancer Therapy. *Biomaterials*. 2012, **33**(14), pp.3770-3782.

70.   Ahn, R.W., Chen, F., Chen, H., Stern, S.T., Clogston, J.D., Patri, A.K., Raja, M.R., Swindell, E.P., Parimi, V., Cryns, V.L. And O'Halloran, T.V. A Novel Nanoparticulate Formulation Of Arsenic Trioxide With Enhanced Therapeutic Efficacy In A Murine Model Of Breast Cancer. *Clinical Cancer Research*. 2010, **16**(14), pp.3607-3617.

71.   Diaz-Garcia, A.M., Fernandez-Oliva, M., Ortiz, M. And Cao, R. Interaction Of Nitric Oxide With Gold Nanoparticles Capped With A Ruthenium(II) Complex. *Dalton Trans.* 2009, (38), pp.7870-7872.

72.   Neuman, D., Ostrowski, A.D., Mikhailovsky, A.A., Absalonson, R.O., Strouse, G.F. And Ford, P.C. Quantum Dot Fluorescence Quenching Pathways With Cr(III) Complexes. Photosensitized NO Production From Trans-Cr(Cyclam)(ONO)2+. *J. Am. Chem. Soc.* 2007, **130**(1), pp.168-175.

73.   Neuman, D., Ostrowski, A.D., Absalonson, R.O., Strouse, G.F. And Ford, P.C. Photosensitized NO Release From Water-Soluble Nanoparticle Assemblies. *J. Am. Chem. Soc.* 2007, **129**(14), pp.4146-4147.

74.   Praseetha P. K., Supriya C. V., Chandraja C. V., Vijayalekshmi B. And Chavalia, M.S. Biosynthesis Of Titanium Nanoparticles And Their Role In Killing Colon Cancer Cells *J. Nanosci. Lett.* 2013, **3**, P.5.

75.   Šponer, J.E., Leszczynski, J. And Šponer, J. Mechanism Of Action Of Anticancer Titanocene Derivatives: An Insight From Quantum Chemical Calculations. *The Journal Of Physical Chemistry B.* 2006, **110**(39), pp.19632-19636.

2. ALUMINIUM COMPLEXES

2.1. Acetylacetonate ligands

In order to study the mechanism of the polymerisation of lactide by the complexes of interest to this project, a ligand system which is tunable for sterics and electronics was required. Acetylacetonate ligands are an excellent candidate for this application as symmetrical or asymmetrical acetylacetone ligands can be synthesised easily *via* Claisen condensation reactions. (Scheme 2.1-1)
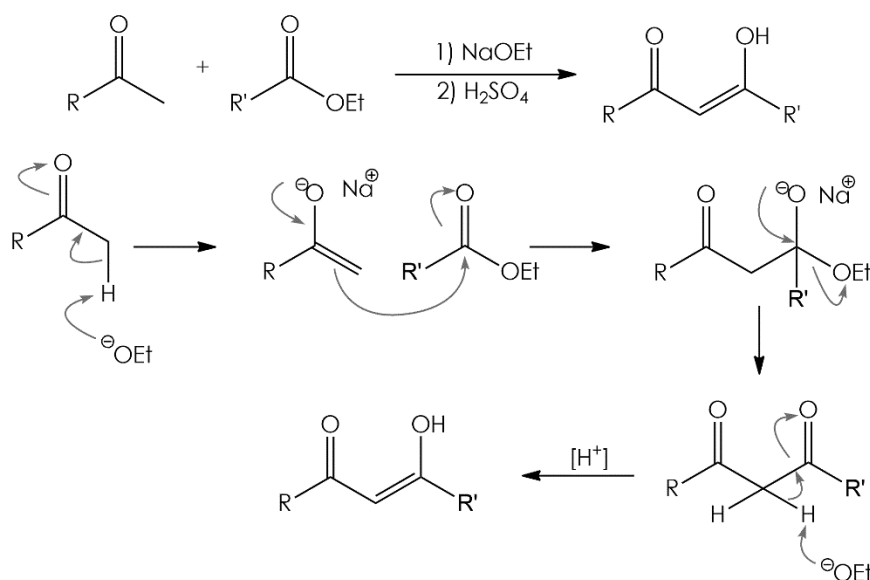
Scheme 2.1-1 – Synthesis of acetylacetone ligands

Asymmetrical ligands where R = substituted phenyl group and R' = methyl group can be prepared by refluxing the relevant acetophenone, or ketone, with base in ethyl acetate. The ligand is acidified and extracted in chloroform from an aqueous solution of the solid obtained in step 1.
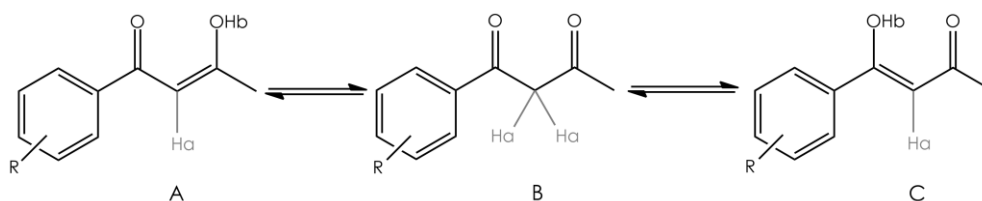
Figure 2.1-1 – Tautomers of acetylacetone ligands

Asymmetrical ligands such as those in Figure 2.1-1 have three possible tautomers, whereas protons labelled Ha in symmetrical acetylacetone molecules are equivalent to one another. In the solid state, the acetylacetone ligands have been found by X-ray crystallography to adopt a delocalised

configuration (Figure 2.1-2), with the C=O bond lengths usually being approximately equal, within error, with an average bond length of 130 pm, half way between a double and single bond.[1-7]
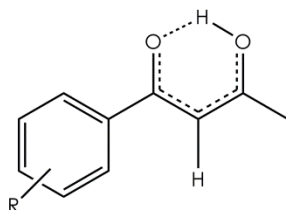
Figure 2.1-2 – Delocalised electron system of a free acetylacetone molecule

The free ligand appears to retain this delocalised structure in solution, with the methinine proton usually appearing between 6.0 – 7.0 ppm in the ^{1}H NMR spectra (Figure 2.1-3). The DEPT 135 experiment offers further evidence that the β-diketonate form is not observed in solution as no significant –ve CH_2 peak is observed in the DEPT 135 ^{13}C NMR spectra (Figure 2.1-1).

Complexes of β-diketonates are synthesised by mixture with a metal source and, if necessary, a base. In the case of the syntheses in this thesis all complexations are ligand substitution reactions where the substituted ligand from the metal acts as a base, removing the extra proton from the free acetylacetone ligand.
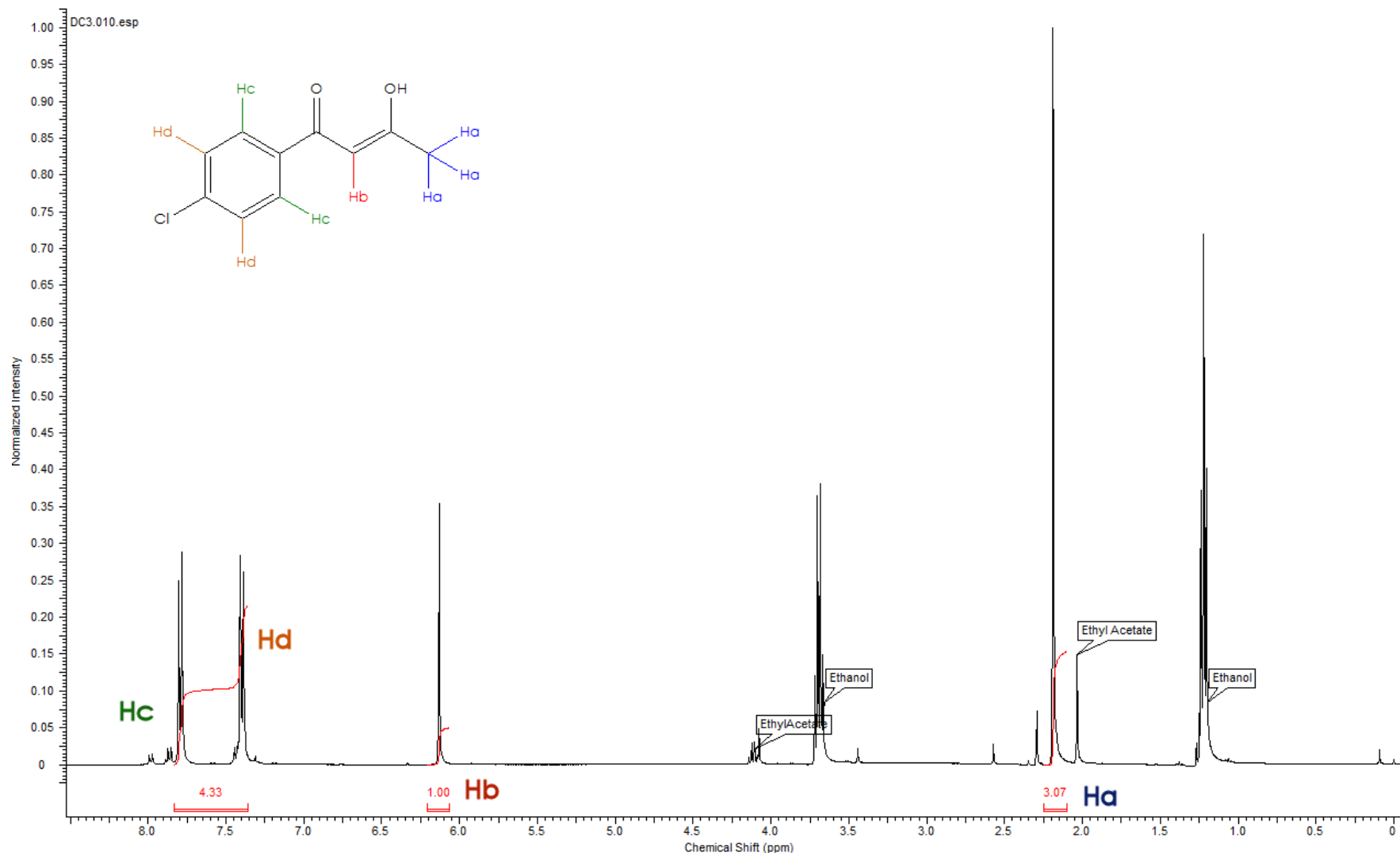
Figure 2.1-1 – Typical ^{1}H NMR spectrum of an acetylacetonate ligand showing likely solvent contaminants
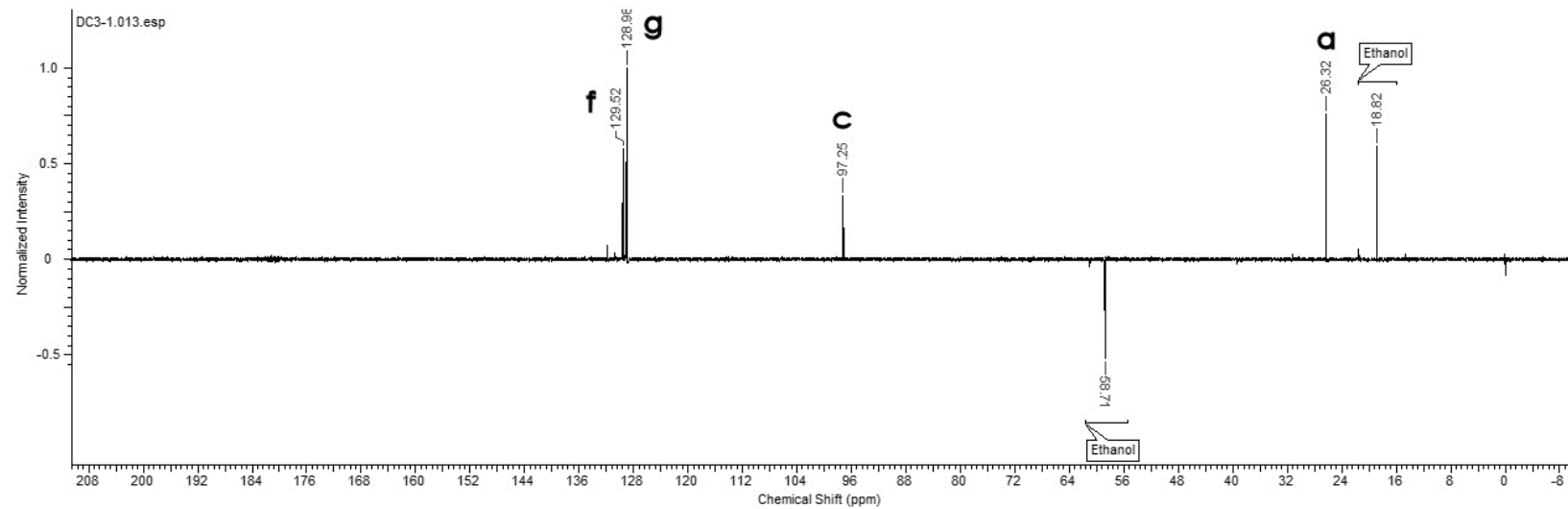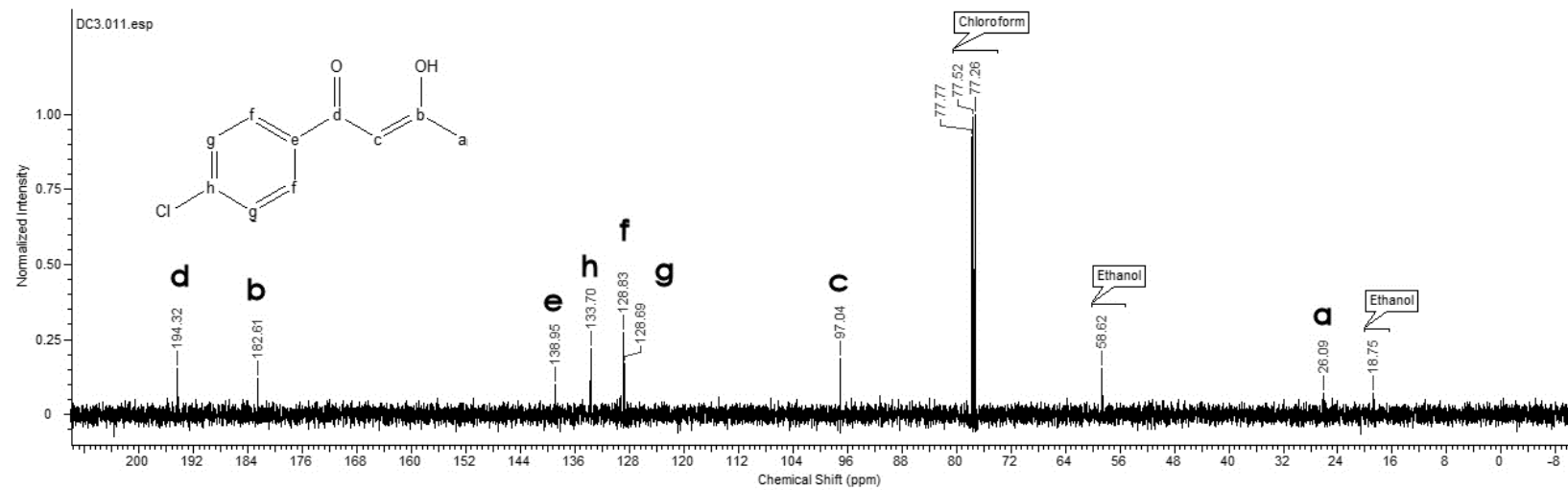
Figure 2.1-2 – Typical ^{13}C NMR spectrum for an acetylacetonate ligand

2.2. Aluminium complexes

Aluminium is well known to the McGowan group to proficiently polymerise lactide. The group has used aluminium complexes to covalently attach functional molecules to poly(lactic acid) chains, allowing the group to synthesise functional plastics which can be spun into fibres for use in garments. [8]

An ideal catalyst for the polymerisation should have a vacant coordination site or should be capable of producing one with little energy input. In this case a dimer structure is ideal, as a dimeric structure can break into two monomeric structures with a vacant coordination site in the presence of a lewis acid. Additionally, aluminium is an ideal metal to form dimeric structures without forming polymeric structures as the metal centre is the smallest of the p-block metals. Trimethylaluminium and triethylaluminium are known to have a dimeric structure in the solid phase.[9, 10] In the case of triethylaluminium there is also evidence the structure can break into monomeric form in the gaseous phase.[10] Ethylaluminium structures have also been explored and a lithium tetraethyl aluminium salt monomer has also been reported.[11] Electron poor structures such as trimethylaluminium and triethylaluminium are known to be pyrophoric, and rapidly react with oxygen in the air, indicating an extremely fragile structure and very reactive metal centres.

It is also possible to synthesise electron precise aluminium dimers using bridging ligands containing lone pair electrons such as halides or alkoxides. Even these types of complex are known to be extremely air sensitive, but not pyrophoric.[12, 13] Some examples using bridging alkoxide ligands have been synthesised in the literature, with examples having been reported by Wengrovius *et al.[14, 15]* and many others.[16-27] However bridged acetylacetonate aluminium dimers have not yet been crystallised, with the closest examples being the malate complexes reported by Seubert *et al. in 2007* and the aluminium β-diketonate alkoxide trimers reported by Wengrovius. [12, 28]

One of the reasons that the dimer structures may not have yet been elucidated is the fragility of the structure. Additional to the air sensitivity of the compound, dimer structures of these sort are also known to 'disproportionate' (though there is no change in oxidation number of the elements in the compound) into the more stable *tris*-acetylaceonate complexes with relatively small inputs of heat.[12]
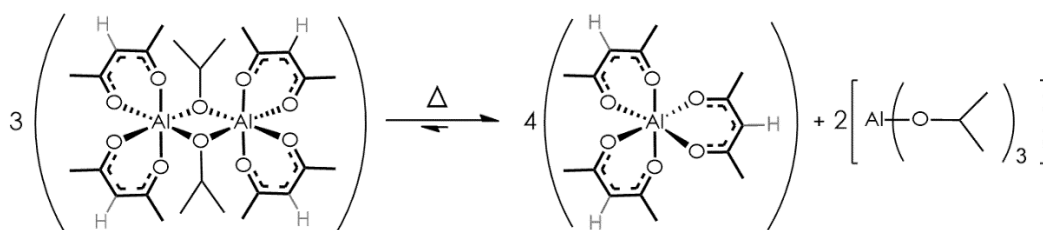
Scheme 2.2-1 – 'Disproportionation' reactions of aluminium dimer structures

Initial attempts to synthesise aluminium dimers focussed on investigating and rationalising the methods used by *Wrengrovius et al*, and considering possible synthetic pathways for making halide bridged analogues of alkoxide bridged compounds previously reported.

2.3. Chloride Bridged Aluminium Dimers

Chloride bridged dimer structures are electron precise. The ligand exchange reaction seems to proceed quickly, driven by the formation of hydrochloric acid and, in this case using bidentate ligands, also driven by the chelate effect.
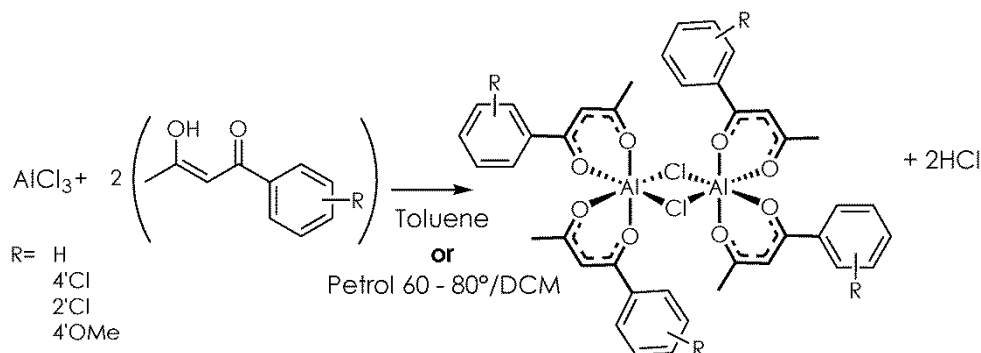
Scheme 2.3-1 – Synthesis of *bis*-(acetylacetonate)aluminium chloride dimer structures

As aluminium chloride is a salt, it was necessary to identify a solvent which allowed full dissolution of the aluminium chloride. If the aluminium chloride was reacted as a solid in suspension, aluminium centres at the surface of the solid crystal lattice may have reacted with a non stoichiometric number of acetylacetonate ligands. Toluene was found to be a good solvent for this reaction as aluminium trichloride readily dissolved in the toluene. However, isolating the product without overheating later became a problem, and a new solvent was sought out which could be removed *in vacuo* at much lower temperatures.

Initial reactions of this type were performed using excess acetylacetonate ligands to investigate the reaction times and suitable solvents. It was found that dissolving aluminium chloride in dichloromethane and adding a solution of the acetylacetonate ligand in petrol 60 - 80° yielded a uniform white solid. When recrystallised by diffusion of pentane into chloroform solution of the solid, hexagonal crystals were isolated, which were found to be *tris*-acetylacetonate aluminium.

Further attempts to identify a reasonable synthetic method followed the method outlined in Scheme 2.3-1. Attempts to synthesise chloride bridged dimers were made with acetylacetonate and substituted phenylacetylacetonate ligands.

To a stirred solution of aluminium (III) chloride in dichloromethane, a solution of acetylacetone in petrol 60-80° was added dropwise with stirring under a dynamic atmosphere of N_2 in Schlenk apparatus. ^{1}H NMR spectra were collected in deuterated

chloroform which had been distilled over calcium hydride and stored in Young's tapped ampoules under N_2.

In the ^{1}H NMR spectrum, complexation can be measured by measuring the shift downfield of the methine proton in the acetylacetonate ligand, labelled 'Hb' in Figure 2.1-4. Shifts of this signal downfield by around 0.1 ppm indicate some complexation.

The number of methine proton signals present in the ^{1}H NMR spectrum between 5.5 -6.5 ppm of an aluminium dimer prepraration is also indicative of the number of products which may have been formed, with *tris*-acetylacetonate aluminium having fewer electrons withdrawn from the methine proton than any form of acetylacetonate aluminium chloride derivative, and expected to have the most upfield shift.

2.3.1. Attempted synthesis of *bis*-(acetylacetonate)aluminium chloride (compound 1)
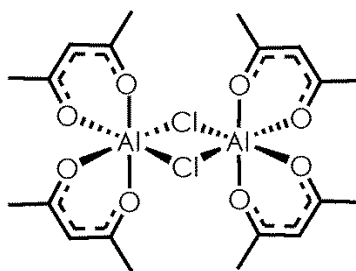
Compound 1 – *bis*-(acetylacetonate)aluminium chloride

Attempts to synthesise compound **1** using the synthetic method laid out in Scheme 2.3-1 were made.

In all syntheses but one using 1, 1.5 and 2 equivalents of acetylacetonate per molecule of aluminium (III) chloride in toluene and dichloromethane/petrol 60-80° mix, a single white product was formed during recrystallisation at - 20 °C from pentane. This product was found to be *tris*-acetylacetonate aluminium by ^{1}H NMR spectroscopy and microanalysis which showed very little chlorine contained within the substance (13.7% expected, 0.35% found).

In one instance where the reaction was performed with two equivalents of acetylacetone with aluminium chloride in pentane and dichloromethane at - 20 °C a crude mixture was formed which suggested some formation of a product with a downfield shift of the methine proton around 0.3 ppm compared to the free ligand. This finding suggests formation of *bis*-acetylacetonate aluminium chloride (compound **1**). The NMR spectrum showed that the compound was impure, with some *tris*-acetylacetonate aluminium also present in the mixture. (Figure 2.3-1)

Attempts to crystallise the product from a chloroform/pentane mixture at 0 °C yielded a crystal suitable for x-ray crystallography, however, midway through solving the compound

was found to be trisacetylacetonealumninium, and the mother liquor changed colour to a light grey on opening the vessel under a flow of N_2.
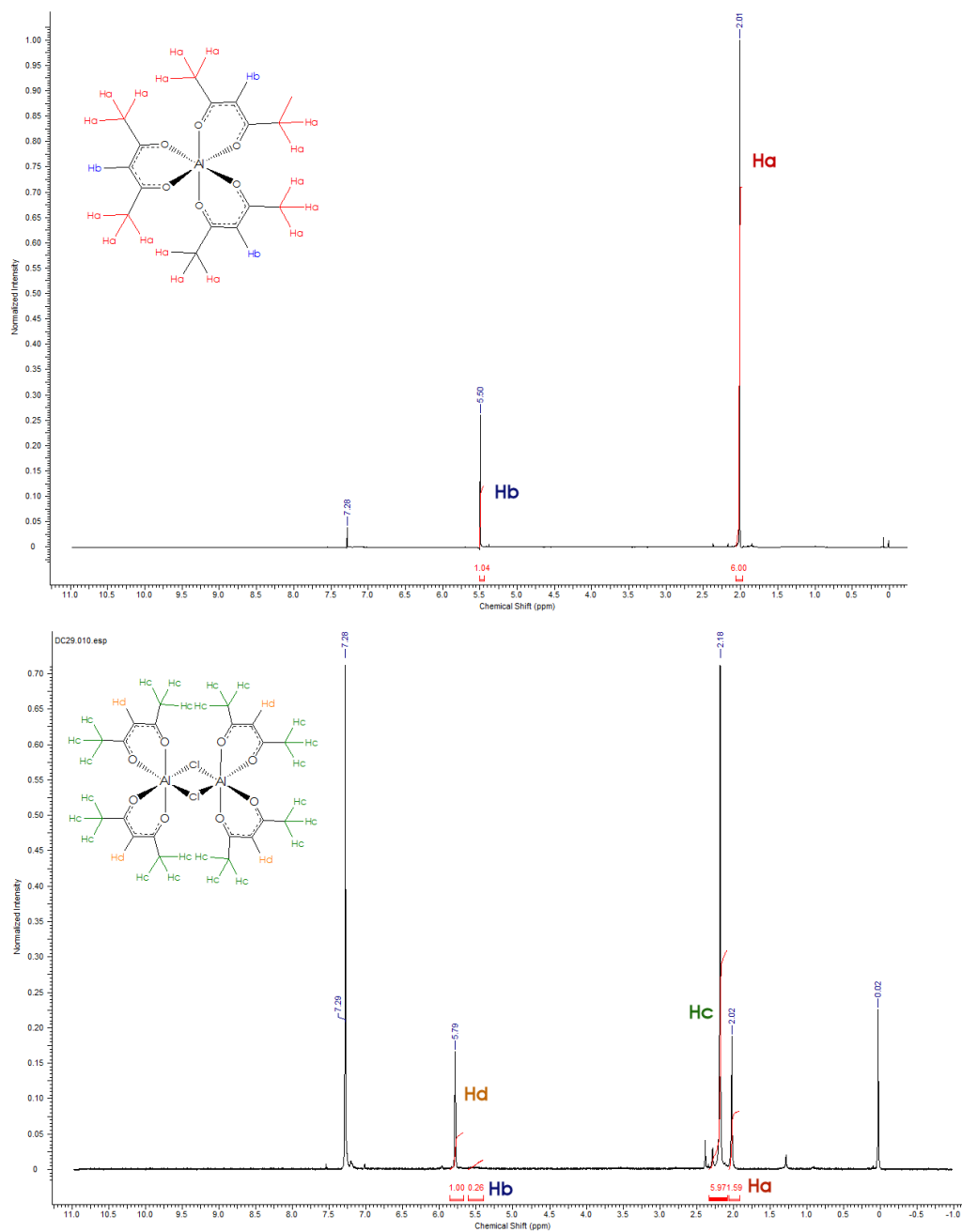
Figure 2.3-1 - ^{1}H NMR spectrum comparison of *tris*-(acetylacetonate)aluminium (top) and crude reaction mixture of attempts to form compound 1 (bottom) collected at 500MHz and 298 K in CDCl₃

2.3.2. Attempted synthesis of *bis*-(phenylacetyacetonate)aluminium chloride
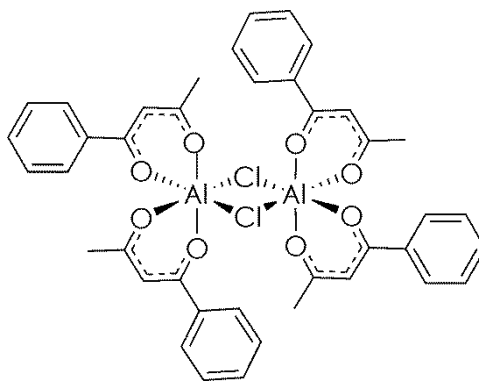
Compound 2 – *bis*-(phenylacetylacetonate)aluminium chloride dimer

Attempts to synthesise *bis*-phenylacetylactonate aluminium chloride using the synthetic method outlined in Scheme 2.3-1 were made. During one reaction a green precipitate was formed. The precipitate was collected by filtration and the crude mixture showed several methine peaks in the ^{1}H NMR spectrum (Figure 2.3-2). The mixture was recrystallised from pentane diffusion into chloroform solution of the crude compound. Recrystallisation had a minor effect on the ^{1}H NMR spectrum (Figure 2.3-2), which showed significant removal of *tris*-phenylacetylacetonate aluminium as the tallest peaks in the crude ^{1}H NMR spectrum are reduced in intensity at 6.45 ppm and 2.31 ppm. As this is the largest expected impurity the method has promise.

Additionally only a single methine proton signal, H_b, remains in the spectrum. This is diagnostic of only a single product formed, as there is only one magnetic environment. If there were a series of products, some monomers, some dimers, some including several chloride ions and some including none, each of these changes should cause significant effects on the aromaticity of the acetylacetonate ligand, and so the magnetic deshielding of the methine proton. However, the overlapping signals of the aromatic protons, H_c, H_d and H_e suggest that there may still be several stereoisomers within the structure, which causes the aromatic protons to experience different magnetic environments as they are forced closer to and further away from the bridging chloride ions in some arrangements of the dimers. This recrystallised product was by far the cleanest and most promising aluminium dimer with bridging chloride product formed during this project. Additional attempts to characterise the complex failed, and attempts to obtain elemental analyses were unsuccessful, possibly due to the extremely air sensitive nature of the complex.
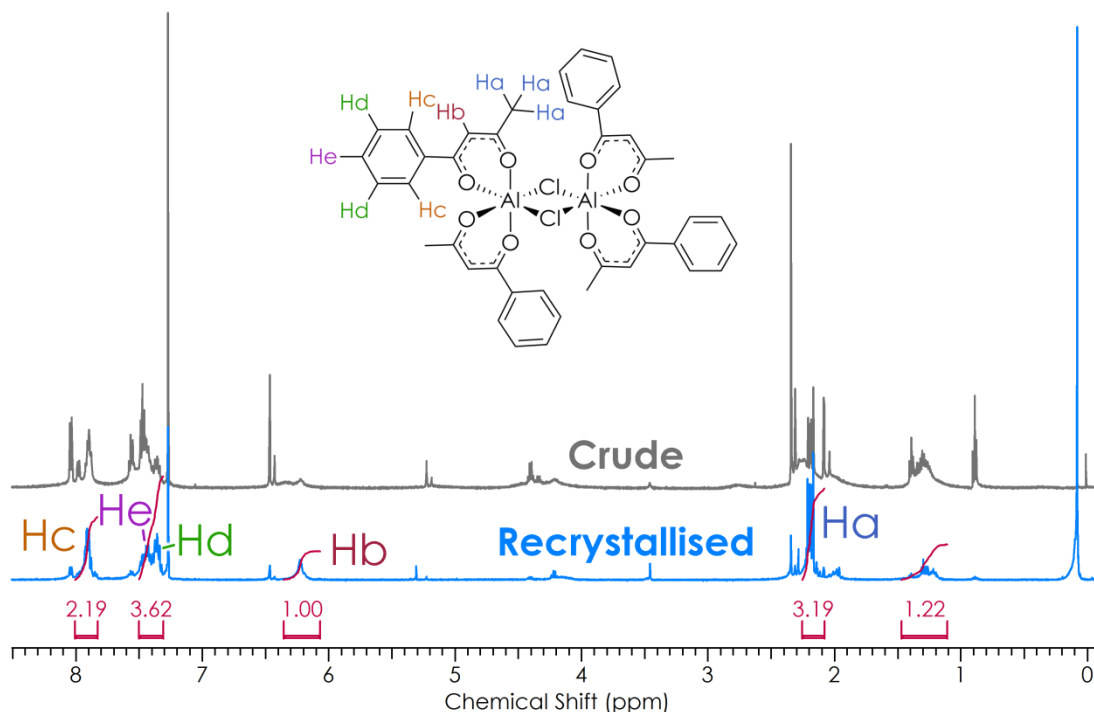
Figure 2.3-2 – Comparative ^{1}H NMR spectrum of crude (top) vs recrystallised (bottom) reaction mixtures resulting from the attempted synthesis of compound 2 collected at 500 MHz at 298 K in CDCl$_3$

2.3.3. Attempted syntheses of *bis*-(4'chlorophenylacetylacetonate)aluminium chloride (compound 3)
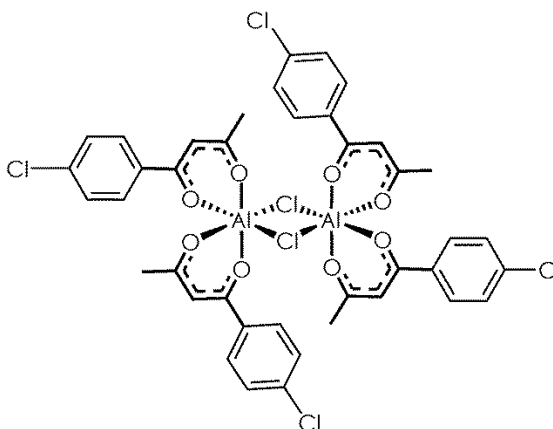
Compound 3 – *bis*-(4-chlorophenylacetylacetonate)aluminium chloride dimer

In other attempted syntheses using substituted phenylacetylacetonate ligands, a similar pattern emerges, with the 4'Cl, 2'Cl and 4'OMe phenylacetylacetonate ligands also forming tris(acetylacetonate)aluminium derivatives, products with single methine peaks in the ^{1}H NMR spectrum.

The exception is attempted syntheses of compound **3** using 4'chlorophenylacetylacetone in dichloromethane and petrol 60 – 80 ° which yielded a slightly green product. The product was recrysallised by pentane diffusion into a chloroform solution of the crude product under N$_2$.
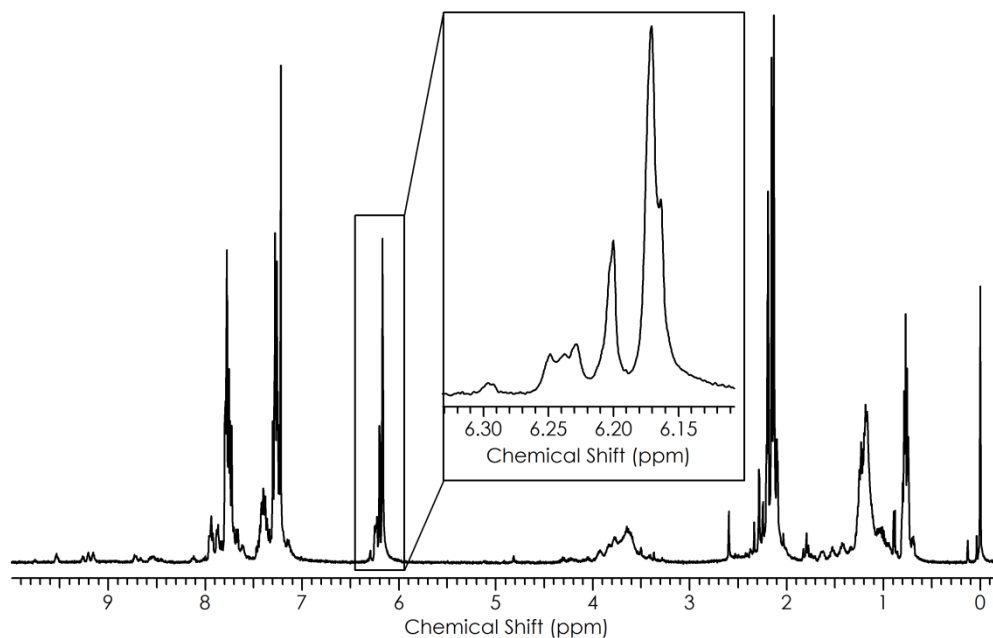
Figure 2.3-3- ^{1}H NMR spectrum of crude product of attempted synthesis of *bis*-4-chlorophenylacetylacetonate aluminium chloride collected at 500 MHz and 223 K in CDCl₃

The ^{1}H NMR spectrum of the solid (Figure 2.3-3) showed that the recrystallised solid contained many different methine proton environments, with seven signals showing between 6.17 and 6.30 ppm, suggesting either several products or several non-magnetically equivalent stereoisomers.

The mass spectrum of the solid suggested some formation of the $[Al(4-Cl'acac)_3]_2$ dimer, showing a major peak of 1249.1 $gmol^{-1}$ which corresponds to $[C_{60}H_{50}Al_2Cl_6NaO_{12}]$. Other major peaks corresponding to $Al(4-ClPhacac)_2$ with a major peak representing $[C_{20}H_{16}AlCl_2O_4]^+$ at 417.0 $gmol^{-1}$ and $Al(4-ClPhacac)_3Na$; 635 $gmol^{-1}$, $[C_{30}H_{24}AlCl_3NaO_6]^+$.

Attempts to grow crystals under N_2 from pentane, chloroform, dichloromethane and diffusion of pentane into chloroform at - 20 °C yielded very small amounts of solid which were unsuitable for analysis.

2.3.4. Synthesis of alkoxide compounds from aluminium chloride precursors
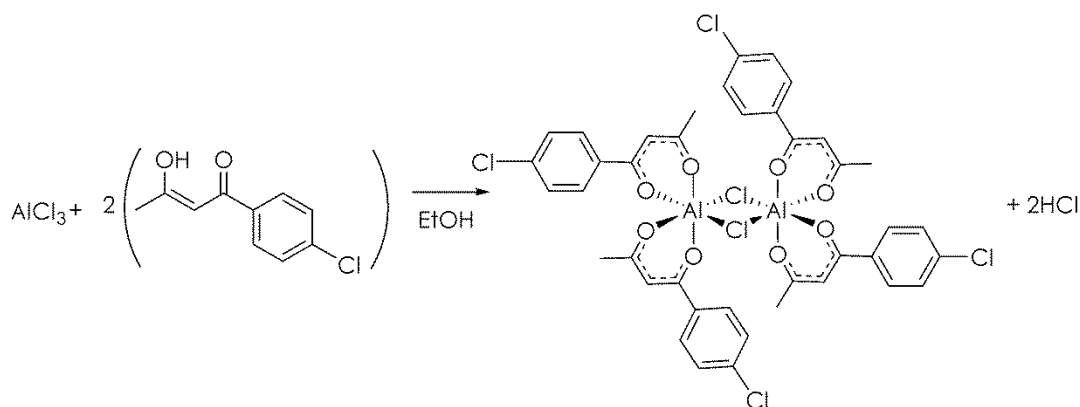
Scheme 2.3-2 – Attempted synthesis of *bis*-(4'chlorophenylacetylacetonate)aluminium chloride dimer

In one attempted synthesis of compound **3**, ethanol was used as a solvent using the scheme outlined in Scheme 2.3-2. As alkoxide bridged compounds were also a target of this investigation, if the chloride ions were able to suitably act as a base to form ethoxide bridging ligands, this would have also been of interest.

The crude product of the reaction was analysed by ^{1}H NMR spectrum (Figure 2.3-4) and shows a shift of the methine peak from 6.09 ppm in the uncomplexed 4'chlorophenylacetylacetone ligand to 6.29 ppm in the crude reaction mixture, suggesting complexation of the ligand to the aluminium centre as expected.

Additionally there is a broadening of the peaks corresponding to the CH_2 protons of the ethanol changing from a doublet at 3.35 ppm to a single broad peak at 3.91 ppm. This large upfield shift of 0.56 ppm suggests that there has been some complexation of ethanol to the metal centre. Downfield there is a large change in the signals, with a new broad signal appearing at 1.29 ppm which may indicate complexation of the ethanol as the usual CH_3 signal appearing around 1.25 ppm of the ethanol shifts significantly. There are additional new peaks at 0.87 ppm which could not be identified.

This method was also thought to have promise as a possible method to form alkoxide complexes as aluminium (III) chloride is not particularly oxygen sensitive, though it is hygroscopic and will react with water if exposed to the atmosphere.[29]
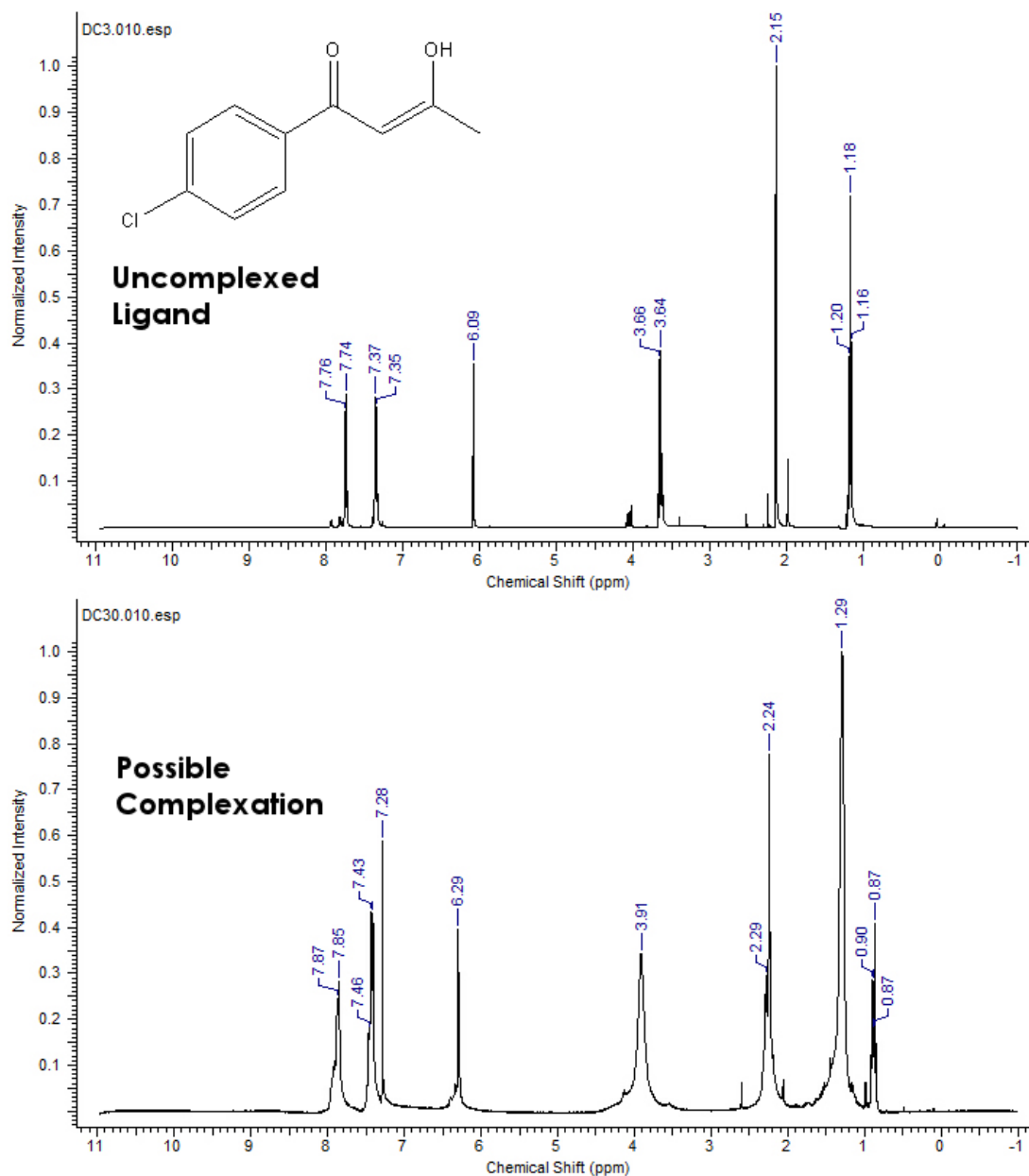
Figure 2.3-4 – Comparative ^{1}H NMR spectrum showing the spectrum of 4'chlorophenylacetylacetone (top) against crude reaction mixture of attempted synthesis of compound 3 using the synthesis described in Scheme 2.3-2, collected at 500 MHz and 298 K in CDCl₃.

The compound was found to be thermally unstable and degraded in the spectrometer awaiting long run collections.

2.3.5. Polymerisation attempts using crude aluminium chloride mixtures

Polymerisation attempts were made with all aluminium compounds synthesised in the most forcing conditions to ascertain whether the acetylacetonate ligands 'turned off' the metal's catalytic ability, and whether the acetylacetonate ligands were able to act as initiators to the polymerisation reaction.

The most forcing polymerisation conditions possible for the polymerisation of lactide is to dry-melt together the lactide and potential catalyst in a ratio of 200:1 lactide to catalyst.

Lactide melts around 100 °C, but can withstand temperatures of 150 °C before thermal decomposition occurs. Using this method the moltern lactide acts as its own solvent for the reaction mixture. A stirrer bead is added to ensure reasonable mixing of the reaction mixture, and the reaction is conducted in a suba-sealed round bottomed flask under nitrogen and submerged in hot oil.

A successful polymerisation results in a solid at the bottom of the round-bottomed flask at 150 °C. Degree of polymerisation is measured by ^{1}H NMR spectrum (see Chapter 3)

The major impurity formed during the synthesis, *tris*-acetylacetonate aluminium, was found not to polymerise lactide in these forcing conditions. Aluminium (III) chloride was also found not to polymerise lactide during control studies to ensure there were no impurities within the purchased samples of the starting materials which may be active for the polymerisation of lactdie. Lactide was found not to self-polymerise in these forcing conditions, establishing the control methods for testing the catalytic ability of the polymers.

All of the *tris*-acetylacetonate compounds tested were found not to polymerise lactide in dry-melt conditions, with ^{1}H NMR spectroscopy confirming no change in the lactide monomer after polymerisation attempts.

However, the impure substance which resulted from attempts to synthesise compound **2** was found to polymerise lactide efficiently in dry melt conditions and 1:200 equivalents of lactide per aluminium centre, to yield a spongy, slightly yellow, solid plastic at 150 °C. This crude reaction mixture represented the most successful attempts to synthesise a chloride bridged aluminium dimer, which acted as a reasonably successful catalyst for the polymerisation of lactide. The ability for aluminium chloride complexes to polymerise lactide has not yet been reported in the literature, although some examples of complexes containing chloride ligands have.[30, 31] This result led to further investigations of the ability of chloride ligands to act as initiating groups to polymerise lactide which are discussed in Chapter 3.

2.4. Synthesis of *bis*-(acetylacetonate)aluminium *sec*-butoxide [Al(acac)$_2$(^{s}BuO)$_2$]$_2$ (Compound 4)

Many attempts at synthesising alkoxide bridged compounds were made during this project. Due to the severely air sensitive nature of these compounds, as well as their heat sensitivity, synthesis and purification of these compounds is extremely challenging. While Wrengrovius *et al* report synthesis of very simple alkoxide bridged dimers, the challenge of crystallisation of the most simple compounds remains. The simplicity of the compounds is of extreme importance.

Examples of large substituted ligands and pheyl bridging alkoxide compounds exist in the literature,[16, 17, 32-37] however these complexes have unrealistic industrial applications. Chapter 1 discusses the current industrial synthetic methods of poly(lactic acid), which

uses a simple catalyst of stannous octoate. Any proposed substitute must be as simple to handle and as cheap as stannous octoate unless that catalyst confers vastly improved synthetic properties such as rate of polymerisation or control of chain length. If an initiator is involved, this should be a common solvent. Some catalysts in the literature require benzoyl alcohol or more expensive compounds still as an initiator, making these catalysts undesirable for industrial use.[38, 39] While the synthesis and purification of the compound described in this section is difficult if the chemist wishes to isolate and characterise the compound, the synthesis is incredibly simple if they are interested only in creating some of the compound *in situ* to use in polymerisation.

In order to investigate more closely the mechanism of action of the catalysts, it is necessary to have an idea of the structure of the compound in the solid state, for further confirmation that the structure of the compound is following the models the mechanism of the polymerisation of the plastic is suspected to be.

This section reports the full synthesis and characterisation of a novel simple alkoxide-bridged aluminium dimer which acts as an efficient catalyst for the polymerisation of lactide at room temperature in solution without the need for an initiator, which is made by simple addition of aluminium (III) *sec*-butoxide and acetylacetone.

Bis-acetylacetonate aluminium *sec*-butoxide (compound **4**) was synthesised under N_2 by slow addition of a solution of acetylacetone in chloroform to a stirred solution of aluminium(III) *sec*-butoxide at - 78 °C. The mixture was stirred for three hours at - 78 °C then allowed to warm up to 0 °C under dynamic nitrogen flow.
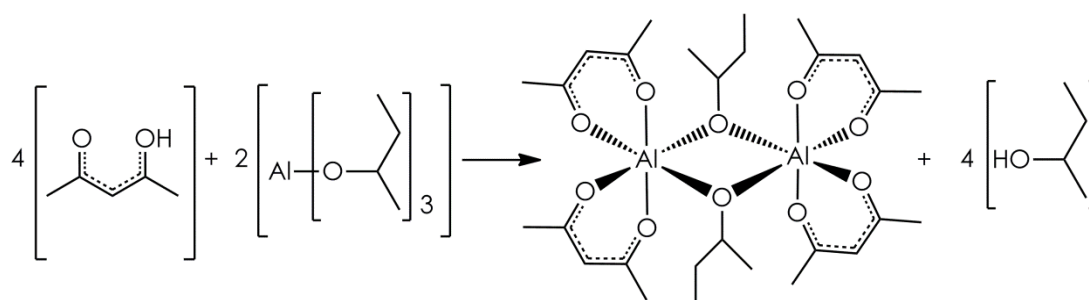
Compound 1 – *bis*-acetylacetonate aluminium *sec*-butoxide

Scheme 2.4-1 – Synthesis of bisacetylactonate aluminium sec-butoxide

The solution was allowed to partially evaporate slowly at 0 °C under nitrogen flow and small colourless crystals suitable for X-ray crystallography were obtained. The crystals were isolated by filtration and were found to be pure by microanalysis.

On further cooling a second crop of large cloudy plates were obtained. These plates were later found to be *tris*-acetylacetonate aluminium by ^{1}H NMR spectroscopy.

2.4.1. Crystallographic analysis of *bis*-(acetylacetonate)aluminium *sec*-butoxide [Al(acac)₂(ˢBuO)₂]₂ (Compound 4)
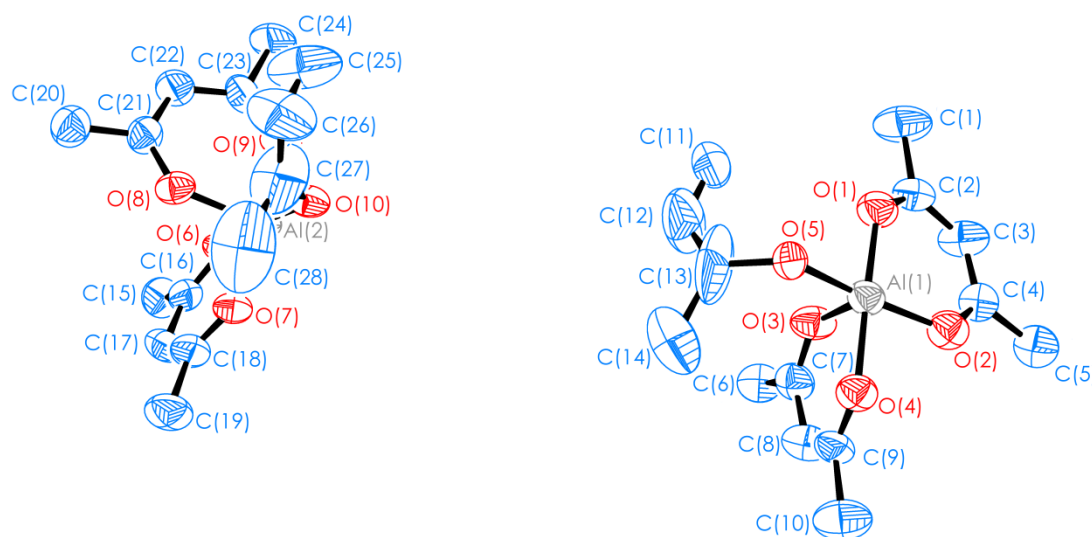
Figure 2.4-1 - ORTEP diagram of the asymmetric unit of Compound 4 with ellipsoids displayed at the 50% probability level, (hydrogen atoms omitted for clarity)

Compound **4** crystallised in a tetragonal unit cell in the space group $I4_1$. The asymmetric unit contains two half-molecules with a total of eight molecules in the unit cell. Bond angles and lengths are included in Table 1.4-1 and Table 1.4-2 respectively.

Each symmetry generated molecule contains only one of the half molecules shown in the asymmetric unit, giving rise to Al(1)-Al(1) molecules and Al(2)-Al(2) molecules in the crystal structure. The two molecules are equivalent within error. The dimer structure contains two octahedral aluminium centres, with bridging *sec*-butoxide O-Al bond lengths measuring 1.882(6) Å and 1.870(6) Å, and an average interatomic Al-Al inter-atomic distance measuring 2.91 Å. This further confirms the electron precise nature of the complex as this bond length is very similar to the bond lengths found in simple aluminium oxide hydroxide minerals such as diaspore of 1.86 Å.[40, 41] The aluminium-acetylacetonate oxygen interactions are all equidistant, within error, measuring an average of 1.90 Å. The bridging centre is sterically strained and there is a significant pinching effect between the aluminium atoms and the bridging oxygen atoms reducing the O(6)-Al(1)-O(6) bond angle to 78.25(3)° (Figure 2.4-3). The bond angles around the *sec*-butoxide oxygen atom seem to exhibit a trigonal planar geometry, with the outside C(13)-O(5)-Al(1) angles measuring 129.6(8)°, and the strained angle inside the bridging structure Al(1)-O(5)-Al(1) measuring 101.5(2)°.
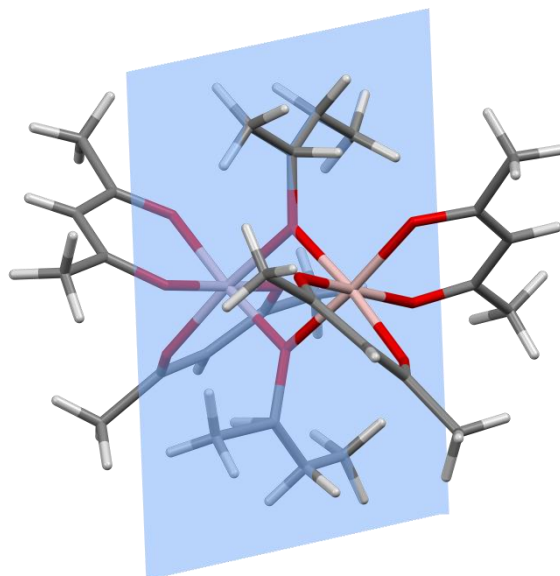
Figure 2.4-2 – Capped stick diagram showing the *sec*-butoxide bridging ligand plane (blue)
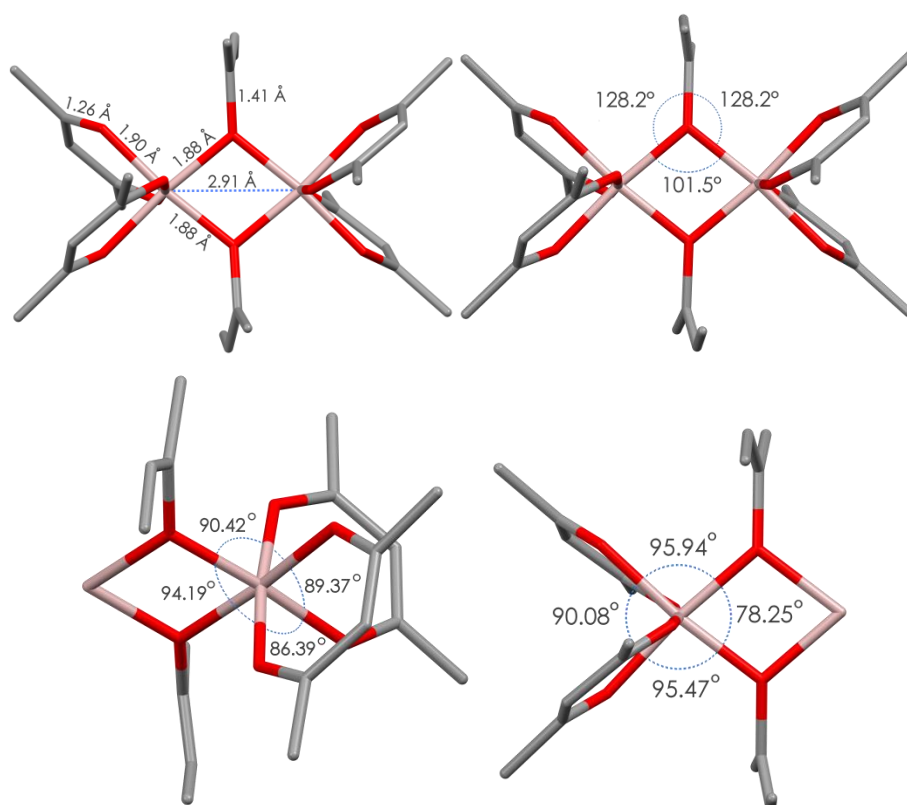
Figure 2.4-3 – Selected bond lengths and angles in the structure of compound 4 (atoms omitted for clarity)

The *sec*-butoxide ligand was shown to have a 2D planar carbon backbone (Figure 2.4-2) which was not expected. The *sec*-butoxide C(13)-O(5) bond measures 1.412(9) Å, indicating a single C-O bond, and sp^3 hybridised oxygen atom, rather than the sp^2 C=O

which is suggested by the planar arrangement of the *sec*-butoxide chain. This planarity may be a result of average motion of the chain, which is supported by the large ellipsoids of the *sec*-butoxide carbon atoms (Figure 2.4-1). This thermal motion leads to an odd placement of the hydrogen atom of the *sec*-butoxide carbon. The other carbon-carbon bond lengths within the *sec*-butoxide carbon backbone are anomalous measuring: C(13)-C(12) 1.223(19)Å, C(13)-C(14) 1.72(2)Å and C(11)-C(12) 1.222(13)Å. Other angles around the aluminium centres were as expected all measuring approximately 90° (Figure 2.4-3 and Figure 2.4-4)
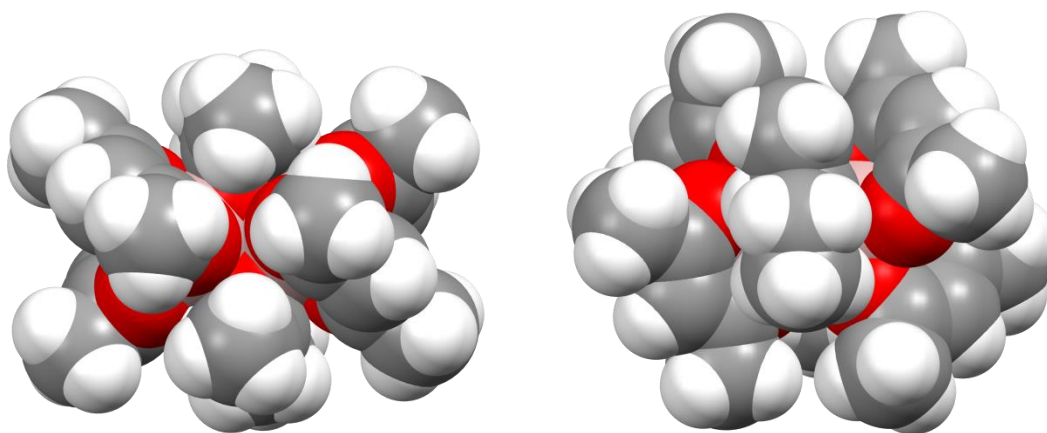
Figure 2.4-4 – Space filling diagram of compound 4

The crystal structure gives us some insight into the reason why the methyl protons of the acetylacetonate ligand might be observed as two separate peaks in the ^{1}H NMR spectrum in Figure 2.4-6. Figure 2.4-4 shows a space filling diagram of compound **4**. Due to the sterically strained nature of the bridging structure the acetylacetone methyl groups are forced together into a very close arrangement, with a methyl carbon - methyl carbon distance measuring 4.89 Å. A 1996 study of observed Van der Waals radii of carbon-hydrogen bonds from crystal structures conducted by Taylor *et al.* was found to be 3.02 Å.[42] With the methyl – methyl distances being so short compared to an expected C-H bond length, it is possible at this distance that the Van der Waals radii of the methyl protons are able to interfere, causing a change in magnetic environment enough for these interacting methyl groups to be differentiated in an NMR spectrum.

Al(1)-Al(1)[(a)]	2.915(5)Å	Al(1)-O(5)	1.882(6)Å
Al(1)-O(5)[(a)]	1.883(6)Å	Al(1)-O(2)	1.902(7)Å
Al(1)-O(3)	1.889(6)Å	Al(1)-O(4)	1.908(7)Å
Al(1)-O(1)	1.902(5)Å	O(5)-Al(1)[(a)]	1.883(6)Å
O(5)-C(13)	1.412(9)Å	O(2)-C(4)	1.283(11)Å
O(3)-C(7)	1.288(9)Å	O(4)-C(9)	1.241(10)Å
O(1)-C(2)	1.263(10)Å	C(1)-C(2)	1.481(11)Å
C(9)-C(10)	1.527(11)Å	C(9)-C(8)	1.393(12)Å
C(2)-C(3)	1.390(11)Å	C(7)-C(8)	1.384(11)Å
C(7)-C(6)	1.494(12)Å	C(4)-C(3)	1.372(13)Å
C(4)-C(5)	1.531(11)Å	Al(2)-Al(2)[(b)]	2.923(5)Å
Al(2)-O(6)	1.888(6)Å	Al(2)-O(8)	1.895(7)Å
Al(2)-O(10)[(b)]	1.875(6)Å	Al(2)-O(10)	1.870(6)Å
Al(2)-O(7)	1.898(8)Å	Al(2)-O(9)	1.902(6)Å
O(6)-C(16)	1.288(9)Å	O(8)-C(21)	1.288(11)Å
O(10)-Al(2)[(b)]	1.875(6)Å	O(10)-C(27)	1.447(11)Å
O(7)-C(18)	1.249(10)Å	O(9)-C(23)	1.254(9)Å
C(24)-C(23)	1.507(10)Å	C(19)-C(18)	1.499(11)Å
C(23)-C(22)	1.389(11)Å	C(16)-C(17)	1.369(11)Å
C(16)-C(15)	1.523(11)Å	C(18)-C(17)	1.408(12)Å
C(22)-C(21)	1.382(13)Å	C(21)-C(20)	1.513(11)Å
C(28)-C(27)	1.72(3)Å	C(11)-C(12)	1.222(13)Å
C(27)-C(26)	1.228(19)Å	C(13)-C(12)	1.223(19)Å
C(13)-C(14)	1.72(2)Å	C(26)-C(25)	1.264(14)Å

Table 2.4-1 – Selected bond lengths for Compound 4 with standard uncertainties listed in parentheses. [(a)/(b)] – Indicates a symmetry generated atom in the second half of the molecule

O(5)-Al(1)-Al(1)[(a)]	39.28(16)°	O(5)[(a)]-Al(1)-Al(1)[(a)]	39.27(16)°
O(5)-Al(1)-O(5)[(a)]	78.5(2)°	O(5)-Al(1)-O(2)	94.6(3)°
O(5)[(a)]-Al(1)-O(2)	90.5(3)°	O(5)[(a)]-Al(1)-O(3)	95.9(3)°
O(5)-Al(1)-O(3)	174.3(3)°	O(5)[(a)]-Al(1)-O(4)	94.6(3)°
O(5)-Al(1)-O(4)	90.2(3)°	O(5)[(a)]-Al(1)-O(1)	174.5(3)°
O(5)-Al(1)-O(1)	96.0(3)°	O(2)-Al(1)-Al(1)[(a)]	93.08(19)°
O(2)-Al(1)-O(4)	173.6(3)°	O(2)-Al(1)-O(1)	89.2(2)°
O(3)-Al(1)-Al(1)[(a)]	135.1(2)°	O(3)-Al(1)-O(2)	86.6(3)°
O(3)-Al(1)-O(4)	89.1(3)°	O(3)-Al(1)-O(1)	89.6(3)°
O(4)-Al(1)-Al(1)[(a)]	93.4(2)°	O(1)-Al(1)-Al(1)[(a)]	135.2(2)°
O(1)-Al(1)-O(4)	86.1(3)°	Al(1)-O(5)-Al(1)[(a)]	101.5(2)°
C(13)-O(5)-Al(1)	129.6(8)°	C(13)-O(5)-Al(1)[(a)]	128.2(8)°

C(4)-O(2)-Al(1)	128.3(5)°	C(7)-O(3)-Al(1)	129.3(5)°
C(9)-O(4)-Al(1)	129.5(6)°	C(2)-O(1)-Al(1)	130.3(5)°
O(4)-C(9)-C(10)	114.6(9)°	O(4)-C(9)-C(8)	124.0(8)°
C(8)-C(9)-C(10)	121.3(8)°	O(1)-C(2)-C(1)	117.9(7)°
O(1)-C(2)-C(3)	122.7(8)°	C(3)-C(2)-C(1)	119.5(8)°
O(3)-C(7)-C(8)	122.6(7)°	O(3)-C(7)-C(6)	115.3(7)°
C(8)-C(7)-C(6)	121.9(8)°	C(7)-C(8)-C(9)	123.3(8)°
O(2)-C(4)-C(3)	124.2(8)°	O(2)-C(4)-C(5)	115.4(9)°
C(3)-C(4)-C(5)	120.4(8)°	C(4)-C(3)-C(2)	123.5(8)°

Table 2.4-2 – Bond angles for compound 4 with standard uncertainties listed in parentheses
[a] – Indicates a symmetry generated atom in the second half of the molecule
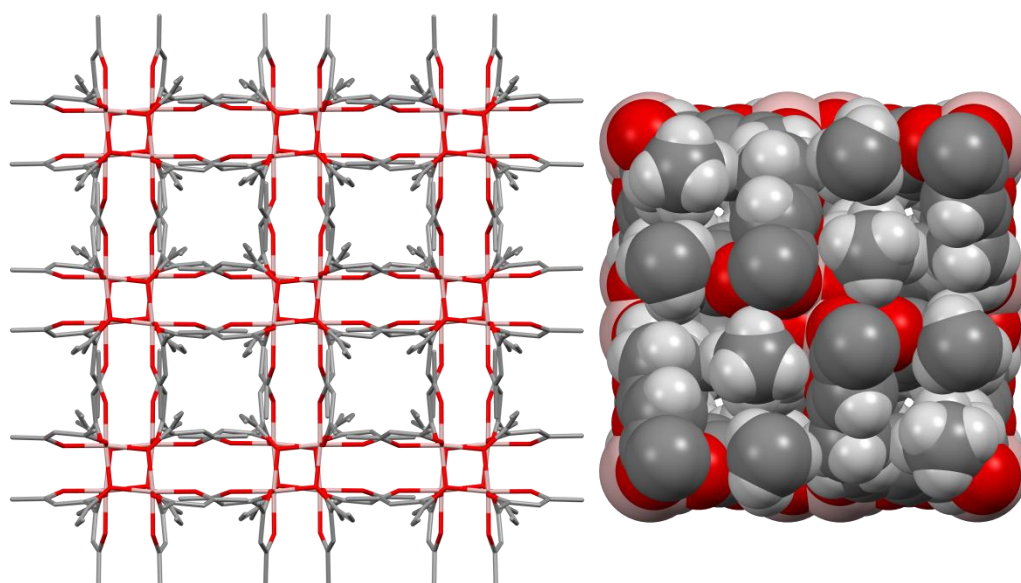
Figure 2.4-5 – Crystal packing of compound 4 viewed down the c-axis of the crystal structure.
Left – Capped Stick Diagram   Right – Space filling diagram

Figure 2.4-5 shows the crystal packing of compound **4** when viewed down the c-axis. The compound shows an interesting structure where the aluminium bridges of the compound stack on top of each other to form an interesting square lattice, and forming tiny channels running down the structure when viewed in the space filling mode are too small for possible hosting applications.

2.4.2. NMR spectroscopic analysis of *bis*-(acetylacetonate)aluminium *sec*-butoxide (Compound 4)

The ^{1}H NMR spectrum of the isolated product shows broad peaks belonging to the aluminium *sec*-butoxide dimer (compound **4**) and sharp peaks identified as belonging to an aluminium *tris*-acetylacetonate. The full ^{1}H NMR spectrum is displayed in Figure 2.4-6.

At room temperature the ^{1}H NMR spectrum is complex. The usual diagnostic peak for the methine proton of the β-diketonate (H_b Figure 2.4-6) is split into two distinct signals at 5.38 ppm and 5.33 ppm which coalesce to a single signal at 5.36 ppm as the sample is heated to 60 °C (Figure 2.4-7).

It is possible that increasing the temperature pushes the formation of *tris*-acetylacetonate aluminium. If this were the case only two products would be formed, *tris*-acetylacetonate aluminium and aluminium (III) *sec*-butoxide. As *tris*-acetylacetonate aluminium is already present in the spectrum, the product formed at 60 °C must be different, otherwise the methine proton labelled b in Figure 2.4-7 would join the signal downfield at 5.15 ppm.

Aluminium is known to form 5 co-ordinate trigonal bipyramidal structures. [43, 44] One possibility is that, at room temperature, the interconversion between the dimeric structure and the monomeric structure as shown in Scheme 2.4-2 is reasonably rapid, and both forms can be seen in the ^{1}H NMR spectrum. As the sample is heated the kinetic product is formed and only one of these forms is seen. As the dimer is known to be the thermodynamic product, forming at - 78 °C, it may be the monomer which predominates in the 60 °C spectrum.
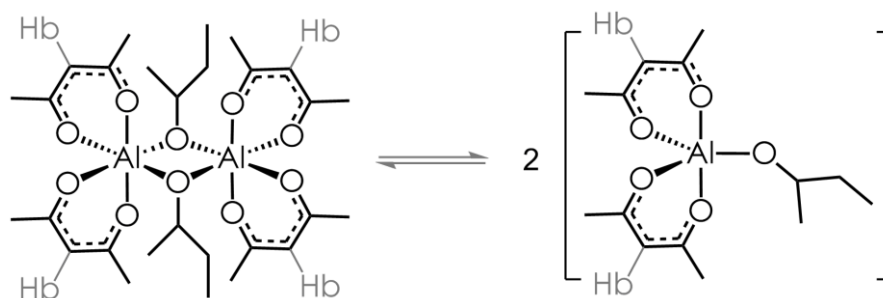
Scheme 2.4-2 – Possible interconversion of aluminium dimers into two aluminium monomers

This mirrors the observations of the methyl group signals of the β-diketonate ligand (H_a) which also displays two separate signals at room temperature which coalesce into one signal on heating to 60 °C.

As the sample is cooled to - 50 °C the methine peak separates into a large number of signals, with three major signals emerging, all displaying significant movements of chemical shift. Again this effect is reflected by the methyl proton signals of the β-diketonate ligand, which also separate into a complex set of peaks. Due to the symmetry

of the aluminium dimer it seems unlikely that the peaks which emerge at - 50 °C could arise from stereochemical isomers of the complex, and must instead arise from structural isomers of the dimer, but at this time it is unclear what these structures may be.

It was unclear whether the aluminium *tris*-acetylacetonate is formed spontaneously on dissolution or if it exists as an impurity in the isolated solid. Attempts to further purify the compound by techniques other than recrystallisation were made. The air-sensitive and electronically deficient nature of the compound made column chromatographic separating methods infeasible, and so sublimation was chosen as a possible method for purification.

Several experiments were conducted to find suitable conditions to purify compound **4** by sublimation. The compound was found to melt at 172 °C under nitrogen while aluminium*tris*-acetylacetonate is known to have a melting point above 190 °C. The sublimation was performed under static vacuum at 160 °C, however it was found that the compound was thermally unstable with NMR analysis of the resulting sublimate showing several decomposition products.
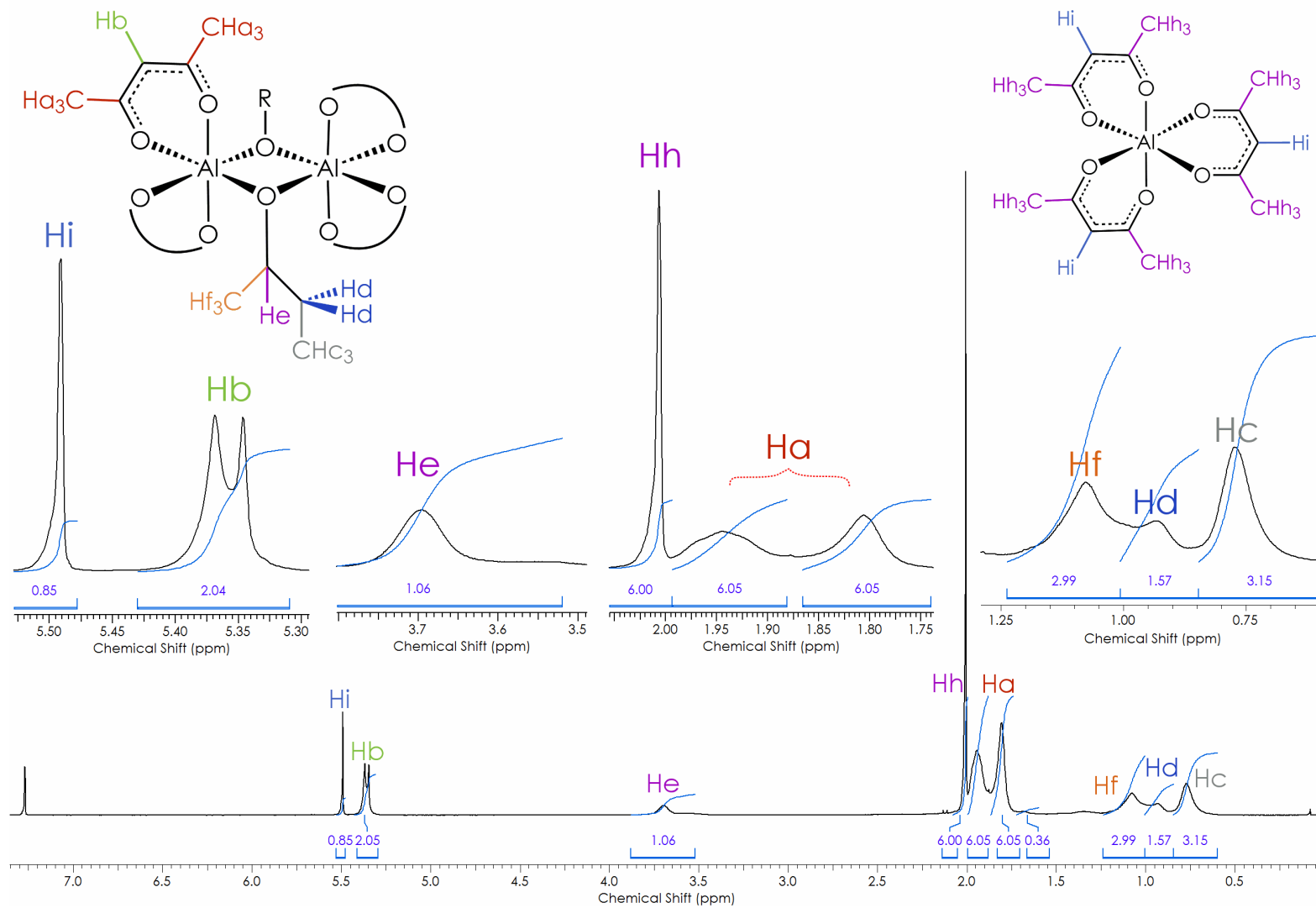
Figure 2.4-1 – Assigned ^{1}H NMR spectrum of compound 4 collected at 500 MHz, 298 K in CDCl$_3$
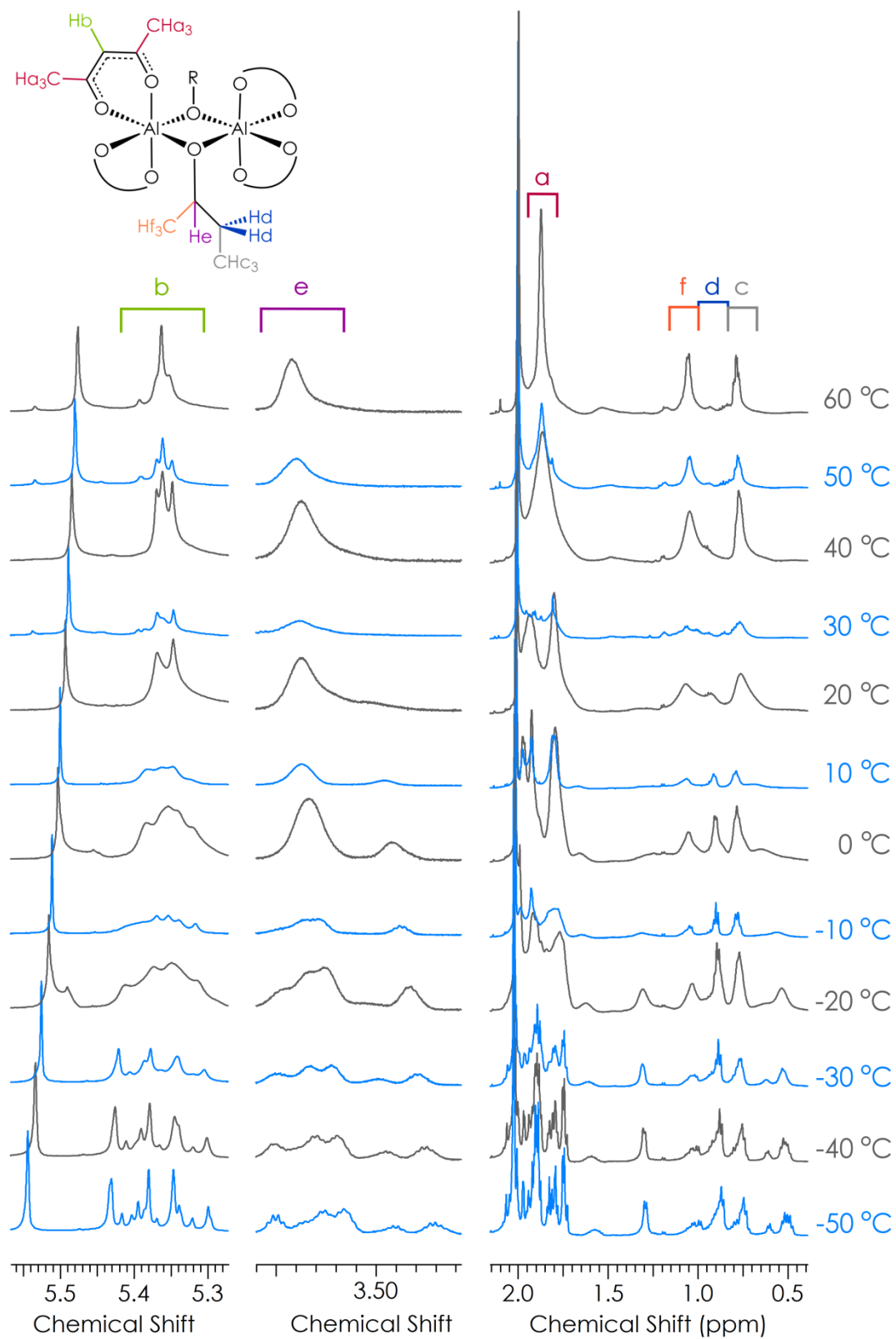
Figure 2.4-7 – Variable temperature ¹H NMR spectrum of compound 4 collected at 500 MHz in CDCl₃
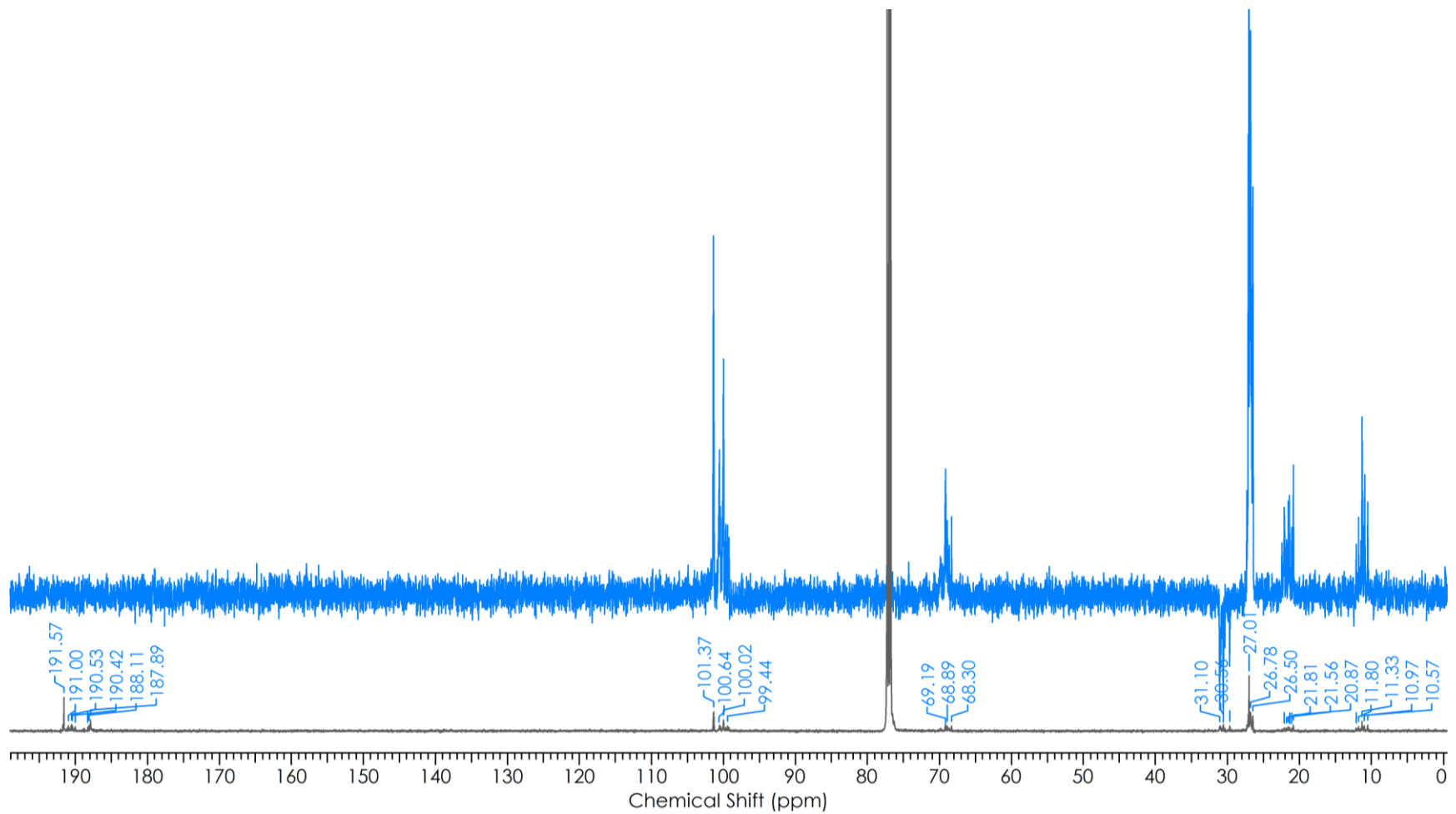
Figure 2.4-8 – ^{13}C {^1H} NMR spectrum of compound 4 (bottom) and DEPT 135 ^{13}C{^1H} spectrum (top) collected at - 50 °C in CDCl$_3$ at 125 MHz

2.4.3. Polymerisation of lactide by *bis*-(acetylacetonate)aluminium *sec*-butoxide (Compound 4)

Compound **4** was found to polymerise 400 equivalents of lactide at 150 °C in dry melt conditions in 5 minutes to yield a white polymer giving a turnover number of 1.32 molecules/s. The compound was also found to polymerise lactide in toluene at 80 °C in under one hour. Compound **4** was synthesised with aluminium *tris*-acetylacetonate as the major impurity, which is known to be inactive to ring opening polymerisation in solution, so the polymerisation activity is assumed to be as shown in Figure 2.4-9.[45]
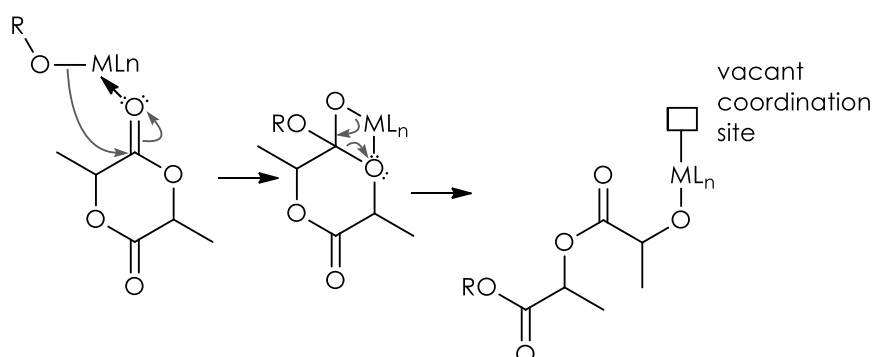
Figure 2.4-9 - Possible mechanism of polymerisation of lactide

The first step of normal polymerisation is thought to be coordination of the lactide molecule to the metal centre. The following step is an alkoxide insertion into the coordinated lactide carbonyl bond. This step allows the migratory group to be covalently bonded into the chain of the polymer, which then acts as a migratory group to insert into the next molecule of lactide.[46]

Compound **4** was added to two equivalents of lactide in $CDCl_3$ (one molecule of lactide per metal centre) and a ^1H spectrum taken at intervals over 24 hours in an attempt to study the first step of the polymerisation (Figure 2.4-10). As time elapses the broad signal at 3.70 ppm labelled He becomes more defined with a slight upfield shift as the flexible R_2HC-O proton of the sec-butoxide (labelled H_e in Figure 2.4-10) moves from an α-position to a Lewis acidic oxygen atom to a well-defined proton in an α-position to an ester. The peaks labelled Hf and Hd at 1.37 ppm and 0.88 ppm respectively also become a defined triplet and doublet confirming the original assignment, however, the final protons belonging to the sec-butoxide bridging group, Hc, does not become defined at all. Furthermore the protons Ha and Hb which belong to the acetylacetonate ligand appear to be diminishing as some intermediate structure is formed with singlet peaks at 1.89 ppm, 2.08 ppm and 5.43 ppm. During the experiment there is a slow reduction in peak height of the protons belonging to the lactide ring labelled Hi at 5.04 ppm. This change in intensity suggests that as this is the most acidic proton on the molecule it may be removed by the sec-butoxide acting as a base. If this is so an upfield shift would be expected as sec-butanol is formed and the oxygen no longer binds to the metal centre, however in this

experiment we observe the opposite occurring as the more defined protons He move downfield and become more defined.
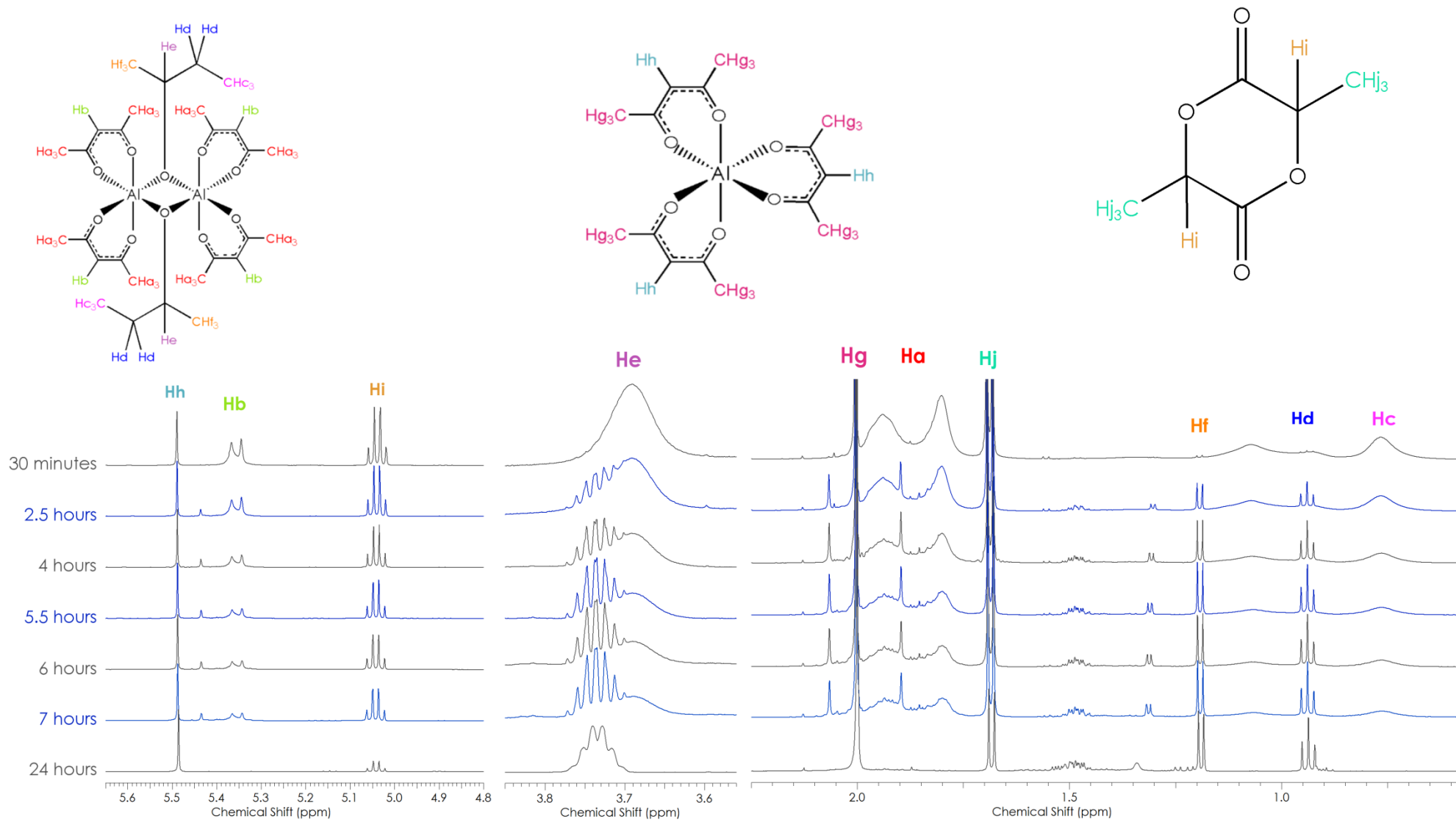
Figure 2.4-10 – ^{1}NMR spectra showing *in situ* polymerisation of lactide using compound 4 over 24 hours, collected at 500 MHz, 298 K in CDCl$_3$

2.5. Conclusion

A route to synthesis and characterisation of a very fragile novel *sec*-butoxide bridged aluminium dimer complex has been found, and structural information for a simple β-diketonate dimer has been reported for the first time. The simplicity of synthesising this catalyst *in situ* makes it an ideal candidate for industrial use, and the structural information reported will contribute to further study into the mechanism of the ring opening polymerisation of aluminium alkoxide complexes. The complex was found to have good activity as a catalyst for the ring opening polymerisation, with catalytic turnover of over one molecule per second at 150 °C yielding an industrially useful colourless polymer. This is somewhat comparable to catalysts used in industry which report turnover numbers between 5-10 molecules per second.

Some attempts to synthesise chloride-bridged aluminium dimers have been made and crude mixtures containing aluminium chloride complexes have been found to polymerise lactide. The synthetic evidence included in this chapter may be enough to put chloride-bridged dimers to use as a catalyst for polymerisation by forming the complex *in situ* if the aluminium chloride complexes are more air and water stable than the aluminium *sec*-butoxide complexes, this may prove a significant industrial advantage.

2.6. Further Work

Further work in this field should be to continue to attempt to crystallise substituted bridged aluminium *sec*-butoxide bridged β-diketonate complexes and study structure -activity relationships with the ability to polymerise and rate of polymerisation as electron withdrawing and electron donating groups are incorporated into the complex.

Further investigation into the industrial applicability of compound **4** to large scale polymerisation experiments may bring the project towards commercial viability as a replacement for toxic tin impurities in commercial beverage plastics.

2.7. Chapter 2 References

1. Casellato, U., Graziani, R., Maccarone, G., Purello, R.R. And Vidali, M. Crystal Structure Of 1-(2-Hydroxyphenyl)-3-(2-Thiomethoxyphenyl)-1,3-Propanedione, $C_{16}H_{14}O_3S$. *Journal Of Crystallographic And Spectroscopic Research*. 1987, **17**(3), pp.323-329.

2. Cicogna, F., Ingrosso, G., Lodato, F., Marchetti, F. And Zandomeneghi, M. 9-Anthroylacetone And Its Photodimer. *Tetrahedron*. 2004, **60**(51), pp.11959-11968.

3. Fan, C. And Et Al. Crystal Structure Of 1-[2-N-Butyl-5-Formyl-3-Thienyl]-2-[2-Cyano-1,5-Dimethyl-4-Pyrryl]-3,3,4,4,5,5-Hexafluoro-Cyclopent-1-Ene, $C_{21}H_{18}F_6N_2OS$. *Zeitschrift Für Kristallographie - New Crystal Structures*. 2013, **228**(2), pp.219-220.

4. Gilli, P., Bertolasi, V., Pretto, L., Ferretti, V. And Gilli, G. Covalent Versus Electrostatic Nature Of The Strong Hydrogen Bond: Discrimination Among Single, Double, And Asymmetric Single-Well Hydrogen Bonds By Variable-Temperature X-Ray Crystallographic Methods In B-Diketone Enol RAHB Systems. *Journal Of The American Chemical Society*. 2004, **126**(12), pp.3845-3855.

5. Jones, R. The Enol Form Of 1-(4-Bromophenyl)-1,3-Butanedione. *Acta Crystallographica Section B*. 1976, **32**(1), pp.301-303.

6. Keller, M., Ianchuk, M., Ladeira, S., Taillefer, M., Caminade, A.-M., Majoral, J.-P. And Ouali, A. Synthesis Of Dendritic B-Diketones And Their Application In Copper-Catalyzed Diaryl Ether Formation. *European Journal Of Inorganic Chemistry*. 2012, **2012**(5), pp.1056-1062.

7. Liu, S.-L., Zhu, J.-L. And Ouyang, T. Crystal Structure Of 1,1'-(Pyridin-2,6-Diyl)Bis-3-P-Tolylpropane-1,3-Dione, C25H21NO4. *Zeitschrift Für Kristallographie - New Crystal Structures*. 2010, **225**(4), pp.643.

8. Macrae, R.O., Pask, C.M., Burdsall, L.K., Blackburn, R.S., Rayner, C.M. And Mcgowan, P.C. The Combined Synthesis And Coloration Of Poly(Lactic Acid). *Angewandte Chemie International Edition*. 2011, **50**(1), pp.291-294.

9. Carlsson, J.O., Gorbatkin, S., Lubben, D. And Greene, J.E. Thermodynamics Of The Homogeneous And Heterogeneous Decomposition Of Trimethylaluminum, Monomethylaluminum, And Dimethylaluminumhydride: Effects Of Scavengers And Ultraviolet-Laser Photolysis. *Journal Of Vacuum Science & Technology B*. 1991, **9**(6), pp.2759-2770.

10. Vass, G., Tarczay, G., Magyarfalvi, G., Bödi, A. And Szepes, L. Hei Photoelectron Spectroscopy Of Trialkylaluminum And Dialkylaluminum Hydride Compounds And Their Oligomers. *Organometallics*. 2002, **21**(13), pp.2751-2757.

11.   Gerteis, R.L., Dickerson, R.E. And Brown, T.L. The Crystal Structure Of Lithium Aluminum Tetraethyl. *Inorganic Chemistry*. 1964, **3**(6), pp.872-875.

12.   Wengrovius, J.H., Garbauskas, M.F., Williams, E.A., Goint, R.C., Donahue, P.E. And Smith, J.F. Aluminum Alkoxide Chemistry Revisited: Synthesis, Structures, And Characterization Of Several Aluminum Alkoxide And Siloxide Complexes. *Journal Of The American Chemical Society*. 1986, **108**(5), pp.982-989.

13.   Reinheckel, H. Metal Alkoxides. Von D. C. Bradley, R. C. Mehrotra, D. P. Gaur; Academic Press, London, New York, San Francisco 1978; 411 Seiten Mit Zahlreichen Bildern Und Tabellen; *Zeitschrift Für Chemie*. 1980, **20**(10), pp.396-396.

14.   Garbauskas, M.F. And Wengrovius, J.H. Structure Of The Aluminium Alkoxide Complex [Al(O-iPr)(3,5-Heptanedione)$_2$]$_2$. *Acta Crystallographica Section C*. 1987, **43**(12), pp.2441-2442.

15.   Garbauskas, M.F., Wengrovius, J.H., Going, R.C. And Kasper, J.S. Structures Of Three Aluminium Alkoxide Complexes Having The Formula [Al(OR)$_2$(acac)]N. *Acta Crystallographica Section C*. 1984, **40**(9), pp.1536-1540.

16.   Cottone, A. And Scott, M.J. Simultaneous Coordination Of A Nucleophile With A Bifunctional Lewis Acid Assembly Incorporating A Linked Phenoxide Ligand System. *Organometallics*. 2000, **19**(25), pp.5254-5256.

17.   Zhang, D. Facile Formation Of Hexacyclic [Al$_3$O$_2$Cl] Aluminum And Alkoxide-Bridged Titanium Complexes: Reactions Of Alme$_3$ With [Ti(L)Cl$_2$] [L = 2,2'-Methylenebis(6-Tert-Butyl-4-Methylphenolato)]. *European Journal Of Inorganic Chemistry* 2007, **2007**(19), pp.3077-3082.

18.   Schwarz, A.D., Chu, Z. And Mountford, P. Sulfonamide-Supported Aluminum Catalysts For The Ring-Opening Polymerization Of Rac-Lactide. *Organometallics*. 2010, **29**(5), pp.1246-1260.

19.   Mcneese, T.J., Wreford, S.S. And Foxman, B.M. Preparation And Molecular Structure Of [Ta{H$_2$Al(OC$_2$H$_4$OMe)$_2$}(Me$_2$PC$_2$H$_4$PMe$_2$)$_2$]$_2$, A Co-Ordinatively Unsaturated Aluminohydride Adduct Of Tantalum(I). *J. Chem. Soc., Chemical Communications*. 1978, (12), pp.500-501.

20.   Janas, Z., Jerzykiewicz, L.B., Przybylak, S., Richards, R.L. And Sobota, P. Syntheses And Structural Characterization Of Vanadium And Aluminum Thiolates. *Organometallics*. 2000, **19**(21), pp.4252-4257.

21.   Kong, W.-L. And Wang, Z.-X. Dinuclear Magnesium, Zinc And Aluminum Complexes Supported By Bis(Iminopyrrolide) Ligands: Synthesis, Structures, And Catalysis Toward The Ring-Opening Polymerization Of ε-Caprolactone And Rac-Lactide. *Dalton Transactions*. 2014, **43**(24), pp.9126-9135.

22. Clegg, W., Henderson, K.W. And Rakov, I.M. Bis-[M-1-(2,4,6-Tri-Methyl-Phenyl)-Ethano-Lato-O:O]-Bis-(Di-Methyl-Aluminium). *Acta Crystallographica Section E.* 2001, **57**(9), pp.M387-M389.

23. Iwasa, N., Katao, S., Liu, J., Fujiki, M., Furukawa, Y. And Nomura, K. Notable Effect Of Fluoro Substituents In The Imino Group In Ring-Opening Polymerization Of ε-Caprolactone By Al Complexes Containing Phenoxyimine Ligands. *Organometallics.* 2009, **28**(7), pp.2179-2187.

24. Dimitrov, A., Koch, J., Troyanov, S.I. And Kemnitz, E. Aluminum Alkoxide Fluorides Involved In The Sol–Gel Synthesis Of Nanoscopic AlF$_3$. *European Journal Of Inorganic Chemistry*. 2009, **2009**(35), pp.5299-5301.

25. Obrey, S.J., Bott, S.G. And Barron, A.R. Aluminum Alkoxides As Synthons For Methylalumoxane (MAO): Product-Catalyzed Thermal Decomposition Of [Me$_2$Al(μ-OCPh$_3$)]$_2$. *Organometallics.* 2001, **20**(24), pp.5162-5170.

26. Liu, Y.-C., Ko, B.-T., Huang, B.-H. And Lin, C.-C. Reduction Of Aldehydes And Ketones Catalyzed By A Novel Aluminum Alkoxide: Mechanistic Studies Of Meerwein−Ponndorf−Verley Reaction. *Organometallics.* 2002, **21**(10), pp.2066-2069.

27. Francis, J.A., Mcmahon, C.N., Bott, S.G. And Barron, A.R. Steric Effects In Aluminum Compounds Containing Monoanionic Potentially Bidentate Ligands: Toward A Quantitative Measure Of Steric Bulk. *Organometallics.* 1999, **18**(21), pp.4399-4416.

28. Happel, O., Harms, K. And Seubert, A. Synthesis And Structural Characterization Of Two Aluminium Malate Complexes. *Zeitschrift Für Anorganische Und Allgemeine Chemie* 2007. **633**(11-12), pp.1952-1958.

29. Scientific, F. *Materials Safety Data Sheet.* 1 Ed. Fishersci.Com: Fisher Scientific, 23/07/2014.

30. Kim, Y., Jnaneshwara, G.K. And Verkade, J.G. Titanium Alkoxides As Initiators For The Controlled Polymerization Of Lactide. *Inorganic Chemistry* 2003, **42**(5), pp.1437-1447.

31. Hou, W., Chen, J., Yan, X., Shi, Z. And Sun, J. A Single Active Site Metal Center Of Neodymocene Chloride For The Ring-Opening Polymerization Of ε-Caprolactone. *Journal Of Applied Polymer Science.* 2012, **123**(2), pp.1212-1217.

32. Rennekamp, C., Wessel, H., Roesky, H.W., Müller, P., Schmidt, H.-G., Noltemeyer, M., Usón, I. And Barron, A.R. An Alternative Approach To Al2O2 Ring Systems By Unexpected Cleavage Of Stable Al−F− And Si−O− Bonds. *Inorganic Chemistry*. 1999, **38**(23), pp.5235-5240.

33. Giri Prasanth, V., Kiran, T., Gopal Aravindan, P., Iyer Sathiyanarayanan, K. And Pathak, M. Synthesis, Structural, And E-Caprolactone Polymerization Studies Of

Heteroleptic Derivatives Of Aluminum(III). *Jounal Of Coordination Chemistry*. 2015, **68**(14), pp.2480-2491.

34. P. Corden, J., Errington, W., Moore, P. And G. H. Wallbridge, M. Stereochemical Control Of *Cis-* And *Trans*-TiCl$_2$ Groups In Six-Coordinate Complexes [(L)TiCl$_2$] (L2- = N$_2$O$_2$-Donor Schiff Base) And Reactions With Trimethylaluminium To Form Cationic Aluminium Species. *Chemical Communications* 1999, (4), pp.323-324.

35. Karpiniec, S.S., Mcguinness, D.S., Gardiner, M.G., Yates, B.F. And Patel, J. Revisiting The Aufbau Reaction With Acetylene: Further Insights From Experiment And Theory. *Organometallics*. 2011, **30**(6), pp.1569-1576.

36. Giesbrecht, G. R., Gordon, J. C., Brady, J. T., Clark, D. L., Keogh, D.W., Michalczyk, R., Scott, B. L. And Watkin, J. G. Interactions Of Remote Alkyl Groups With Lanthanide Metal Centers: Synthesis, Characterization And Ligand Redistribution Reactions Of Heterobimetallic Species Containing Trialkylaluminum Fragments. *European Journal Of Inorganic Chemistry* 2002, **2002**(3), pp.723-731.

37. Benn, R., Janssen, E., Lehmkuhl, H., Rufińska, A., Angermund, K., Betz, P., Goddard, R. And Krüger, C. Drei- Oder Vierfach-Koordination Des Aluminiums In Alkylaluminiumphenoxiden Und Deren Unterscheidung Durch ^{27}Al-NMR-Spektroskopie. *Journal Of Organometallic Chemistry*. 1991, **411**(1–2), pp.37-55.

38. Hormnirun, P., Marshall, E.L., Gibson, V.C., White, A.J.P. And Williams, D.J. Remarkable Stereocontrol In The Polymerization Of Racemic Lactide Using Aluminum Initiators Supported By Tetradentate Aminophenoxide Ligands. *Journal Of The American Chemical Society*. 2004, **126**(9), pp.2688-2689.

39. Liu, Y.C., Ko, B.T. And Lin, C.C. A Highly Efficient Catalyst For The "Living" And "Immortal" Polymerization Of ε-Caprolactone And L-Lactide. *Macromolecules*. 2001, **34**(18), pp.6196-6201.

40. Ewing, F.J. The Crystal Structure Of Diaspore. *The Journal Of Chemical Physics*. 1935, **3**(4), pp.203-207.

41. Pauling, L. *The Nature Of The Chemical Bond And The Structure Of Molecules And Crystals: An Introduction To Modern Structural Chemistry*. 3rd Edition Ed. Cornell University: Cornell University Press; 3 Edition (January 31, 1960), 1960.

42. Rowland, R.S. And Taylor, R. Intermolecular Nonbonded Contact Distances In Organic Crystal Structures: Comparison With Distances Expected From Van Der Waals Radii. *The Journal Of Physical Chemistry*. 1996, **100**(18), pp.7384-7391.

43. Bonamico, M. And Dessy, G. The Crystal Structure Of Aluminosiloxanes: X-Ray Analysis Of A Compound Of Formula C$_8$H$_{24}$Al$_3$Br$_5$O$_6$Si$_4$. *Journal Of The Chemical Society A: Inorganic, Physical, Theoretical*. 1968, (0), pp.291-297.

44. Benn, R., Rufińska, A., Lehmkuhl, H., Janssen, E. And Krüger, C. 27Al-NMR Spectroscopy: A Probe For Three-, Four-, Five-, And Sixfold Coordinated Al Atoms In Organoaluminum Compounds. *Angewandte Chemie International Edition In English.* 1983, **22**(10), pp.779-780.

45. Stephen, R., Sunoj, R.B. And Ghosh, P. 2011. A Computational Insight Into A Metal Mediated Pathway For The Ring-Opening Polymerization (ROP) Of Lactides By An Ionic {(NHC)$_2$Ag}+X- (X = Halide) Type N-Heterocyclic Carbene (NHC) Complex. *Dalton Transactions.* **40**(39), pp.10156-10161.

46. Routaray, A., Nath, N., Maharana, T. and Sutar, A.K. 2015. Ring-Opening Polymerization Of Lactide By Aluminium Catalyst. *Catalysis Science & Technology.*

47. Bourissou, D., Martin-Vaca, B., Dumitrescu, A., Graullier, M. and Lacombe, F. 2005. Controlled Cationic Polymerization Of Lactide. *Macromolecules.* **38**(24), pp.9993-9998.

3. TITANIUM CHLORIDE COMPLEXES FOR POLYMERISATION OF LACTIDE

3.1. Titanium chloride complexes as anti-cancer drugs

Previous work in the McGowan group by Dr. James Mannion, Dr Andrew Hebden and Dr. Benjamin Crossley have reported the anti-cancer activity of Budotitane derivatives featuring monodentate halide ligands.[1-3] The general preparation is detailed in Scheme 3.1. Compounds with a *cis*-chloride or *cis*-bromide motif were found to be cytotoxic with some IC_{50} values comparable to those of *cis*-platin, and most within an order of magnitude on the A2780 ovarian carcinoma and MCF-7 breast cancer cell lines.
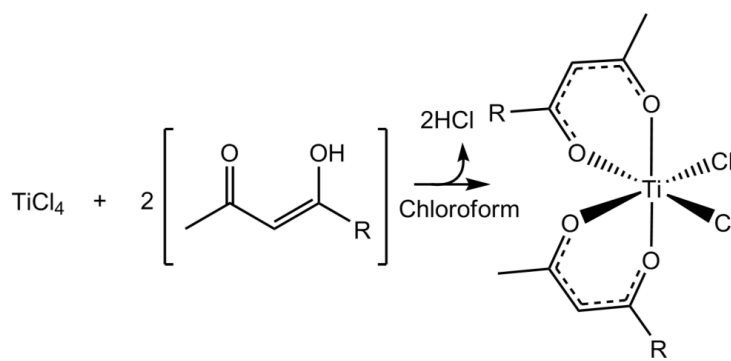
Scheme 3.1- General preparation of titanium halide complexes

It is well known that titanium is able to act as a catalyst for the ring opening polymerisation of lactide with titanatranes,[4] titanium alkoxide complexes[5-7] titanium oxide clusters[8] and amidotitanium[9] complexes all reported to be active. Titanium has also been used in conjunction with other metals in bimetallic complexes and on its own to polymerise lactide.[10] Usually, when titanium complexes are used for this purpose an alkoxide group is included in the complex, or an alcohol initiator is used to add an alkoxide group to the complex.[11, 12] A small number of examples of titanium chloride complexes have been found to polymerise lactide without initiator.[5, 13, 14] The mechanism for the ring opening polymerisation of lactide is not yet well characterised, but is assumed to proceed by a coordination-insertion mechanism in which the lactide first coordinates, then a labile group inserts into the ester C-O bond, causing the lactide ring to open and the addition of the labile group into the chain of the polymer (Figure 3.1-1).
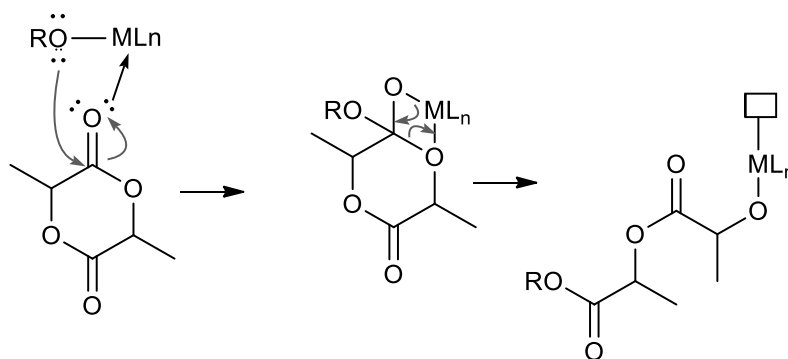
Figure 3.1-1 – Proposed mechanism of the ring opening polymerisation of lactide

The anti-cancer active titanium chloride complexes were synthesised and tested for ability to polymerise lactide. Attempts were made to assess whether the titanium species retains anti-cancer ability after the polymerisation and kinetic information about the rate of polymerisation was also collected.

3.1.1. In solution polymerisations

Polymerisations were conducted using three titanium chloride complexes previously synthesised by Dr James Mannion.[3] These complexes were chosen as they have structures well defined by the McGowan group with crystal structures of all three having been collected. The steric bulk of the ligand increases in the order **1** < **2** < **3** and also has electron withdrawing properties increasing in the same order.
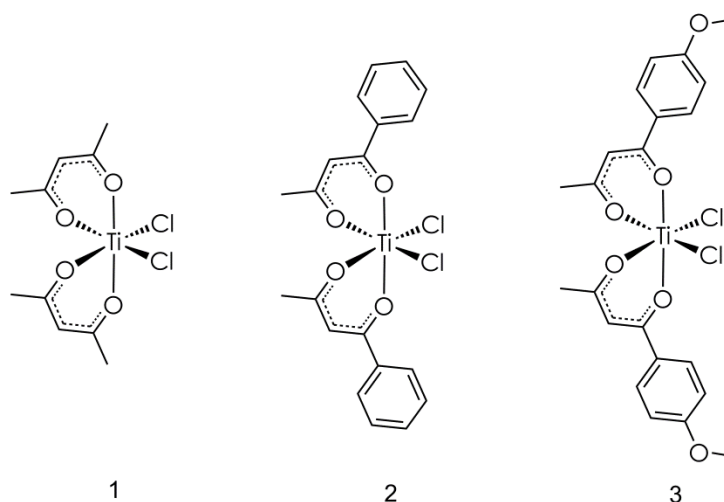
Figure 3.1-2– Titanium chloride complexes investigated for polymerisation of lactide

Bis-acetylacetonate titanium(IV) chloride complexes were synthesised by the slow addition of two equivalents of the relevant acetylacetone to titanium(IV)chloride with vigorous stirring in chloroform. After 16 hours a red precipitate was formed and the solvent removed by filtration. The red solid was dried *in vacuo* and purity was assessed by microanalysis.

Polymerisations in solution were investigated using Schlenk line techniques in dry toluene. Solutions of **1**, **2** and **3** with 200 equivalents of *rac*-lactide were heated at 70 °C and refluxed at 110 °C with vigorous stirring in all cases. The solutions were precipitated in ice after 24 hours, reduced *in vacuo* and the resulting pink solids were found to be unchanged from initial mixtures of catalyst and lactide by ^{1}H NMR spectroscopy. This suggests that titanium (IV) chloride complexes are inactive catalysts for the ring opening polymerisation of lactide in solution, or at low temperatures.

3.1.2. Dry Melt Polymerisations

A preliminary study was conducted by preparing mixtures of titanium complexes **1, 2** or **3** and *rac*-lactide in a ratio of 1:200 respectively under anhydrous glove box conditions. The flask was closed with a suba seal, and release of expanding gas was allowed through a pin hole in the seal. The body of the flask was submerged in oil and heated to 150 °C while stirring for 2 days. As the polymerisation was found not to proceed in solution there was no need for addition of a specific quenching agent before analysing the polymers in $CDCl_3$. If any residual active species were present they would be quenched by exposing the plastic to air and with addition of wet deuterated chloroform. The degree of polymerisation was measured by integration of ^{1}H NMR signals of the ester proton of the lactide molecule against the downshifted ester proton of the poly(lactic acid) chain. The spectra of poly(L-lactic acid) or poly(D-lactic acid) are fairly simple with only one polymer environment. As the enantiomeric environment becomes more complicated so does the NMR spectrum.[15]
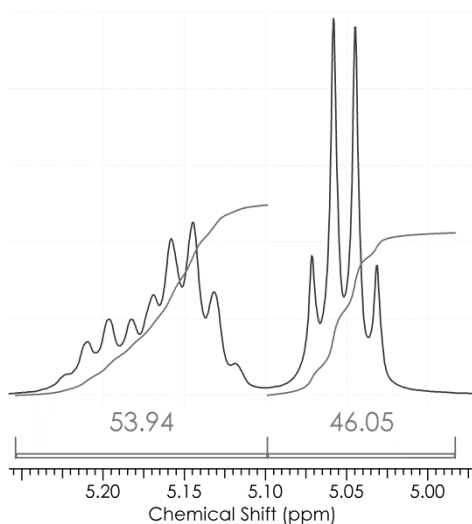
Figure 3.1-3 – Example integration of unreacted lactide quartet (right) against polymer chain signals (left)

Compounds **1, 2** and **3** were found to polymerise *rac*-lactide under dry melt conditions (200 eq lactide, 150 °C, N_2 atmosphere, 2 days) giving poly(lactic acid) with varying degrees of conversion to polymers (**1** = 80% conversion **2** = 54% conversion, **3** = 14% conversion). In all three cases the polymer mixture was brown in colour.

This data correlates as expected with the ring opening mechanism described in Figure 3.1-1. The first step of the polymerisation involves the coordination of lactide to the metal centre. The more electron donating the β-diketonate ligand on the catalyst the slower this preliminary step and each additional coordination of lactide will be afterwards. The order of degree of electron withdrawing of the ligand from the metal is **1** > **2** > **3** which correlates with the conversions, the largest conversion observed when compound **1** is used as a catalyst and smaller observed conversions when a more withdrawing methoxy substituted catalyst is used.
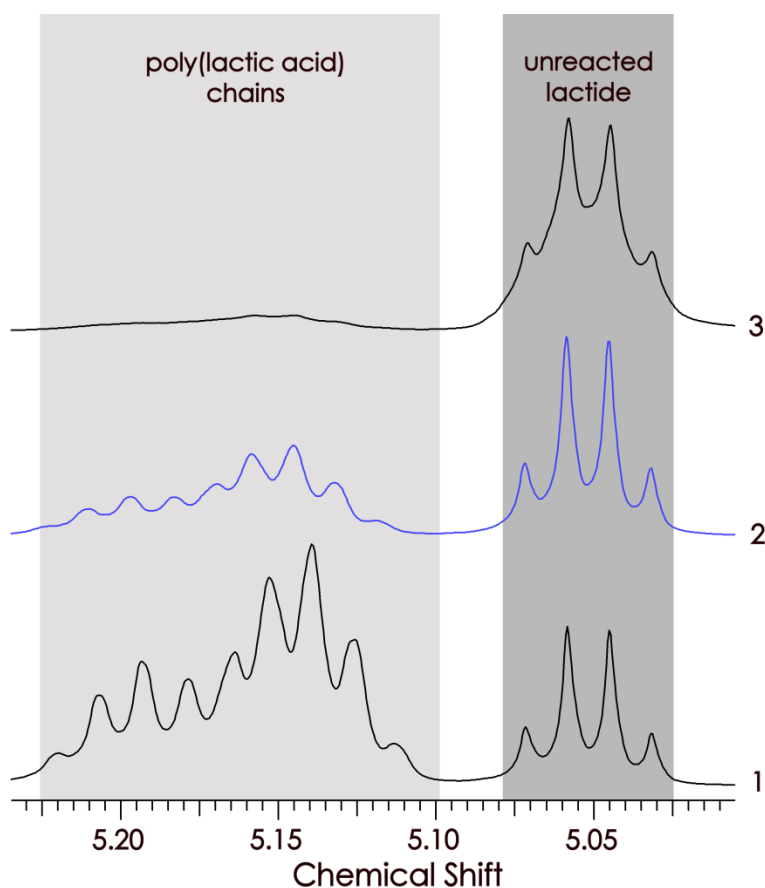
Figure 3.1-4 – ^{1}H NMR spectrum of resulting polymer/lactide mixture after stirring at 150 °C for two days.

It could be argued that the larger the electronic withdrawal to the metal centre, the more likely a C=O lone pair of the lactide will form a dative coordination to the metal centre, and so more likely the monodentate ligand is to insert into the π* of the C=O of a coordinated lactide molecule. If this is the case this data may provide some argument to the idea that the coordination of the lactide to the metal centre is the rate determining step of the polymerisation. A variation of the catalyst loading may offer additional insight into the mechanism.

Several studies probing the mechanism of the polymerisation were undertaken. Compound **2** was reacted with 3, 5, 10 and 200 equivalents of *rac*-lactide under anhydrous conditions. The mixtures were stirred at 150 °C for 2 days under partial vacuum. Sublimed lactide was returned to the reaction mixture by heating the body of the flask periodically. Mass spectrometry was utilised to analyse the polymers. The mass spectra of all of the polymerisations followed the expected pattern

of peaks separated by a gap of 72 gmol^{-1}, corresponding to a single repeating lactic acid unit. (Figure 3.1-5)

In an attempt to identify whether the ligand itself is acting as an initiating group for the ring opening reaction or the chloride, the mass spectra were studied in detail to identify chains of poly(lactic acid) with an additional chloride atom.

Table 3.1-1 and Table 3.1-2 show assignments of the major peaks of the mass spectra of the mixtures of 3 and 10 equivalents of lactide to catalyst respectively. Solutions of polymer in dry chloroform were compared against sodium formate calibrant. The sample was subjected to electrospray ionisation. Each peak found was matched to the closest possible ion or adduct found by calculation of all possible values of $Ti_n(C_3H_4O_2)_mCl_x(C_{10}H_9O_2)_y+Na_z$ up to the detection limit of the instrument, 2000 gmol^{-1}. Phenylacetonate has been shortened to (L) for clarity. Each spectrum shows some evidence of chloride inclusion into a lactide chain (peaks **9**, **17**, **25** and **27**) however there is as much evidence for inclusion of the ligand into the chain before ionisation (peaks **10, 18, 22** and **26**). As the polymer/catalyst mixture is fairly complex the spectrum features many overlapping peaks, making isotopic matching more difficult, however some examples of short oligomers of lactic acid with possible acylchloride terminals were found with matching isotopic patterns, showing there was at least some initiation by the chloride moieties. Figure 3.1-6 shows one such isolated peak representing 5 repeating units of lactic acid, with an additional chloride atom. The observed peak has excellent correlation with the predicted isotopic abundances and may be the acylchloride species the mechanism predicts. However, as always with mass spectrometry, it is possible that the observed species is simply an ionisation product formed in the instrument. Further evidence was sought using NMR spectroscopy.
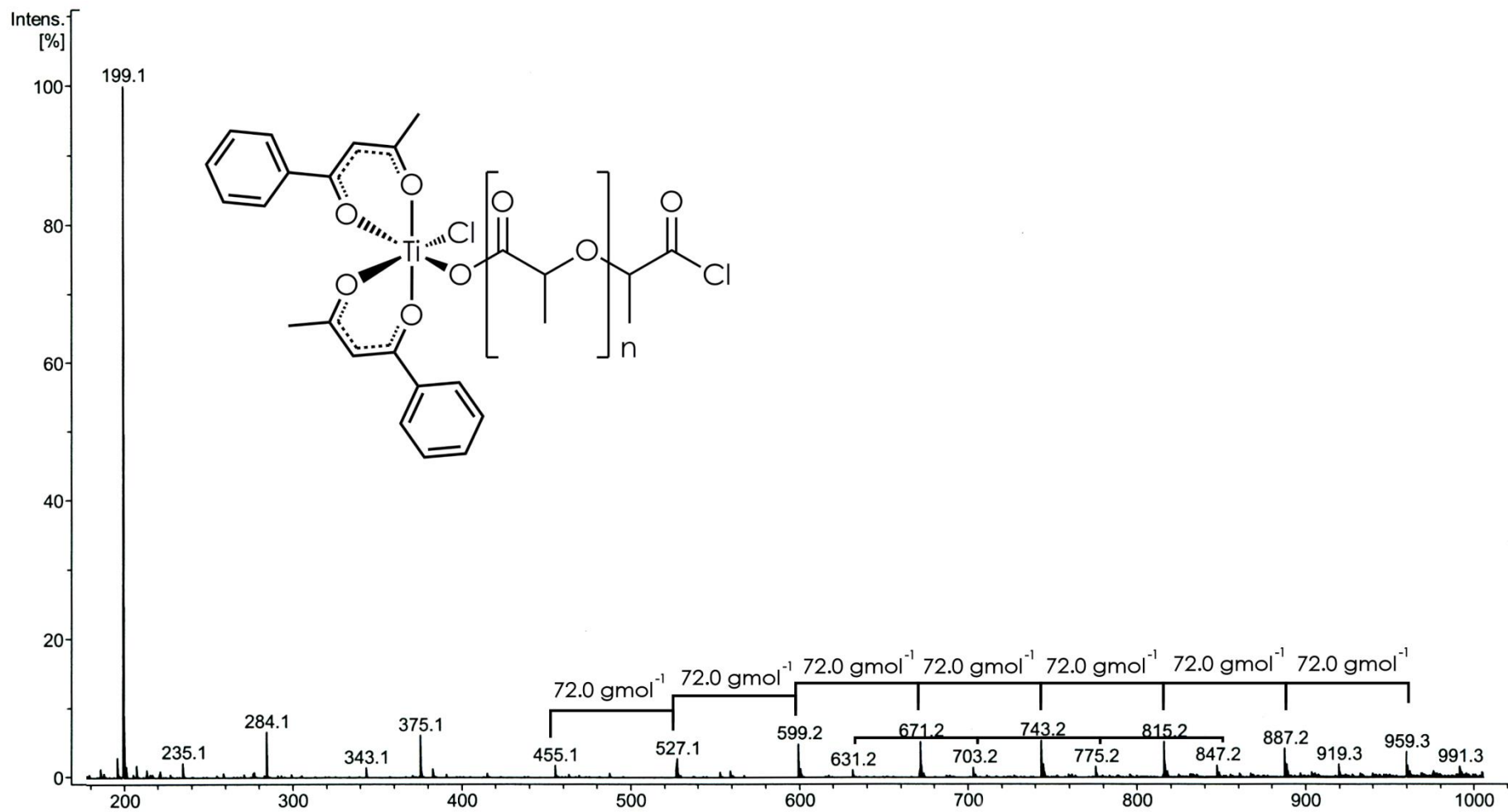
Figure 3.1-1 – Mass spectrum of polymer mixture of compound 2 with 200 equivalents of *rac*-lactide.
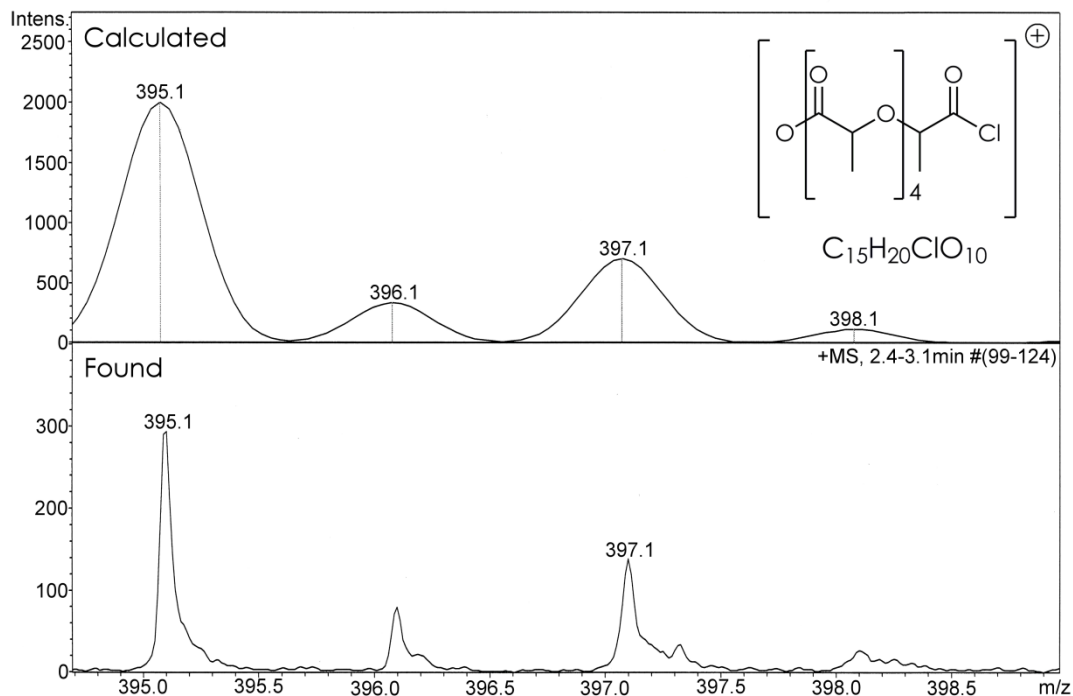
Figure 3.1-6 – Isotopic pattern calculated (top) and found (bottom) for a fragment of poly(lactic acid) chain containing a chlorine atom.

Peak number	m/z	Assignment	Chemical Formula
1	429.1	0.5(lactide)Cl(L)$_2$	C$_{23}$H$_{22}$O$_6$Cl
2	483.1	1.5(lactide)Ti(L) + Na	C$_{19}$H$_{21}$O$_8$TiClNa
3	511.2	0.5(lactide) Ti(L)$_2$Cl$_2$ – H	C$_{23}$H$_{23}$O$_6$TiCl$_2$
4	527.1	3.5(lactide) + Na	C$_{21}$H$_{28}$O$_{14}$Na
5	589.2	2(lactide)TiCl$_2$(L) + Na	C$_{22}$H$_{24}$O$_{10}$TiCl$_2$Na
6	684.4	2.5(lactide)TiCl$_2$(L) + 2Na	C$_{25}$H$_{29}$O$_{12}$TiCl$_2$Na$_2$
7	701.2	3.5(lactide)Cl (L)	C$_{31}$H$_{37}$O$_{16}$Cl
8	815.2	5.5(lactide)Na	C$_{33}$H$_{44}$O$_{22}$Na
9	971.3	6.5(lactide)Cl	C$_{39}$H$_{52}$O$_{26}$Cl
10	999.3	5.5(lactide)(L) + 2Na	C$_{43}$H$_{53}$O$_{24}$Na$_2$

Table 3.1-1 – Major peaks from the mass spectrum of dry melt of 3 equivalents of lactide with 1 equivalent of compound 2. (L) = phenylacetylacetonate

Peak number	m/z	Assignment	Chemical Formula
11	327.1	0.5(lactide) Ti (L) + 2Na	$C_{13}H_{13}O_4TiNa_2$
12	387.1	1(lactide) Cl (L) + 2Na +H	$C_{16}H_{18}O_6ClNa_2$
13	429.1	0.5(lactide) Cl (L)$_2$	$C_{23}H_{22}O_6Cl$
14	483.1	1.5(lactide) Ti Cl (L) + Na	$C_{19}H_{21}O_8TiClNa$
15	511.2	0.5(lactide) Ti Cl$_2$ (L)$_2$ -H	$C_{23}H_{21}O_6TiCl_2$
16	527.1	3.5(lactide) +Na	$C_{21}H_{28}O_{14}Na$
17	611.1	4(lactide) Cl	$C_{24}H_{32}O_{16}Cl$
18	689.2	3.5(lactide) (L) +Na +H	$C_{31}H_{38}O_{16}Na$
19	795.1	3.5(lactide) Ti Cl (L) + 2Na + H	$C_{34}H_{38}O_{16}TiClNa_2$
20	815.2	5.5(lactide) + Na	$C_{33}H_{44}O_{22}Na$
21	897.2	3.5(lactide) Ti (L)$_2$ + Na	$C_{41}H_{46}O_{18}TiNa$
22	999.3	5.5(lactide) (L) + 2Na	$C_{43}H_{33}O_{24}Na_2$
23	1091.6	7(lactide) Ti Cl	$C_{42}H_{56}O_{28}TiCl$
24	1181.2	6.5(lactide) Ti Cl (L) + H	$C_{49}H_{62}O_{28}TiCl$
25	1283.3	8.5(lactide) Cl + Na + H	$C_{51}H_{69}O_{34}ClNa$
26	1353.4	7(lactide) (L)$_2$ Na	$C_{62}H_{74}O_{32}Na$
27	1449.7	9.5(lactide) Cl + 2Na	$C_{57}H_{76}O_{38}ClNa_2$

Table 3.1-2 - Major peaks from the mass spectrum of dry melt of 10 equivalents of lactide with 1 equivalent of compound 2. (L) = phenylacetylacetonate

3.2. NMR Spectroscopy For Polymer Analysis

Several papers on the proton NMR environments of polymers of lactide are available in the literature.[16-23] The two chemical environments in L-lactide are identical to those in D-lactide; upfield, around 1.68 ppm, there is a doublet arising from methyl protons in β arrangement with a carbonyl group. Downfield there is a quartet at 5.05 ppm arising from a methine proton in the α arrangement to the ester carbonyl. On polymerisation the methyl protons shift upfield around 0.11 ppm, while the α proton shifts downfield around 0.12ppm. However, the spectra of the polymer formed by these catalysts are more complex.

As the polymerisation of *rac*-lactide proceeds in the presence of catalyst it is assumed to be equally likely that a D-lactide molecule or L-lactide will complex to the catalyst and join into a polymer chain. As each monomer is added it can be described as being either isotactic with the last molecule, i.e. having the same stereochemistry, or as syndiotactic with the last monomer, i.e. having opposite stereochemistry. An isotactic diad of lactic

acid repeating units could be –RR- or –SS-, both of which would be expected to have equivalent signals by NMR spectroscopy (Figure 3.2-1).
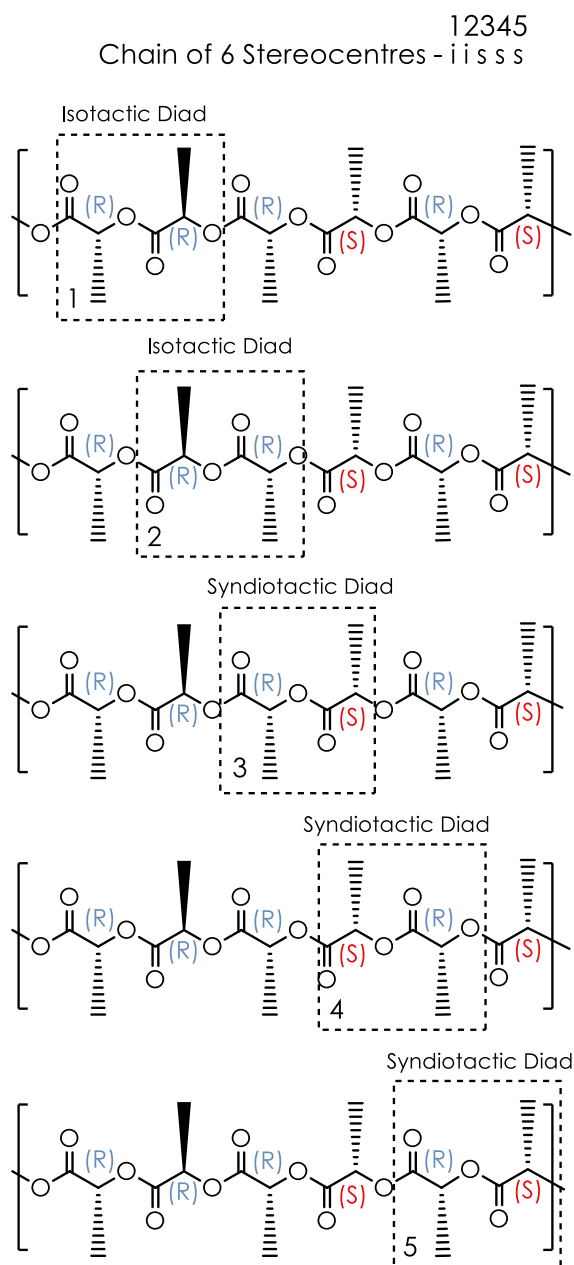
Figure 3.2-1 – Figure showing the isotactic and syndiotactic naming system for a hexad of lactic acid repeating units. Note that 'iisss' would also give describe a hexaad with where the sequence of configuration of chiral centres is "S,S,S,R,S,R"

A syndiotactic diad would have configurations of either –RS- or –SR-, again these would be expected to be equivalent in the ^{1}H NMR spectra. A diad of lactic acid units with opposite chirality can therefore be described simply as 's', and two acid units with the same arrangement would be described as 'i'.

Chains of units can be denoted by describing each one as 'i' or 's' to the one preceding, for example a chain containing perfectly alternating –RSRSRS- stereocentres would be described as having each stereocentre in the opposite configuration to the last, the first

pair (-*RS*-) is syndiotactic, the pair starting on the second stereocentre (-*SR*-) is syndiotactic. So the –RSRSRS- hexad could be described as sssss. All five diads in syndiotactic arrangements. More stereoirregular chains can also be described. -*RSRR*- can be described as ssi, and -*RRRSRS*- would be described as iisss (Figure 3.2-1).

Each set of unique chiral tetrads and hexads of the lactic acid repeating unit are distinguishable, having unique chemical shifts in both ^{1}H and ^{13}C spectra due to having different magnetic environments. This nomenclature of the lactic acid chain allows us to assign peaks to chiral environments, regardless of whether the chiral environment is left handed or right handed. While ssi represents the -*RSRR*- string mentioned earlier, it also represents the chemically and magnetically identical tetrad –*SRSS*-.

However there has been discussion in the literature about which chemical shifts represent which stereochemical assignment. Preliminarily Kriechldorf *et al.* performed Bernoullian statistical analyses of the outcomes of polymerisations of *meso*-lactide and *rac*-lactide and correlated integrations from homonuclear decoupled experiments to assign the peaks to the relevant tetrads to each peak.[19] Later Chisholm *et al.* performed HETCOR experiments to correlate ^{13}C signals to their corresponding ^{1}H signals. The Chisholm group found a correlation between ^{1}H signals suggested to arise from reported sis tetramers (-*RSSR*-, or –*SRRS*-) and ^{13}C signals for iss/ssi configurations of lactic acid units, suggesting that one of these assignments was incorrect, prompting the group to propose a new assignment of the peaks.[23] Further discussion from Thakur *et al.* suggested that the chemical shift differentiation between chiral tetrads arises asymmetrically; i.e. two stereo units in one direction and only one unit in the other, and that the direction of asymmetry in the case of ^{13}C NMR and ^{1}H NMR spectroscopy were opposite, leading to confusion from the HETCOR experiments. Most recently Kasperczyk conducted high resolution HETCOR experiments and agreed with the original assignments reported by Kriechldorf.[24]

In the case of polymers of *rac*-lactide stereocentres can only join in pairs with chain configurations following a pattern of –*RRRR*- or –*RRSS*- and their opposites. It is, therefore, impossible for an ss triad to appear as this would represent a fragment such as –*RSR*- or –*SRS*-. It is possible for one of the stereocentres to undergo nucleophilic attack and be inverted during the reaction, or undergo transesterification reactions, but this effect is expected to be rare and not observed in these spectra as the titanium atoms act as lewis acids, preventing formation of large concentrations of free nucleophiles.
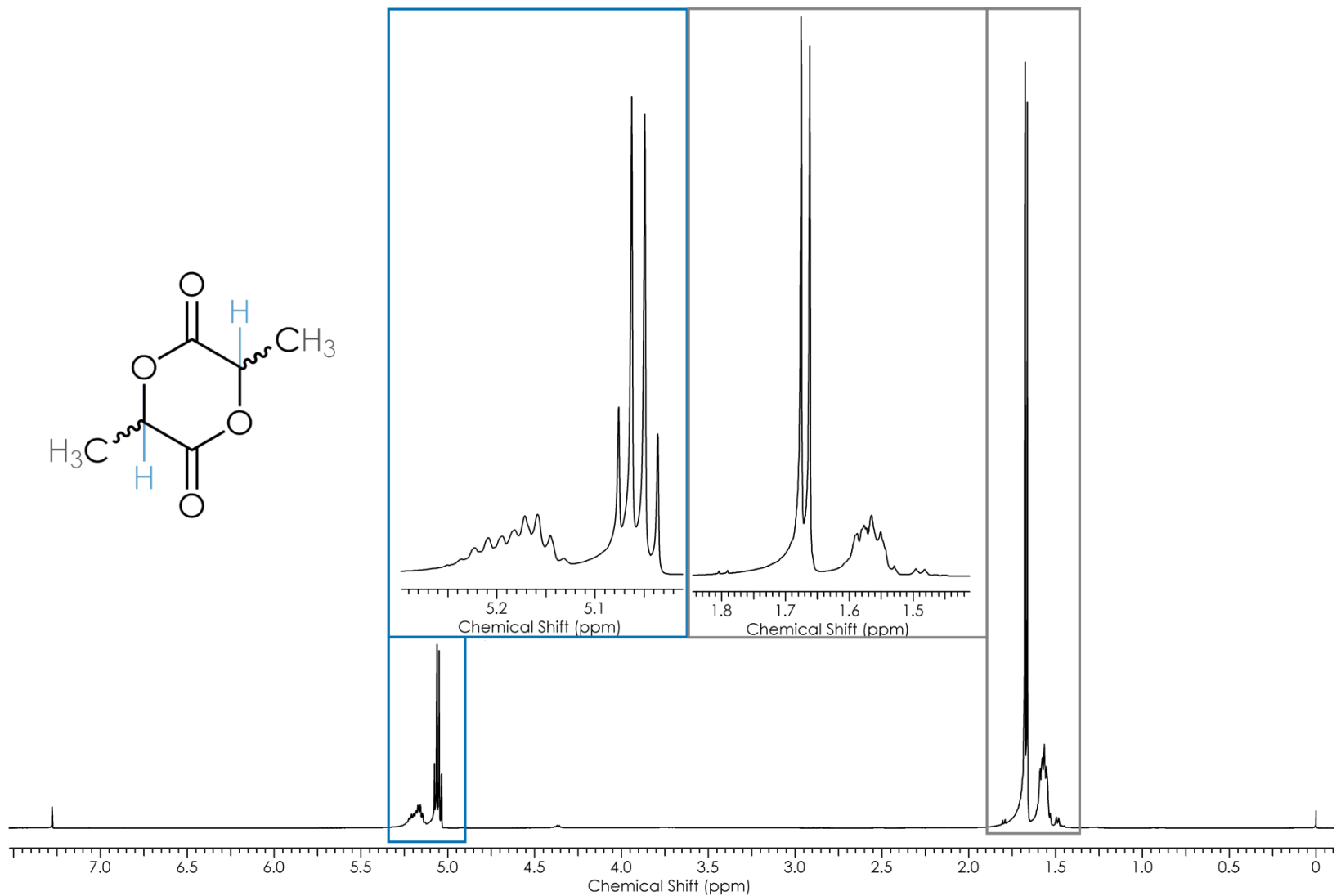
Figure 3.2-1 – ¹H spectrum of reaction mixture of dry melt of 200 equivalents of lactide with 1 equivalent of compound 2 collected at 298 K at 500 MHz in CDCl₃

Figure 3.2-2 shows the ^{1}H NMR spectrum of the resulting polymer from mixture of compound **2** and 200 equivalents of *rac*-lactide in CDCl$_3$. The major peaks in this spectrum are well defined, belonging to unreacted lactide at 5.05 ppm and 1.68 ppm. The multiplet at 5.16 ppm arises from the stereoisomers of the polymer chain. At least two overlapping quartets can be observed, one at 5.16 ppm and the other at 5.20 ppm. Neither peak is well defined with additional peaks appearing on the left and right of the multiplet, suggesting several overlapping peaks.

Similarly the expected doublet at 1.58ppm representing the poly(lactic acid) shows at least two overlapping doublet signals with smaller signals at 1.49 ppm and 1.54 ppm.

The chemical shifts of each of the peaks of the polymer in the spectrum are obscured by the splitting patterns of the proton peaks. A much clearer picture of the stereochemical environments of the polymer can be obtained using decoupled spectra. Figure 3.2-3 shows a 14,000 scan [13]C{[1]H} spectrum of the resulting bulk polymers of mixture of 200 equivalents of lactide with one equivalent of compound **2**, with the peaks labelled 'd', arising from the carbon next to the ester carbonyl, which is typically used to deduce whether the polymer is atactic as expected and whether the catalyst is capable of distinguishing between specific diastereomers of lactide as they are included. Figure 3.2-4 shows the expected shift and approximate areas of the two possible carbon environments of polymers of *rac*-lactide, assuming random incorporation of diastereomers of lactide to the polymer chain as described by Kasperczyk.[24] The major peaks of the ^{13}C{^{1}H} NMR spectra show good agreement with the predicted spectra, with both major peaks at the correct chemical shift. The peak height ratio of the calculated spectrum is 1:3 for isi:iii peaks. In the real spectrum the peak areas have a ratio of 1:2.5, which given the noise in the signal, as well as the nuclear Overhauser enhancement used in the process of acquiring decoupled spectra, is close enough to say that the catalyst has no diastereo preference as expected.

Figure 3.2-4 also shows a comparison between the calculated ^{1}H NMR spectrum and the experimental spectrum. The pattern of having a larger area in the upfield isis, isii, iii and siii signal region of the polymer quartet around 5.16 ppm and areas of expected lower signal around 5.20 ppm representing iiis, iisi and sisi tetrads is observed in the ^{1}H NMR spectrum, however the signal overlap does not allow us to take meaningful measurements of the comparative size ratios of those signals.
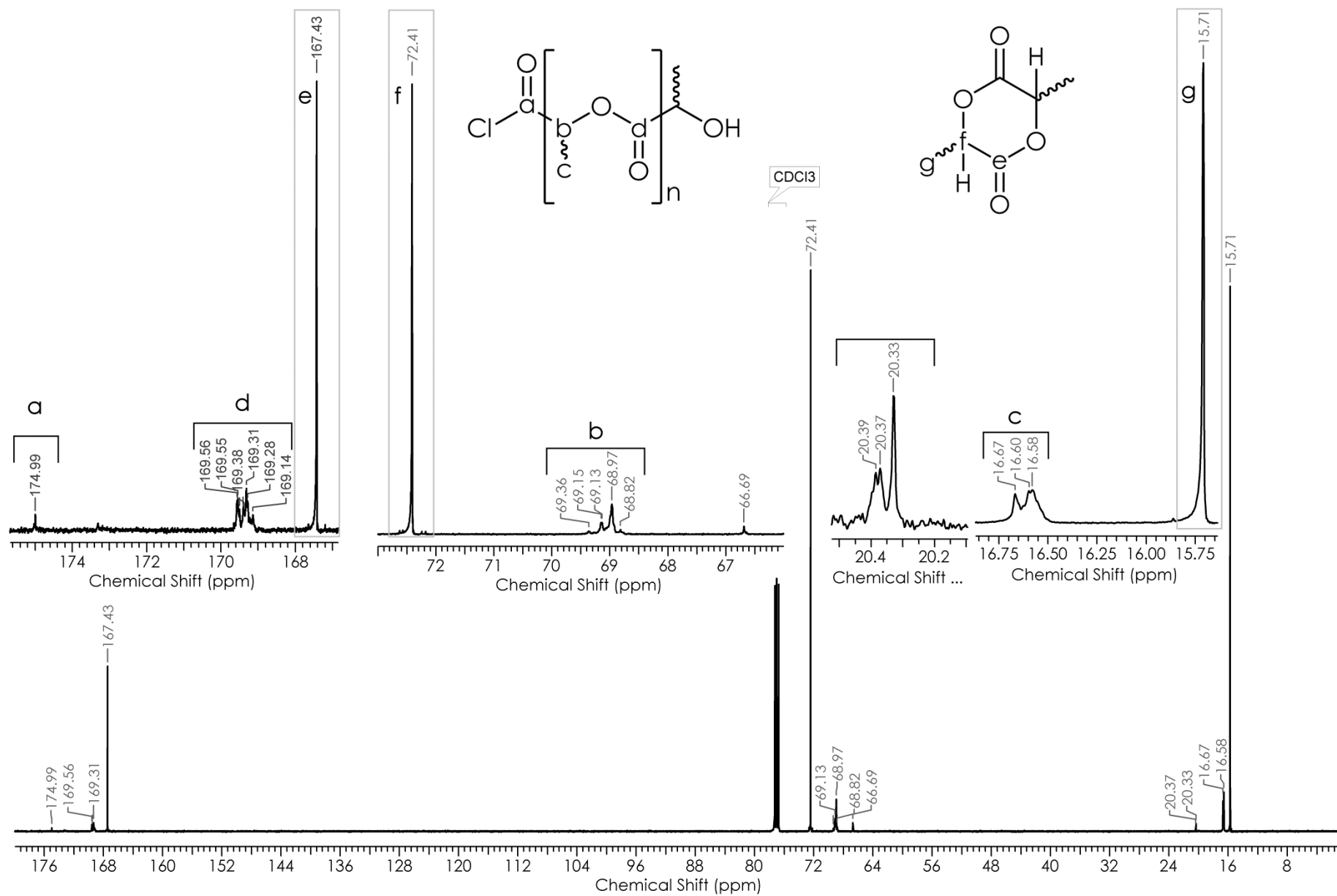
Figure 3.2-2 – $^{13}C\{^1H\}$ spectrum of reaction mixture of 48 hour dry melt of 200 equivalents of lactide with 1 equivalent of compound 2.
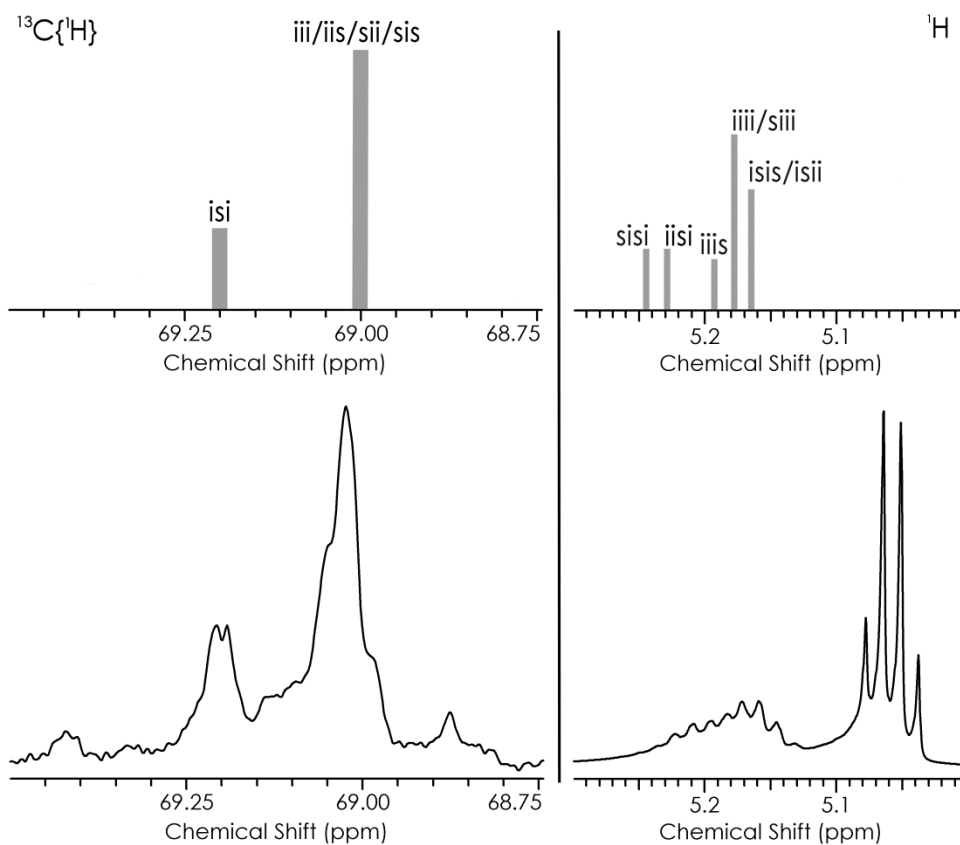
Figure 3.2-4 – Expected chemical shifts of poly(*rac*-lactic acid) tetramers and pentamers (top) with observed peaks (bottom)[24]

A ^{13}C DEPT 135 experiment shows the signals a, d, e and f to belong to quaternary carbon atoms, and agreement with the literature led to the assignments of the peaks given in Figure 3.2-3.[17, 19, 23, 24]
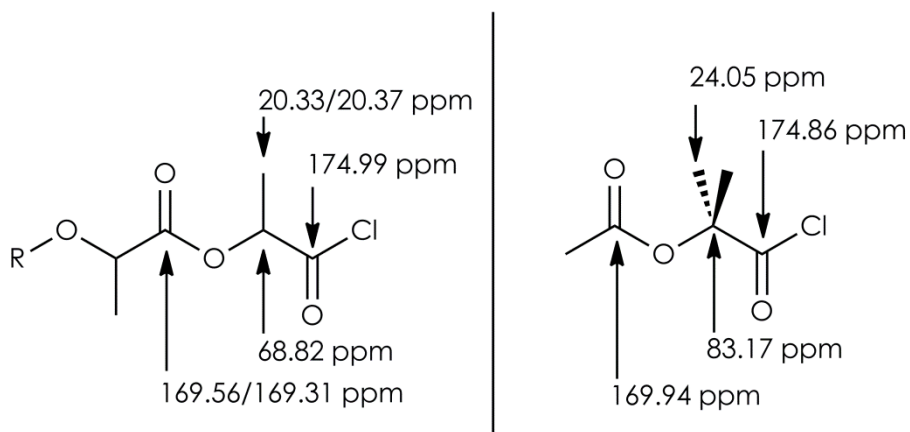
Figure 3.2-5 – Comparison of the observed signals to 1-chloro-2-methyl-1-oxopropan-2-yl acetate[25]

Further analysis of the $^{13}C\{^1H\}$ NMR spectrum shows evidence of an acylchloride group outside of the vigorous conditions of the electrospray ionising source. The peak labelled 'a' at 174.99 ppm was found to correlate very closely with the chemical shift of an analogous molecule, 1-chloro-2-methyl-1-oxopropan-2-ylacetate, reported in the literature.[26] (Figure 3.2-5)

3.3. In situ polymerisation kinetics

As the previously described bulk method introduced errors of unknown size, a new method for investigating the activity of the titanium chloride complexes was sought to eliminate removal of lactide from the polymerisation mixture by sublimation and to ensure a thoroughly anaerobic atmosphere throughout the reaction. It was decided that the samples should be prepared in a glove box to ensure environments of O_2 concentrations <5 ppm and H_2O concentrations <1ppm. Bulk samples were prepared and crushed with a pestle and mortar to ensure homogenicity. HPLC vials were prepared with approximately equal amounts of lactide/catalyst mixtures and sealed using a PTFE/rubber/aluminium crimp cap. The vials were then submerged in oil at the desired temperature with vigorous stirring to ensure continuous tumbling and, therefore, complete mixing of the mixture inside the vials. Preliminary experiments showed the degree of conversion to be much higher using this method than stoppered flasks. Control vials charged with only L-lactide and stirred using this method were found to be unchanged after stirring for 24 hours.

In situ polymerisation studies were carried out by submerging several vials at the same time and removing vials at the appropriate time. Each vial was analysed by NMR spectroscopy with wet $CDCl_3$ and percentage conversion calculated by integration of the unreacted lactide quartet against the PLA quartet. To simplify this measurement L-lactide was used as it has only one stereo environment in the NMR spectrum, that of the iii tetrad. Three separate proton acquisitions were run on each HPLC vial. A sample of compound **3** was prepared with 200.06 equivalents of L-lactide. Several sample vials were prepared and a graph of % conversion against time was plotted.
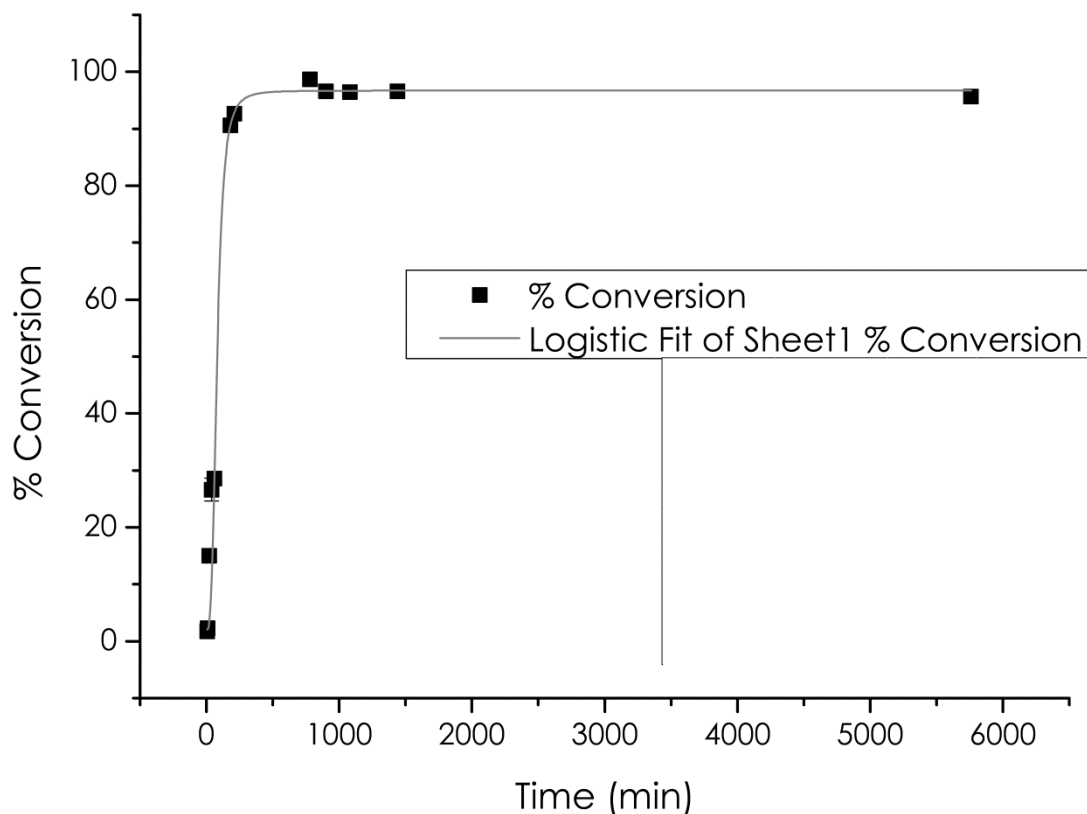
Figure 3.3-1 – Graph of % conversion against time for polymerisation of 200 equivalents of lactide with one equivalent of compound 3 in tumbling vials dry melt polymerisation.

The most suitable line of best fit seemed to be a log dose response line of best fit giving curves with the general formula represented in Equation 3.3-1, where A1, A2, x0 and p were all constants found by the best-fitting algorithm of Origin Pro 8.0.

$$y = A2 + \frac{(A1 - A2)}{(1 + \left(\frac{x}{x0}\right)^{p})}$$

Equation 3.3-1 – General formula of a logarithmic line of best fit for % conversion curves against time for the polymerisation of lactide by titanium chloride complexes.

For each data point, a standard deviation was calculated and is also plotted on the graph.

As the curve of best fit is essentially straight for the first portion of the graph the initial slope can be calculated from the time it takes to reach 50% conversion.

Rearrangement of Equation 3.3-1gives:

$$x = e^{\frac{\ln(-\frac{-y+A1}{-y+A2})}{p}} x0$$

Equation 3.3-2 – Rearrangement of Equation 3.3-1 for x

Inserting the values from the equation calculated for the line of best fit and inserting y = 50 the time taken for the polymerisation to reach 50 % (EC$_{50}$) conversion is 79.9 ± 1.3 minutes.

The gradient is dy/dx and is calculated to be 0.62 %min^{-1} or 0.010 %s^{-1}. As the catalyst has been added in a ratio 1:200 the turnover number for the catalyst is 0.021 molecules/s and the maximum conversion is 96% at 150 °C.

A second experiment was performed by heating, under dry melt conditions at 150 °C, 1 equivalent of compound **3** with 2000 equivalents of L-lactide. The experiment showed that compound **3** has an EC_{50} of 429 ± 120 minutes at this catalyst loading. The slope was calculated as 0.11% min^{-1} or 0.0018% s^{-1}. The turnover number of 0.04 molecules/s and a maximum conversion of 97%. This is comparatively slow compared to compound 4 which had a turnover number of over 1 molecule/s and catalysts reported to be used industrially for the polymerisation of lactide with turnover numbers between 5-10 molecules/s.

3.4. Conclusion

Aims of this experiment were to attempt to find structure activity relationships between the electron donating or withdrawing properties of titanium chloride catalysts and their ability to catalyse the ring opening polymerisation of lactide, and to study the ability of titanium chloride complexes to polymerise lactide, given they have only recently been discovered to be active.

All titanium (IV) chloride catalysts in this work are relatively slow, with very poor turnover numbers less than 0.1 molecule per second. The chloride ligand is not well known to initiate polymerisation, and further information about the conditions that affect the ligand's ability to polymerise lactide may offer insight into other ligands which have previously been thought to be inactive to ring opening polymerisation.

3.5. Further Work

Further work in this field should take the form of finding more well defined and pure examples of titanium chloride catalysts to continue to expand the data on the effect of subtle changes in sterics and electron donation or withdrawal from the metal centre and the ability of the metal to polymerise. Finding a method that allows *in-situ* measurements of the degree of polymerisation of the plastic without introducing air and moisture would be advantageous to allow studies of the polymerisation to occur with minimal intteruption to the reaction compared to an alliquot-removal method.

Attempts to gain insights into whether the titanium(IV) chloride complexes maintain their cytoxic activity after polymerisation were made. In these attempts a polymer synthesised using *bis*(4-fluorophenylacetylacetonate)titanium(IV) chloride as a catalyst was exposed to air and exposed to the HT-29 human ovarian cancer cell line by Dr Aida Basri at the institute of cancer therapeutics, University of Bradford. After exposure to the plastic for 3 days there was found to be no increased cell death compared to the control cells.

This inactivity may be due to the limited volume of solvent used by the cell-line testing procedures and the purposeful insolubility of the resulting poly(lactic acid) plastics. The large amount of plastic required to collect significant concentrations of the titanium(IV) complex within the plastic means that the solvents used in the cell line testing must be changed to become more soublising to the plastics. These changes to the solvent system would remove the *in vitro* method further from realistic conditions found within a multi-organ system. It may be that the plastic requires a different environment to break down and release the drug and expose the cells to the titanium centres. The titanium(IV) complex may also simply be inactive once the plastic has been formed. New methods would need to be identified which would allow exposure of cancer cells to the metal-dispersed plastics over a larger amount of time than is usual in *in vitro* assays, and give a measure of cytotoxic ability.

3.6. Chapter Three References

1.   Crossley, B.D. Ph.D. Thesis, University Of Leeds, 2011.

2.   Hebden, A.J. Ph.D. Thesis, University Of Leeds, 2010.

3.   Mannion, J.J. Ph.D. Thesis, University Of Leeds, 2009.

4.   Kim, Y. And Verkade, J.G. Novel Titanatranes With Different Ring Sizes: Syntheses, Structures, And Lactide Polymerization Catalytic Capabilities. *Organometallics*. 2002, **21**(12), pp.2395-2399.

5.   Kim, Y., Jnaneshwara, G.K. And Verkade, J.G. Titanium Alkoxides As Initiators For The Controlled Polymerization Of Lactide. *Inorganic Chemistry* 2003, **42**(5), pp.1437-1447.

6.   Russell, S.K., Gamble, C.L., Gibbins, K.J., Juhl, K.C.S., Mitchell, W.S., Tumas, A.J. And Hofmeister, G.E. Stereoselective Controlled Polymerization Of D/L-Lactide With [Ti(Trisphenolate)O-^{i}Pr]$_2$ Initiators. *Macromolecules*. 2005, **38**(24), pp.10336-10340.

7.   Gregson, C.K.A., Blackmore, I.J., Gibson, V.C., Long, N.J., Marshall, E.L. And White, A.J.P. Titanium-Salen Complexes As Initiators For The Ring Opening Polymerisation Of Rac-Lactide. *Dalton Transactions*. 2006, (25), pp.3134-3140.

8.   Gowda, R.R., Chakraborty, D. And Ramkumar, V. Controlled Hydrolysis Of [Ti(O-2,4,6-Br$_3$C$_6$H$_2$)$_2$(O-^{i}Pr)$_2$]$_2$: Synthesis, Structural Characterization And Studies On Bulk Polymerization Of Cyclic Esters And Lactide. *Inorganic Chemistry Communications*. 2011, **14**(11), pp.1777-1782.

9.   Takashima, Y., Nakayama, Y., Hirao, T., Yasuda, H. And Harada, A. Bis(Amido)Titanium Complexes Having Chelating Diaryloxo Ligands Bridged By Sulfur Or Methylene And Their Catalytic Behaviors For Ring-Opening Polymerization Of Cyclic Esters. *Journal Of Organometallic Chemistry*. 2004, **689**(3), pp.612-619.

10.   Chen, H.Y., Liu, M.Y., Sutar, A.K. And Lin, C.C. Synthesis And Structural Studies Of Heterobimetallic Alkoxide Complexes Supported By Bis(Phenolate) Ligands: Efficient Catalysts For Ring-Opening Polymerization Of L-Lactide. *Inorganic Chemistry*. 2009, **49**(2), pp.665-674.

11.   Jeong Go, M., Min Lee, J., Mun Lee, K., Hwa Oh, C., Park, K.H., Kim, S.H., Kim, M., Park, H.-R., Park, M.H., Kim, Y. And Lee, J. Titanium Complexes Containing Bidentate Benzotriazole Ligands As Catalysts For The Ring Opening Polymerization Of Lactide. *Polyhedron*. 2014, **67**, pp.286-29

12.   Takashima, Y., Nakayama, Y., Watanabe, K., Itono, T., Ueyama, N., Nakamura, A., Yasuda, H., Harada, A. And Okuda, J. Polymerizations Of Cyclic Esters Catalyzed By Titanium Complexes Having Chalcogen-Bridged Chelating Diaryloxo Ligands. *Macromolecules*. 2002, **35**(20), pp.7538-7544.

13.   Lee, J., Kim, Y. And Do, Y. Novel Chlorotitanium Complexes Containing Chiral Tridentate Schiff Base Ligands For Ring-Opening Polymerization Of Lactide. *Inorganic Chemistry*. 2007, **46**(19), pp.7701-7703.

14.   Frediani, M., Sémeril, D., Mariotti, A., Rosi, L., Frediani, P., Rosi, L., Matt, D. And Toupet, L. Ring Opening Polymerization Of Lactide Under Solvent-Free Conditions

Catalyzed By A Chlorotitanium Calix[4]arene Complex. *Macromolecules Rapid Communication.* 2008, **29**(18), pp.1554-1560.

15. Ovitt, T.M. And Coates, G. W. Stereoselective Ring-Opening Polymerization Of Rac-Lactide With A Single-Site, Racemic Aluminum Alkoxide Catalyst: Synthesis Of Stereoblock Poly(Lactic Acid). *Journal Of Polymer Science Part A: Polymer Chemistry.* 2000, **38**(S1), pp.4686–4692.

16. Thakur, K.A.M., Kean, R.T., Hall, E.S., Kolstad, J.J. And Munson, E.J. Stereochemical Aspects Of Lactide Stereo-Copolymerization Investigated By ^{1}H NMR: A Case Of Changing Stereospecificity. *Macromolecules.* 1998, **31**(5), pp.1487-1494.

17. Thakur, K.A.M., Kean, R.T., Zell, M.T., Padden, B.E. And Munson, E.J. An Alternative Interpretation Of The HETCOR NMR Spectra Of Poly(Lactide). *Chem. Commun.* 1998, (17), pp.1913-1914.

18. Kricheldorf, H.R., Kreiser-Saunders, I., Jürgens, C. And Wolter, D. Polylactides - Synthesis, Characterization And Medical Application. *Macromolecular Symposia.* 1996, **103**(1), pp.85-102.

19. Kricheldorf, H.R., Boettcher, C. And Tönnes, K.-U. Polylactones: 23. Polymerization Of Racemic And MesoD,L-Lactide With Various Organotin Catalysts—Stereochemical Aspects. *Polymer.* 1992, **33**(13), pp.2817-2824.

20. Schindler, A. And Harper, D. Poly (Lactic Acid). I. Stereosequence Distribution In The Polymerization Of Racemic Dilactide. *Journal Of Polymer Science: Polymer Letters Edition.* 1976, **14**(12), pp.729-734.

21. Chabot, F., Vert, M., Chapelle, S. And Granger, P. Configurational Structures Of Lactic Acid Stereocopolymers As Determined By [13]C·{^{1}H} NMR *Polymer.* 1983, **24**(1), pp.53-59.

22. Lillie, E. And Schulz, R.C. ^{1}H- And ^{13}C-{^{1}H}-NMR Spectra Of Stereocopolymers Of Lactide. *Die Makromolekulare Chemie.* 1975, **176**(6), pp.1901-1906.

23. H. Chisholm, M., S. Iyer, S. And E. Matison, M. Concerning The Stereochemistry Of Poly(Lactide), PLA. Previous Assignments Are Shown To Be Incorrect And A New Assignment Is Proposed. *Chemical Communications.* 1997, **0**(20), pp.1999-2000.

24. Kasperczyk, J.E. HETCOR NMR Study Of Poly(*rac*-lactide) And Poly(*meso*-lactide). *Polymer.* 1999, **40**(19), pp.5455-5458.

25. Yamaji, T.S. Hayamizu, K. Yanagisawa, M. And Yamamoto, O. *Spectral Database For Organic Compounds.* [Online]. 2013. [Accessed 30/03/2016]. Available From: http://sdbs.db.aist.go.jp/sdbs/cgi-bin/cre_index.cgi

26. Yamaji, T.S. Hayamizu, K. Yanagisawa, M. And Yamamoto, O. *Spectral Database For Organic Compounds SDBS No.:15004.* [Online]. 2013. [Accessed 30/03/2016]. Available From: http://sdbs.db.aist.go.jp/sdbs/cgi-bin/cre_index.cgi

4. TITANIUM ETHOXIDE COMPLEXES

4.1. Titanium complexes in the McGowan group
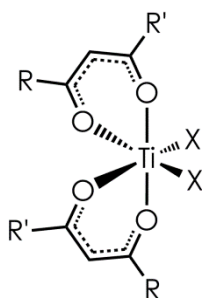
Figure 4.1-1 – General structure of titanium (IV) complexes synthesised by the McGowan group.

Titanium (IV) complexes in this chapter have been synthesised towards two aims:

1. For the polymerisation of lactide
2. For use as anti-cancer drugs

Previous work in the McGowan group has focussed on the synthesis of titanium(IV) complexes with the aim to further improve our understanding of the structure/activity relationship of metallodrugs of the type shown in Figure 4.1-1. The group has synthesised a large library of compounds varying the symmetry of the β-diketonate ligand, the position and strength of the electron donating and withdrawing groups on the chelating ligand and the nature of the labile monodentate ligand, X.[1] Thus far, complexes with halide ligands have been researched with chloride and bromide complexes being the lead compounds of interest. However titanium β-diketonates containing ethoxide labile groups are known to be cytotoxic with one example, Budotitane, progressing to Phase II trials.[2]
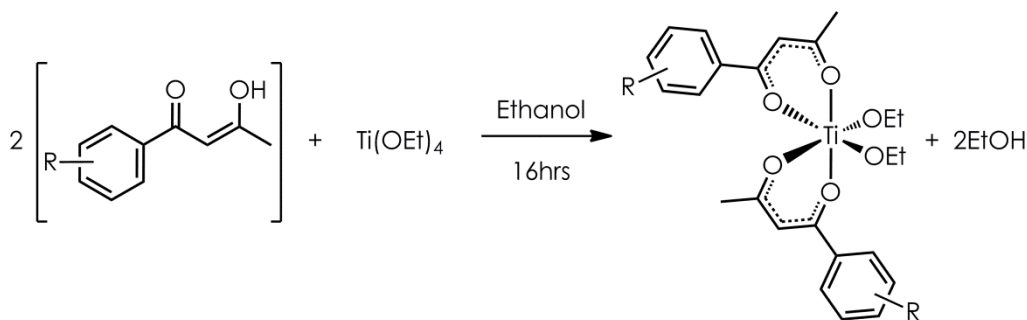
Scheme 4.1-1 – Synthesis of titanium ethoxide complexes

Bis-acetylacetonate titanium ethoxide complexes are synthesised using the procedure outlined in Scheme 4.1-1, a synthetic pathway used previously in the McGowan group.[3] Due to the asymmetry of the β-diketonate ligand and the inclusion of two monodentate ligands each structure can exist in 5 structural isomers (Figure 4.1-2), which are named first according to the monodentate ligands, then the benzoyl-adjacent oxygen atom of the acetylacetonate ligand, and finally by the methyl-adjacent oxygen atom of the acetylacetonate ligand using similar methods to the Cahn-Ingold-Prelog priority rules.[4, 5] *Keppler et al* reported that titanium β-diketonate halide complexes adopt only those structures with the monodentate ligand in the *cis* position in solution.[6] These three forms are known to interconvert in solution giving rise to broad ^{1}H NMR signals, This process is purported to be acid catalysed.[4, 7, 8]

Unlike titanium chloride or bromide complexes, titanium ethoxide complexes form basic solutions, and so the interconversion between the structural isomers is expected to be slow, or not observed. Fay *et al.* have suggested rate constants for the exchange between isomers containing three halide ligands to be between 6.7×10^2 and 1.6×10^4 s^{-1}, the fastest conversion happening when chloride ligands are occupying the *cis* positions, and with activation energies around $+11.3 \pm 0.5$ kcalmol^{-1} or $+47.31$ kJmol^{-1}.[8]

trans-trans-trans   *trans-cis-cis*

cis-cis-trans   *cis-cis-cis*   *cis-trans-cis*
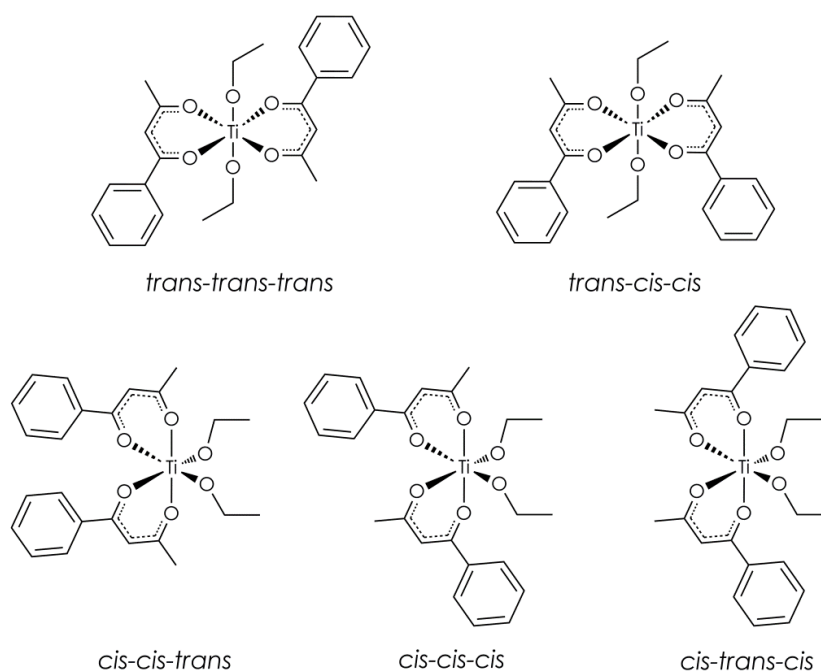
Figure 4.1-2 – Possible structural isomers of β-diketonate ethoxide complexes

This chapter will investigate the methods of conversion of the titanium ethoxide complexes, and investigate whether there is structural stability benefit to using an ethoxide complex over a chloride or bromide complex.

Chapter 3 of this work describes the use of well-studied titanium chloride complexes as catalysts for the polymerisation of lactide, and discusses the evidence that the initiating ligand is incorporated into the chain. Alkoxide ligands are much more traditional initiators for the polymerisation of lactide.[9-16] This chapter will also investigate the use of titanium ethoxide complexes for polymerisation of lactide, as well as trying to gather evidence of the efficiency of the polymerisation.

Firstly this chapter reports the synthesis and characterisation of a series of novel titanium (IV) ethoxide complexes, then reports on a series of experiments to investigate the mechanism of the transition of the titanium (IV) ethoxide complexes between the five isomers shown in Figure 4.2-1.

4.2. Synthesis of *bis*-(4-fluorophenylacetylacetonate)titanium(IV) ethoxide [Ti(4'F-Phacac)$_2$(OEt)$_2$] (Compound 5)
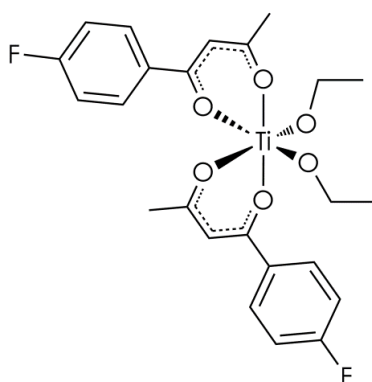
Compound 5 - *bis*-(4'fluoroacetylacetonate)titanium(IV) ethoxide

Figure 4.2-1 – Structure of compound 5

Bis-(4'fluorophenylacetylacetonate)titanium(IV) ethoxide (compound **5**) was synthesised *via* the scheme outlined in Scheme 4.1-1. To a solution of titanium(IV) ethoxide under anhydrous conditions, 2 equivalents of 4-fluorophenylacetylacetone was added drop wise with vigorous stirring. The mixture was stirred for 16 hours. The resulting cream precipitate was isolated by filtration, washed with pentane and remaining organic solvent removed *in vacuo*. The compound was recrystallised from hot ethanol to give crystals suitable for X-ray diffraction. The compound was further analysed by microanalysis, ^{1}H and ^{13}C NMR spectroscopy and mass spectrometry.

4.2.1. Crystallographic analysis of *bis-*(4-fluorophenylacetylacetonate)titanium(IV) ethoxide (Compound 5)
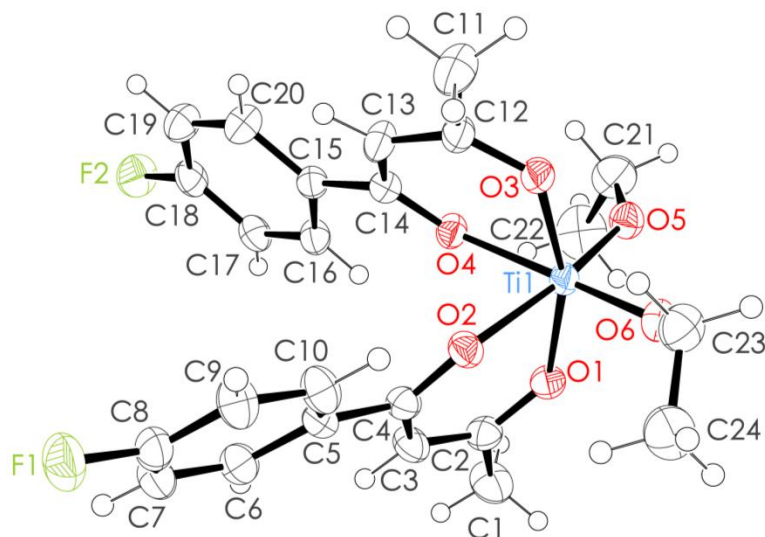
Figure 4.2-2 – ORTEP diagram of Compound 5 with displacement ellipsoids showing 50% probability

Compound **5** was found to crystallise in a monoclinic unit cell in the space group P2$_1$/n. The asymmetric unit contains one molecule with a total of four molecules in the unit cell. Bond lengths and selected angles from the crystal structure can be viewed in

Table 4.2-1 and Table 4.2-2. The β-diketonate ligand is planar as expected, with C-O bond lengths of 1.311(3) Å, 1.284(3) Å, 1.296(3) Å and 1.288(3) Å, giving an average of 1.295 Å. As expected this bond length is between the normal bond length for a C-O single and double bond, confirming, along with the planar nature of the ligand, the aromaticity of the chelate. The ethoxide ligand oxygen atoms (O5 and O6) are in a *cis* configuration, as are the oxygen atoms closest to the phenyl rings of the β-diketonate ligand (O2 and O4). The oxygen atoms closest to the methyl groups (O1 and O3) are in an *trans* position around the titanium centre. The complex is, therefore, in the *cis-cis-trans* configuration. The ellipsoids of the ethoxide carbon atoms (C21-C24) are slightly larger than the more rigidly cooridnated acetylactoneate carbon atoms, showing increased motion of the ethoxide chains.

Additionally there is a difference between the Ti-O bond lengths for the chelating oxygen atoms and the monodentate ethoxide Ti-O bond length. The monodentate Ti-OEt bond lengths are 1.827(2)Å and 1.833(2) Å, giving an average value of 1.830 Å. The chelating oxygen-metal bonds are significantly longer with values of 2.018(2) Å, 2.092(2) A, 2.030(2)Å and 2.098(2)Å. This gives an average value of 2.064 Å, or a 12 % increase in bond length for chelating oxygen atoms.
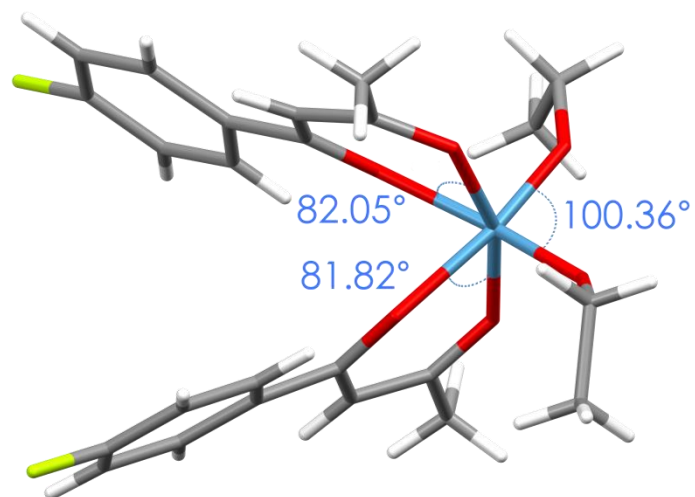
Figure 4.2-3 – Capped stick diagram showing the distorted octahedral geometry of the titanium centre of compound 5

The geometry of the titanium metal centre shows significant distortion, with the ethoxide-ethoxide bond angle of 100.36(7)°, a significant widening caused by the steric bulk of the two ethyl chains (Figure 4.2-4). Figure 4.2-3 also shows the pinched angles between the two chelating oxygen atoms in the acetylacetonate ligand. In this case the angle is much smaller than the expected 90°, due to the strain of the chelating ring.

Ti(1)-O(5)	1.8278(18)	Å	Ti(1)-O(6)	1.8335(17)	Å
Ti(1)-O(1)	2.0189(17)	Å	Ti(1)-O(3)	2.0301(16)	Å
Ti(1)-O(4)	2.0925(17)	Å	Ti(1)-O(2)	2.0987(17)	Å
O(2)-C(4)	1.284(3)	Å	O(3)-C(12)	1.311(3)	Å
O(5)-C(21)	1.434(3)	Å	C(3)-C(2)	1.412(4)	Å
C(3)-C(4)	1.428(3)	Å	C(4)-C(5)	1.511(3)	Å
O(1)-C(2)	1.296(3)	Å	O(4)-C(14)	1.288(3)	Å
C(2)-C(1)	1.525(3)	Å	C(15)-C(20)	1.418(3)	Å
C(15)-C(16)	1.425(3)	Å	C(15)-C(14)	1.515(3)	Å
C(14)-C(13)	1.423(3)	Å	C(13)-C(12)	1.419(3)	Å
O(6)-C(23)	1.456(3)	Å	F(4)-C(18)	1.375(3)	Å
C(5)-C(10)	1.417(3)	Å	C(5)-C(6)	1.419(3)	Å
C(21)-C(22)	1.533(5)	Å	C(23)-C(24)	1.509(5)	Å
C(18)-C(19)	1.398(4)	Å	C(18)-C(17)	1.404(3)	Å
C(16)-C(17)	1.402(3)	Å	C(9)-C(10)	1.390(4)	Å
C(9)-C(8)	1.416(4)	Å	C(20)-C(19)	1.408(4)	Å
C(7)-C(8)	1.385(4)	Å	C(7)-C(6)	1.401(4)	Å
C(12)-C(11)	1.516(3)	Å	C(8)-F(1)	1.384(3)	Å

Table 4.2-1 – Interatomic distances for compound 5 with standard uncertainties listed in parentheses

O(5)-Ti(1)-O(6)	100.19(8)°	O(5)-Ti(1)-O(1)	93.18(8)°
O(6)-Ti(1)-O(1)	100.74(8)°	O(5)-Ti(1)-O(3)	100.36(7)°
O(6)-Ti(1)-O(3)	89.50(7)°	O(3)-Ti(1)-O(4)	82.05(6)°
O(5)-Ti(1)-O(4)	88.19(7)°	O(6)-Ti(1)-O(2)	90.98(8)°
O(1)-Ti(1)-O(4)	85.65(7)°	O(3)-Ti(1)-O(2)	82.47(7)°
O(1)-Ti(1)-O(2)	81.82(7)°	C(4)-O(2)-Ti(1)	130.09(15)°
O(4)-Ti(1)-O(2)	81.10(7)°	C(21)-O(5)-Ti(1)	141.34(19)°
C(2)-C(3)-C(4)	122.0(2)°	O(2)-C(4)-C(3)	122.6(2)°
C(2)-O(1)-Ti(1)	131.43(16)°	C(3)-C(4)-C(5)	121.6(2)°
O(1)-C(2)-C(3)	124.6(2)°	O(1)-C(2)-C(1)	114.8(2)°
C(7)-C(6)-C(5)	121.0(2)°	O(6)-C(23)-C(24)	111.8(2)°
F(1)-C(8)-C(9)	117.4(2)°	F(1)-C(8)-C(7)	119.5(2)°

Table 4.2-2 – Selected bond angles for compound 5 with standard uncertainties listed in parentheses
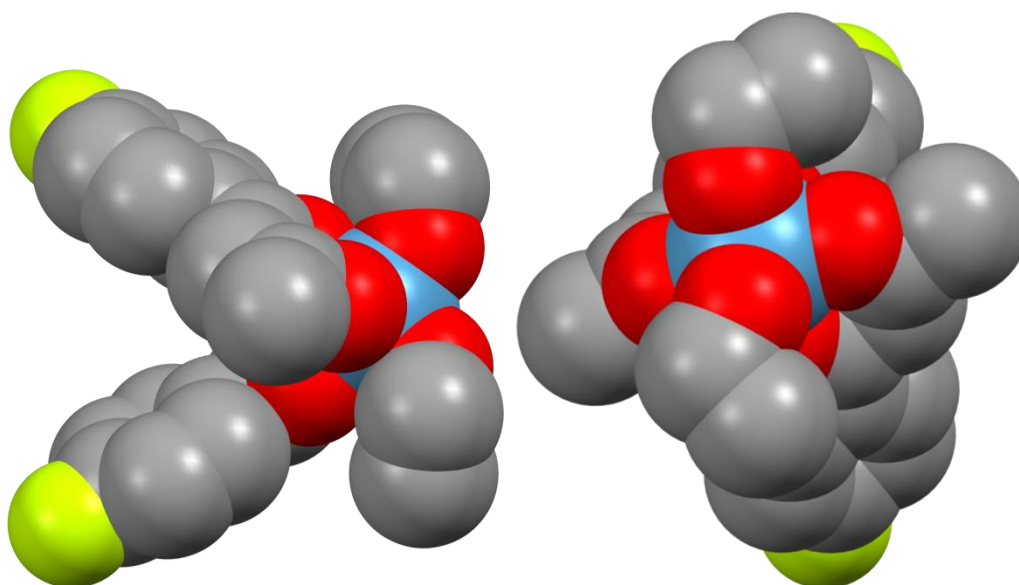
Figure 4.2-4 – Space filling diagram showing the Van der Waals radii of the ligands around the titanium centre of compound 5. Hydrogen atoms omitted for clarity.
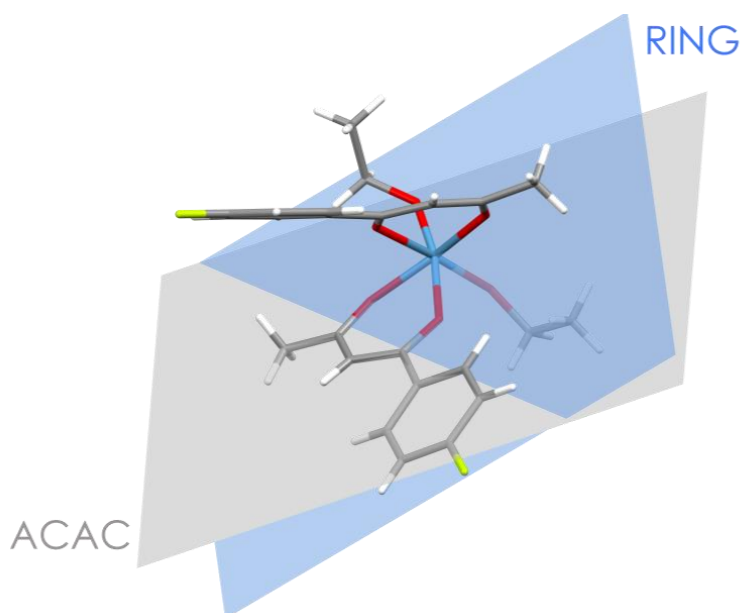
Figure 4.2-5 – Capped stick representation of compound 5 showing the planes of the acetylacetonate backbone (lighter grey layer) and the plane of the 4'fluorophenyl ring (darker blue layer)

The 4'fluorophenyl ring was found to twist slightly out of the plane of the acetylacetonate ligand, as can be seen in Figure 4.2-5, displaying a torsion angle of 10.22(8)°. The observed torsion may be due to the hydrogen bonds in the solid state as seen in Figure 4.2-6.
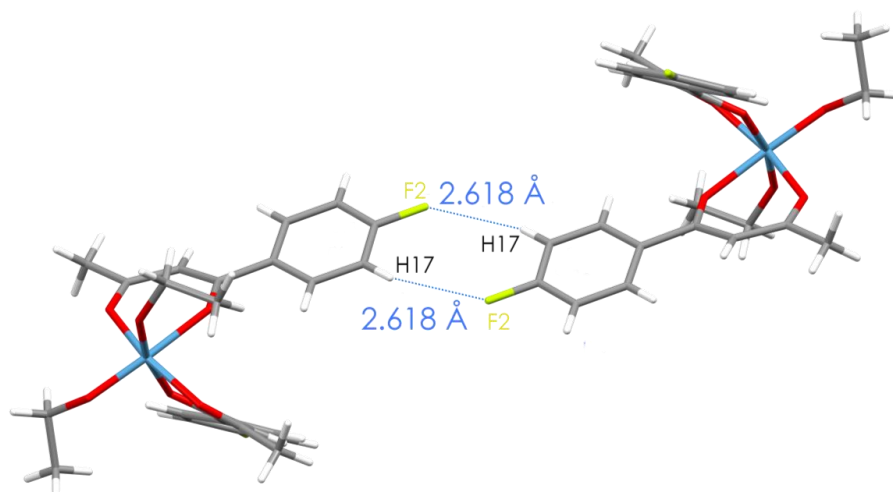
Figure 4.2-6 - Hydrogen bonding of the fluorophenyl fluorine atom with the adjacent hydrogen atom of the nearest molecule
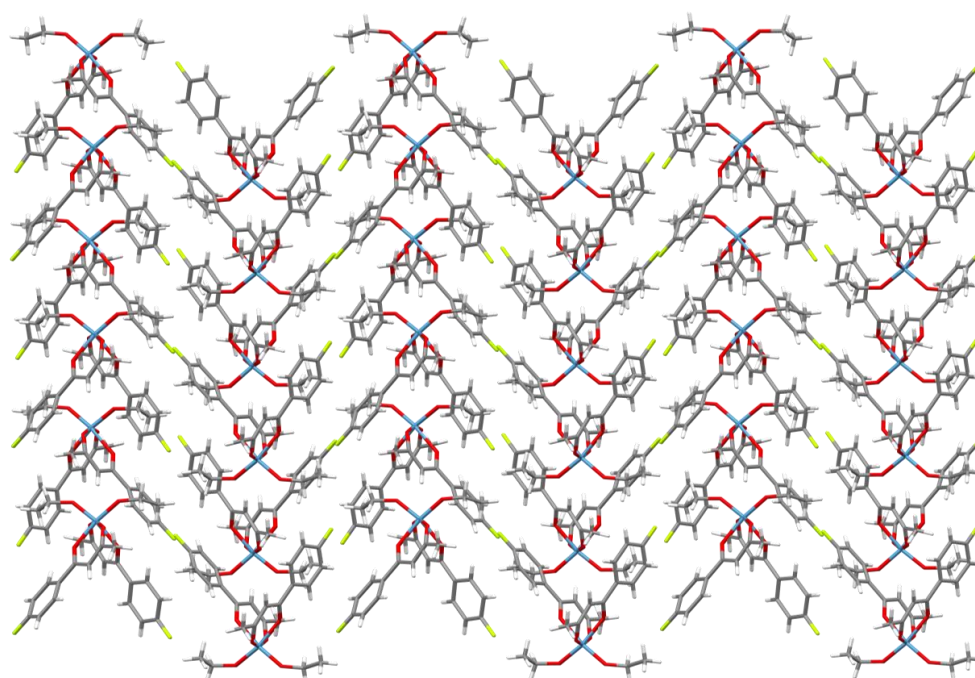
Figure 4.2-7 – Crystal packing of compound 5 viewed down the a axis of the crystal structure

When viewed down the a axis of the crystal structure, compound **5** packs in an interesting herringbone structure as seen in Figure 4.2-7, showing each molecule stacking on top of each other in the vertical direction and an alternating orientation of the molecules along the horizontal axis. This mirrors the findings of the group with the analogous titanium complexes with chloride bridging ligands which often form a herringbone structure. [3, 17, 18]

4.2.2. NMR spectroscopic analysis of *bis*-(4-fluorophenylacetylacetonate)titanium(IV) ethoxide (compound 5)
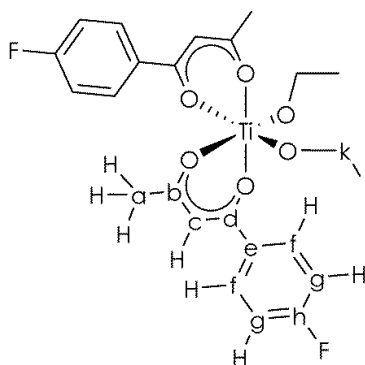
Figure 4.2-8 – Labelled structure of compound 5

Figure 4.2-6 shows a labelled structure of compound **5** which will be used for the assignments of the ^{1}H, ^{1}H-^{1}H COSY and ^{13}C NMR spectrum in Figure 4.2-9 and Figure 4.2-10 .
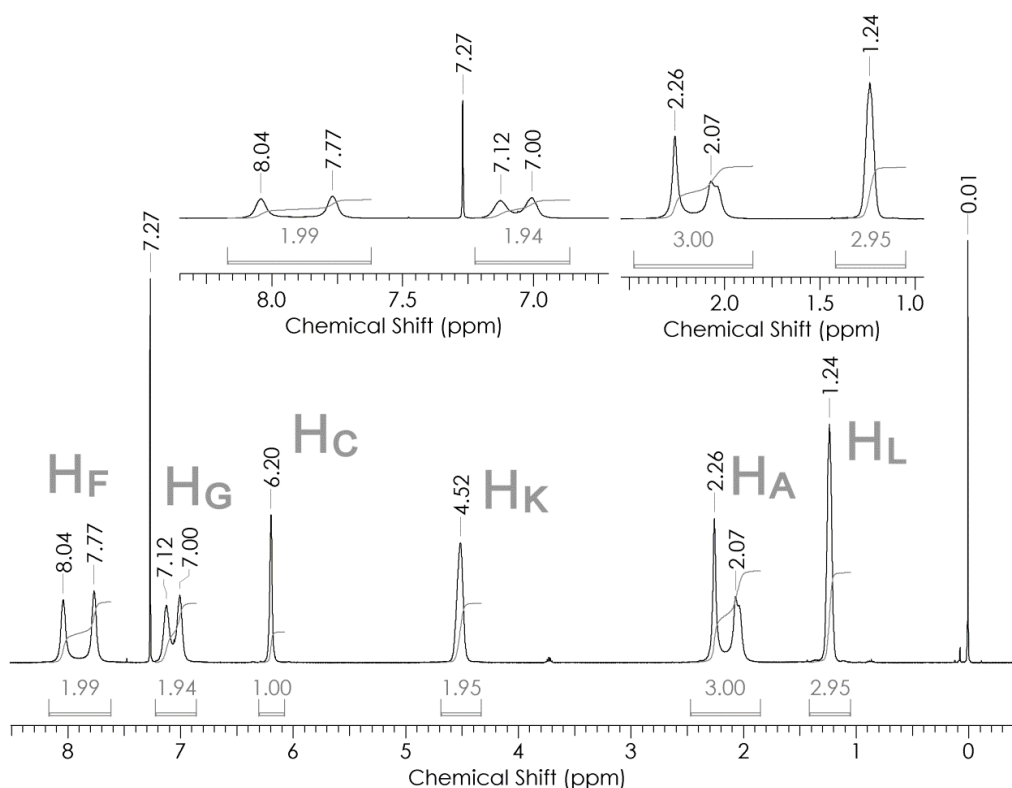
Figure 4.2-9 - 500MHz ^{1}H NMR spectrum of compound 5 in CDCl$_3$ showing chemical shifts and integrals at 300K

At room temperature the spectrum is broad, suggesting that the interconversion between the structural isomers is occurring and is rapid. All of the signals arising from the acetylacetonate protons, except the methine proton, split into two separate peaks. Peak assignments are listed in Table 4.2-3.
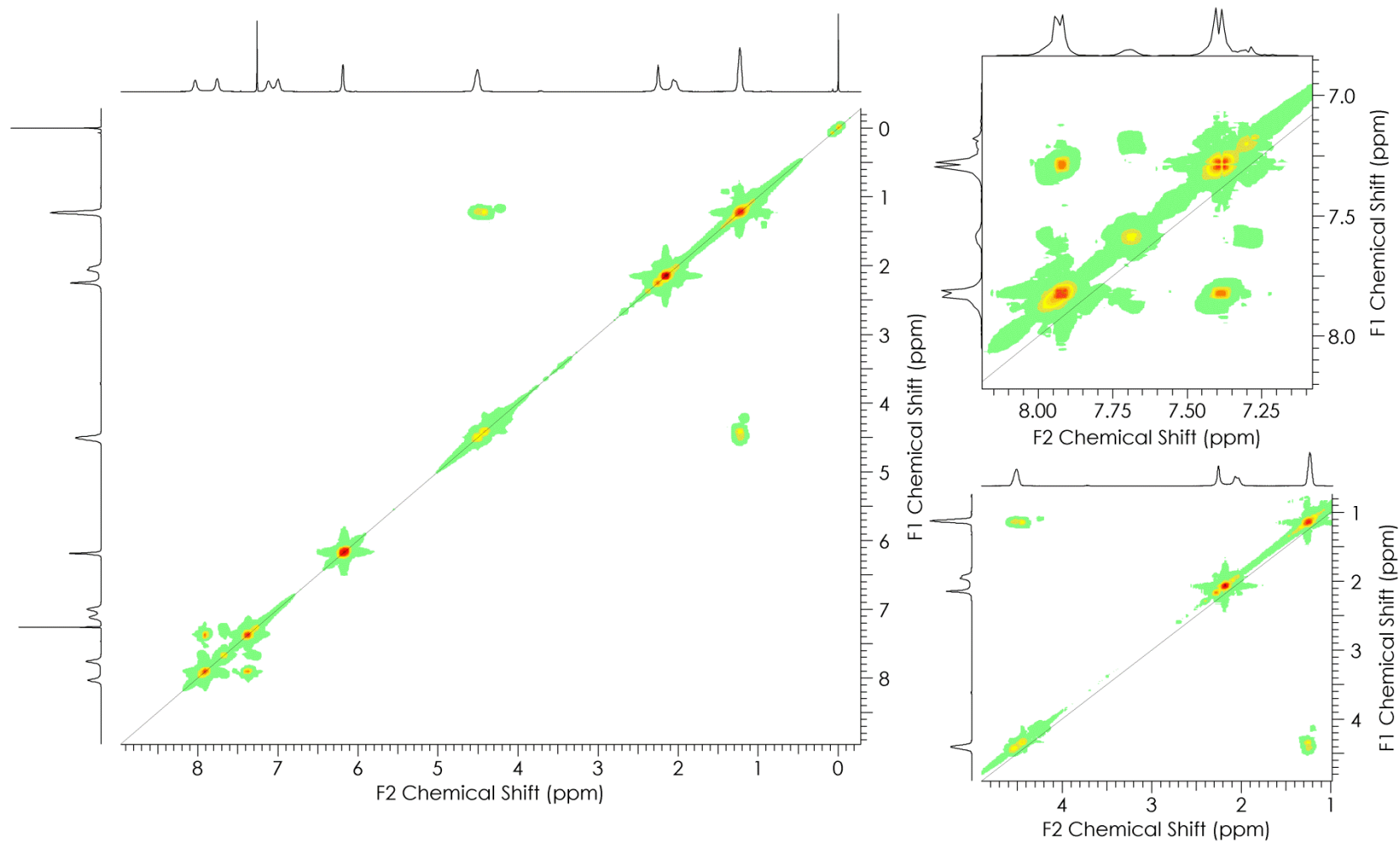
Figure 4.2-10 – 500MHz ^{1}H-^{1}H COSY spectrum in CDCl$_3$ collected at room temperature

^{1}H Chemical Shift (σ)	Integration, multiplicity	Assignment	Chemical Shift	^{13}C Assignment
1.24 ppm	3H, s	H$_L$	18.51 ppm	l
2.07 ppm 2.26 ppm	3H, s	H$_A$	33.62 ppm	a
4.52 ppm	2H, as	H$_K$	72.38 ppm	k
6.20 ppm	1H, s	H$_C$	111.48 ppm	f
7.00 ppm 7.12 ppm	2H, as	H$_G$	130.17 ppm	g
7.77 ppm 8.04 ppm	2H, as	H$_F$	133.41 ppm	h
			140.00 ppm	e
			164.03 ppm	d
			166.05 ppm	b

Table 4.2-3 – NMR spectroscopic assignments for compound 5

One explanation for the appearance of two signals for each expected proton environment of the acetylacetonate ligand in the ^{1}H NMR spectrum is some form of coupling to the fluorine atom in the structure. If this were correct, H-C-C-F coupling values observed for the protons labelled H$_g$ are calculated to be 135 Hz, which is two orders of magnitude larger than the expected coupling constant of 1-4 Hz.[19] Like the aromatic acetylacetonate protons, the methyl acac protons labelled H$_a$ are split between two significantly different signals. It is unlikely that this is a splitting effect from the fluorine atom of 95 Hz over ^{9}J.

Another possibility is that compound **5** forms two products in solution, but crystallises with the ethoxide ligands in the *cis* position in the solid state. If this were the case, two different methine peaks would be expected, assuming that the structures have significant enough magnetic difference to cause the protons within the phenyl ring and methyl group of the acetylacetonate ligand to have such differences in the chemical shifts of the protons. Additionally the signals belonging to H$_K$ and H$_L$, the ethoxide ligand signals, would also be split into two defined signals, assuming significant magnetic difference. The signals at 7.77 ppm and 8.04 ppm each integrate with an area of one proton within error, suggesting that if there were two products they are present at a 1:1 ratio. This finding is mirrored in the integrations of the signals at 7.00 ppm and 7.12 ppm and with the methyl protons of the acetylacetonate ligand (H$_L$) where the upfield signal at 2.07 ppm integrates to the same area as the signal at 2.26 ppm.

A third possibility is that the hydrogen bonding shown in the solid state in Figure 4.2-6 also exists in solution, restricting the ability of the phenyl ring to rotate, causing the apparently equivalent phenyl protons labelled H$_G$ to be locked into position, and so stopping these protons experiencing equivalent magnetic environments. This would account for the 1:1

integration ratio observed between each of the phenyl signals within the ^{1}H NMR spectrum.

The final possibility is the formation in solution of isomers of the compound which have two inequivalent actylacetonate ligands. This would also explain the approximately equal signal area for the two signals observed for proton environments H_A, H_F and H_G, however it would suggest that all of the isomers formed *in situ* within the NMR spectrometer have inequivalent acetylacetonate ligands, even when very symmetrical.

The ^{1}H-^{1}H COSY spectrum in Figure 4.2-10 confirms the assignment of the protons H_A as these protons do not couple to any other signal in the spectrum. The protons H_K ad H_L are found to couple as expected, and do not couple to any other signals, again confirming the assignment of these signals. In the expansion (right) we can see that only the two signals 8.04 ppm 7.77 ppm couple on the phenyl ring, and in this case they only couple to one another. The aromatic signals at 7.00 ppm and 7.12 ppm are found not to couple to any other proton in the spectrum which is unusual, but indicates that these protons are undergoing additional coupling to the fluorine atom and confirms the assignment as the protons closest to the fluorine atom.

4.3. Synthesis of *bis*-(4-bromophenylacetylacetonate)titanium(IV) ethoxide [Ti(4'Br-Phacac)$_2$(OEt)$_2$] (Compound 6)
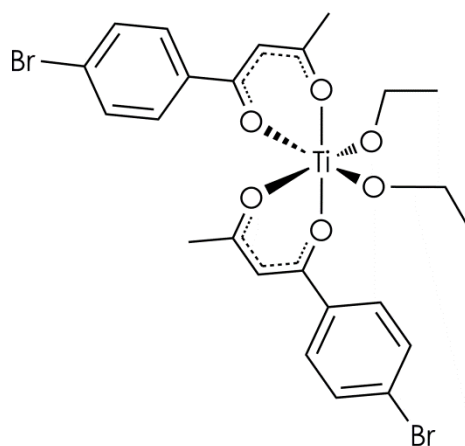
Compound 6 - *bis*-(4-bromophenylacetylacetonate)titanium(IV) ethoxide

Figure 4.3-1- Structure of compound 6

Bis-(4'bromophenylacetylacetonate)titanium(IV) ethoxide was synthesised using the synthesis in Scheme 4.1-1. two equivalents of 4'bromophenylacetylacetone was slowly added to a solution of titanium(IV)ethoxide in ethanol under rigorous anhydrous conditions. The resulting precipitate was filtered, washed with pentane and all remaining solvent removed *in vacuo*. The cream solid was then recrystallised from hot ethanol in anhydrous conditions to yield single crystals suitable for X-ray diffraction.

4.3.1. Crystallographic analysis of *bis*-(4-bromophenylacetylacetonate)titanium(IV) ethoxide (compound 6)
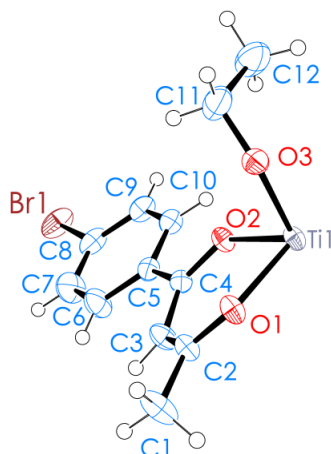
Figure 4.3-2 – ORTEP diagram of the asymmetric unit only of compound 6 with ellipsoids displayed at the 50% probability level

Compound **6** crystallised in an orthorhombic unit cell in the space group Ccc2. The asymmetric unit contains half a molecule with 4 molecules in the unit cell. The molecule is arranged in a *cis-cis-trans* arrangement with the ethoxide ligands showing a *cis* arrangement, the oxygen atoms closest to the phenyl ring of the β-diketonate ligand (O2 and O2(a)) taking a *cis* arrangement. The oxygen atoms of the β-diketonate closest to the methyl groups of the ligand (O1 and O1(a)) take a trans-configuration. Figure 4.3-3 shows the arrangement of the ethyl chains of the ethoxide groups. In compound **6** the chains take a Z shape arrangement, with each ethyl chain pointing in an opposite direction. In compound **5** the ethoxide groups take a C-shape arrangement in the solid-state as seen in Figure 4.2-4. Bond lengths and selected angles of compound **6** can be seen in Table 4.3-1and Table 4.3-2 respectively. The acetylacetonate ligand is planar with average aromatic C=O bond length of 1.292 Å.
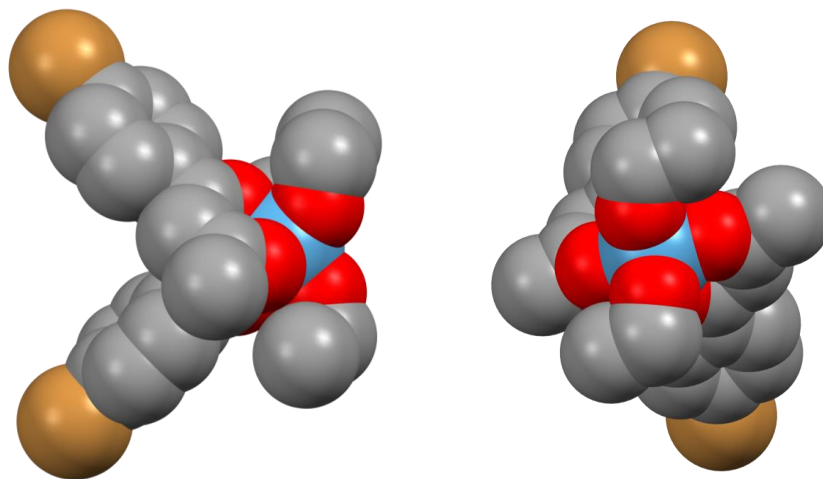
Figure 4.3-3 – Space-filling representation of the structure of compound 6 showing a Z-shape arrangement of the ethyl chains of the ethoxide ligand

Br(1)-C(8)	1.9148(17)	Å	Ti(1)-O(2)	2.0897(12)	Å
Ti(1)-O(3)	1.8264(12)	Å	Ti(1)-O(1)	2.0119(9)	Å
O(2)-C(4)	1.2894(18)	Å	O(3)-C(11)	1.409(2)	Å
C(6)-C(7)	1.402(3)	Å	O(1)-C(2)	1.2946(17)	Å
C(7)-C(8)	1.405(3)	Å	C(6)-C(5)	1.419(2)	Å
C(5)-C(4)	1.504(2)	Å	C(8)-C(9)	1.391(3)	Å
C(1)-C(2)	1.519(2)	Å	C(5)-C(10)	1.409(2)	Å
C(3)-C(4)	1.418(2)	Å	C(2)-C(3)	1.410(2)	Å
C(11)-C(12)	1.527(3)	Å	C(9)-C(10)	1.408(2)	Å

Table 4.3-1 – Average bond lengths of compound 6 with standard uncertainties listed in parentheses

O(3)[a]-Ti(1)-O(3)	99.44(8)°	O(2)[a]-Ti(1)-O(3)	169.12(5)°
O(2)[a]-Ti(1)-O(3)[a]	90.11(5) °	O(2)-Ti(1)-O(3)[a]	169.12(5)°
O(2)-Ti(1)-O(3)	90.11(5) °	O(2)[a]-Ti(1)-O(2)	80.89(7)°
O(1)[a]-Ti(1)-O(3)	91.06(4) °	O(1)[a]-Ti(1)-O(3)[a]	98.77(4)°
O(1)-Ti(1)-O(3)[a]	91.06(4) °	O(1)-Ti(1)-O(3)	98.77(4)°
O(1)[a]-Ti(1)-O(2)	86.15(4) °	O(1)[a]-Ti(1)-O(2)[a]	82.30(4)°
O(1)-Ti(1)-O(2)[a]	86.15(4) °	O(1)-Ti(1)-O(2)	82.30(4)°

O(1)[a]-Ti(1)-O(1)	164.81(6)°	C(11)-O(3)-Ti(1)	145.30(14)°
C(4)-O(2)-Ti(1)	131.18(9)°	C(2)-O(1)-Ti(1)	132.40(9)°
C(5)-C(6)-C(7)	120.87(15)°	C(8)-C(7)-C(6)	119.06(16)°
C(7)-C(8)-Br(1)	119.45(14)°	C(9)-C(8)-Br(1)	119.36(14)°
C(9)-C(8)-C(7)	121.19(17)°	C(4)-C(5)-C(6)	118.78(13)°
C(10)-C(5)-C(6)	118.65(14)°	C(10)-C(5)-C(4)	122.57(13)°
C(1)-C(2)-O(1)	115.22(14)°	C(3)-C(2)-O(1)	124.58(13)°
C(3)-C(2)-C(1)	120.19(14)°	C(4)-C(3)-C(2)	121.79(14)°
C(5)-C(4)-O(2)	116.28(12)°	C(3)-C(4)-O(2)	123.47(14)°
C(3)-C(4)-C(5)	120.19(13)°	C(10)-C(9)-C(8)	119.60(16)°
C(9)-C(10)-C(5)	120.58(16)°	C(12)-C(11)-O(3)	113.37(16)°

Table 4.3-2 – Bond angles of compound 6 with standard uncertainties listed in parentheses

[a] – Indicates a symmetry generated atom in the second half of the molecule

The Ti-OEt bond lengths in compound **6** are significantly shorter than the Ti-O bonds of the acetylacetonate chelating ligand, with chelating Ti-O bond lengths measuring 2.0119(9) Å and 2.0897(12) Å and Ti-OEt bond length measuring 1.826 Å. This continues to confirm the aromaticity of the acetylacetonate ligand as the electrons responsible for bonding are spread across the ligand and so the bonds to titanium are weaker as expected.

The geometry of the titanium centre is distorted. The steric bulk of the ethoxide groups causes a widening of the ethoxide-ethoxide bond angles measuring 99.44(8)° as opposed to the usual 90° expected. There is also a significant pinching effect of the chelating ligand with acetylacetone O-Ti-O bond angles measuring 82.30(4)°. These two factors leave the titanium centre with a large angle for approach of the lactide molecule to the titanium centre and ligand exchange reactions as can be seen in Figure 4.3-3, the space filling diagram of compound **6**. Due to the small bite angle of the chelating ligands and the otherwise normal unconstrained angle in between the acetylacetonate ligands, once there is exchange of the ethoxide ligands, nearly half of the coordination sphere of the titanium atom is exposed. This is ideal for a catalyst for the ring opening polymerisation of lactide.
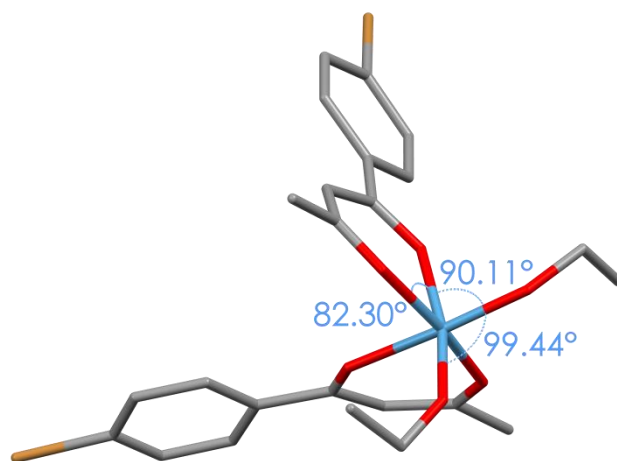
Figure 4.3-4 – Capped stick diagram of compound 6 showing the distorted octahedral geometry of the titanium metal centre (hydrogen atoms omitted for clarity)
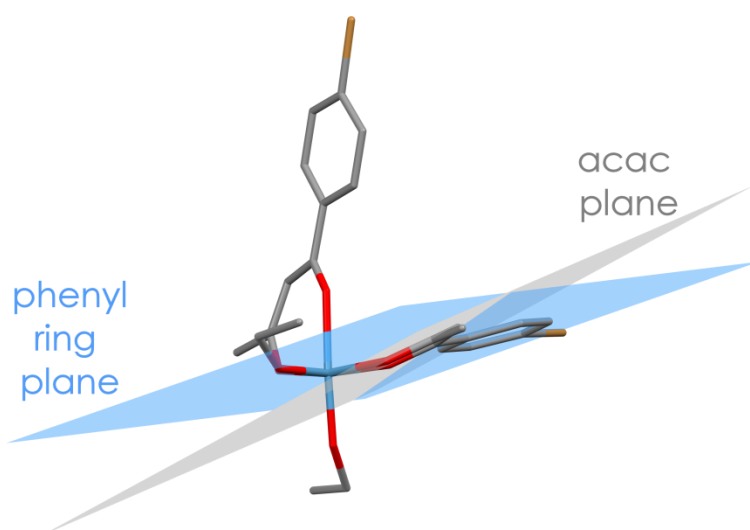
Figure 4.3-5 – Capped stick representation of compound 6 showing the planes of the acetylacetonate backbone (light grey layer) and the plane of the 4'bromophenyl ring of the ligand.

The phenyl ring of the acetylacetonate ligand is slightly out of plane, with the torsion angle between the ring and the acetylacteonate backbone measuring 11.78° (Figure 4.3-5).

The compound was found to pack in layers, with each molecule oriented in the same direction when viewed down the a-axis. There was no hydrogen bonding, T-stacking or π-π stacking found in this structure, leading to an untemplated structure as seen in Figure 4.3-6.
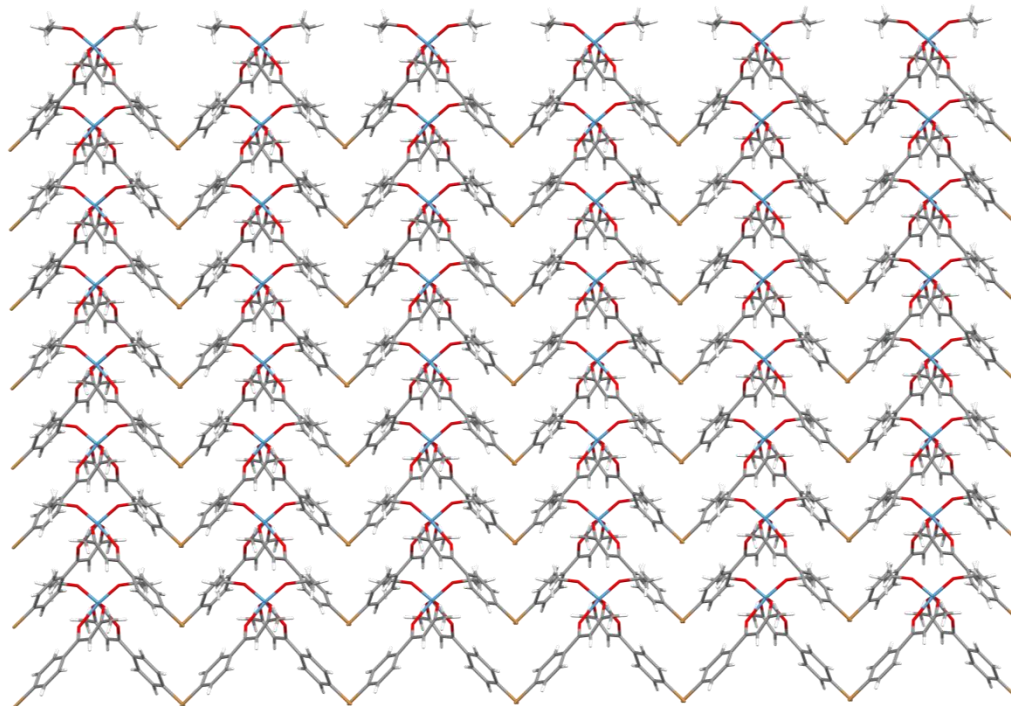
Figure 4.3-6 – Crystal packing of compound 6 viewed down the a-axis of the crystal structure.

4.3.2. NMR spectroscopic analysis of *bis*-(4-bromophenylacetylacetonate)titanium(IV) ethoxide (Compound 6)
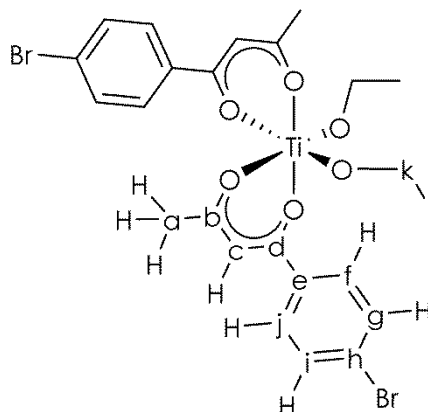
Figure 4.3-7 – Labelled structure of compound 6

Figure 4.3-7 shows a structure of compound **6** showing the labels which will be used for the assignments of the ^{1}H, ^{13}C{^{1}H} and correlation NMR spectra.
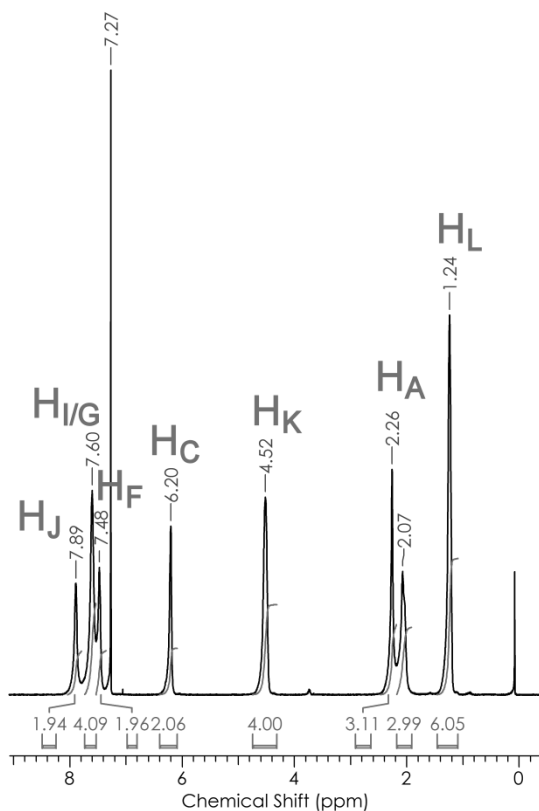
Figure 4.3-8 – 500MHz 1H NMR spectrum of compound 6 in CDCl$_3$ showing chemical shifts and integrals at 300K

The proton NMR spectrum of the crystals of compound **6** confirmed successful complexation of the 4-bromoacetylacetonate ligand with a shift in the methine proton of 0.05ppm downfield over the free ligand. Due to the broad signals of the NMR splitting patterns cannot be used to assign the NMR resonances, so correlation spectroscopy offers information on connectivity.

The most upfield shift at 1.24 ppm arises from the terminal methyl group of the ethoxide ligand, and the COSY spectrum along with the integration shows the expected correlation with the ethoxide CH_2 peak at 4.52 ppm (Figure 4.3-9). A HMBC spectrum shows coupling over several bonds, and the HMBC spectrum of compound **6** in Figure 4.3-11 shows the signals at 4.52 ppm and 1.25 ppm to only couple with each other over 2-3 bonds, confirming the assignment of these protons as the carbon atoms in the ethoxide ligand.

The aromatic peaks at 7.48 ppm, 7.60 ppm and 7.89 ppm collectively arise from the four aromatic protons. Instead of the two expected signals, the peaks split into three signals, with each signal integrating to represent 1:2:1 protons respectively. The ^1H-^1H COSY spectrum (Figure 4.3-9) shows that the signal at 7.49 ppm couples to the signal at 7.60 ppm, but not the signal at 7.89 ppm.

The NOESY spectrum (Figure 4.3-12) shows the same pattern where the protons responsible for the signal at 7.48 ppm are close in physical space to those at 7.60 ppm but not the one responsible for the peak at 7.89 ppm.

^1H Chemical Shift (σ)	Integration, multiplicity	Assignment	^{13}C Chemical Shift (σ)	Assignment
1.24	6H, s	H_L	18.49	l
2.07	3H, as	H_A	27.01	a
2.26	3H, as	H_A	27.69	a
4.52	4H, as	H_K	72.46	k
6.20	2H, as	H_C	98.86	c
7.48	2H, as	H_F	99.33	c
7.60	4H, as	H_I and H_G	126.49	h
7.89	2H, as	H_J	129.12	f or j
			131.60	g and i
			136.09	e
			178.70	d
			181.70	d
			181.78	d
			190.63	b
			193.55	b

Table 4.3-3 – NMR spectroscopic assignments of compound 6
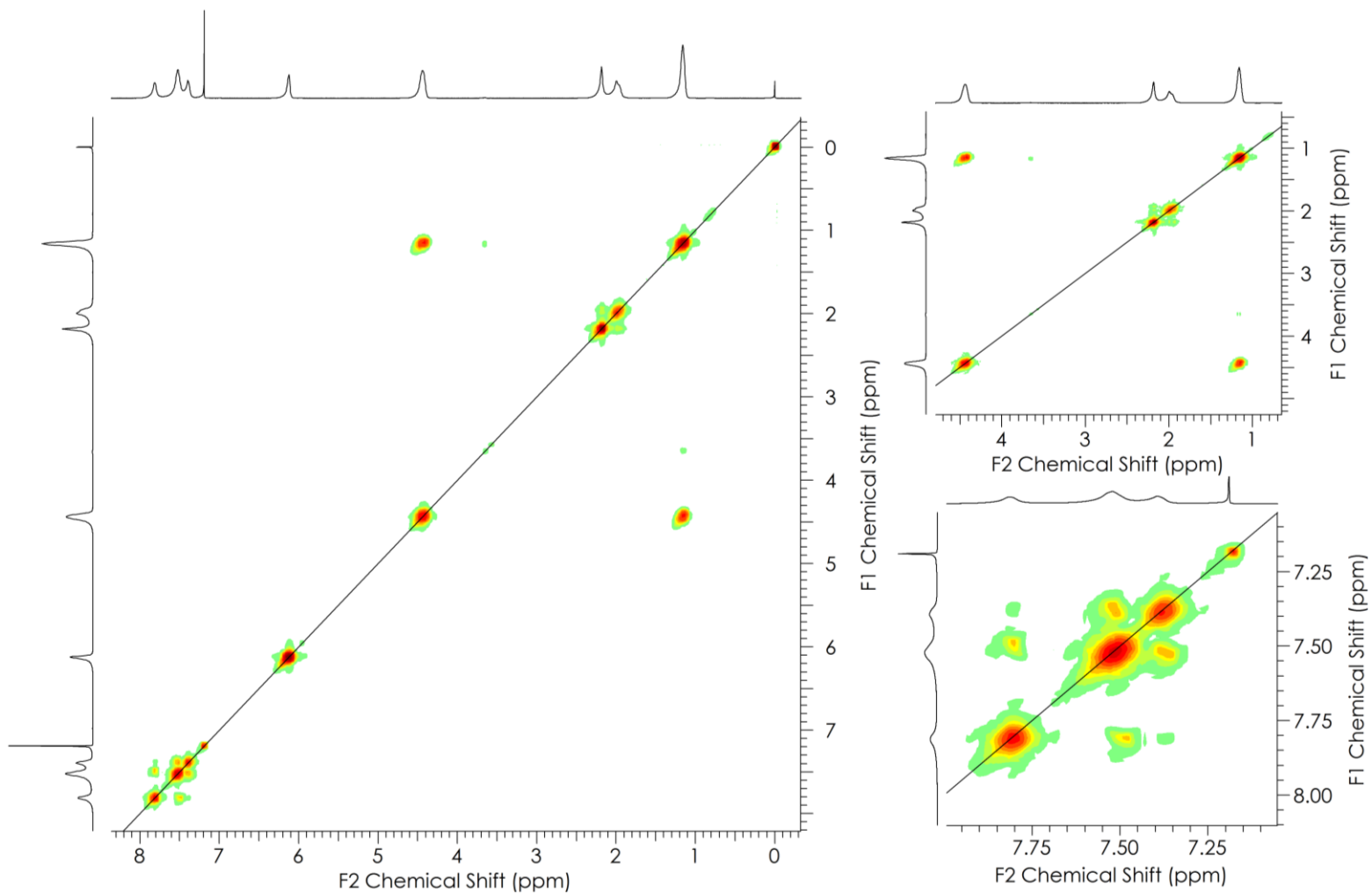
Figure 4.3-9 – 500 MHz ^1H-^1H COSY spectrum in CDCl$_3$

The HMQC spectrum (Figure 4.3-10) shows the carbon signals with their corresponding proton signals. The spectrum shows the signals at 129.1 ppm and 131.6 ppm on the ^{13}C vertical axis each appear to couple to more than one proton signal. Equally, the broad ^{1}H signal at 7.60 ppm encompasses signals which correlate with more than one significantly different ^{13}C environment.
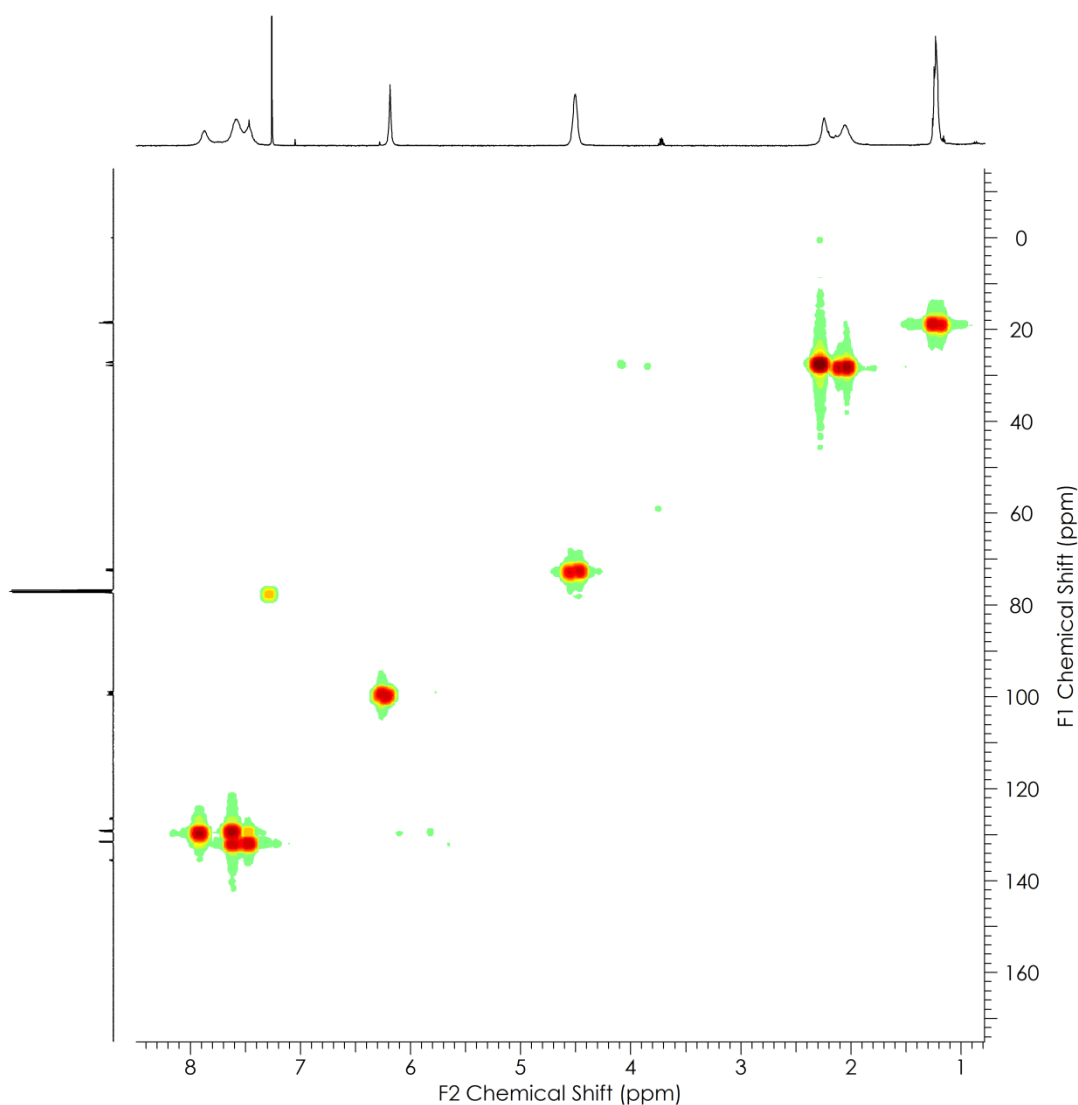
Figure 4.3-10 – 500 MHz HMQC spectrum of compound 6 collected in CDCl$_3$ at 298 K

The HMBC spectrum (Figure 4.3-11) shows that the most downfield aromatic proton signal at 7.89 ppm is coupled to the other two aromatic signals at 7.48 ppm and 7.60 ppm over several bonds. The most deshielded aromatic proton peak is attached to a carbon atom which couples over several bonds to the methine proton. None of the other carbon atoms couple to the methine proton as strongly. In aromatic systems the maximum coupling expected to be observed in HMBC spectroscopy is coupling over ^{4}J. This signal also shows

weak signal in the NOESY spectrum (Figure 4.3-12) with the methine proton, suggesting the proton responsible for the signal at 7.89 ppm to be close in physical space to the methine acetylacetonate proton, suggesting that the proton is on the phenyl ring in a position closest to the ketone and has been assigned as H_j

The remaining ^1H signals to be assigned, H_f, H_g and H_i were resolved by variable temperature studies in section 4.3.3.
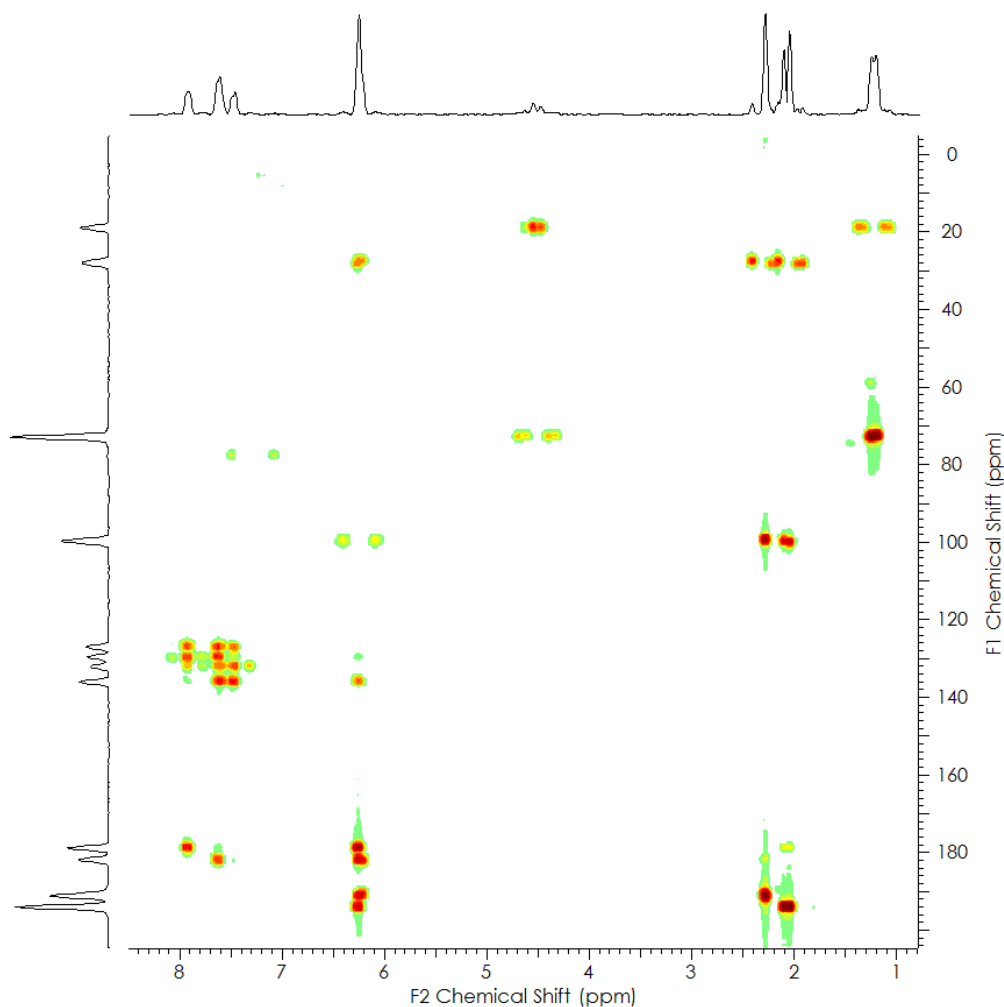
Figure 4.3-11 – 500 MHz HMBC spectrum of compound 6 collected at 253 K

The HMBC spectrum allows us to assign the identity of the $^{13}C\{^1H\}$ NMR spectroscopic signals arising at 178.7 ppm and 190.6 ppm. The more upfield shift at 190.6 ppm is coupled over several bonds with the diagnostic methine proton at 6.20 ppm and the acetylacetonate methyl proton at 2.07 ppm and 2.26 ppm confirming these signals to be assigned to the ketone carbonyl carbon on the methyl side of the acetylacteonate ligand. The more downfield shift at 181.7 ppm couples with the aromatic signals mentioned before at 7.48 ppm, 7.60 ppm and 7.89 ppm, showing this shift to be assigned to the carbonyl carbon closest to the phenyl ring.
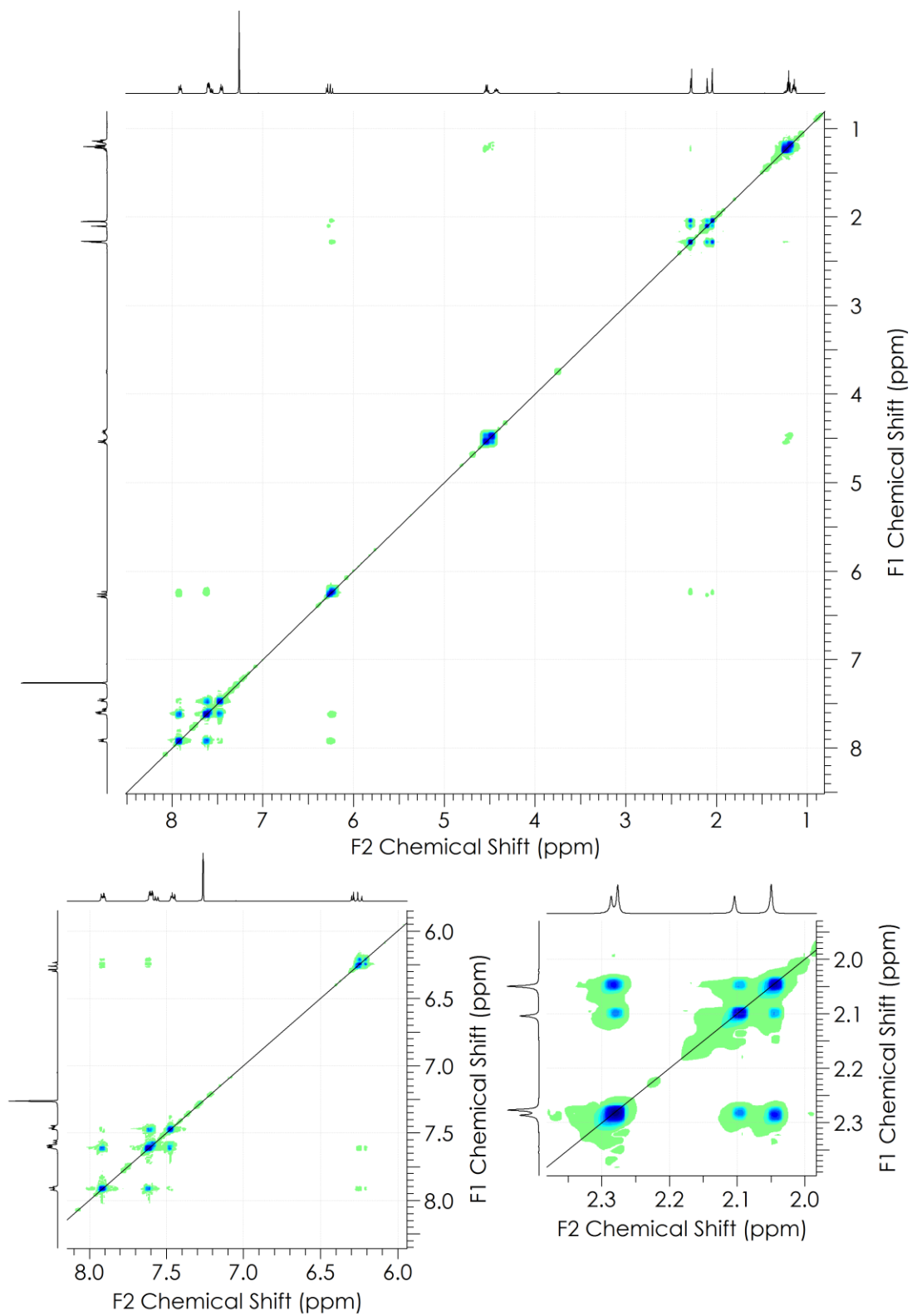
Figure 4.3-12 – 500 MHz NOESY spectrum of compound 6 collected at 253 K

4.3.3. Variable temperature studies of *bis*-(4-bromophenylacetylacetonate)titanium(IV) ethoxide (Compound 6)

Figure 4.3-13 shows the 500 MHz ^{1}H NMR spectrum of compound **6** collected at several temperatures. At room temperature only one broad methine proton (H_c, Figure 4.2-8) is observed. The methine proton is isolated from any other protons in the system by two ketone carbon atoms. As such it is not expected to exhibit any coupling. As the sample is cooled to 213 K, the single broad methine peak caused by rapid interconversion of the isomers of the complex is isolated into four sharp peaks as the interconversion processes decrease in rate. The structural isomers of bis(acetylacetonate) titanium ethoxide complexes are shown in Figure 4.1-2. The *cis-cis-trans* and *cis-trans-cis* isomers have equivalent methine protons on the acetylacetonate backbone. However, the *cis-cis-cis* isomer contains two non-equivalent acetylacetoneate ligands. Therefore the *cis-cis-cis* isomer would be responsible for two methine peaks in the ^{1}H NMR spectrum. [8] A similar increase in the resolution of the acetylacetonate methyl group is also observed, with peaks arising in the region of 2.10 – 2.30 ppm. The presence of four peaks gives strong evidence of the existence of 3 structural isomers in solution at a time, and the apparent thermodynamic stability of the isomers with *cis* monodentate ligand indicated by the collection of all crystal structures of titanium (IV) β-diketonate complexes within the group so far exhibiting this arrangement, suggests that those three isomers may be the *cis-cis-trans, cis-cis-cis* and *cis-trans-cis* isomers.

All other broad peaks are also resolved at 213 K to confirm the original assignments of the protons. The aromatic peaks between 7.48 – 7.90 ppm resolve into several doublet peaks, confirming the *para* substitution of the halide on the phenyl ring of the acetyl acetonate ligand. This finding suggests that the proton environment H_f is inequivalent to H_j which could only with restricted rotation of the phenyl ring of the acetylacetonate ligand.

The peak at 4.52 ppm resolves into a series of quartets confirming the assignment of the CH_2 group of the ethoxide ligand and the peaks between 1.15 – 1.25 ppm resolve into a series of overlapping triplets corresponding to the CH_3 group of the ethoxide ligand.

The changes in the $^{13}C\{^1H\}$ NMR spectra in Figure 4.3-14 are less subtle, with acetylacetonate carbonyl resonances 178.7 and 193.6 ppm splitting into only two separate resonances, but with the methine $^{13}C\{^1H\}$ resonances at 98.86 and 99.3 ppm splitting into four well defined resonances at 99.4, 99.6, 99.9, and 100.2 ppm, mirroring the ^{1}H NMR spectroscopic experimental results.
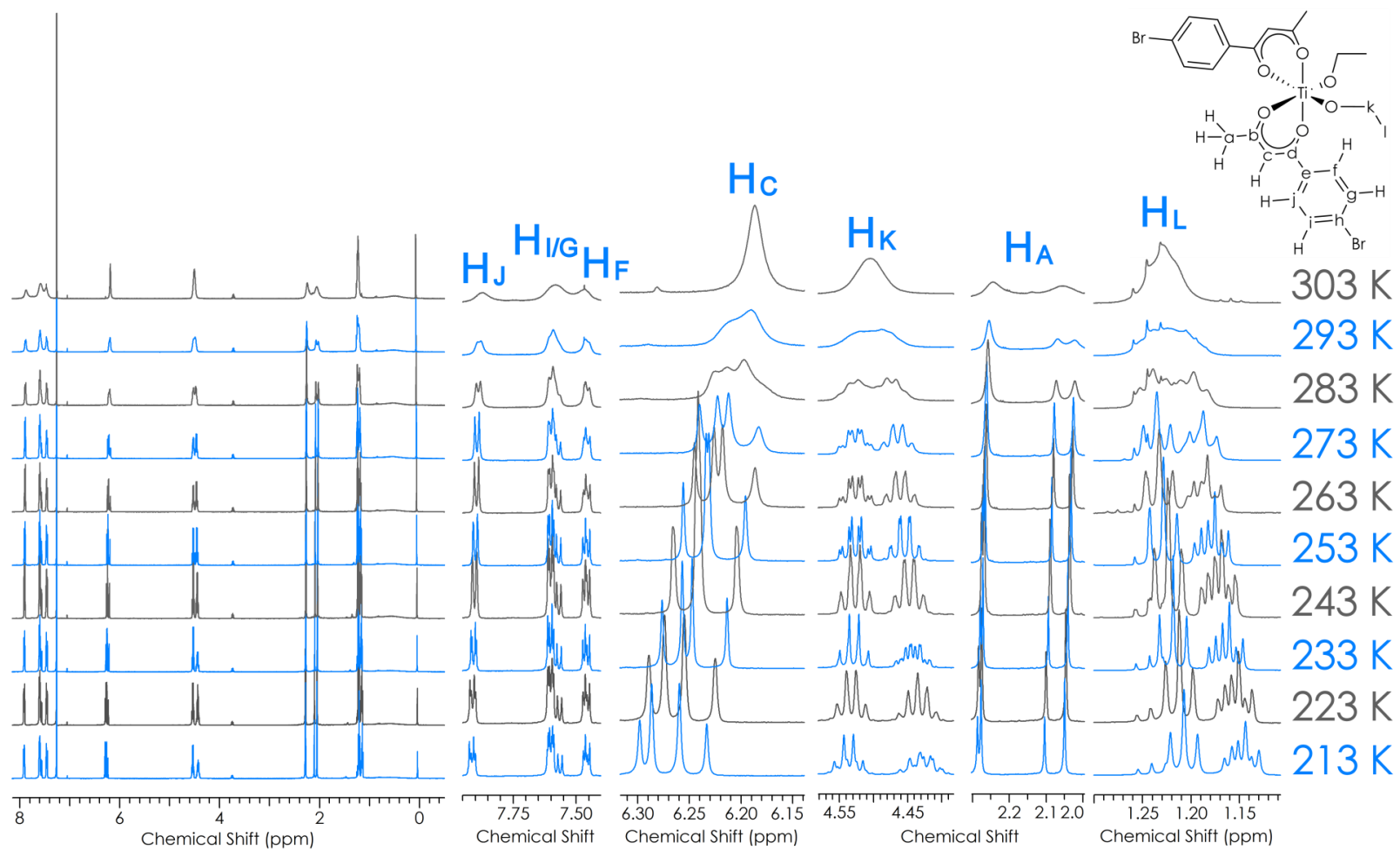
Figure 4.3-13 – Variable temperature 500 MHz ^{1}H NMR spectra of compound 6 in CDCl$_3$. Expansions provided (right) Temperatures listed against the spectra.
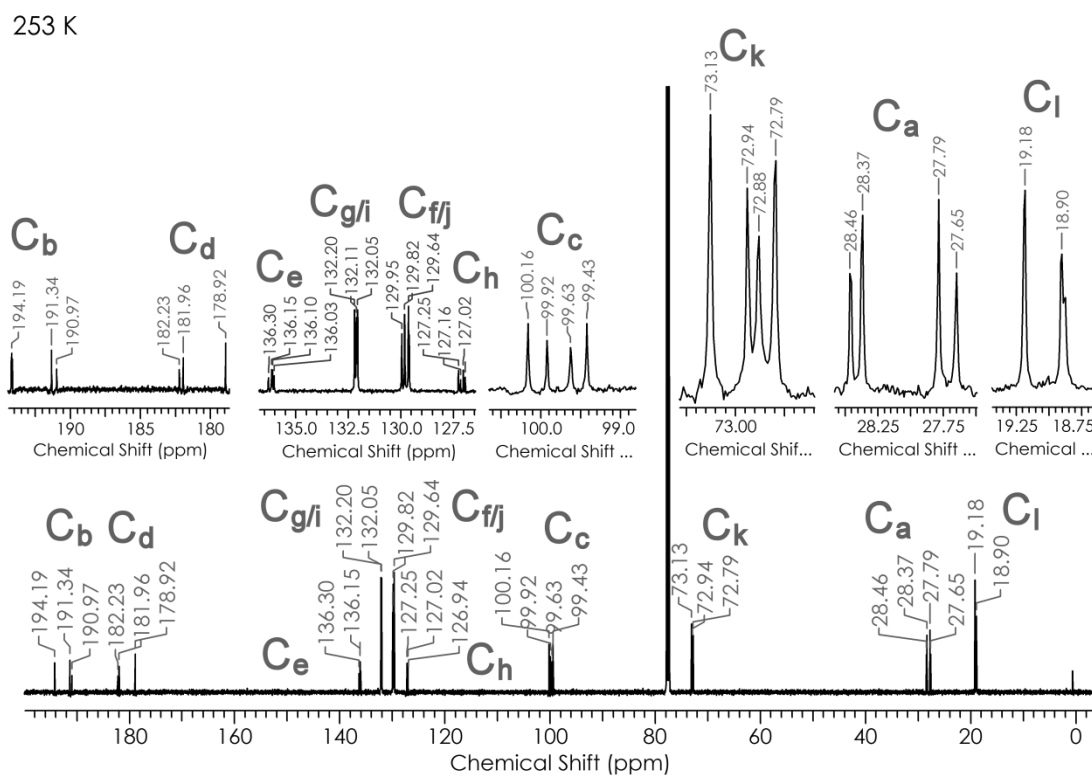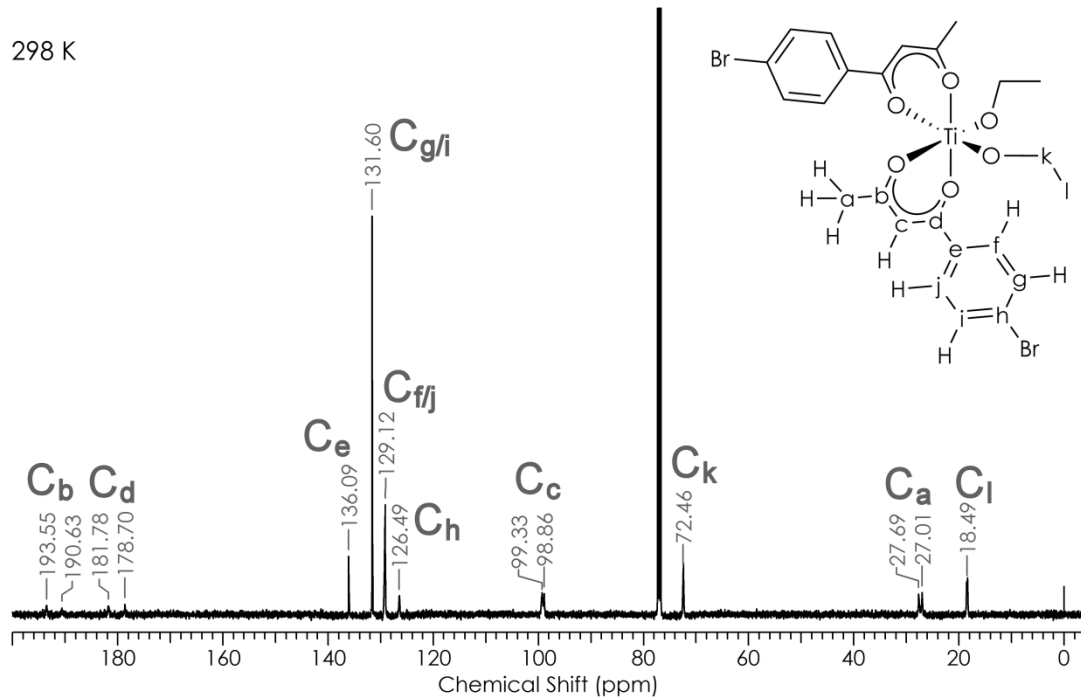
Figure 4.3-14 – 175 MHz ^{13}C{1H} NMR spectra of compound 6 collected in CDCl$_3$ at 298 K (top) and at 253 K (bottom)

4.4. Synthesis of *bis*-(4-iodophenylacetylacetonate)titanium(IV) ethoxide [Ti(4′I-Phacac)₂(OEt)₂] (Compound 7)
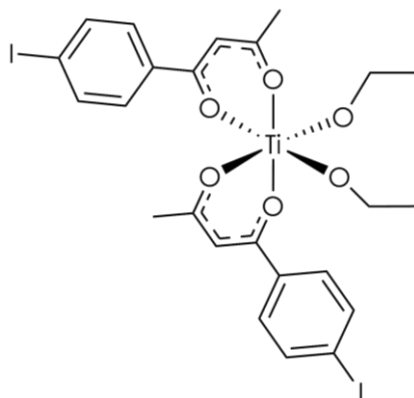
Compound 7 - *bis*-(4-iodophenylacetylacetonate)titanium(IV) ethoxide

Figure 4.4-1 - Structure of compound 7

Bis-(4-iodophenylacetylacetonate)titanium(IV) ethoxide was synthesised *via* the synthesis outlined in Scheme 4.1-1. 2 equivalents of 4'iodophenylacetylacetone was slowly added to a solution of titanium(IV) ethoxide in ethanol under rigorous anhydrous conditions. The resulting precipitate was filtered, washed with pentane and all remaining solvent removed *in vacuo*. The solid was then recrystallised from hot ethanol to yield an analytically pure brown powder.

4.4.1. NMR spectroscopic analysis of *bis*-(4-iodophenylacetylacetonate)titanium(IV) ethoxide (Compound 7)
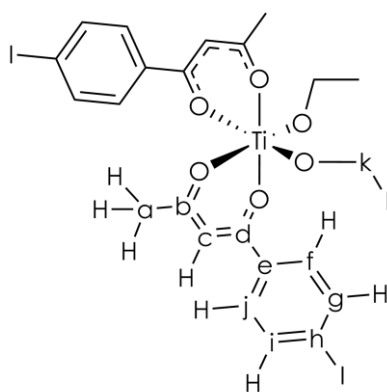
Figure 4.4-2 – Labelled structure of compound 7

The ^{1}H NMR spectrum of compound **7** shows a similar pattern to the other titanium ethoxide complexes with *para*-substituted acetylacetonate ligands, with significant signal broadening observed within the spectrum at 298 K. The acetylactetonate methyl proton signal splits into two peaks at 2.07 and 2.26 ppm, while the diagnostic methine proton remains a single broad peak. In the aromatic region there are two signals at 7.46 and 7.74 ppm with signals integrating to 3 and 1 proton respectively. The ^{13}C{^{1}H} spectrum echoes the findings of the ^{1}H spectrum, with signals for the acetylacetonate methyl and methine protons showing two separate peaks at 27.03 ppm and 27.67 ppm and 98.89 ppm and 99.31 ppm respectively.
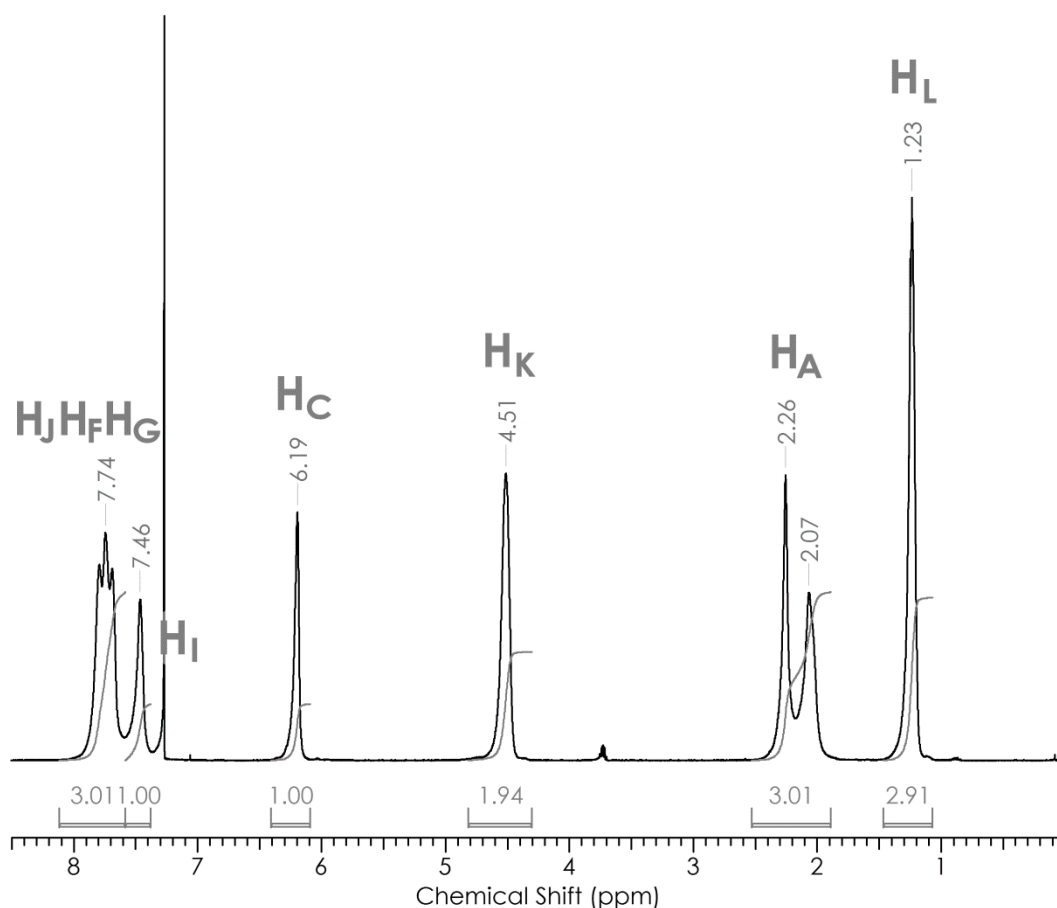
Figure 4.4-3 – 500 MHz ^{1}H NMR spectrum of compound 7 collected at 298 K in CDCl$_3$

¹H Chemical Shift (σ)	Integration, multiplicity	Assignment	¹³C Chemical Shift (σ)	Assignment
1.23 ppm	3H, s	H$_L$	18.55 ppm	l
2.07 ppm 2.26 ppm	3H, s	H$_A$	27.03 ppm 27.67 ppm	a
4.51 ppm	2H, as	H$_K$	72.42 ppm	k
6.19 ppm	1H, as	H$_C$	98.89 ppm	c
7.46 ppm	1H, as	H$_I$	99.31 ppm	c'
7.74 ppm	3H, multiplet	H$_F$, H$_G$ and H$_J$	129.13 ppm	g and i
			136.68 ppm	f
			137.62 ppm	j
			178.91 ppm	h
			182.07 ppm	e
			190.77 ppm	b
			193.67 ppm	d

Table 4.4-1 – ¹H and ¹³C{¹H} assignments of compound 7

The ¹H spectrum in Figure 4.4-3 mirrors earlier findings with the methyl group of the acetylacetonate ligand again separating into two signals which integrate to three protons only when added together. The ¹H NMR spectrum exhibits only one signal for the methine proton at 6.19 ppm suggesting, again, that there is only one type of compound present (i.e a centre containing the same number of bidentate and monodentate ligands), switching rapidly between stereochemical isomers as the broadening of the signals of the ¹H NMR spectrum indicates. The aromatic region shows a similar pattern observed in compound **5** and compound **6** where each aromatic proton exists in a different magnetic environment and, in this case, there is severe overlap of the signals.
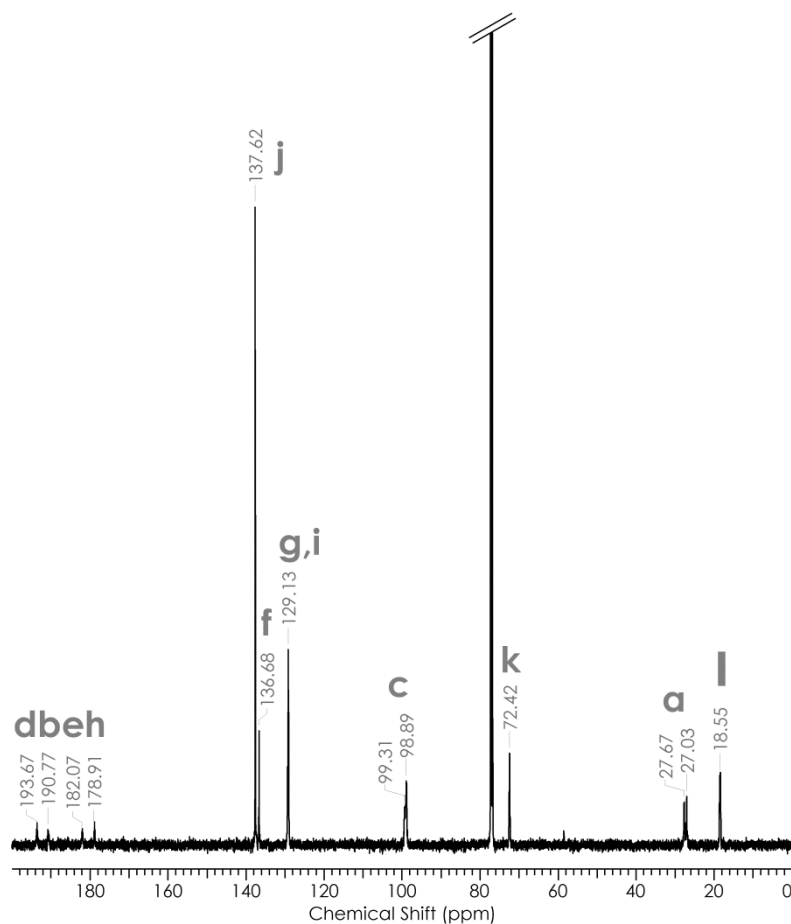
Figure 4.4-4 – 175 MHz ^{13}C{^{1}H} NMR spectrum collected at 298 K in CDCl$_3$. The CDCl$_3$ peak has been truncated

Figure 4.4-4 shows the ^{13}C{^{1}H} NMR spectrum of compound **7**. In the spectrum collected at room temperature we see two separate signals at 99.3 ppm caused by the methine carbon, suggesting two distinct magnetic environments and possibly two distinct stereoisomers within the solution, or perhaps both *cis* and *trans* binding modes of the monodentate ligand which causes the methine carbon atoms to experience such different magnetic environments. The integration of the methine peaks of the acetylacetonate ligand of the ^{1}H NMR spectrum again show a 1:1 ratio between the two peaks, suggesting either a ratio close to 1:1 of two different isomers or a methyl group which interacts closely with another atom or group to allow the protons of the methyl group to experience two different magnetic environments.

If the complex undergoes rapid interconversion between all five structural isomers of the complex equally, this may explain these observations, as there are two structural isomers with monodentate ligands in the *trans* arrangement and three with monodentate ligands in the *cis* arrangement as seen in Figure 4.1-2. The significant difference in structure

between the *cis* and *trans* arrangement of the monodentate ligands may cause two distinct signals in the NMR spectrum, while allowing for many ^{1}H signals to overlap in the NMR spectrum into the broad singlet we observe at room temperature.

Assuming equal distribution of isomers, there is a 2:3 ratio of isomers with dissimilar magnetic environments, which correlates with an approximately equal integrations of the methyl acetylacetonate signals in the ^{1}H NMR spectrum. The activation energy for rearrangement of titanium complexes with chloride monodentate ligands was found to be +47.31 kJmol[-1].[8] If the activation energy for these ethoxide complexes is of a similar magnitude it could be feasible to suggest that this rapid interconversion between all forms of the isomers may be possible.

4.5. Synthesis of *bis*-(di-1,3-methoxyphenylpropan-1,3-diketonate)titanium(IV) ethoxide [Ti(4'OEtPhacacPh4'OEt)$_2$(OEt)$_2$] (Compound 8)
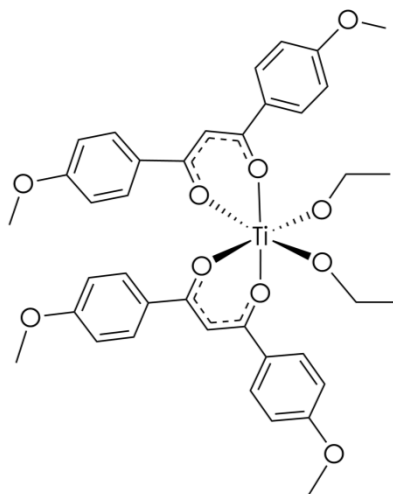
Compound 8 - *bis*-(di-1,3-methoxyphenylpropan-1,3-diketonate)titanium(IV) ethoxide

Figure 4.5-1 - Structure of compound 8

Compound **8** was synthesised using the scheme shown in Scheme 4.5-1. Two equivalents of bis(4'methoxydiphenyl)acetylacetone was slowly added to a solution of titanium(IV) ethoxide in ethanol under rigorously anhydrous conditions. The resulting precipitate was filtered, washed with pentane and all remaining solvent removed *in vacuo*. The cream solid was then recrystallised from hot ethanol in anhydrous conditions to yield an analytically pure yellow powder.
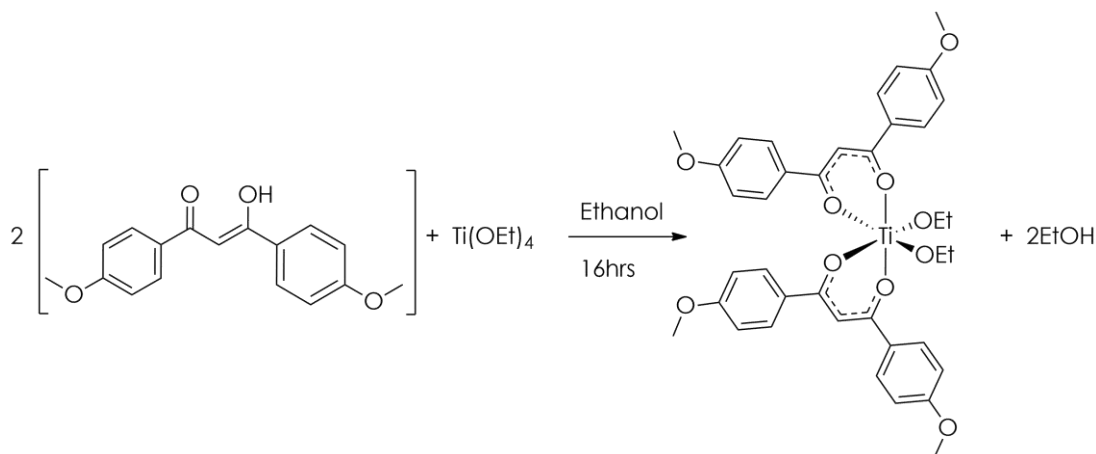
Scheme 4.5-1 – Synthesis of symmetrical *bis*-(acetylacetonate)titanium(IV) ethoxide complexes.

4.5.1. NMR spectroscopic analysis of *bis*-(di-1,3-methoxyphenylpropan-1,3-diketonate)titanium(IV) ethoxide (Compound 8)
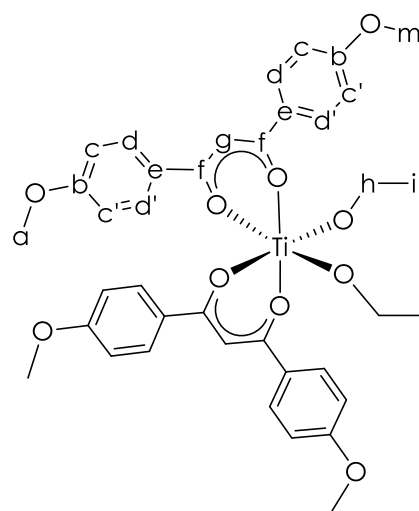
Figure 4.5-2 – Labelled structure of compound 8

Figure 4.5-4 shows the ^{1}H NMR spectrum of compound **8**. Due to the high symmetry of this molecule the spectrum is remarkably clear and even with slight broadening, the symmetry of the molecule is such that the expected triplet and quartet structure can be observed on the ethoxide proton signals at 1.26 ppm 4.57 ppm respectively, with normal coupling of around 7 Hz measured.

There are two signals at 3.78 ppm and 3.91 ppm arising from the acetylacetonate methoxy group protons. The two expected aromatic proton signals each split into two signals, one pair at 8.16 ppm and 7.78 ppm and one pair at 7.01 ppm and 6.78 ppm. The COSY

spectrum (Figure 4.5-5) shows that only one of the signal in each identified pair couples to one another, both upfield peaks at 7.78 ppm and 6.78 ppm couple and both peaks at 8.16 and 7.01 ppm couple. This may suggest that the phenyl rings of the ligand become inequivalent on formation of the complex, or that there is restricted rotation of the phenyl groups, making the protons pointing towards the titanium centre inequivalent to those pointing out.

Due to the symmetry of the acetylacetonate ligand there are now only two possible isomers of the compound. (Figure 4.5-3) So far, every *bis*-acetylacetonate complex synthesised by the McGowan group has crystallised with monodentate ligands in the *cis* position, indicating a thermodynamic stability of the *cis* isomers. The $^{13}C\{^{1}H\}$ NMR spectrum in Figure 4.5-6 shows a single signal for the methine proton of the acetylacetonate ligand at room temperature, which suggests that there is only one configuration of the monodentate ligands, so the duplication of peaks within the ^{1}H NMR spectrum might be explained by restricted rotation of the phenyl groups once complexed.
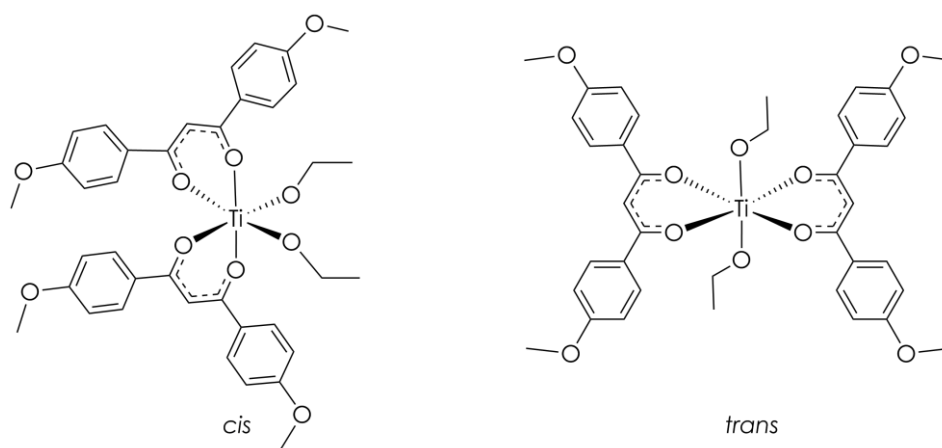
Figure 4.5-3 – Possible isomers of compound 8

The results of the ^{1}H-^{1}H COSY suggest most prominently that there is restricted rotation about the phenyl rings, and those rings on the inside experience increased deshielding from interaction with overlapping Van der Waals radii, and exhibit downfield chemical shifts in the ^{1}H NMR spectrum. The two downfield shifts couple together, meaning they are next to each other in physical space, leading to an assignment of these atoms as $H_{C'}$ and $H_{D'}$ to their counterparts pointing to the outside of the complex H_C and H_D, which experience less deshielding from the interference of the Van der Waals radii, and so exhibit upfield chemical shifts, and couple together as seen in the COSY.

The idea of restricted rotation does not explain the inequivalent OMe proton signals in the ^{1}H NMR spectrum at 3.78 ppm and 3.91 ppm. In the *cis* arrangement of ethoxide ligands shown in Figure 4.5-3, the two phenyl methoxy groups on the left of the drawing are forced close to one another by the *cis* arrangement of the Ti-O bonds to the β-diketonate ligand, while the methoxy groups where the Ti-O bonds to the β-diketonate are *trans* to one another, the groups point out into space. Again those groups which experience interference of the Van der Waals radii shift downfield, and their counterparts remain upfield. This evidence further supports the notion that the molecule retains the *cis* arrangement of monodentate ligands in solution, as the *trans* equivalent would not exhibit inequivalent OMe groups.
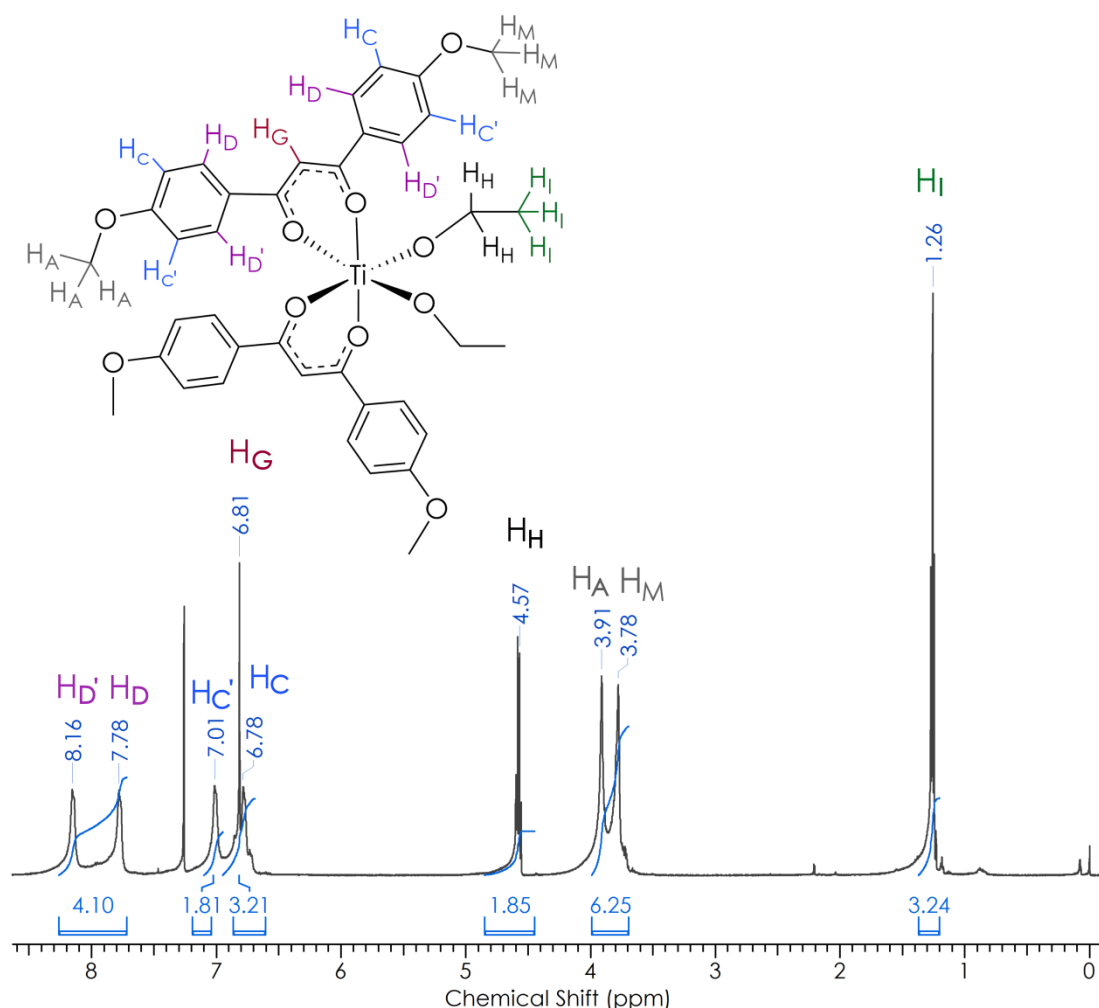
Figure 4.5-4 - 500 MHz ^{1}H NMR spectrum of compound 8 collected at 298 K in CDCl₃

^1H Chemical Shift (σ)	Integration, multiplicity	Splitting Frequency	Assignment	^{13}C Chemical Shift (σ)	Assignment
1.26 ppm	3H, t	6.9 Hz	H_I	18.70 ppm	i
3.77 ppm 3.91 ppm	6H, s		H_A	55.44 ppm	a
4.57 ppm	2H, q	7.1 Hz	H_H	71.55 ppm	f
6.78 ppm	2H, s		H_C	94.50 ppm	g
6.81 ppm	1H, s		H_G	113.54 ppm	d
7.01 ppm	2H, s		$H_{C'}$	113.70 ppm	d'
7.78 ppm	2H, s		H_D	129.66 ppm	c
8.15 ppm	2H. s		$H_{D'}$	130.47 ppm	b
				162.52 ppm	e

Table 4.5-1 – NMR spectroscopic assignments of the ^1H and $^{13}C\{^1H\}$ spectra of compound 8
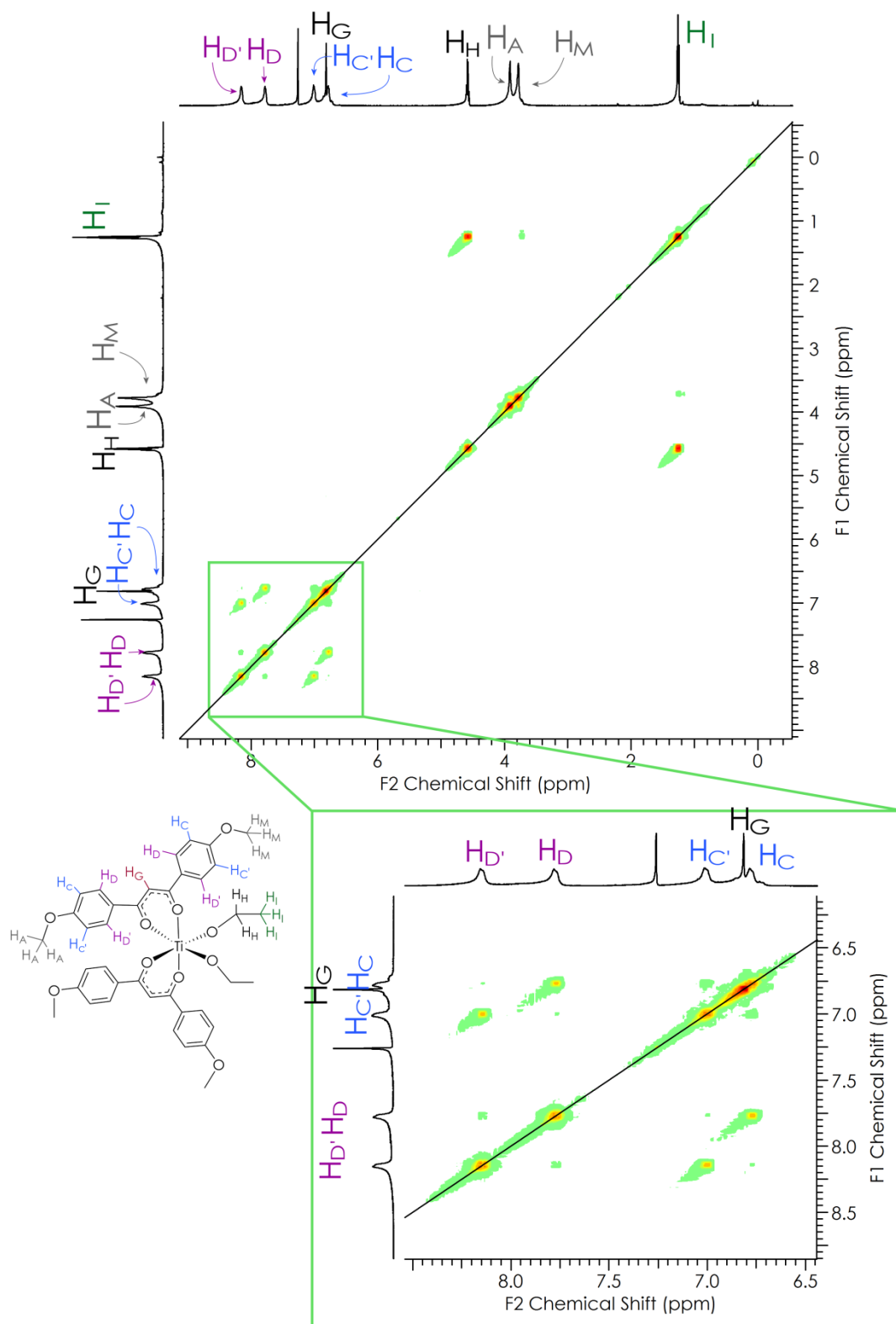
Figure 4.5-5 – 500 MHz ^{1}H COSY NMR spectrum of compound 8 collected at 298K in CDCl$_3$
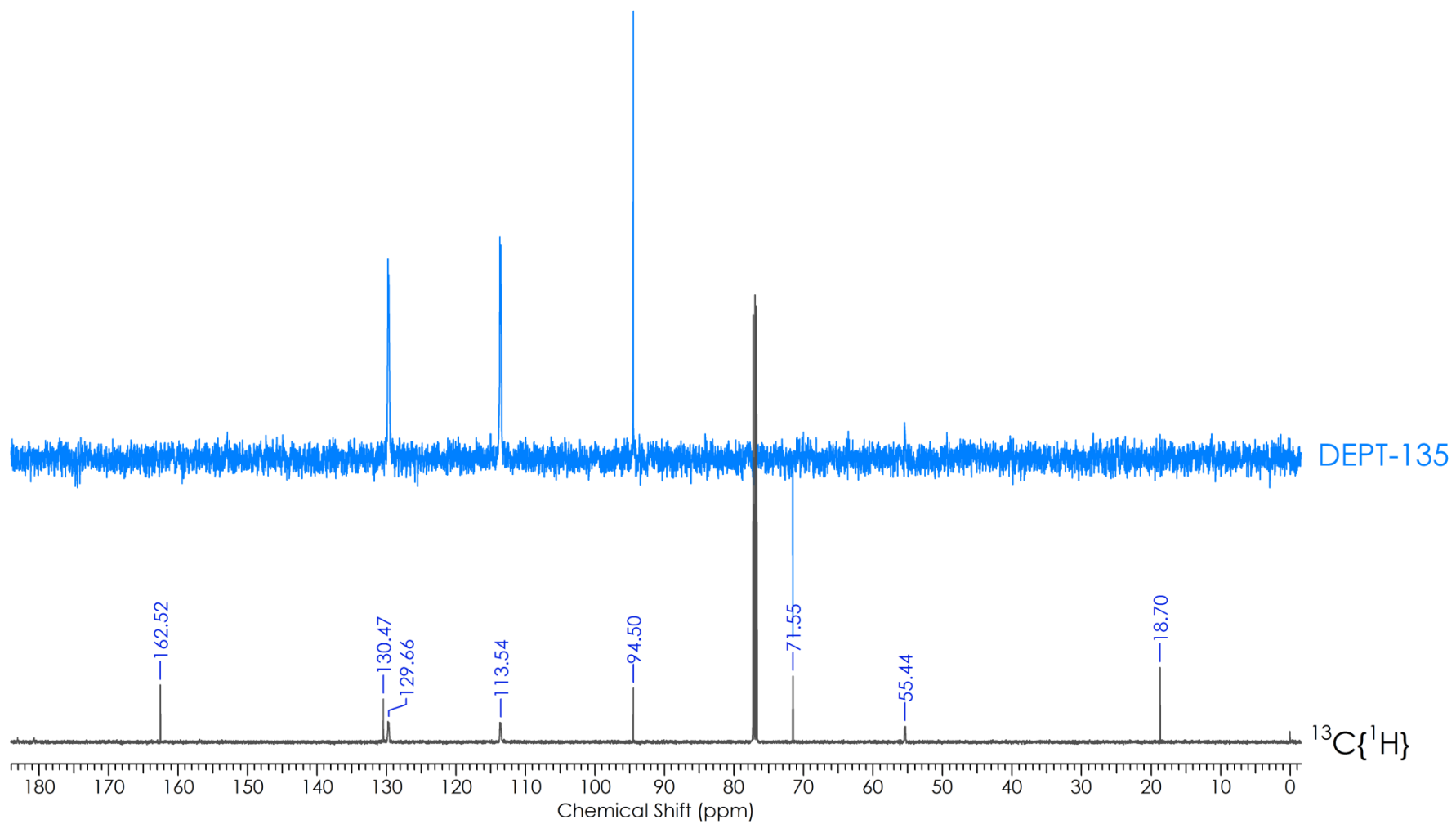
Figure 4.5-6 – DEPT-135 (top) and $^{13}C\{^1H\}$ (bottom) NMR spectra of compound 8 collected at 298 K on a 175 MHz spectrometer.

4.6. Titanium(IV) Ethoxide complexes for polymerisation of lactide

Compound **5**, compound **6** and compound **7** were found not to polymerise lactide in solution. In all three cases a solution of the compound with 200 equivalents of lactide in chloroform was unchanged after being stirred at 60 °C for 2 days and in toluene at 110 °C reflux for 1 day.

However, all three compounds were found to efficiently polymerise lactide in dry-melt conditions. A small amount of each sample was dissolved in 200 equivalents of molten lactide and stirred under anhydrous conditions at 150 °C. Each complex yielded a slightly yellow polymer after four hours of stirring and polymerisation was confirmed by ^{1}H NMR spectroscopy with all three compounds generating excellent percentage conversions over 95%.

Attempts to measure the efficiency of titanium (IV) ethoxide catalysts were made by completing polymerisations in dry melt at several temperatures. Compound **5** was mixed with 210 equivalents of L-lactide and the mixture crushed with a pestle and mortar. 10 mg samples of the mixture were added to glass vials with aluminium/PTFE crimped caps and were submerged in agitated oil at various temperatures. Three vials were removed from the oil during the polymerisation, cooled quickly and the reaction quenched with wet deuterated chloroform. This was repeated several times during the experiment.

The sample vials were stripped of identifiers and a ^{1}H NMR spectrum was collected for each sample. The area of the peaks of the ^{1}H NMR spectrum belonging to poly(lactic acid) were integrated against those belonging to unreacted lactide in a blind experiment, ensuring no influence from the author, in order to calculate a degree of conversion, and the results of the experiment are plotted in Figure 4.6-1.
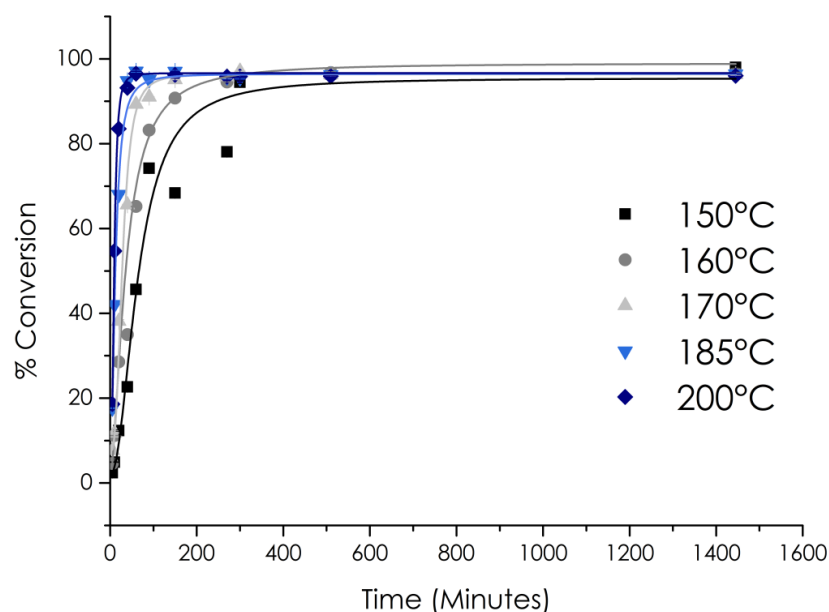
Figure 4.6-1 – Logarithmic curves of best fit showing degree of polymerisation of samples of lactide at 150 °C, 160 °C, 170 °C, 185 °C and 200 °C with a 1:210 equivalents catalyst loading of compound 5.

At all of the temperatures used in this experiment, compound **5** polymerises lactide to give final degrees of conversion around 97 % (Table 4.6-1).

As the temperature of the polymerisation conditions is increased, the time taken for the catalyst to convert 50% of the lactide into poly(lactic acid) (EC_{50}) decreases, indicating an increased rate of polymerisation with increasing temperature. Figure 4.6-2 shows the change in EC_{50} as temperature increases, showing an exponential decrease in the amount of time taken to convert 50% of the lactide into poly(lactic acid) and so a logarithmic increase in rate of polymerisation with temperature.

Temperature	EC_{50}	Degree of conversion (%)	Error		
150 °C	66.4 min	97.90	±	0.09	%
160 °C	35.8 min	96.67	±	0.19	%
170 °C	27.6 min	96.28	±	0.16	%
185 °C	12.0 min	96.40	±	0.02	%
200 °C	9.3 min	96.01	±	0.25	%

Table 4.6-1 – EC_{50} Time taken for a 1:200 equivalents catalyst loading of compound 5 to lactide to reach 50% conversion at a range of temperatures.
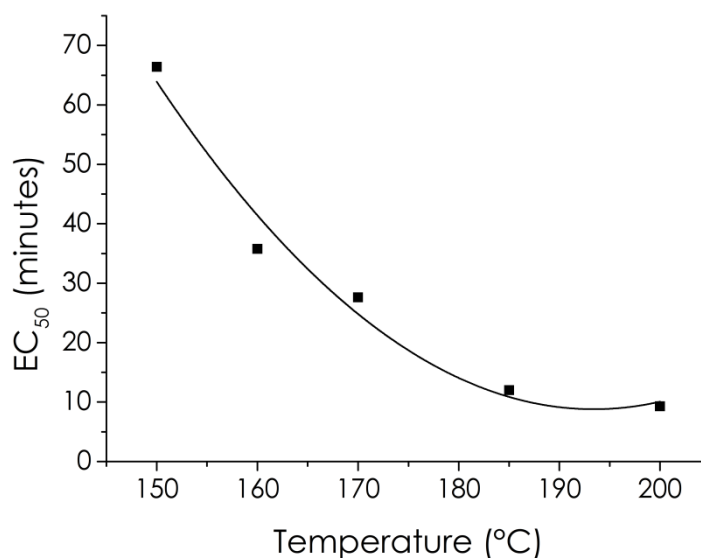
Figure 4.6-2 – Change in the rate of polymerisation with varying temperature of compound 5 with 210 equivalents of lactide.

At the fastest rate, compound **5** was found to have a turnover number of 0.13 molecules/second for the polymerisation of lactide, which represents moderate catalytic ability. The best organic catalysts in the literature generating turnover numbers of up to 1,000,000 molecules/second,[20] but most good catalysts having a turnover number of 10-50 molecules per second.

While titanium (IV) ethoxide complexes might seem to have poor performance for the polymerisation of lactide, the intersection of this ability with the anti-cancer activity of the complexes may enhance the desirability of using titanium (IV) ethoxide complexes to synthesise metal dispersed polymers.
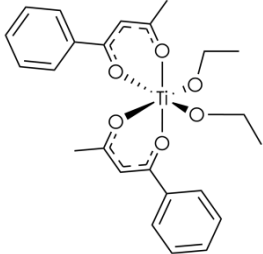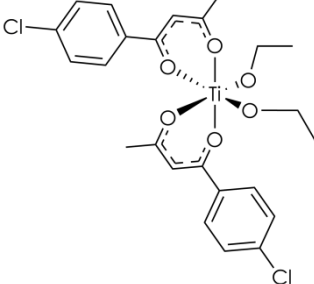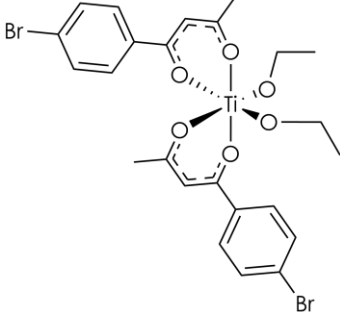
4.7. *In vitro* cell line testing of *para*-substituted budotitane derivatives

Recent work in the McGowan group has focussed on finding relationships between the structure of group IV β-diketonate drugs and their *in vitro* efficacy against many cancer cell lines.

Work undertaken by Dr. Benjamin Crossley and Dr. James Mannion in the group found that titanium(IV) complexes containing halide and *bis*-β-diketonate ligands to be particularly effective in causing cell death of the A2780 human ovarian carcinoma cell-line, with bromide ligands being seemingly the most effective for titanium metallodrugs containing *para*-substituted acetylacetonate ligands, and ethoxide ligands performing equally well within error of the experiment.[3, 18]

Tshuva *et al* recently reported that source titanium alkoxide and chloride compounds, $Ti(O^iPr)_4$ and $TiCl_4(THF)_2$, were not active against cancer cell lines due to the high rate of aggregate formation in normoxic and aqueous conditions *in vitro*.[21]

A series of *para*-substituted drugs were synthesised by the author and tested for cytotoxic activity against the HT-29 ovarian cancer cell line by Dr Aida Basri at the institute of cancer therapeutics, University of Bradford, with low IC_{50} values representing complexes which are able to cause effective cell death at low concentrations. (Table 4.7-1)

Drug	IC_{50}
Cis-platin	3.2 ± 0.3 μM
 Budotitane **Compound 9 – Budotitane**	25.6 ± 0.3 μM IC_{50} test compound/ IC_{50} *cis*-platin $= 8.0$ Somewhat active
 Bis-4'chlorophenylacetylacetonatetitanium(IV) ethoxide first prepared by Benjamin Crossley at the University of Leeds.	30.73 ± 0.9 μM IC_{50} test compound/ IC_{50} *cis*-platin $=9.6$ Somewhat active
 Bis-4'bromophenylacetylacetonatetitanium(IV) ethoxide **Compound 6**	27.5 ± 0.8 μM IC_{50} test compound/ IC_{50} *cis*-platin $= 8.6$ Somewhat active
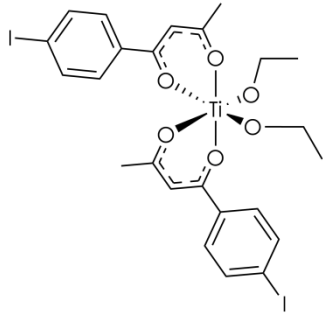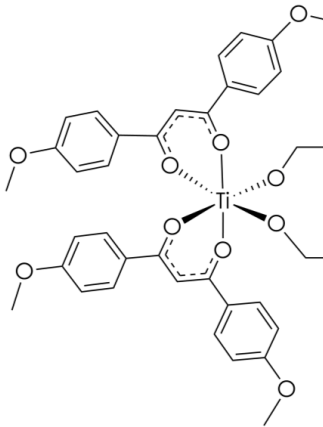
 Bis-4'iodophenylacetylacetonatetitanium(IV) ethoxide **Compound 7**	25.7± 0.2 µM IC_{50} test compound/ IC_{50} *cis*-platin = 8.0 Somewhat active
 Compound 8	> 100 µM Inactive

Table 4.7-1 – IC_{50} values of a series of *para*-substituted Budotitane derivatives.

During cell line testing, a series of wells of cells are exposed to varying concentrations of the compound under investigation, with row of wells untreated to act as a control against the drug. The cells are provided growth medium and are incubated for 3 days while exposed to the drug. After exposure the cells undergo the MTT assay, described in section 1.3.1. Cells which are alive convert yellow MTT into a purple formazan compound. A UV/vis spectrometer is used to calculate the degree of conversion of the MTT compared to the control wells, and the concentration of the drug exposure can be plotted against the degree of cell death to find the IC_{50} value of the drug. The cell line results show that there is little electronic contribution to the activity of the titanium ethoxide complexes, as adding withdrawing halides in the *para* position of the phenylacetylacetonate ligand seems to have had very little effect on the IC_{50} values of these complexes when compared to a non-substituted drug like Budotitane (compound **9**). There is also no observable trend in the activity of the drugs against the decreasing withdrawing strength of the *para*-substituted chlorine, bromine and iodine complexes as you might expect if electronics

were to play a large part activating or deactivating the activity of the drug, nor the steric effects of the larger halides atoms on the phenyl ring. The complexity of even this basic biological system makes it difficult to hypothesise as to the efficacy of the shape and electronics of the complex, and so further work to continue building a library to obtain large amounts of data is needed.

Compound **6** and compound **7** were found to have moderate anti-cancer activity, with required dosages around 8 times the required dosage of *cis*-platin to cause cell death of 50% of the population exposed.

Compound **8** was found to be inactive against the HT-29 human ovarian cancer cell line with concentrations of compound 8 exceeding 100 µmoldm^{-3} and exhibiting essentially no cytotoxic activity. This may be due to the sensitivity of the complex to oxygen, or this may be an indication of an unusual configuration of compound **8** causing it to have reduced activity compared to the asymmetrical phenylacetylacetonate ligands.

4.8. Mechanistic studies of the interconversion of isomers of the titanium ethoxide complexes

The broad signals of the ^{1}H NMR spectra of the titanium (IV) ethoxide complexes in this chapter raises the questions;

- How many isomers exist in solution?
- During the mechanism of interconversion of the structural isomers of the complexes, does the acetylacetonate ligand partially or completely dissociate?

4.9. Mechanism of interconversion of titanium ethoxide complexes

The McGowan group has previously studied the interconversion of the different possible isomers of asymmetrical biacetylacetonatetitanium halide complexes. Work undertaken by Dr Andrew Hebden found that when *bis*-(phenylacetylacetonate)titanium(IV) chloride and *bis*-(4-fluorophenylacetylacetonate)titanium(IV) chloride were mixed in CDCl$_3$, a ligand exchange reaction occurred during which the two separate compounds formed (phenylacetylacetonate)(4-chlorophenylacetylacetonate)titanium(IV) chloride. The reaction was observed by NMR spectroscopy *in situ*. [17]
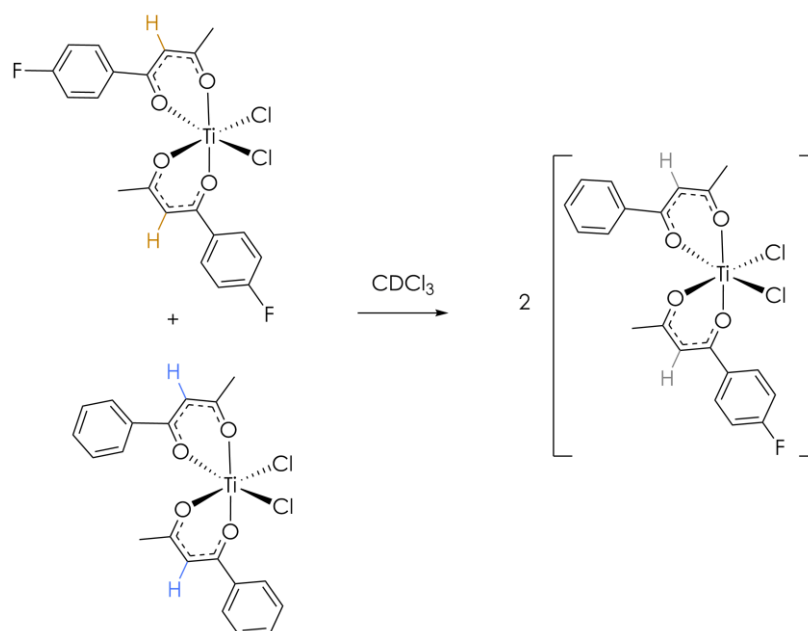
Figure 4.9-1 – Ligand exchange reactions of *bis*-(acetylacetonate) titanium chloride complexes. *Bis*-(4-chlorophenylacetylacetonate)titanium(IV) chloride (top left) and *bis*-(phenylacetylacetonate)titanium(IV) chloride (bottom left) are mixed together in deuterated chloroform to form a cross-product (right)

During the experiment the methine protons of the two complexes initially exhibited two separate, well defined chemical shifts, separated by 0.06 ppm. During the course of the experiment the two methine signals were found to coalesce into one single signal with a chemical shift halfway between the two original chemical shifts. This proves that, for *bis*-acetylacetonate titanium chloride complexes, the mechanism for interconversion can include complete dissociation of the acetylacetonate ligand from the metal centre. The group have suggested that this process is acid-catalysed, which can be formed from photolysis of the CDCl₃. Equally, any trace acetylacetone ligands left from the synthesis can also act as weak acids and may allow the catalysis of the ligand exchange reaction. In order to further investigate this phenomenon bis(phenylacetylacetonate)titanium(IV) ethoxide (compound **9**) and bis-(4'fluorophenylacetylacetonate)titanium(IV) ethoxide (compound **5**) were mixed together in distilled, dry deuterated chloroform in a Young's NMR tube as described in Scheme 4.9-1. Several ^{1}H NMR spectra of the mixture were recorded as the mixture was left for 3 days to react (Figure 4.9-2).

As the titanium ethoxide complexes are basic, the concentration of acid available to catalyse a ligand exchange reaction is low. Over the course of several days there is no cross product methine peak observed upon mixing of the ethoxide complexes, unlike the effect which is observed with the analogous titanium chloride complexes. However, the peaks of the spectrum remain broad, suggesting rapid intramolecular conversion of the compounds between isomers. This suggests that the mechanism of interconversion does

not require that a β-diketonate completely dissociate from the complex in order to allow the interconversion of the complexes, and instead may only require a single oxygen atom to dissociate.
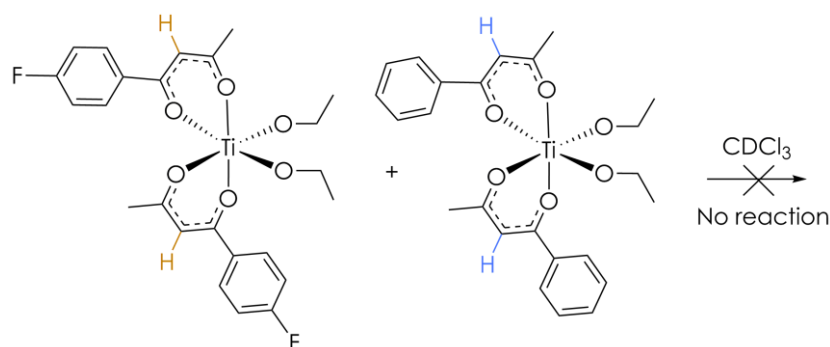
Scheme 4.9-1 – Ligand exchange reactions of *bis*-(acetylacetonate) titanium ethoxide complexes. *Bis*-(4-fluorophenylacetylacetonate)titanium(IV) ethoxide (left) and *bis*-(phenylacetylacetonate)titanium(IV) chloride (right) are mixed and no reaction is observed

It can also be observed that the intensity of the peaks reduces over time even when the number of scans in the experiment remains constant. The solution was found to change colour, beginning a light yellow colour and ending a light green.

The loss of intensity may be caused by a process by which the titanium(IV) is reduced to titanium (III) and becomes paramagnetic. This causes the chemical shifts of the protons of the magnetic complex to move into much higher chemical shifts. A spectrum with broad scan width was collected, however no additional peaks to those displayed in Figure 4.10-1 were observed. As time elapses an additional peak forms in the spectrum at 9.80 ppm suggesting the formation of an aldehyde, with the peak having a quartet structure. This suggests that during the process the ethoxide ligand is oxidised to ethanal. A low sweep scan of the mixture showed that there is no hydride formed during the process.

Similar experiments were performed with the pure complexes and the same phenomenon of colour change and reduced signal intensity in ^{1}H NMR spectra was observed. compound **5**, compound **6** and compound **7** were all found to exhibit similar behaviour when left in sunlight, with no change in the spectra observed when the sample was kept in the dark for several weeks, but when the compound was exposed to sunlight the indicative change in colour was observed and formation of the aldehyde observed in the ^{1}H spectra. It is not suggested that sunlight may initiate the interconversion of isomers of the complexes, as even in the dark, the titanium ethoxide complexes exhibit broad shifts in their ^{1}H NMR spectra.
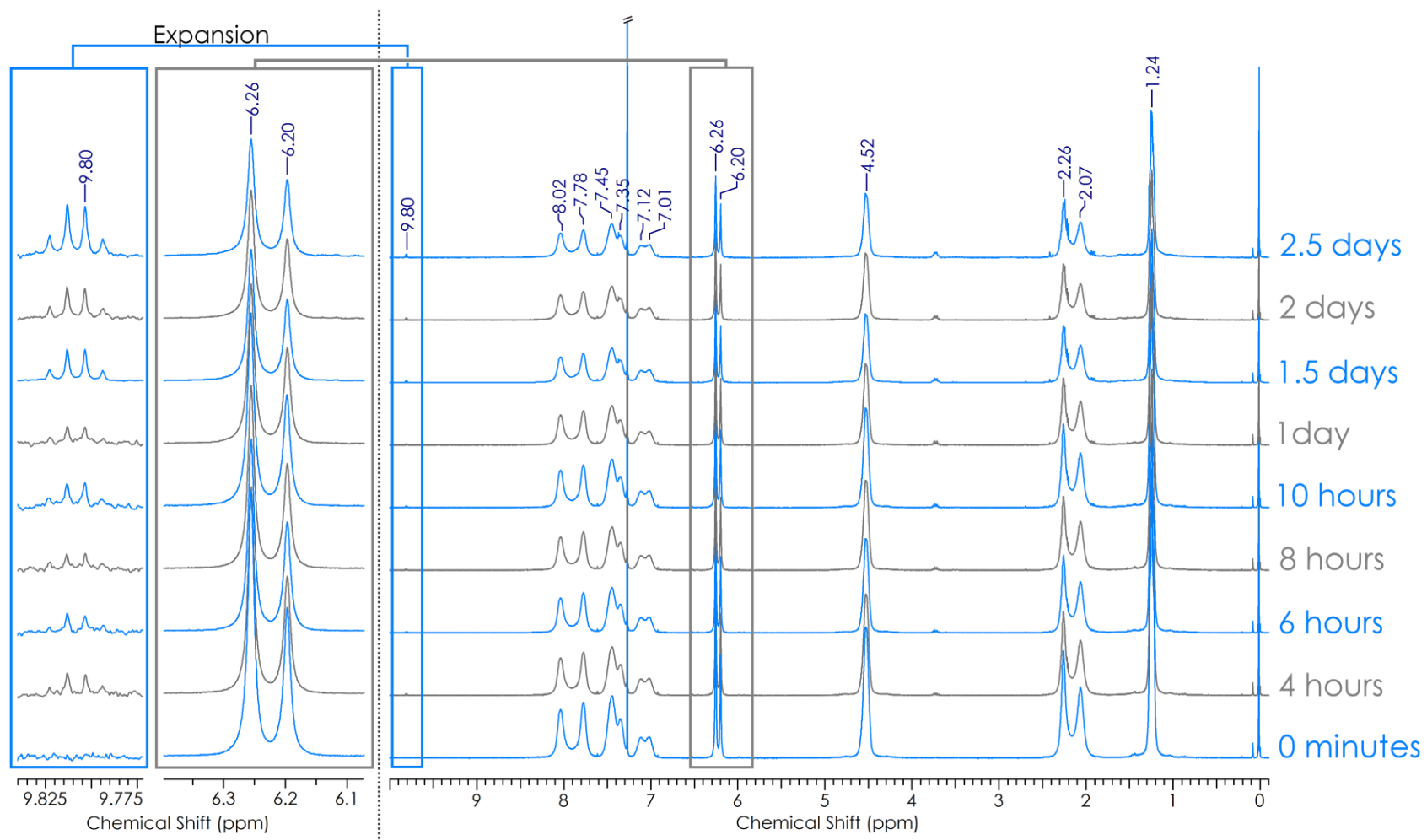
Figure 4.9-2 – *In situ* ^{1}H NMR spectroscopy mechanistic study of a mixture of compound 5 and compound 9

4.9.1. Attempted polymerisation with reduced titanium (IV) species

An anhydrous solution of compound **5** in deuterated chloroform was exposed to sunlight for 1 day until a colour change was observed. One thousand equivalents of lactide were added to the solution, maintaining the anhydrous conditions in the solution. The solution was further exposed to sunlight for two days and a ^{1}H NMR spectrum was collected.
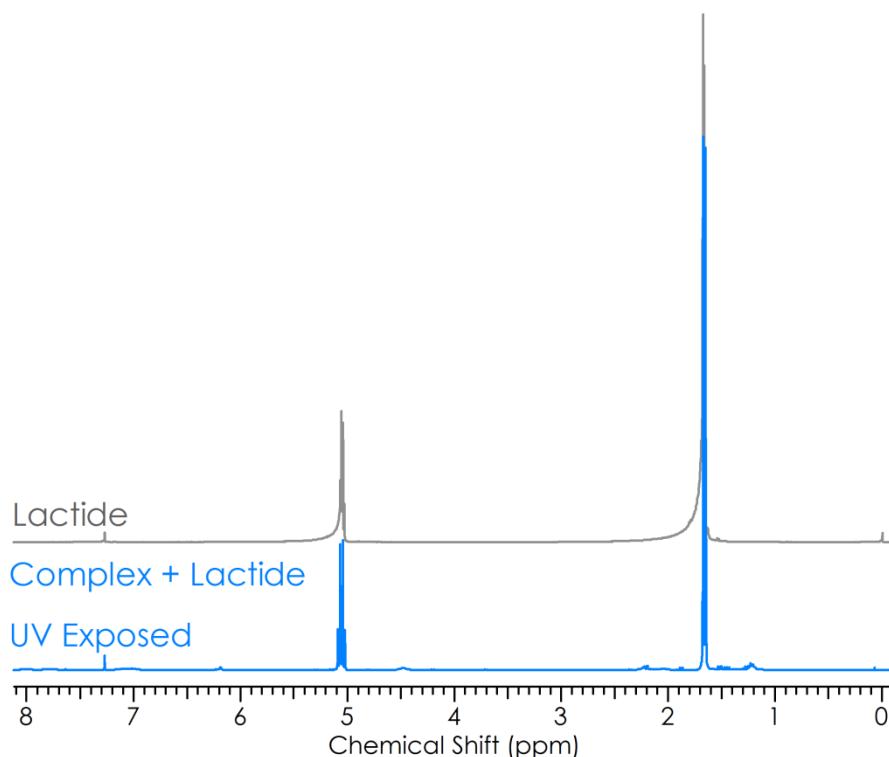
Figure 4.9-3 - ^{1}H NMR spectrum of a UV exposed mixture of compound 5 and lactide (bottom) and ^{1}H NMR spectrum of lactide (top) in CDCl$_3$ collected at 300 MHz

The ^{1}H NMR in Figure 4.9-3 shows that despite UV 'activation', the resulting titanium complex remains inactive for the polymerisation of lactide at room temperature in solution.

4.10. Possible oxygenated products

Titanium alkoxide complexes are well known to the group to degrade in aqueous or normoxic conditions. The complexes are prepared in rigorously anhydrous conditions, but *in vitro* cell line testing is carried out in a normoxic atmosphere, usually exposing the drugs to water and oxygen for several days. As such, if a drug shows activity even in these environments the oxygenated product may also be reactive. Compound **8** was exposed to oxygen during recrystallisation. Crystals of the oxygen-exposed product of compound **8** were collected and stored under oil. A crystal structure of the crystals was obtained, though the quality of the crystals were such that it was not possible to resolve the initial solution fully. However the data was of sufficient quality to solve, and can give some idea of the connectivity of the product of the oxidation of compound **8.**
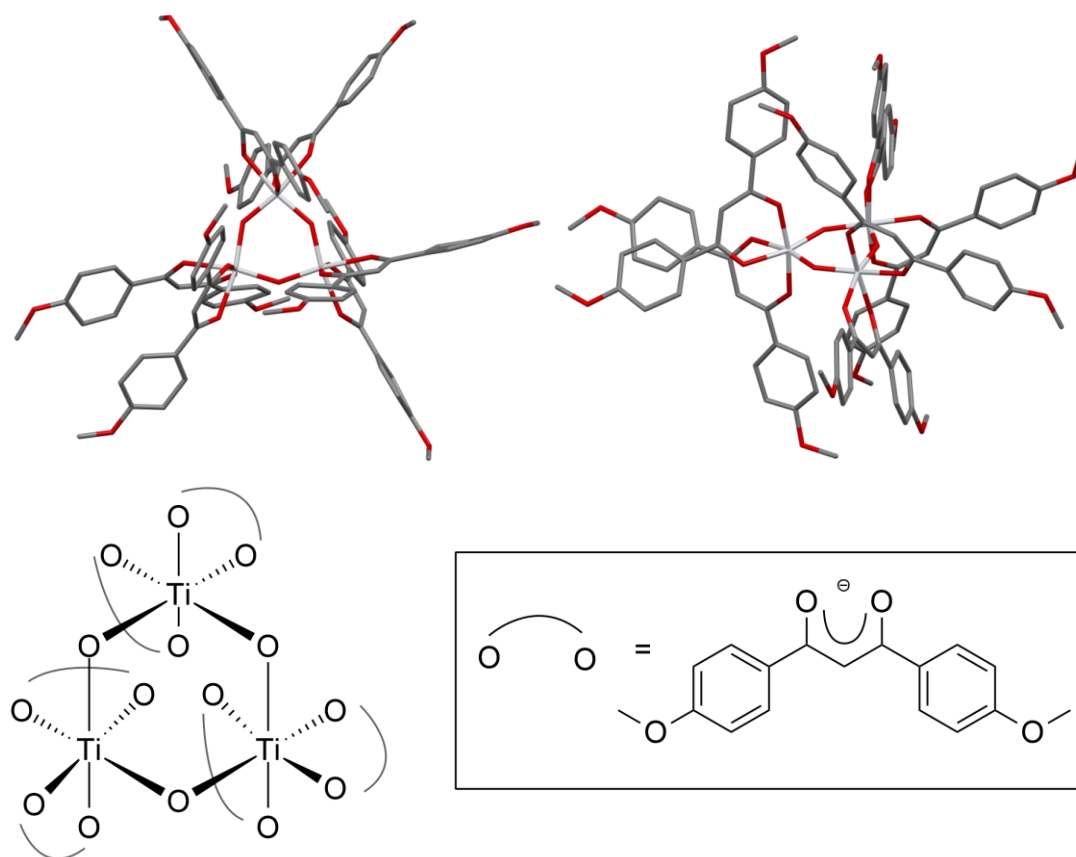
Figure 4.10-1 – Structure solution of the oxygenated product of compound 8. (Hydrogen atoms omitted for clarity)

Figure 4.10-1 shows the initial solution of the crystal data. The product is a trimer comprising of three titanium centres with three oxide bridges to form a six-membered ring of Ti-O bonds. Each titanium centre remains chelated to two β-diketonate ligands, suggesting that the coordination of the chelating ligands is air and water stable. The metal centre has a *cis* configuration with respect to the oxide bridge, leaving each metal centre reasonably protected by the steric bulk of the ligands around the metal centre. This result suggests that when titanium (IV) ethoxide complexes are exposed to air and water *in vivo* they may not necessarily form large aggregate structures, and instead could form small molecules.

While the structure is not resolved enough to measure bond angles with accuracy, an idea of the magnitude of the angles can be obtained. Figure 4.10-2 shows an expansion of a view of the crystal structure, showing the central 6 membered Ti-O-Ti ring and typical bond angles around the oxygen atoms and aluminium atoms. In this case the oxygen atom is expected to bond in an sp^3 hybridised manner, to give an expected Ti-O-Ti bond angle of 109°. In this structure this angle is much wider than expected, measuring around 143°. The structure exhibits Ti-O bonds of approximate length 1.80 Å, which is similar to the Ti-OEt bond lengths observed in the crystal structures of compound **5** and compound **6** without

any particular constraints on the bond lengths. The O-Ti-O bond length measures approximately 99 ° which is significantly larger than the expected 90 ° for an octahedral complex. This large deviation from typical bond angles in the geometries found in this structure must be driven by the required bond lengths, which seem to be typical of Ti-O single bond lengths.
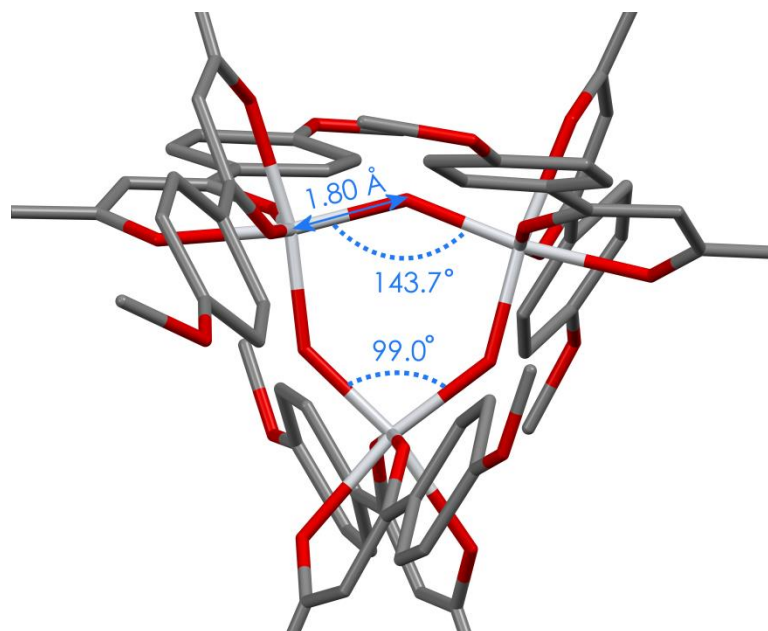
Figure 4.10-2 – Truncated view of the Ti-O-Ti ring of the oxygenated product of compound 8. Titanium – light grey   Oxygen - red

4.11. **Attempted syntheses**

During this project many target compounds were identified and many syntheses were attempted. During purification, it was often found that solids of the target molecules would form glasses, solids which appear crystalline, but have no long range order, or into powders. Several solvent systems were identified as likely candidates for recrystallisation systems, with medium polarity solvents such as ethanol and chloroform achieving the most success. The following two compounds crystallised within oils of the compound, and as such while the compounds were successfully synthesised, additional characterisation of the compounds was not possible due to the small amount of product isolated.

4.11.1. Synthesis of *bis*-(4-methylphenylacetylacetone)Titanium(IV) ethoxide [Ti(4'MePhacac)$_2$(OEt)$_2$] - compound 10
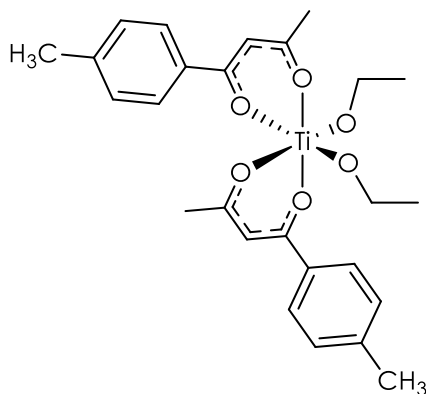
Compound 10 - *bis*-(4-methylphenylacetylacetone)Titanium(IV) ethoxide

Figure 4.11-1 - Structure of compound 10

Bis-(4'methylphenylacetylacetonate)titanium(IV) ethoxide (compound **10**) was synthesised *via* the scheme outlined in Scheme 4.1-1. To a solution of titanium(IV) ethoxide under anhydrous conditions, 2 equivalents of 4-methylphenylacetylacetone was added drop wise in ethanol solution with vigorous stirring. The mixture was stirred for 16 hours. The resulting oil was isolated *in vacuo*. Attempts to purify the compound by recrystallisation from ethanol, chloroform, diethylether and vapour diffusion of pentane into chloroform at - 20 °C were unsuccessful. An aliquot of the pure oil of the compound was left in the fridge for several months. On returning inspection of the flask small brown crystals suitable for X-ray had formed in the oil.

The crystal structure was collected and solved by Dr. Christopher Pask using an Agilant SuperNova diffractometer at 250 K. The reason for the relatively high temperature collection is that the crystals of compound **10** were found to fracture at the usual collection temperature of 100 K. The crystal structure of the compound shows significant disorder around the ethoxide ligands, with one of the ethoxide ligands being solved in two parts, and the other being solved in three parts. The asymmetric unit contains one whole molecule, and the unit cell is monoclinic, in the P2$_1$/C space group, leading to four whole molecules in the unit cell. There is very little disorder around the acetylacetonate ligand, and the overall structure solution has an R$_1$ of 6.97 % and R$_{int}$ of 5.99 %
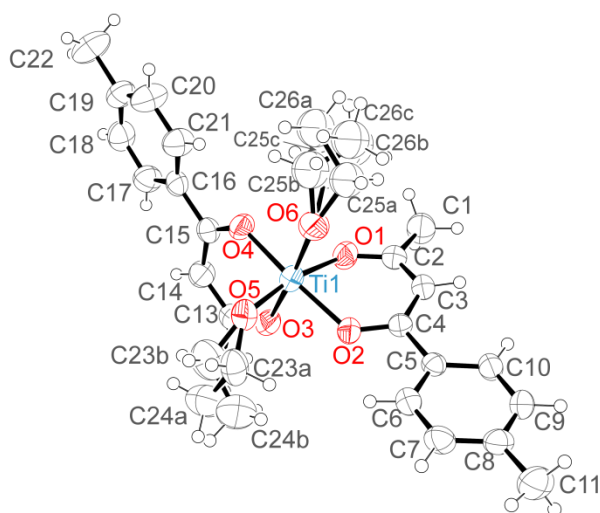
Figure 4.11-2 - ORTEP diagram of the asymmetric unit of with ellipsoids displayed at the 50% probability level

The crystal structure of compound **10** exhibits a very large ethoxide-ethoxide angle of 100.87°, comparable to those already observed from cis-ethoxide complexes earlier in this chapter. The bite angle of the acetylacetonate ligand is 82.62° suggesting a relatively strained ligand interaction with the titanium centre in the solid state. The remaining unconstrained angle around the titanium centre, the angle between the ethoxide oxygen atom and the nearest acetylacetonate oxygen atom, is fairly large at 98.14° compared with the expected 90° angles expected in a true octahedral complex. Again this complex exhibits a large empty coordination sphere, and the complex exhibits *cis-trans-cis* configuration.
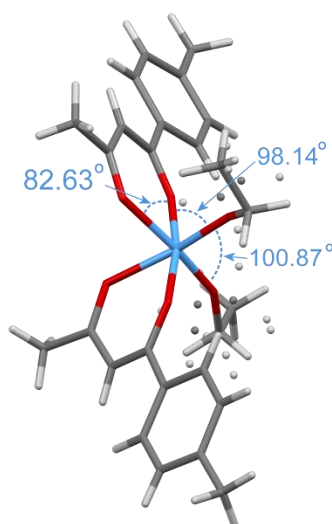
Figure 4.11-3 – Capped stick model of compound 10 with annotated bite angles of the acetylacetonate ligand
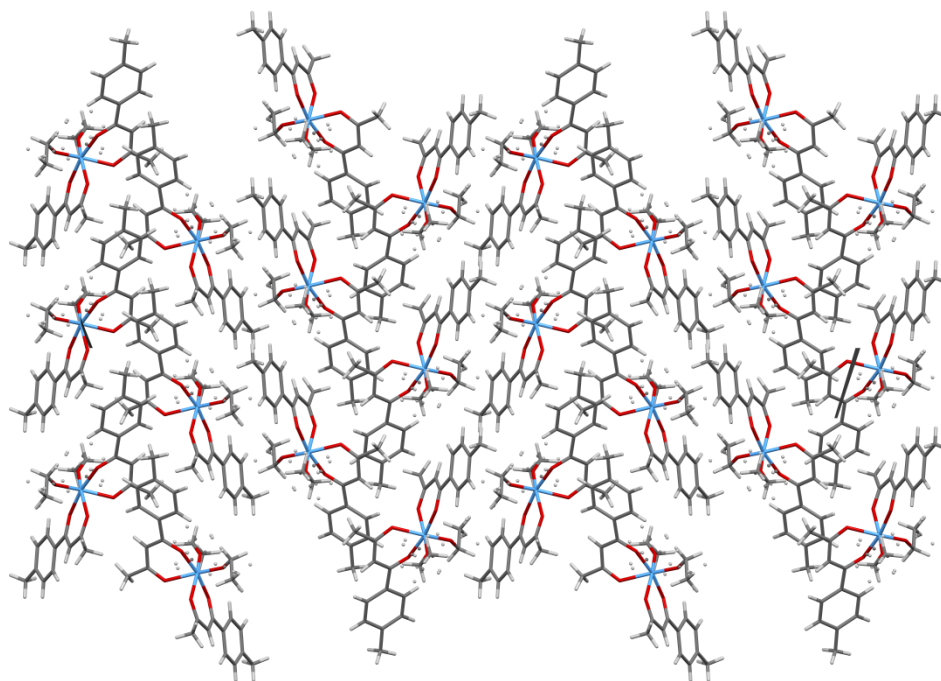
Figure 4.11-4 - Crystal packing of compound 10 viewed down the a-axis of the crystal structure.

In the solid state, compound **10** exhibits a steep herringbone packing when viewed down the a-axis of the unit cell, but seems not to have any π or T-stacking interactions (Figure 4.11-4). This finding mirrors the crystal packing of compound **5** despite the lack of hydrogen bonding interactions.

Ti(1)-O(1)	2.060(2) Å	Ti(1)-O(2)	1.9939(19) Å
Ti(1)-O(3)	2.057(2) Å	Ti(1)-O(4)	2.006(2) Å
Ti(1)-O(5)	1.795(2) Å	Ti(1)-O(6)	1.790(2) Å
O(1)-C(2)	1.268(3) Å	C(1)-C(2)	1.498(4) Å
O(2)-C(4)	1.289(3) Å	C(2)-C(3)	1.394(4) Å
O(3)-C(13)	1.253(4) Å	C(3)-C(4)	1.387(4) Å
O(4)-C(15)	1.268(3) Å	C(4)-C(5)	1.491(4) Å
O(5)-C(23a)	1.406(9) Å	O(5)-C(23b)	1.412(11) Å
C(5)-C(6)	1.391(4) Å	C(5)-C(10)	1.394(4) Å
O(6)-C(25a)	1.419(15) Å	O(6)-C(25b)	1.405(11) Å
O(6)-C(25c)	1.509(12) Å	C(6)-C(7)	1.380(4) Å
C(7)-C(8)	1.382(5) Å	C(8)-C(9)	1.381(4) Å
C(8)-C(11)	1.510(4) Å	C(9)-C(10)	1.380(4) Å

144

C(12)-C(13)	1.500(4) Å	C(13)-C(14)	1.393(4) Å
C(14)-C(15)	1.389(4) Å	C(15)-C(16)	1.500(4) Å
C(16)-C(17)	1.377(4) Å	C(16)-C(21)	1.370(4) Å
C(17)-C(18)	1.371(4) Å	C(18)-C(19)	1.372(5) Å
C(19)-C(20)	1.368(5) Å	C(19)-C(22)	1.505(4) Å
C(20)-C(21)	1.399(5) Å	C(23a)-C(24a)	1.512(13) Å
C(23b)-C(24b)	1.463(13) Å	C(25a)-C(26a)	1.489(17) Å
C(25b)-C(26b)	1.40(2) Å	C(25c)-C(26c)	1.451(18) Å

Table 4.11-1 - Interatomic distances for compound 10 with standard uncertainties listed in parentheses

Table 4.11-1 shows bond lengths within the structure. The structure shows the aromatic C-O bonds in the acetylacetonate ligand to have lengths of 1.268(3) Å, 1.253(4) Å, 1.289(3) Å and 1.268(3) Å. These lengths are much shorter than the single C-O sigma bonds in the OEt ligands whose lengths are reported to be 1.406(9) Å, 1.419(15) Å, 1.509(12) Å, 1.412(11) Å and 1.405(11) Å.

4.11.2. Crystallographic analysis of *bis*-(1,3-diphenylpropan-1,3-diketonate)titanium(IV) ethoxide [Ti(1,3-diphenylpropan-1,3,diketonate)$_2$(OEt)$_2$] (Compound 11)
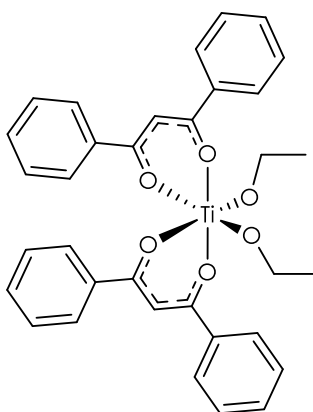
Compound 11 - *bis*-(1,3-diphenylpropan-1,3-diketonate)titanium(IV) ethoxide

Figure 4.11-5 – Structure of *bis*-(1,3-diphenylpropan-1,3-diketonate)titanium(IV) ethoxide

Bis-(1,3-diphenylpropan-1,3-diketonate)titanium(IV) ethoxide (compound **11**) was synthesised *via* the scheme outlined in Scheme 4.1-1. To a solution of titanium(IV) ethoxide under anhydrous conditions, 2 equivalents of 1,3-diphenylpropan-1,3-dione was added drop wise in ethanol solution with vigorous stirring. The mixture was stirred for 36 hours. The

resulting oil was isolated *in vacuo*. Attempts to purify the compound by recrystallisation from ethanol, and chloroform were unsuccessful. An aliquot of the pure oil of the compound was left at - 20 °C for two days yielding crystals suitable for X-ray diffraction.
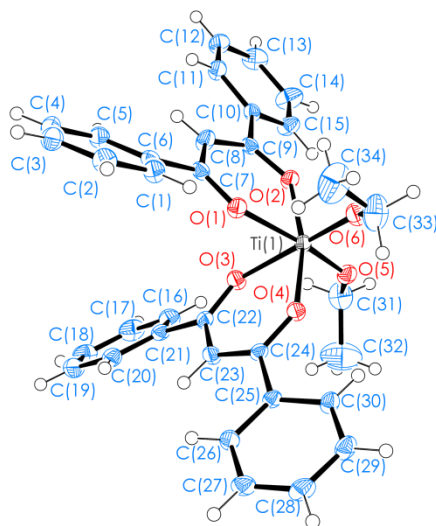
Figure 4.11-6 – ORTEP diagram of compound 11 with displacement ellipsoids showing 50% probability

Compound **11** crystallised in a monoclinic unit cell in the space group $P2_1/c$. The asymmetric unit contains one molecule, with a total of four molecules in the unit cell. Selected bond lengths and angles are included in Table 4.11-2 and Table 4.11-3 respectively. As we have seen earlier with similar complexes, the Ti-O bond lengths of the ethoxide ligand oxygen atoms O(6) and O(5) are significantly shorter than those of the oxygen atoms of the acetylacetonate ligand O(2), O(3), O(4) and O(5), where the ethoxide Ti-O bond lengths measure an average of 1.827 Å compared to the acetylacetonate Ti-O bond lengths measuring an average of 2.062 Å. With standard uncertainties measuring 0.07 % of the bond lengths this is a significant difference between the bonding modes.

Ti(1)-O(2)	2.0194(16)	Å	Ti(1)-O(3)	2.0960(16)	Å
Ti(1)-O(6)	1.8189(16)	Å	Ti(1)-O(4)	2.0293(16)	Å
Ti(1)-O(5)	1.8349(17)	Å	Ti(1)-O(1)	2.1036(16)	Å
O(2)-C(9)	1.305(3)	Å	O(3)-C(22)	1.284(3)	Å
O(1)-C(7)	1.290(3)	Å	O(4)-C(24)	1.306(3)	Å
O(6)-C(33)	1.435(3)	Å	C(26)-C(25)	1.417(3)	Å
O(5)-C(31)	1.431(3)	Å	C(9)-C(8)	1.413(3)	Å
C(22)-C(21)	1.516(3)	Å	C(6)-C(7)	1.514(3)	Å
C(25)-C(30)	1.423(3)	Å	C(23)-C(24)	1.414(3)	Å
C(10)-C(11)	1.420(3)	Å	C(8)-C(7)	1.425(3)	Å
C(10)-C(9)	1.520(3)	Å	C(31)-C(32)	1.521(5)	Å

Table 4.11-2 – Selected interatomic distances for compound 11 with standard uncertainties listed in parentheses

O(3)-Ti(1)-O(2)	86.77(6) °	O(6)-Ti(1)-O(2)	100.46(7) °
O(6)-Ti(1)-O(3)	168.62(7) °	O(4)-Ti(1)-O(2)	166.17(7) °
O(4)-Ti(1)-O(3)	82.75(6) °	O(4)-Ti(1)-O(6)	88.63(7) °
O(5)-Ti(1)-O(2)	90.84(7) °	O(5)-Ti(1)-O(3)	88.55(7) °
O(5)-Ti(1)-O(6)	100.01(8) °	O(5)-Ti(1)-O(4)	97.87(7) °
O(1)-Ti(1)-O(2)	83.22(6) °	O(1)-Ti(1)-O(3)	80.28(7) °
O(1)-Ti(1)-O(6)	91.78(7) °	O(1)-Ti(1)-O(4)	86.12(6) °
O(1)-Ti(1)-O(5)	167.61(7) °	C(24)-C(23)-C(22)	122.8(2) °
C(31)-O(5)-Ti(1)	137.82(16) °	O(4)-C(24)-C(25)	115.47(18) °
C(12)-C(11)-C(10)	121.1(2) °	C(7)-C(8)-C(9)	123.0(2) °
C(6)-C(7)-O(1)	117.44(18) °		

Table 4.11-3 – Selected bond angles for compound 11 with standard uncertainties listed in parentheses

Twisted phenyl
ring
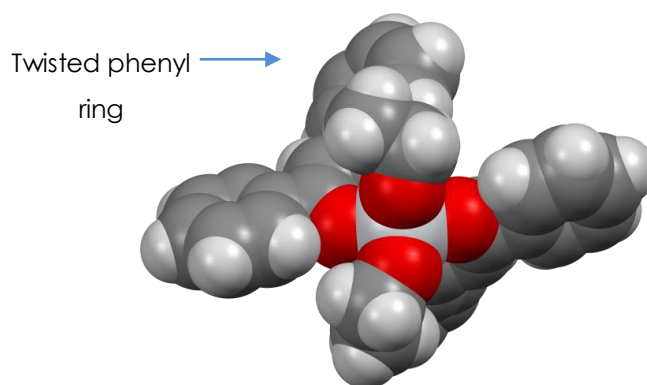
Figure 4.11-7 – Space filling diagram showing the Van der Waals radii of the atoms of the ligands around the complex and showing significant bowing of the acetylacetonate ligand.

Figure 4.11-7 shows a space filling diagram of compound **11** viewed with the ethoxide ligands pointing towards the viewer. In this arrangement it is clear the complex exhibits a *cis* configuration with regards to the ethoxide ligands as usual, however the acetylacetonate backbone of the molecule is unusually bowed, with significant torsion of one of the phenyl rings of the ligand 29.29 ° away from the plane of each the ligands (Figure 4.11-8). This finding is interesting as this molecule does not form hydrogen bonds between molecules. The molecules do not exhibit π – π stacking nor form T-bonding interactions. This suggests that the torsion is caused only by the steric strain around the molecule, possibly due to interaction with the ethoxide ligands of the complex, which in this molecule are asymmetrical.
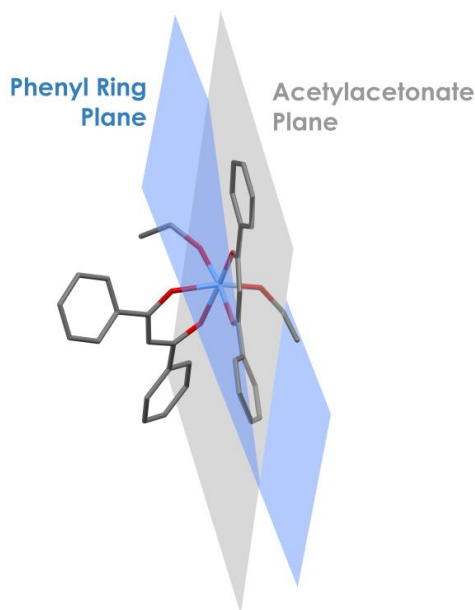
Figure 4.11-8 – Capped stick representation of compound 11 showing the planes of the acetylacetonate ligand (grey) and the plane of the twisted phenyl ring of the ligand (blue)

4.12. Dimeric analogues of bridging aluminium *sec*-butoxide dimers

Several attempts were made to prepare dimeric titanium analogues of the bridged aluminium complexes synthesised in Chapter 2. Attempts to synthesise molecules with the target structure shown in Figure 4.12-1 were made by adding only one equivalent of the acetylacetonate ligand to titanium(IV) ethoxide in anhydrous conditions at -78 °C and 35 °C. The solutions were stirred for 2 hours, at which point a precipitate formed. The precipitates were isolated by filtration and washed with pentane. The precipitates were often found to contain several products, with the bulk of the material being the normal *bis*-acetylacetonatetitanium(IV) ethoxide complexes and unreacted titanium(IV) ethoxide.

R_1=Ph, R_2= Me
R_1=Ph, R_2=Ph
R_1=4'ClPh, R_2=Me
R_1=4'FPh, R_2=Me
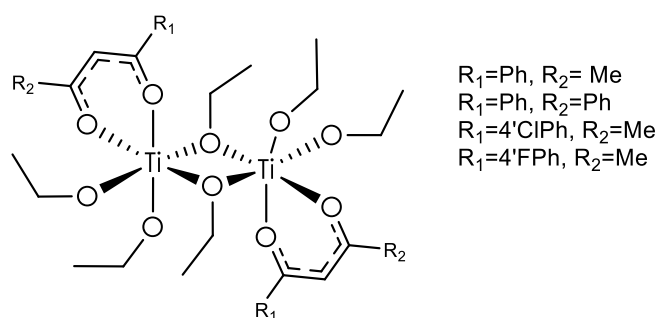
Figure 4.12-1 – Target bridged titanium dimer compounds

The filtrate was reduced *in vacuo* and the remaining residue was found to consist of unreacted titanium(IV) ethoxide in all cases.

4.13. Conclusion

This chapter reports the synthesis and characterisation of several novel titanium (IV) ethoxide complexes, and contributes structural information about these complexes to the library of compounds made by the McGowan group.

The ability for titanium (IV) ethoxide complexes to polymerise has been studied, and an in-depth study into the effect of temperature on the rate of polymerisation for one compound has been conducted.

The anti-cancer activity of a small range of these compounds has been assessed and the complexes have been found to show moderate activity against human ovarian cancer cell lines. Attempts to test the ability of a polymer produced using titanium (IV) ethoxide complexes has been attempted, however these attempts were unsuccessful due to the nature of the cell line assay.

The mechanism for interconversion of titanium (IV) ethoxide complexes between the structural isomers has been studied, and it was found that titanium (IV) ethoxide complexes are able to interconvert between isomers without complete dissociation of the β-diketonate ligand, which indicates that it is possible to switch on and off the ability for the chelating ligand to dissociate by swapping the nature of the monodentate ligands.

The nature of the decomposition of titanium (IV) ethoxide complexes has also been investigated, and a crystal structure of a complex exposed to oxygen has been collected.

4.14. **Further Work**

The focus of future work in this field might investigate further the nature of the photo-reduction of the titanium (IV) complexes, possibly to titanium (III) complexes, and isolating the structure of the reduced species.

Titanium (IV) complexes have been of interest to the McGowan group in order to build up a library of structure-activity relationships and further work in this regard would be to attempt to synthesise *meta* and *ortho* substituted phenyl β-diketonate complexes to investigate whether increased asymmetry has any effect on the anti-cancer activity of the complexes.

The potential of titanium (IV) ethoxide complexes for a combined polymerisation/anti-cancer application seems ripe. A delivery system based on titanium dispersed poly(lactic acid) implants could be developed into a potentially low-cost continual delivery system of localised drugs to a tumor site, reducing the whole body exposure to anti-cancer active compounds in the future. One current barrier to this testing procedure is the DMSO solvent system used in *in vitro* cell line testing, and alternative methods of exposing cells to the decomposing plastic would have to be identified.

4.15. **Chapter Four References**

1. Lord, R.M., Mannion, J.J., Hebden, A.J., Nako, A.E., Crossley, B.D., Mcmullon, M.W., Janeway, F.D., Phillips, R.M. And Mcgowan, P.C. Mechanistic And Cytotoxicity Studies Of Group IV B-Diketonate Complexes. *Chemmedchem*. 2014, **9**(6), pp.1136-1139.

2. Keppler, B.K., Friesen, C., Moritz, H.G., Vongerichten, H. And Vogel, E. Tumor-Inhibiting Bis(B-Diketonato) Metal Complexes. Budotitane, *Cis*-Diethoxybis(1-Phenylbutane-1,3-Dionato)Titanium(IV). *Bioinorganic Chemistry*. 1991, pp.97-127.

3. Crossley, B.D. *Ph.D. Thesis*. University Of Leeds, 2011.

4. Serpone, N. And Fay, R.C. Stereochemistry And Lability Of Dihalobis(β-Diketonato)Titanium(IV) Complexes II Benzoylacetonates And Dibenzoylmethanates. *Inorganic Chemistry*. 1967, **6**(10), pp.1835-1843.

5. Cahn, R.S., Ingold, C. And Prelog, V. Specification Of Molecular Chirality. *Angewandte Chemie International Edition In English*. 1966, **5**(4), pp.385-415.

6. Comba, P. Jakob, H. Nuber, B. And Keppler, B.K. Solution Structures And Isomer Distributions Of *Bis*(β-Diketonato) Complexes Of Titanium(IV) And Cobalt(III). *Inorganic Chemistry*. 1994, **33**(15), pp.3396-3400.

7. Fay, R.C. And Lowry, R.N. Stereochemistry And Lability Of Dihalobis(β-Diketonato)Titanium(V) Complexes. I. Acetylacetonates. *Inorganic Chemistry*. 1967, **6**(8), pp.1512-1519.

8. Fay, R.C. And Lowry, R.N. Structure And Lability Of Dihalobis(Acetylacetonato)Titanium(IV) Complexes. *Inorganic And Nuclear Chemistry Letters*. 1967, **3**(4), pp.117-120.

9. Lawan, N., Muangpil, S., Kungwan, N., Meepowpan, P., Lee, V.S. And Punyodom, W. Tin (IV) Alkoxide Initiator Design For Poly (D-Lactide) Synthesis Using DFT Calculations. *Computational And Theoretical Chemistry*. 2013, **1020**, pp.121-126.

10. Umare, P.S., Tembe, G.L., Rao, K.V., Satpathy, U.S. And Trivedi, B. Catalytic Ring-Opening Polymerization Of L-Lactide By Titanium Biphenoxy-Alkoxide

Initiators. *Journal Of Molecular Catalysis A: Chemical.* 2007, **268**(1–2), pp.235-243.

11.   Kim, Y., Jnaneshwara, G.K. And Verkade, J.G. Titanium Alkoxides As Initiators For The Controlled Polymerization Of Lactide. *Inorganic Chemistry.* 2003, **42**(5), pp.1437-1447.

12.   Chmura, A.J., Cousins, D.M., Davidson, M.G., Jones, M.D., Lunn, M.D. And Mahon, M.F. Robust Chiral Zirconium Alkoxide Initiators For The Room-Temperature Stereoselective Ring-Opening Polymerisation Of Rac-Lactide. *Dalton Transactions.* 2008, (11), pp.1437-1443.

13.   Gibson, V.C., Marshall, E.L., Navarro-Llobet, D., White, A.J.P. And Williams, D.J. A Well-Defined Iron(II) Alkoxide Initiator For The Controlled Polymerisation Of Lactide. *Journal Of The Chemical Society, Dalton Transactions.* 2002, (23), pp.4321-4322.

14.   Bhaw-Luximon, A., Jhurry, D. And Spassky, N. Controlled Polymerization Of DL-Lactide Using A Schiff's Base Al-Alkoxide Initiator Derived From 2-Hydroxyacetophenone. *Polymer Bulletin.* 2000, **44**(1), pp.31-38.

15.   Spassky, N., Wisniewski, M., Pluta, C. And Le Borgne, A. Highly Stereoelective Polymerization Of *Rac*-(D,L)-Lactide With A Chiral Schiff's Base/Aluminium Alkoxide Initiator. *Macromolecular Chemistry And Physics.* 1996, **197**(9), pp.2627-2637.

16.   Hormnirun, P., Marshall, E.L., Gibson, V.C., White, A.J.P. And Williams, D.J. Remarkable Stereocontrol In The Polymerization Of Racemic Lactide Using Aluminum Initiators Supported By Tetradentate Aminophenoxide Ligands. *Journal Of The American Chemical Society.* 2004, **126**(9), pp.2688-2689.

17.   Hebden, A.J. Ph.D. Thesis Thesis, University Of Leeds, 2010.

18.   Mannion, J.J. *Ph.D. Thesis*. Ph. D. Thesis, University Of Leeds, 2008.

19.   Lichter, R.L. And Wasylishen, R.E. Fluoropyridines. Carbon-13 Chemical Shifts And Carbon-Fluorine Coupling Constants. *Journal Of The American Chemical Society.* 1975, **97**(7), pp.1808-1813.

20.   Ishikawa, T. *Superbases For Organic Synthesis: Guanidines, Amidines, Phosphazenes And Related Organocatalysts.* 1st Edition Ed. Wiley-Blackwell, 2009.

21.   Tshuva, E.Y. And Peri, D. Modern Cytotoxic Titanium(IV) Complexes; Insights On The Enigmatic Involvement Of Hydrolysis. *Coordination Chemistry Reviews.* 2009, **253**(15–16), pp.2098-2115

5. EXPERIMENTAL

5.1. Apparatus

All syntheses stated as being performed under N_2 or under anhydrous conditions were performed using Schlenk line techniques under an atmosphere of N_2 which was passed over a dual column of phosphorus pentoxide and activated 4Å molecular sieves.

All glassware, canulae and filter canulae used in the above syntheses stated as being performed "under N_2" or "under anhydrous conditions" were stored in an oven at 160 °C prior to use. Volumes of liquid reagents were measured using N_2 purged needles and syringes.

Unless otherwise stated, all ligands used in this project were synthesised by the author using a modified synthesis originally reported by Hollick *et al.*[1] All solid ligands were recrystallised and dessicated before use. Acetylacetone was purified by distillation and stored over 3Å molecular sieves under dry nitrogen. Titanium starting materials including titanium(IV) ethoxide and titanium(IV) chloride were stored under dry nitrogen in a sealed ampoule and were purchased from Sigma-Aldrich Chemical Company. All other reagents were purchased from Sigma-Aldrich Chemical Company, Acros Organics, Fisher Scientific, VWR International or the in-house stores in the School of Chemistry, University of Leeds.

Ethanol, hexane, methanol, toluene, dichloromethane, tetrahydrofuran and diethylether were dried by passing solvents over a copper catalyst and activated alumnia columns using a Pure Solvent MD Solvent Purification System. Pentane, petrol 40-60°, petrol 60-80°, petrol 80-100° and petrol 100-120° were distilled over wired sodium and stored under dry nitrogen after degassing using three freeze-pump-thaw cycles. Chloroform was dried by refluxing over calcium hydride and stored under dry nitrogen after degassing using three freeze-pump-thaw cycles. After drying all solvents were stored in Young's tapped glass ampoules.

5.2. Analysis and instrumentation

Deuterated NMR solvents were purchased from Sigma-Aldrich Chemical Company, Acros Organics or GOSS Scientific. All NMR solvents used in this project were distilled over calcium hydride under dry dinitrogen and stored under nitrogen with 4 Å molecular sieves in an ampoule fitted with a Young's tap, except deuterated benzene which was degassed using three freeze-pump-thaw cycles and stored over a sodium mirror.

All NMR, microanalysis and mass spectrometry samples were prepared in a Braun Labmaster 100 glove box and sealed under oxygen free nitrogen.

NMR spectra were collected by the author or Mr. Simon Barrett using Bruker DRX 500 MHz spectrometers or a Bruker DPX 300 MHz spectrometer.

Microanalyses were collected by Mr. Ian Blakeley and Ms. Tanya Marinko-Covell at the University of Leeds microanalysis service.

Mass spectra were collected by Ms. Tanya Marinko-Covell at the University of Leeds mass spectrometry service, with electrospray being the source of ionisation unless otherwise stated.

X-ray diffraction data was collected by the author, Dr Christopher Pask or Miss Rianne Lord on a Bruker X8 diffractometer using monochromated Mo-Ka (graphite) X-ray radiation of wavelength 0.71073 Å. Diffraction data was detected using a Kappa Apex II CCD detector. Suitable crystals were mounted on a MiTeGen micromesh and cooled to 150K using an Oxford cryostream low temperature device.[2]

The data was scaled and prepared using APEX2 software and error calculations were found using SADABS. The data was solved by direct methods using the Olex2 GUI[3] and ShelXL or SuperFlip[4] packages. Structure refinement was achieved using ShelXS[5] or olex.refine packages.[3]

5.3. Aluminium Complexes

5.3.1. Attempted synthesis of *bis*(acetylacetonate)aluminium chloride – (Compound 1)

Anhydrous aluminium(III) chloride (0.5g, 3.7 mmol) was added to toluene (30 ml). The solution was heated and stirred until full desolution. Acetylacetone (0.73 ml, 0.75 g, 7.5 mmol) was added under an atmosphere of N_2. The resulting forest green solution was stirred for 10 hours.

Characterisation data:

Compound was found to have 0 % chlorine by elemental analysis. Mass spectrometry found a major peak of $Na[Al(acetylacetonate)_3]_2$ at 671.22 gmol[-1].

5.3.2. Attempted synthesis of *bis*(acetylacetonate)aluminium chloride – (Compound 1)

Anhydrous aluminium(III) chloride (0.5 g) was added to petrol 60 - 80° (30 ml). The solution was stirred for three days until full desolution. Acetylacetone (0.74 ml, 0.75 g, 7.5 mmol) was added under an atmosphere of N_2 to yield a milky white precipitate. The filtrate was isolated and the remaining solvent removed *in vacuo* to yield a white solid.

Characterisation data

Compound was found to contain large amounts of $Na[Al(acetylacetonate)_3]_2$ by mass spectrometry, major peak at 671.22 gmol[-1]. The compound was found to have 0% chlorine by elemental analysis.

5.3.3. Attempted synthesis of *bis*-(phenylacetylacetonate)aluminium chloride dimer – (Compound 2)

To a solution of anhydrous aluminium(III) chloride (0.75 g, 5.6 mmol) in chloroform (~40 ml) was added a solution of phenylacetylacetone (1.81 g, 11.2 mmol) in DCM dropwise. A colour change was observed from orange to green. The crude product was dissolved in chloroform and allowed to recrystallise in an atmosphere of pentane under anhydrous conditions.

Characterisation data
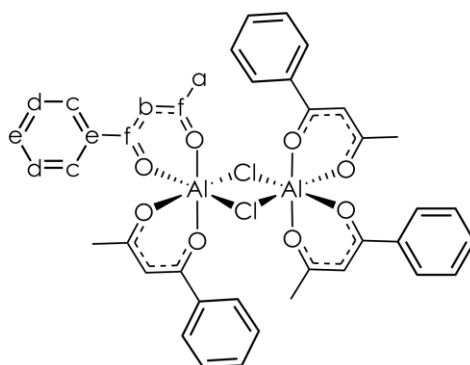
Figure 5.3-1 – Lettered structure of compound 2 used for the assignment of ^{1}H NMR peaks

500 MHz, 298 K, CDCl$_3$, ^{1}H NMR: (See Figure 5.3-1)

2.20 ppm 3H, s, [[PhCOCHCOC**H$_3$**]$_2$AlCl]$_2$] **H$_a$**
6.25 ppm 1H, s, [PhCOC**H**COCH$_3$]$_2$AlCl]$_2$ **H$_c$**
7.45 ppm 3.5H, m [[C**H**(C$_2$**H$_2$**)(C$_2$H$_2$)CHCOCHCOCH$_3$]$_2$AlCl]$_2$ Overlapping signals **H$_e$** and **H$_d$** (and additional impurity)
7.93 ppm 2H, m [[CH(C$_2$H$_2$)(C$_2$**H$_2$**)CHCOCHCOCH$_3$]$_2$AlCl]$_2$ **H$_c$**

5.3.4. Attempted synthesis of *bis*(acetylacetonate)aluminium chloride dimer – (Compound 3)

To a solution of anhydrous aluminium(III) chloride (0.5 g, 3.7 mmol) in DCM was added a solution of 4'chlorophenylacetylacetonate (1.46 g, 7.4 mmol) in petrol 60-80 °. The solution was stirred for 16 hours to yield 1.2 g, 2.6 mmol of white solid (70 % yield).

Characterisation data

500 MHz, 298 K, CDCl$_3$, ^{1}H NMR:

2.18 ppm 6H, s, [[**H$_3$**CCOCHCOC**H$_3$**]$_2$AlCl]$_2$]
5.79 ppm 1H, s, [H$_3$CCOC**H**COCH$_3$]$_2$AlCl]$_2$

Suggested synthesis of the desired product, but significant impurities of Al(acac)$_3$

[H$_3$CCOCHCOCH$_3$]$_3$Al]: 500 MHz, 298 K, CDCl$_3$, ^{1}H NMR:

2.01 ppm (0.2 Equivalents) 6H, s, [**H$_3$**CCOCHCOC**H$_3$**]$_3$Al]

5.79 ppm (0.2 Equivalents) 1H, s, [H$_3$CCOC**H**COCH$_3$]$_3$Al]

5.3.5. Successful Synthesis of *bis*-(acetylacetonate)aluminium secbutoxide dimer - (Compound 4)

Aluminium secbutoxide (1.82 g, 7.4 mmol) was dissolved in petrol (60 – 80 °) and cooled to -78 °C in a cardice/acetone slurry bath. To which a solution of acetylacetone (1.48 g, 14.8 mmol) in chloroform was added slowly with vigorous stirring under nitrogen. The solution was allowed to warm to 0 °C under dynamic nitrogen flow to yield colourless crystals suitable for X-ray diffraction. (0.52 g, 0.87 mmol 23 % yield)

Characterisation data:

500 MHz, 298 K, CDCl$_3$, ^{1}H NMR:	175 MHz, CDCl$_3$, ^{13}C NMR:
0.76 ppm [3H, bs, H$_3$CC**H$_2$**CHOCH$_3$] butoxide	11.34 ppm [alkyl H$_3$**C**CH$_2$CHOCH$_3$]
0.93 ppm [2H, bs, **H$_3$**CCH$_2$CHOCH$_3$] butoxide	20.87 ppm [alkyl H$_3$CCH$_2$CHO**C**H$_3$]
1.08 ppm [3H, H$_3$CCH$_2$CHO**CH$_3$**] butoxide	26.50 ppm [methyl, H$_3$**C**COCHCO**C**H$_3$]
1.80 ppm [6H, bs, **CH$_3$**COCHCOCH$_3$] acac	30.56 ppm [alkyl, H$_3$C**C**H$_2$CHOCH$_3$]
1.94 ppm [6H, bs, CH$_3$COCHCO**CH$_3$**]	69.16 ppm [H$_3$CCO**C**HCOCH$_3$]
3.69 ppm [1H, bs, CH$_3$COC**H**COCH$_3$]	100.02 ppm [H$_3$CCH$_2$**C**HOCH$_3$]
5.35/5.49 ppm [2H, ad, CH$_3$COC**H**COCH$_3$]	187.89 ppm [H$_3$CCOCH**C**OCH$_3$]
	191.57 ppm [H$_3$C**C**OCHCOCH$_3$]

Microanalysis: Calculated - C: 56.37%, H: 7.77% Found – C: 55.80%, H: 7.55%

ES-MS (CHCl$_3$, m/z) : 425.1 – ((M+Al) – 2 x acac) – C$_{18}$H$_{32}$Al$_3$O$_6^+$

5.3.6. Polymerisation of L-Lactide using *bis*-(acetylacetonate)aluminium chloride dimer – (Compound 2)

Recrystallised sample of compound **2** (0.014 g, 0.032 mmol) was added to L-lactide (0.91 g, 6.3 mmol, 200 equivalents per aluminium centre) in an atmosphere of N$_2$. The reaction mixture was heated to 150 °C for 4 hours and solidified leaving a slightly yellow plastic.

Degree of conversion – 87.1 %, measured by integration of lactide methine proton against unreacted lactide methine proton.

Characterisation
Poly(lactic acid)
500 MHz, CDCl$_3$, 298 K ^{1}H NMR:
1.58 ppm [3H, t, [OCH(C**H$_3$**)CO]$_n$]

5.17 ppm [1H, q, [OC**H**(CH$_3$)CO]$_n$]

Lactide
1.67 ppm [3H, t, [OCH(C**H$_3$**)CO]$_2$]
5.04 ppm [1H, q, [OC**H**(CH$_3$)CO]$_2$]

5.3.7. Polymerisation of L-Lactide using *bis*-(acetylacetonate)aluminium secbutoxide - (Compound 4)

Recrystallised sample of compound **4** (0.002 g, 0.033 mol) was added to L-lactide (1.56 g, 10.831 mmol, 200 equivalents per aluminium centre) in an atmosphere of N$_2$. The reaction mixture was heated to 150 °C for 10 minutes and solidified leaving a white solid.

Degree of conversion – 94.49 %, measured by integration of lactide methine proton against unreacted lactide methine proton.

Characterisation
Poly(lactic acid)
500 MHz, CDCl$_3$, 298 K ^{1}H NMR:
1.58 ppm [3H, t, [OCH(C**H$_3$**)CO]$_n$]
5.17 ppm [1H, q, [OC**H**(CH$_3$)CO]$_n$]
Lactide
1.67 ppm [3H, t, [OCH(C**H$_3$**)CO]$_2$]
5.04 ppm [1H, q, [OC**H**(CH$_3$)CO]$_2$]

5.4. Titanium Complex Synthesis

5.4.1. *Bis*-(4'Fluorophenylacetylacetonate)titanium(IV) ethoxide - compound 5

2 equivalents of 4'fluorophenylacetylactone (2.37 g, 13.1 mmol) was dissolved in ethanol and added to titanium(IV) ethoxide (1.5 g, 6.57 mmol) solution. The mixture was allowed to stir for 16 hours and the resulting cream precipitate was isolated by filtration. The powder was then recrystallised from hot ethanol to yield light yellow crystals suitable for X-ray diffraction (2.61 g, 5.26 mmol, 80% yield).

500 MHz, CDCl$_3$, 298 K ^{1}H NMR:
1.24 ppm [3H, s, TiOCH$_2$**CH$_3$**]
2.07/2.26 ppm [3H, s 4'FPhCOCHCO**CH$_3$**]
4.52 ppm [2H, as, TiO**CH$_2$**CH$_3$]
6.20 ppm [1H, s, 4'FPhCO**CH**COCH$_3$]
7.00/7.12 ppm [2H, as, **H-**ortho to fluorine atom on phenyl ring]
7.77/8.04 ppm [2H, d, **H-**meta to fluorine atom on phenyl ring].

175 MHz, CDCl$_3$, 298K, ^{13}C{^{1}H} NMR:

18.5 ppm [alkyl, TiOCH$_2$**C**H$_3$]

33.6 ppm [alkyl, 4'FPhCOCHCO**C**H$_3$]

72.4 ppm [alkoxide, TiO**C**H$_2$CH$_3$]

111.4 ppm [aromatic, **C**-meta to fluorine atom on phenyl ring]

130.2 ppm [aromatic, **C**-ortho to fluorine atom in phenyl ring]

133.4 ppm [aromatic, F-**C** of phenyl ring]

140.0 ppm [aromatic, quaternary Ph**C**-C=O of acetylacetonate]

164.0 ppm [carbonyl, 4'FPhCOCH**C**OCH$_3$]

166.0 ppm [carbonyl, 4'FPh**C**OCHCOCH$_3$].

Microanalysis: Calculated - C: 57.84%, H:5.66% Found – C:57.70%, H:5.25%

ES-MS (CHCl$_3$, m/z) : 519.1 (M+Na) - C$_{24}$H$_{26}$F$_2$NaO$_6$Ti$^+$

See Appendix for crystallographic data

5.4.2. *Bis*-(4-bromophenylacetylacetonate)titanium(IV) ethoxide (Compound 6)

2 equivalents of 4'bromophenylacetylactone (0.50 g, 2.09 mmol) was dissolved in ethanol and added to titanium(IV) ethoxide (0.24 g, 1.05 mmol) solution. The mixture was allowed to stir for 16 hours and the resulting cream precipitate was isolated by filtration. The powder was then recrystallised from hot ethanol to yield light yellow crystals suitable for X-ray diffraction.

500 MHz, CDCl$_3$, 298 K ^{1}H NMR:

1.24 ppm [6H s, TiOCH$_2$**CH$_3$**]

2.07 ppm [3H, as, 4'BrPhCOCHCO**CH$_3$**]

2.26 ppm [3H, s, 4'BrPhCOCHCO**CH$_3$**]

4.52 ppm [4H, as, TiO**CH$_2$**CH$_3$]

6.20 ppm [2H, s, 4'BrPhCO**CH**COCH$_3$]

7.48 ppm [2H, as, **H-**meta to bromine atom on phenyl ring]

7.60 ppm [4H, as, **H-**ortho to bromine atom on phenyl ring]

7.89 ppm [2H, d, **H-**meta to bromine atom on phenyl ring]

175 MHz, CDCl$_3$, 298K, ^{13}C{^{1}H} NMR:

18.5 ppm [alkyl, TiOCH$_2$**C**H$_3$]

27.0 ppm [alkyl, 4'FPhCOCHCO**C**H$_3$]

27.7 ppm [alkyl, 4'BrPhCOCHCO**C**H$_3$]

72.5 ppm [alkoxide, TiO**C**H$_2$CH$_3$]

98.9/99.3 ppm [methine, 4'BrPhCO**C**HCOCH$_3$]

131.6 ppm [aromatic, **C**-ortho to bromine atom in phenyl ring]

129.1 ppm [aromatic, **C**-meta to bromine atom on phenyl ring]

126.5 ppm [aromatic, Br-**C** of phenyl ring]

140.0 ppm [aromatic, quaternary **C**-C=O of acetylacetonate]

178.7/181.7/181.8 ppm [carbonyl, 4'BrPhCOCH**C**OCH₃]

190.6/193.6 ppm [carbonyl, 4'BrPh**C**OCHCOCH₃].

See Appendix for crystallographic data

5.4.3. *Bis*-(4-iodophenylacetylacetonate)titanium(IV) ethoxide (Compound 7)

2 equivalents of 4'iodophenylacetyllactone (0.50 g, 1.74 mmol) was dissolved in ethanol and added to titanium(IV) ethoxide (0.20 g, 0.88 mmol) in ethanol. The mixture was allowed to stir for 16 hours and the resulting brown precipitate was isolated by filtration. The powder was then recrystallised from hot ethanol to yield a dark brown solid.

500 MHz, CDCl₃, 298 K ¹H NMR:

1.23 ppm [3H, s, TiOCH₂**CH₃**]

2.07/2.26 ppm [3H, s, 4'IPhCOCHCO**CH₃**]

4.51 ppm [2H, as, TiO**CH₂**CH₃]

6.19 ppm [4'IPhCO**CH**COCH₃]

7.46 ppm [1H as, **H**-ortho to the iodine atom of the phenyl ring]

7.74 ppm [3H, m, **H**-ortho to the iodine atom of the phenyl ring, **H**-meta to the iodine atom of the phenyl ring].

175 MHz, CDCl₃, 298K, ¹³C{¹H} NMR:

18.6 ppm [alkyl, TiOCH₂**C**H₃]

27.0/27.7 ppm [methyl, 4'IPhCOCHCO**C**H₃]

72.4 ppm [alkoxide, TiO**C**H₂CH₃]

98.9 ppm [methine, 4'IPhCO**C**HCOCH₃]

129.1 ppm [aromatic, **C atoms**-ortho to the iodine atom of the phenyl ring]

136.7/137.6 ppm [aromatic, **C atoms** – meta to the iodine atoms of the phenyl ring],

178.9 ppm [aromatic quaternary, **C**-I]

182.1 ppm [aromatic quaternary, **C**-C=O]

190.8 ppm [carbonyl, 4'IPhCOCH**C**OCH₃]

193.7 ppm [carbonyl, 4'IPh**C**OCHCOCH₃].

Microanalysis – Calculated – C: 40.48%, H: 3.68%. Found – C: 40.80% H: 3.55%

5.4.4. Synthesis of *Bis*-(1,3-di-4-methoxyphenylpropan-1,3-diketonate)titanium(IV) ethoxide (Compound 6)

1 equivalent of *bis*-4'methoxyphenylacetyllactone (0.3 g, 1.01 mmol) was dissolved in ethanol and added to titanium(IV) ethoxide (0.24 g, 1.05 mmol) in ethanol. The mixture was allowed to stir for 16 hours and the resulting white precipitate was isolated by filtration. The powder was then recrystallised from hot ethanol to yield a white powder.

500 MHz, CDCl$_3$, 298 K ^{1}H NMR:

1.26 ppm [3H, t, ^{2}J = 6.9 Hz, TiOCH$_2$**CH$_3$**]

3.77/3.91 ppm [6H, s, **H$_3$**COPhCOCHCOPhOC**H$_3$**]

4.57 ppm [2H, q, ^{2}J = 7.1 Hz, TiO**CH$_2$**CH$_3$]

6.78 ppm [2H, s, **H-atoms** ortho to the methoxy group of the phenyl ring]

6.81 ppm [1H, s, H$_3$COPhCO**CH**COPhOCH$_3$]

7.01 ppm [2H, s, **H-atoms** ortho to the methoxy group of the phenyl ring]

7.78 ppm [2H, s, **H-atoms** meta to the methoxy group of the phenyl ring]

8.15 ppm [2H, s, **H-atoms** meta to the methoxy group of the phenyl ring]

175 MHz, CDCl$_3$, 298K, ^{13}C{^{1}H} NMR:

18.7 ppm [alkyl, TiOCH$_2$**C**H$_3$]

55.4 ppm [methoxy, H$_3$**C**OPhCOCHCOPhO**C**H$_3$]

71.6 ppm [alkoxy, TiO**C**H$_2$CH$_3$]

94.5 ppm [methine, H$_3$COPhCO**C**HCOPhOCH$_3$]

113.5 ppm [aromatic, **C-atoms** meta to the methoxy group of the phenyl ring]

113.7 ppm [aromatic, **C-atoms** meta to the methoxy group of the phenyl ring]

129.7 ppm [aromatic, **C-atoms** ortho to the methoxy group of the phenyl ring]

130.5 ppm [aromatic, C-OCH$_3$]

162.5 ppm [carbonyl, H$_3$COPh**C**OCH**C**OPhOCH$_3$]

Elemental Analysis – Calculated – C:64.78%, H:5.72%, Found – C:64.75%, H:5.65%

ES-MS (CHCl$_3$, m/z) : 673.2 (M+H) - C$_{38}$H$_{41}$O$_8$Ti

5.5. Bulk polymerisations

5.5.1. Bulk polymerisation of lactide with *bis*-(acetylacetonate)titanium chloride (Compound 2)

200 equivalents of *rac*-lactide was mixed with one equivalent of bisacetylacteonate titanium chloride. The mixture was ground in a pestle and mortar and sealed in a round bottomed flask with a suba seal. The flask was then submerged in oil at 150°C.

Degree of conversion – 80 %, measured by integration of lactide methine proton against unreacted lactide methine proton.

Characterisation
Poly(lactic acid)
500 MHz, CDCl$_3$, 298 K ^{1}H NMR:
1.58 ppm [3H, t, [OCH(C**H$_3$**)CO]$_n$]
5.17/5.19 ppm [1H, m, [OC**H**(CH$_3$)CO]$_n$]
Lactide
1.67 ppm [3H, t, [OCH(C**H$_3$**)CO]$_2$]
5.04 ppm [1H, q, [OC**H**(CH$_3$)CO]$_2$]

5.5.2. Bulk polymerisation of lactide with *bis-*(4'methoxyphenylacetylacetonate) titanium(IV) chloride

200 equivalents of *rac*-lactide was mixed with one equivalent of bis-4'methoxyphenylacetylacteonate titanium chloride. The mixture was ground in a pestle and morter and sealed in a round bottomed flask with a suba seal. The flask was then submerged in oil at 150°C.

Degree of conversion – 54 %, measured by integration of lactide methine proton against unreacted lactide methine proton.

Characterisation
Poly(lactic acid)
500 MHz, CDCl$_3$, 298 K ^{1}H NMR:
1.58 ppm [3H, t, [OCH(C**H$_3$**)CO]$_n$]
5.17/5.19 ppm [1H, m, [OC**H**(CH$_3$)CO]$_n$]
Lactide
1.67 ppm [3H, t, [OCH(C**H$_3$**)CO]$_2$]
5.04 ppm [1H, q, [OC**H**(CH$_3$)CO]$_2$]

5.5.3. *In situ* polymerisation of lactide with *bis-*(4'methoxyphenylacetylacetonate) titanium(IV) chloride

A bulk mixture of 200 equivalents of L-lactide was mixed with one equivalent of bis-4'methoxyphenylacetylacteonate titanium chloride. The mixture was ground in a pestle and mortar and sealed into glass crip-cap vials with aluminium caps and PTFE plugs. The vials were submerged into rigorously stirred oil at 150°C. Three sample vials were removed at 5 minutes, 10 minutes, 20 minutes, 40 minutes, 60 minutes, 3 hours, 4 hours,13 hours and 15 hours. Each sample vial was exposed to air and the polymer inside analysed by ^{1}H NMR. The NMR spectra were randomised and each data set was given a random number. The degree of polymerisation was calculated by single-blind integration of the area under the peaks of polymerised lactide against total area of unreacted and polymerised lactide and the percentage conversion calculated for each of the vials. The average was calculated and plotted using orgin pro 8.

Degree of conversion – 14%, measured by integration of lactide methine proton against unreacted lactide methine proton.

Characterisation
Poly(lactic acid)
500 MHz, CDCl$_3$, 298 K ^{1}H NMR:
1.58 ppm [3H, t, [OCH(C**H$_3$**)CO]$_n$]
5.17/5.19 ppm [1H, m, [OC**H**(CH$_3$)CO]$_n$]
Lactide

1.7 ppm [3H, t, [OCH(C**H₃**)CO]₂]

5.0 ppm [1H, q, [OC**H**(CH₃)CO]₂]

5.5.4. In-Situ polymerisation studies of lactide with compound 5

A bulk mixture of 210 equivalents of L-lactide was mixed with one equivalent of compound **5**. The mixture was ground in a pestle and mortar and sealed into glass crip-cap vials with aluminium caps and PTFE plugs. The vials were submerged into rigorously stirred oil at 150 °C. Three sample vials were removed at 5 minutes, 10 minutes, 20 minutes, 40 minutes, 60 minutes, 90 minutes, 150 hours, 4 hours, 5 hours and 8.5 hours and 12 hours. Each sample vial was exposed to air and the polymer inside analysed by ^{1}H NMR in wet CDCl₃. This process was repeated in oil baths at 160 °C, 170 °C, 185 °C and 200 °C. The NMR spectra were randomised and each data set was given a random number. The degree of polymerisation was calculated by single-blind integration of the area under the peaks of polymerised lactide against total area of unreacted and polymerised lactide and the percentage conversion calculated for each of the vials. The average was calculated and plotted using Origin pro 8. Origin was further used to model appropriate lines of best fit for all of the data points, and a logarithmic fit was selected, using origin to interpolate variables for A1, A2, x, x0 and p which best fit the data set satisfying equations with general formula as shown in Equation 3.3-1. The general formula was rearranged to make x the subject of the equation and y=50 inserted with the variables interpolated by Origin Pro (Equation 3.3-2). Full calculations are included in the appendix.

5.6. Chapter Five References

1. Hollick, J.J., Golding, B.T., Hardcastle, I.R., Martin, N., Richardson, C., Rigoreau, L.J.M., Smith, G.C.M. And Griffin, R.J. 2,6-Disubstituted Pyran-4-one And Thiopyran-4-one Inhibitors Of DNA-Dependent Protein Kinase (DNA-PK). *Bioorganic & Medicinal Chemistry Letters.* 2003, **13**(18), pp.3083-3086.

2. Cosier, J. And Glazer, A.M. A Nitrogen-Gas-Stream Cryostat For General X-Ray Diffraction Studies. *Journal Of Applied Crystallography.* 1986, **19**(2), pp.105-107.

3. Dolomanov, O.V., Bourhis, L.J., Gildea, R.J., Howard, J.A.K. And Puschmann, H. OLEX2: A Complete Structure Solution, Refinement And Analysis Program. *Journal Of Applied Crystallography.* 2009, **42**(2), pp.339-341.

4. Palatinus, L. And Chapuis, G. SUPERFLIP - A Computer Program For The Solution Of Crystal Structures By Charge Flipping In Arbitrary Dimensions. *Journal Of Applied Crystallography.* 2007, **40**(4), pp.786-790.

5. Sheldrick, G.M. And Schneider, T.R. [16] SHELXL: High-Resolution Refinement. In: Charles W. Carter Jr, R.M.S. Ed. *Methods In Enzymology*. Academic Press, 1997, pp.319-343.

6. APPENDICES

6.1. Crystallographic information for compound 4

Table 1 Crystal data and structure refinement for DC46_0M.

Identification code	DC46_0M
Empirical formula	$C_{28}H_{39}Al_2O_{10}$
Formula weight	589.55
Temperature/K	150
Crystal system	tetragonal
Space group	$I4_1$
a/Å	14.8759(2)
b/Å	14.8759(2)
c/Å	29.5961(6)
α/°	90
β/°	90
γ/°	90
Volume/Å^3	6549.4(2)
Z	8
ρ_{calc}mg/mm^3	1.196
m/mm^{-1}	0.138
F(000)	2504.0
Crystal size/mm^3	0.06 × 0.02 × 0.01
Radiation	MoKa (λ = 0.71073)
2Θ range for data collection	3.064 to 56.714°
Index ranges	-19 ≤ h ≤ 19, -19 ≤ k ≤ 19, -39 ≤ l ≤ 39
Reflections collected	59082
Independent reflections	8169 [R_{int} = 0.0459, R_{sigma} = 0.0275]
Data/restraints/parameters	8169/1/373
Goodness-of-fit on F^2	1.055
Final R indexes [I>=2σ (I)]	R_1 = 0.0705, wR_2 = 0.1717

Final R indexes [all data]		R₁ = 0.1101, wR₂ = 0.2085		

Final R indexes [all data] $R_1 = 0.1101, wR_2 = 0.2085$

Largest diff. peak/hole / e Å⁻³   0.38/-0.45

Flack parameter   0.48(13)

Table 2 Fractional Atomic Coordinates (×10⁴) and Equivalent Isotropic Displacement Parameters (Å²×10³) for DC46_0M. U_{eq} is defined as 1/3 of of the trace of the orthogonalised U_{IJ} tensor.

Atom	x	y	z	U(eq)
Al1	−14305.8(17)	−9308.6(15)	−11105.2(8)	49.2(5)
O5	−15565(4)	−9432(3)	−11107(2)	47.8(11)
O2	−14207(4)	−9311(3)	−10464.5(19)	50.7(14)
O3	−13036(3)	−9308(3)	−11116.5(17)	54.1(13)
O4	−14307(4)	−9201(4)	−11748(2)	55.4(15)
O1	−14298(4)	−8030(3)	−11095.2(17)	52.7(13)
C1	−14088(6)	−6519(6)	−10885(3)	67(2)
C9	−13685(7)	−8991(6)	−12007(3)	59(2)
C2	−14114(5)	−7492(6)	−10778(3)	55.7(19)
C7	−12499(5)	−9072(5)	−11437(3)	53.3(19)
C10	−13967(7)	−8854(8)	−12498(3)	84(3)
C8	−12789(6)	−8925(6)	−11875(3)	64(2)
C4	−14008(6)	−8654(7)	−10202(3)	61(2)
C3	−13919(6)	−7779(6)	−10342(3)	66(2)
C6	−11525(6)	−9056(6)	−11314(3)	71(2)
C5	−13840(7)	−8907(7)	−9708(3)	78(3)
Al2	−19303.8(17)	−5693.2(16)	−11105.7(9)	49.2(5)
O6	−18035(4)	−5692(4)	−11116.0(19)	58.5(14)
O8	−19205(4)	−5686(4)	−10467(2)	54.2(14)
O10	−20554(4)	−5559(4)	−11107(3)	53.1(12)
O7	−19313(4)	−5803(4)	−11744(2)	60.1(16)

Atom				
O9	−19294(4)	−6972(3)	−11095.2(19)	58.6(14)
C24	−19084(6)	−8485(5)	−10890(3)	64(2)
C19	−18963(8)	−6132(8)	−12491(3)	86(3)
C23	−19113(6)	−7498(5)	−10777(3)	54.7(19)
C16	−17509(5)	−5925(5)	−11442(3)	52.9(19)
C18	−18691(6)	−6011(5)	−12008(3)	54.6(19)
C17	−17785(7)	−6085(6)	−11875(3)	68(2)
C22	−18909(6)	−7224(7)	−10340(3)	69(3)
C21	−19001(6)	−6341(7)	−10202(3)	59(2)
C20	−18856(7)	−6099(7)	−9711(3)	80(3)
C15	−16520(6)	−5943(6)	−11310(3)	66(2)
C28	−21507(10)	−6336(10)	−10473(6)	164(7)
C11	−16404(8)	−8466(9)	−11758(3)	117(5)
C27	−21245(9)	−6228(10)	−11036(7)	137(6)
C13	−16238(9)	−8773(9)	−11050(7)	141(6)
C26	−21556(9)	−6664(8)	−11352(4)	129(4)
C12	−16564(8)	−8333(8)	−11359(4)	129(5)
C14	−16543(10)	−8660(10)	−10492(6)	146(6)
C25	−21408(9)	−6518(9)	−11766(4)	115(5)

Table 3 Anisotropic Displacement Parameters ($\text{Å}^2 \times 10^3$) for DC46_0M. The Anisotropic displacement factor exponent takes the form: $-2\pi^2[h^2a^{*2}U_{11}+2hka^*b^*U_{12}+\dots]$.

Atom	U_{11}	U_{22}	U_{33}	U_{23}	U_{13}	U_{12}
Al1	59.9(14)	50.2(12)	37.4(9)	2.6(10)	−0.6(10)	15.1(10)
O5	56(3)	42(2)	45(2)	1(2)	−4(2)	20(2)
O2	62(3)	54(3)	36(3)	8(2)	4(2)	7(2)
O3	60(3)	61(3)	42(3)	6(3)	4(3)	16(2)
O4	65(4)	64(4)	38(3)	0(2)	−3(2)	18(3)

O1	76(3)	45(3)	37(2)	2(2)	−4(3)	12(2)
C1	83(6)	54(5)	65(5)	3(4)	2(5)	−14(4)
C9	80(6)	53(5)	42(4)	0(4)	−3(4)	−10(4)
C2	50(4)	72(5)	45(4)	8(4)	7(3)	−1(3)
C7	63(5)	46(4)	51(5)	7(3)	1(4)	−9(3)
C10	100(7)	117(9)	36(4)	11(5)	0(5)	−19(6)
C8	64(5)	77(6)	50(5)	6(4)	6(4)	−15(4)
C4	62(5)	86(6)	37(4)	−2(4)	4(4)	−1(4)
C3	85(6)	69(6)	43(5)	−10(4)	−1(4)	−17(5)
C6	76(6)	69(6)	70(6)	2(5)	10(5)	−7(4)
C5	103(8)	88(7)	42(4)	10(5)	1(5)	−16(5)
Al2	58.3(14)	49.5(12)	39.9(9)	−2.1(10)	−0.3(10)	−4.4(10)
O6	64(3)	60(3)	52(3)	−5(3)	4(3)	2(2)
O8	60(3)	60(3)	42(3)	−4(2)	2(2)	7(2)
O10	60(3)	47(3)	53(3)	−3(3)	−4(3)	−13(2)
O7	72(4)	62(4)	46(4)	−4(3)	3(3)	−4(3)
O9	79(4)	53(3)	44(3)	−4(3)	−4(3)	7(3)
C24	79(6)	49(4)	63(5)	−9(4)	−5(4)	15(4)
C19	109(8)	111(9)	38(4)	−12(5)	−3(5)	21(6)
C23	53(4)	62(5)	49(4)	0(4)	12(3)	6(3)
C16	53(4)	49(4)	57(5)	−3(3)	7(4)	13(3)
C18	66(5)	53(4)	46(4)	0(3)	−6(4)	11(4)
C17	78(6)	77(6)	49(5)	−7(4)	−1(4)	27(5)
C22	83(6)	81(6)	43(5)	2(4)	−2(4)	29(5)
C21	63(5)	75(6)	38(4)	1(4)	3(4)	1(4)
C20	102(8)	93(7)	46(5)	−15(5)	−1(5)	18(6)
C15	70(6)	64(5)	64(5)	−9(4)	1(4)	9(4)
C28	143(12)	126(11)	223(17)	88(12)	43(13)	−23(9)

C11	125(9)	157(11)	69(6)	−21(6)	5(6)	82(8)
C27	88(8)	92(9)	232(17)	14(10)	−13(9)	−50(6)
C13	74(7)	80(7)	267(18)	−12(9)	−2(9)	55(5)
C26	145(10)	126(9)	116(9)	−34(7)	26(7)	−81(8)
C12	148(9)	130(9)	108(8)	31(7)	12(7)	96(8)
C14	141(12)	119(10)	180(14)	−55(10)	23(11)	45(9)
C25	122(10)	154(12)	69(6)	22(6)	−7(6)	−61(8)

Table 4 Bond Lengths for DC46_0M.

Atom	Atom	Length/Å	Atom	Atom	Length/Å
Al1	Al1[1]	2.915(5)	Al2	O10[2]	1.875(6)
Al1	O5[1]	1.883(6)	Al2	O10	1.870(6)
Al1	O5	1.882(6)	Al2	O7	1.898(8)
Al1	O2	1.902(7)	Al2	O9	1.902(6)
Al1	O3	1.889(6)	O6	C16	1.288(9)
Al1	O4	1.908(7)	O8	C21	1.288(11)
Al1	O1	1.902(5)	O10	Al2[2]	1.875(6)
O5	Al1[1]	1.883(6)	O10	C27	1.447(11)
O5	C13	1.412(9)	O7	C18	1.249(10)
O2	C4	1.283(11)	O9	C23	1.254(9)
O3	C7	1.288(9)	C24	C23	1.507(10)
O4	C9	1.241(10)	C19	C18	1.499(11)
O1	C2	1.263(10)	C23	C22	1.389(11)
C1	C2	1.481(11)	C16	C17	1.369(11)
C9	C10	1.527(11)	C16	C15	1.523(11)
C9	C8	1.393(12)	C18	C17	1.408(12)
C2	C3	1.390(11)	C22	C21	1.382(13)
C7	C8	1.384(11)	C21	C20	1.513(11)

Atom	Atom	Bond Length	Atom	Atom	Bond Length
C7	C6	1.494(12)	C28	C27	1.72(3)
C4	C3	1.372(13)	C11	C12	1.222(13)
C4	C5	1.531(11)	C27	C26	1.228(19)
Al2	Al2[2]	2.923(5)	C13	C12	1.223(19)
Al2	O6	1.888(6)	C13	C14	1.72(2)
Al2	O8	1.895(7)	C26	C25	1.264(14)

[1]-3-X,-2-Y,+Z; [2]-4-X,-1-Y,+Z

Table 5 Bond Angles for DC46_0M.

Atom	Atom	Atom	Angle/°	Atom	Atom	Atom	Angle/°
O5	Al1	Al1[1]	39.28(16)	O8	Al2	Al2[2]	92.95(18)
O5[1]	Al1	Al1[1]	39.27(16)	O8	Al2	O7	173.8(3)
O5	Al1	O5[1]	78.5(2)	O8	Al2	O9	89.3(3)
O5[1]	Al1	O2	90.5(3)	O10[2]	Al2	Al2[2]	38.64(18)
O5	Al1	O2	94.6(3)	O10	Al2	Al2[2]	38.76(16)
O5	Al1	O3	174.3(3)	O10	Al2	O6	173.7(3)
O5[1]	Al1	O3	95.9(3)	O10[2]	Al2	O6	96.4(3)
O5	Al1	O4	90.2(3)	O10[2]	Al2	O8	90.4(3)
O5[1]	Al1	O4	94.6(3)	O10	Al2	O8	94.6(3)
O5	Al1	O1	96.0(3)	O10	Al2	O10[2]	77.4(2)
O5[1]	Al1	O1	174.5(3)	O10	Al2	O7	90.0(3)
O2	Al1	Al1[1]	93.08(19)	O10[2]	Al2	O7	94.7(3)
O2	Al1	O4	173.6(3)	O10[2]	Al2	O9	173.9(3)
O2	Al1	O1	89.2(2)	O10	Al2	O9	96.6(3)
O3	Al1	Al1[1]	135.1(2)	O7	Al2	Al2[2]	93.2(2)
O3	Al1	O2	86.6(3)	O7	Al2	O9	86.0(3)
O3	Al1	O4	89.1(3)	O9	Al2	Al2[2]	135.3(2)
O3	Al1	O1	89.6(3)	C16	O6	Al2	128.2(6)

O4	Al1	Al1^1	93.4(2)	C21	O8	Al2	128.5(6)
O1	Al1	Al1^1	135.2(2)	Al2	O10	Al2^2	102.6(2)
O1	Al1	O4	86.1(3)	C27	O10	Al2^2	127.1(9)
Al1	O5	Al1^1	101.5(2)	C27	O10	Al2	129.3(8)
C13	O5	Al1^1	128.2(8)	C18	O7	Al2	129.6(6)
C13	O5	Al1	129.6(8)	C23	O9	Al2	129.6(6)
C4	O2	Al1	128.3(5)	O9	C23	C24	116.5(8)
C7	O3	Al1	129.3(5)	O9	C23	C22	124.3(8)
C9	O4	Al1	129.5(6)	C22	C23	C24	119.1(8)
C2	O1	Al1	130.3(5)	O6	C16	C17	124.5(8)
O4	C9	C10	114.6(9)	O6	C16	C15	113.6(7)
O4	C9	C8	124.0(8)	C17	C16	C15	121.7(7)
C8	C9	C10	121.3(8)	O7	C18	C19	115.1(8)
O1	C2	C1	117.9(7)	O7	C18	C17	123.7(8)
O1	C2	C3	122.7(8)	C17	C18	C19	121.0(8)
C3	C2	C1	119.5(8)	C16	C17	C18	122.3(8)
O3	C7	C8	122.6(7)	C21	C22	C23	122.1(8)
O3	C7	C6	115.3(7)	O8	C21	C22	124.2(8)
C8	C7	C6	121.9(8)	O8	C21	C20	116.1(8)
C7	C8	C9	123.3(8)	C22	C21	C20	119.8(8)
O2	C4	C3	124.2(8)	O10	C27	C28	111.6(13)
O2	C4	C5	115.4(9)	C26	C27	O10	121.3(16)
C3	C4	C5	120.4(8)	C26	C27	C28	127.1(11)
C4	C3	C2	123.5(8)	O5	C13	C14	111.6(13)
O6	Al2	Al2^2	135.1(2)	C12	C13	O5	124.3(17)
O6	Al2	O8	86.5(3)	C12	C13	C14	124.1(10)
O6	Al2	O7	89.5(3)	C27	C26	C25	125.6(12)
O6	Al2	O9	89.6(3)	C11	C12	C13	123.9(12)

^{1}-3-X,-2-Y,+Z; ^{2}-4-X,-1-Y,+Z

Table 6 Hydrogen Atom Coordinates ($Å×10^4$) and Isotropic Displacement Parameters ($Å^2×10^3$) for DC46_0M.

Atom	x	y	z	U(eq)
H1A	-13698	-6418	-11147	101
H1B	-13851	-6188	-10624	101
H1C	-14696	-6307	-10954	101
H10A	-14403	-9318	-12583	126
H10B	-13437	-8898	-12694	126
H10C	-14241	-8259	-12532	126
H8	-12355	-8771	-12097	77
H3	-13713	-7346	-10130	79
H6A	-11421	-8596	-11083	107
H6B	-11166	-8917	-11583	107
H6C	-11348	-9646	-11196	107
H5A	-14414	-8929	-9546	117
H5B	-13449	-8456	-9568	117
H5C	-13549	-9497	-9694	117
H24A	-19684	-8687	-10982	96
H24B	-18888	-8825	-10625	96
H24C	-18660	-8584	-11139	96
H19A	-19098	-6767	-12548	129
H19B	-18471	-5940	-12689	129
H19C	-19499	-5769	-12554	129
H17	-17349	-6251	-12095	82
H22	-18698	-7658	-10129	83
H20A	-18667	-5469	-9688	120
H20B	-18389	-6487	-9582	120

H20C	-19418	-6183	-9543	120
H15A	-16339	-5348	-11200	99
H15B	-16157	-6102	-11575	99
H15C	-16426	-6390	-11072	99
H28A	-21048	-6035	-10290	246
H28B	-21529	-6975	-10393	246
H28C	-22094	-6061	-10415	246
H11A	-16728	-8025	-11942	176
H11B	-16599	-9074	-11841	176
H11C	-15757	-8407	-11812	176
H27	-21724	-5762	-11074	165
H13	-16713	-9242	-11092	169
H26A	-22217	-6645	-11315	155
H26B	-21374	-7295	-11297	155
H12A	-17224	-8375	-11324	154
H12B	-16402	-7698	-11299	154
H14A	-17118	-8964	-10441	220
H14B	-16602	-8021	-10418	220
H14C	-16081	-8932	-10300	220
H25A	-21717	-6972	-11948	172
H25B	-20760	-6548	-11824	172
H25C	-21632	-5919	-11846	172

Experimental

Single crystals of $C_{28}H_{39}Al_2O_{10}$ **[DC46_0M]** were **[Recrystallised by slow evaporation from chloroform]**. A suitable crystal was selected and **[MiTeGen Mesh]** on a **'Bruker APEX-II CCD'** diffractometer. The crystal was kept at 150 K during data collection. Using Olex2 [1], the structure was solved with the ShelXS [2] structure solution program using Direct Methods and refined with the ShelXL [3] refinement package using Least Squares minimisation.

Dolomanov, O.V., Bourhis, L.J., Gildea, R.J, Howard, J.A.K. & Puschmann, H. (2009), J. Appl. Cryst. 42, 339-341.

Sheldrick, G.M. (2008). Acta Cryst. A64, 112-122

Sheldrick, G.M. (2008). Acta Cryst. A64, 112-122

Crystal structure determination of [DC46_0M]

Crystal Data for $C_{28}H_{39}Al_2O_{10}$ (M =589.55): tetragonal, space group $I4_1$ (no. 80), a = 14.8759(2) Å, c = 29.5961(6) Å, V = 6549.4(2) Å^3, Z = 8, T = 150 K, μ(MoKα) = 0.138 mm^{-1}, $Dcalc$ = 1.196 g/mm^3, 59082 reflections measured (3.064 ≤ 2Θ ≤ 56.714), 8169 unique (R_{int} = 0.0459, R$_{sigma}$ = 0.0275) which were used in all calculations. The final R_1 was 0.0705 (I > 2σ(I)) and wR_2 was 0.2085 (all data).

Refinement model description

Number of restraints - 1, number of constraints - unknown.

Details:

```
1.                           Fixed                              Uiso
 At                1.2                 times                      of:
  All       C(H)        groups,        All       C(H,H)        groups
 At                1.5                 times                      of:
  All                       C(H,H,H)                           groups
2.a    Ternary    CH    refined    with    riding    coordinates:
 C27(H27),                                              C13(H13)
2.b    Secondary    CH2    refined    with    riding    coordinates:
 C26(H26A,H26B),                              C12(H12A,H12B)
2.c    Aromatic/amide    H    refined    with    riding    coordinates:
 C8(H8),          C3(H3),          C17(H17),          C22(H22)
2.d    Idealised    Me    refined    as    rotating    group:
 C1(H1A,H1B,H1C),  C10(H10A,H10B,H10C),  C6(H6A,H6B,H6C),  C5(H5A,H5B,H5C),
 C24(H24A,H24B,H24C),      C19(H19A,H19B,H19C),      C20(H20A,H20B,H20C),
C15(H15A,H15B,
 H15C),   C28(H28A,H28B,H28C),   C11(H11A,H11B,H11C),   C14(H14A,H14B,H14C),
C25(H25A,
 H25B,H25C)
```

6.2. Crystallographic information of compound 5

Table 1 Crystal data and structure refinement for compound **5**

Identification code	DC94
Empirical formula	$C_{24}H_{26}F_2O_6Ti$
Formula weight	143.86
Temperature/K	173.15
Crystal system	monoclinic
Space group	$P2_1/n$
a/Å	11.2553(10)
b/Å	19.6468(19)
c/Å	11.3094(11)
α/°	90
β/°	90.178(5)
γ/°	90
Volume/Å^3	2500.8(4)
Z	4
ρ_{calc}mg/mm^3	0.3821
m/mm^{-1}	0.328
F(000)	281.4
Crystal size/mm^3	$0.02 \times 0.03 \times 0.02$
Radiation	Mo Kα (λ = 0.71073)
2Θ range for data collection	4.14 to 69.6°
Index ranges	$-17 \leq h \leq 13, -29 \leq k \leq 31, -17 \leq l \leq 12$
Reflections collected	46103
Independent reflections	9026 [R_{int} = 0.0754, R_{sigma} = 0.1400]
Data/restraints/parameters	9026/0/28
Goodness-of-fit on F^2	5.519
Final R indexes [I>=2σ (I)]	R_1 = 0.5455, wR_2 = 0.8418
Final R indexes [all data]	R_1 = 0.6230, wR_2 = 0.8677
Largest diff. peak/hole / e Å^{-3}	11.13/-16.20

Table 2 Fractional Atomic Coordinates ($\times 10^4$) and Equivalent Isotropic Displacement Parameters (Å$^2\times 10^3$) for DC94. U$_{eq}$ is defined as 1/3 of of the trace of the orthogonalised U$_{IJ}$ tensor.

Atom	x	y	z	U(eq)
Ti2	9219(3)	2576.6(14)	1538(3)	21.4(9)
O4	9180(20)	3374(13)	2700(20)	68(6)
O8	8974(18)	3246(10)	324(19)	50(5)
O10	9500(40)	2110(20)	2350(40)	130(13)
O11	11033(18)	2831(11)	1200(20)	54(5)
O18	9550(20)	1848(13)	160(20)	67(6)
O38	7512(17)	2414(9)	1303(18)	46(4)

Table 3 Bond Lengths for DC94.

Atom	Atom	Length/Å	Atom	Atom	Length/Å
Ti2	O4	2.05(3)	Ti2	O11	2.14(2)
Ti2	O8	1.92(2)	Ti2	O18	2.15(3)
Ti2	O10	1.34(4)	Ti2	O38	1.96(2)

Table 4 Bond Angles for DC94.

Atom	Atom	Atom	Angle/°	Atom	Atom	Atom	Angle/°
O8	Ti2	O4	86.1(9)	O18	Ti2	O10	90(2)
O10	Ti2	O4	95(2)	O18	Ti2	O11	81.7(9)
O10	Ti2	O8	174.6(18)	O38	Ti2	O4	100.9(9)
O11	Ti2	O4	87.7(9)	O38	Ti2	O8	82.9(8)
O11	Ti2	O8	81.2(8)	O38	Ti2	O10	102.0(19)
O11	Ti2	O10	93.6(19)	O38	Ti2	O11	161.4(9)
O18	Ti2	O4	168.5(10)	O38	Ti2	O18	88.1(9)
O18	Ti2	O8	87.8(10)				

Experimental

Single crystals of $C_{24}H_{26}F_2O_6Ti$ **[DC94]** were **[obtained from recrystallisation from hot ethanol]**. A suitable crystal was selected and **[Crystal mounted on MiTeGen loop under flombilin]** on a **'Bruker APEX-II CCD'** diffractometer. The crystal was kept at 173.15 K during data collection. Using Olex2 [1], the structure was solved with the ShelXS [2] structure solution program using Patterson Method and refined with the ShelXL [3] refinement package using CGLS minimisation.

1. Dolomanov, O.V., Bourhis, L.J, Gildea, R.J, Howard, J.A.K. & Puschmann, H. (2009), J. Appl. Cryst. 42, 339-341.
2. Sheldrick, G.M. (2008). Acta Cryst. A64, 112-122
3. Sheldrick, G.M. (2008). Acta Cryst. A64, 112-122

Crystal structure determination of [DC94]

Crystal Data for $C_{24}H_{26}F_2O_6Ti$ (M =143.86): monoclinic, space group $P2_1/n$ (no. 14), a = 11.2553(10) Å, b = 19.6468(19) Å, c = 11.3094(11) Å, β = 90.178(5)°, V = 2500.8(4) Å^3, Z = 4, T = 173.15 K, μ(Mo Kα) = 0.328 mm^{-1}, $Dcalc$ = 0.3821 g/mm^3, 46103 reflections measured (4.14 ≤ 2Θ ≤ 69.6), 9026 unique (R_{int} = 0.0754, R_{sigma} = 0.1400) which were used in all calculations. The final R_1 was 0.5455 (I>=2u(I)) and wR_2 was 0.8677 (all data).

Refinement model description

Number of restraints - 0, number of constraints - 0.

Details:
```
1. Fixed Uiso
 At 1.2 times of:
  All C(H) groups, All C(H,H) groups
 At 1.5 times of:
  All C(H,H,H) groups
2.a Secondary CH2 refined with riding coordinates:
 C22(H22A,H22B), C23(H23A,H23B)
2.b Aromatic/amide H refined with riding coordinates:
 C6(H6), C19(H19), C16(H16), C10(H10), C17(H17), C9(H9), C20(H20), C7(H7)
2.c Idealised Me refined as rotating group:
 C11(H11A,H11B,H11C), C1(H1A,H1B,H1C), C21(H21A,H21B,H21C),
C24(H24A,H24B,H24C)
```

6.3. Crystallographic information of compound 6

Table 1 Crystal data and structure refinement for DC133.

Identification code	DC133
Empirical formula	$C_{11}H_{14}O_3TiBr$
Formula weight	309.07
Temperature/K	150.0
Crystal system	orthorhombic
Space group	Ccc2
a/Å	11.4688(12)
b/Å	22.418(2)
c/Å	10.6590(12)
$\alpha/°$	90
$\beta/°$	90
$\gamma/°$	90
Volume/$\mathring{A}^3$	2740.5(5)
Z	8
ρ_{calc}mg/mm^3	1.4981
m/mm^{-1}	3.261
F(000)	1239.6
Crystal size/mm^3	$0.01 \times 0.02 \times 0.02$
Radiation	Mo Kα ($\lambda = 0.71073$)
2Θ range for data collection	3.64 to 67.1°
Index ranges	$-17 \le h \le 17, -34 \le k \le 22, -16 \le l \le 16$
Reflections collected	19850
Independent reflections	5371 [$R_{int} = 0.0238$, $R_{sigma} = 0.0410$]
Data/restraints/parameters	5371/0/151
Goodness-of-fit on F^2	0.964
Final R indexes [I>=2σ (I)]	$R_1 = 0.0281$, wR_2 = N/A
Final R indexes [all data]	$R_1 = 0.0380$, $wR_2 = 0.0714$
Largest diff. peak/hole / e Å^{-3}	1.09/-0.46
Flack parameter	0.016(7)

Table 2 Fractional Atomic Coordinates ($\times 10^4$) and Equivalent Isotropic Displacement Parameters ($\mathring{A}^2 \times 10^3$) for DC133. U_{eq} is defined as 1/3 of of the trace of the orthogonalised U_{IJ} tensor.

Atom	x	y	z	U(eq)
Br1	2149.0(2)	4970.04(8)	9611.39(18)	48.27(7)
Ti1	2500	7500	3142.8(3)	20.54(7)
O3	2380.4(8)	6881.5(5)	2035.1(12)	27.2(2)
O2	2219.9(9)	6912.5(5)	4634.8(12)	24.76(19)
O1	791.5(8)	7665.6(5)	3392.3(9)	25.5(2)
C10	2664.3(13)	6158.1(8)	6631.9(16)	28.9(3)

C9	2844.6(15)	5722.8(8)	7556.0(18)	33.5(3)
C8	1926.8(16)	5579.0(7)	8374.7(16)	35.7(4)
C5	1572.0(12)	6449.8(7)	6514.5(14)	24.7(3)
C1	−1087.3(14)	7879.8(10)	4222.8(18)	44.8(5)
C2	98.2(11)	7582.8(7)	4334.8(15)	26.2(3)
C3	368.7(14)	7234.6(8)	5397.2(16)	30.1(3)
C4	1404.0(12)	6890.4(6)	5465.7(13)	22.5(3)
C7	857.7(18)	5869.7(8)	8301.0(19)	47.5(4)
C6	680.5(16)	6308.2(8)	7374.5(17)	40.9(4)
C11	2540.9(17)	6264.1(9)	1859(2)	44.1(5)
C12	3800.3(18)	6062.3(9)	2051(3)	56.8(6)

Table 3 Anisotropic Displacement Parameters ($Å^2×10^3$) for DC133. The Anisotropic displacement factor exponent takes the form: $-2\pi^2[h^2a*^2U_{11}+2hka*b*U_{12}+…]$.

Atom	U_{11}	U_{22}	U_{33}	U_{12}	U_{13}	U_{23}
Br1	83.92(15)	28.98(9)	31.91(9)	−1.85(8)	−8.18(11)	7.86(8)
Ti1	17.09(11)	30.30(17)	14.23(13)	−2.27(12)	−0	0
O3	25.8(5)	32.7(6)	23.2(5)	−1.5(4)	−2.4(4)	−4.7(5)
O2	21.9(4)	31.3(5)	21.1(5)	−0.1(4)	2.7(4)	3.2(5)
O1	19.7(4)	38.2(5)	18.7(5)	−1.8(4)	−0.5(3)	3.1(4)
C10	32.1(8)	27.6(8)	27.1(8)	−1.7(5)	−1.8(6)	1.0(7)
C9	39.2(8)	27.9(8)	33.3(9)	0.4(6)	−8.3(7)	0.8(7)
C8	59.2(10)	24.7(7)	23.1(8)	−4.1(7)	−6.0(7)	1.8(6)
C5	29.6(7)	25.4(7)	19.2(6)	−4.0(5)	0.1(5)	−0.6(6)
C1	29.7(8)	69.6(13)	35.0(9)	15.2(8)	8.1(7)	14.4(9)
C2	20.4(5)	34.5(8)	23.8(8)	−0.1(5)	1.8(5)	1.1(6)
C3	27.8(6)	41.0(9)	21.5(7)	4.1(6)	6.6(6)	5.4(7)
C4	25.1(6)	25.3(7)	17.0(6)	−2.2(5)	−0.2(5)	−0.9(5)
C7	57.6(10)	45.2(10)	39.6(11)	0.4(8)	14.9(9)	16.8(9)
C6	39.2(9)	44.3(10)	39.1(10)	3.9(7)	12.0(8)	15.5(8)
C11	41.5(9)	33.0(9)	58.0(14)	−5.8(7)	−6.8(9)	−3.4(9)
C12	45(1)	36.2(9)	89.1(18)	6.9(8)	−7.4(12)	−5.4(12)

Table 4 Bond Lengths for DC133.

Atom	Atom	Length/Å	Atom	Atom	Length/Å
Br1	C8	1.9148(17)	C10	C5	1.419(2)
Ti1	O3	1.8264(12)	C9	C8	1.405(3)
Ti1	O3[1]	1.8264(12)	C8	C7	1.391(3)
Ti1	O2[1]	2.0897(12)	C5	C4	1.504(2)
Ti1	O2	2.0897(12)	C5	C6	1.409(2)
Ti1	O1	2.0119(9)	C1	C2	1.519(2)
Ti1	O1[1]	2.0119(9)	C2	C3	1.410(2)

O3	C11	1.409(2)	C3	C4	1.418(2)
O2	C4	1.2894(18)	C7	C6	1.408(2)
O1	C2	1.2946(17)	C11	C12	1.527(3)
C10	C9	1.402(3)			

[1]1/2-X,3/2-Y,+Z

Table 5 Bond Angles for DC133.

Atom	Atom	Atom	Angle/°	Atom	Atom	Atom	Angle/°
O3[1]	Ti1	O3	99.44(8)	C5	C10	C9	120.87(15)
O2	Ti1	O3	90.11(5)	C8	C9	C10	119.06(16)
O2	Ti1	O3[1]	169.12(5)	C9	C8	Br1	119.45(14)
O2[1]	Ti1	O3	169.12(5)	C7	C8	Br1	119.36(14)
O2[1]	Ti1	O3[1]	90.11(5)	C7	C8	C9	121.19(17)
O2[1]	Ti1	O2	80.89(7)	C4	C5	C10	118.78(13)
O1	Ti1	O3[1]	91.06(4)	C6	C5	C10	118.65(14)
O1	Ti1	O3	98.77(4)	C6	C5	C4	122.57(13)
O1[1]	Ti1	O3[1]	98.77(4)	C1	C2	O1	115.22(14)
O1[1]	Ti1	O3	91.06(4)	C3	C2	O1	124.58(13)
O1	Ti1	O2	82.30(4)	C3	C2	C1	120.19(14)
O1	Ti1	O2[1]	86.15(4)	C4	C3	C2	121.79(14)
O1[1]	Ti1	O2	86.15(4)	C5	C4	O2	116.28(12)
O1[1]	Ti1	O2[1]	82.30(4)	C3	C4	O2	123.47(14)
O1[1]	Ti1	O1	164.81(6)	C3	C4	C5	120.19(13)
C11	O3	Ti1	145.30(14)	C6	C7	C8	119.60(16)
C4	O2	Ti1	131.18(9)	C7	C6	C5	120.58(16)
C2	O1	Ti1	132.40(9)	C12	C11	O3	113.37(16)

[1]1/2-X,3/2-Y,+Z

Table 6 Hydrogen Atom Coordinates ($Å×10^4$) and Isotropic Displacement Parameters ($Å^2×10^3$) for DC133.

Atom	x	y	z	U(eq)
H10	3281.7(13)	6259.1(8)	6077.0(16)	34.7(4)
H9	3577.1(15)	5527.9(8)	7627.6(18)	40.2(4)
H1a	−986.5(17)	8313.3(11)	4174(16)	67.1(7)
H1b	−1480(6)	7737(6)	3463(9)	67.1(7)
H1c	−1561(6)	7781(6)	4959(8)	67.1(7)
H3	−157.1(14)	7230.3(8)	6085.8(16)	36.1(4)
H7	250.6(18)	5773.1(8)	8872.3(19)	57.0(5)
H6	−46.3(16)	6510.4(8)	7328.7(17)	49.0(5)
H11a	2033.4(17)	6045.7(9)	2454(2)	53.0(6)
H11b	2293.0(17)	6157.1(9)	998(2)	53.0(6)
H12a	4319(2)	6304(5)	1525(12)	85.2(9)

H12b	4016(5)	6112(7)	2934(4)	85.2(9)
H12c	3875(4)	5641(2)	1816(15)	85.2(9)

Experimental

Single crystals of $C_{11}H_{14}O_3TiBr$ **[DC133]** were **[obtained from recrystallisation with hot ethanol]**. A suitable crystal was selected and **[mounted on a MiTeGen crystal mount]** on a **Bruker X8** diffractometer. The crystal was kept at 150.0 K during data collection. Using Olex2 [1], the structure was solved with the Superflip [2] structure solution program using Charge Flipping and refined with the olex2.refine [3] refinement package using Gauss-Newton minimisation.

1. Dolomanov, O.V., Bourhis, L.J., Gildea, R.J, Howard, J.A.K. & Puschmann, H. (2009), J. Appl. Cryst. 42, 339-341.
2. Palatinus, L. & Chapuis, G. (2007). J. Appl. Cryst., 40, 786-790; Palatinus, L. & van der Lee, A. (2008). J. Appl. Cryst. 41, 975-984; Palatinus, L., Prathapa, S. J. & van Smaalen, S. (2012). J. Appl. Cryst. 45, 575-580
3. Bourhis, L.J., Dolomanov, O.V., Gildea, R.J., Howard, J.A.K., Puschmann, H. (2013). in preparation

Crystal structure determination of [DC133]

Crystal Data for $C_{11}H_{14}O_3TiBr$ (*M* =309.07): orthorhombic, space group Ccc2 (no. 37), *a* = 11.4688(12) Å, *b* = 22.418(2) Å, *c* = 10.6590(12) Å, *V* = 2740.5(5) Å^3, *Z* = 8, *T* = 150.0 K, μ(Mo Kα) = 3.261 mm^{-1}, *Dcalc* = 1.4981 g/mm^3, 19850 reflections measured ($3.64 \leq 2\Theta \leq 67.1$), 5371 unique ($R_{int}$ = 0.0238, R_{sigma} = 0.0410) which were used in all calculations. The final R_1 was 0.0281 (I>=2u(I)) and wR_2 was 0.0714 (all data).

Refinement model description

Number of restraints - 0, number of constraints - 21.
Details:
```
1. Fixed Uiso
 At 1.2 times of:
  All C(H) groups, All C(H,H) groups
 At 1.5 times of:
  All C(H,H,H) groups
2.a Secondary CH2 refined with riding coordinates:
 C11(H11a,H11b)
2.b Aromatic/amide H refined with riding coordinates:
 C10(H10), C9(H9), C3(H3), C7(H7), C6(H6)
2.c Idealised Me refined as rotating group:
 C1(H1a,H1b,H1c), C12(H12a,H12b,H12c)
```

6.4. Crystallographic data of compound 11

Table 1 Crystal data and structure refinement for dc150.

Identification code	dc150
Empirical formula	$C_{34}H_{32}O_6Ti$
Formula weight	425.32
Temperature/K	150
Crystal system	monoclinic
Space group	$P2_1/c$
a/Å	11.2203(12)
b/Å	15.8876(16)
c/Å	20.1373(19)
α/°	90
β/°	121.131(6)
γ/°	90
Volume/Å^3	3072.8(6)
Z	4
ρ_{calc}mg/mm^3	0.919
m/mm^{-1}	0.113
F(000)	850.0
Crystal size/mm^3	$0.083 \times 0.072 \times 0.011$
Radiation	MoKα (λ = 0.71073)
2Θ range for data collection	3.486 to 60.484°
Index ranges	$-15 \leq h \leq 15$, $-22 \leq k \leq 22$, $-28 \leq l \leq 24$
Reflections collected	37033
Independent reflections	8994 [R_{int} = 0.0621, R_{sigma} = 0.0646]
Data/restraints/parameters	8994/0/378
Goodness-of-fit on F^2	1.021
Final R indexes [I>=2σ (I)]	R_1 = 0.0612, wR_2 = 0.1674
Final R indexes [all data]	R_1 = 0.0932, wR_2 = 0.1908
Largest diff. peak/hole / e Å^{-3}	1.16/-0.64

Table 2 Fractional Atomic Coordinates (×10^4) and Equivalent Isotropic Displacement Parameters (Å^2×10^3) for dc150. U_{eq} is defined as 1/3 of of the trace of the orthogonalised U_{IJ} tensor.

Atom	x	y	z	U(eq)
Ti1	1966.9(4)	2223.5(3)	3486.6(2)	20.00(12)
O3	711.0(17)	3112.8(11)	3607.1(9)	24.0(3)
O2	474.3(17)	1416.3(11)	3479.5(9)	23.6(3)
O1	585.4(17)	2274.8(10)	2333.6(9)	23.5(3)
O4	2934.4(17)	2181.9(10)	4660.7(9)	22.9(3)
O6	2964.7(17)	3095.9(11)	3413.6(10)	25.1(4)
O5	3033.6(18)	1338.7(11)	3530.3(10)	27.6(4)

Atom	x	y	z	U(eq)
C21	-486(2)	3984.4(14)	4047.6(13)	21.5(4)
C7	-727(2)	2070.9(14)	1908.0(13)	19.4(4)
C26	5061(2)	2015.4(15)	6191.6(14)	22.5(5)
C25	3736(2)	2330.6(13)	6006.6(13)	18.8(4)
C29	4485(3)	2256.1(16)	7387.0(14)	27.6(5)
C19	-1869(3)	5204.8(17)	3305.4(16)	35.0(6)
C18	-2483(3)	5234.4(16)	3760.2(16)	33.1(6)
C6	-1469(2)	2364.8(14)	1069.2(13)	20.3(4)
C30	3461(3)	2450.1(15)	6612.0(13)	22.6(5)
C22	600(2)	3328.3(14)	4188.0(13)	19.9(4)
C11	-3142(2)	846.4(15)	2799.9(14)	25.1(5)
C14	-1771(3)	-311.0(16)	4018.6(15)	29.8(5)
C15	-994(3)	181.8(15)	3798.5(14)	25.5(5)
C24	2666(2)	2506.5(14)	5165.7(13)	18.3(4)
C28	5791(3)	1942.4(17)	7559.8(15)	30.1(5)
C9	-817(2)	1296.8(14)	2958.3(13)	20.2(4)
C2	-1478(3)	3262.4(18)	82.0(16)	38.0(7)
C4	-3514(3)	2407.7(18)	-252.5(15)	30.8(6)
C16	-1107(2)	4025.1(15)	4503.5(14)	25.1(5)
C23	1494(2)	3019.0(15)	4958.2(14)	21.9(4)
C8	-1462(3)	1617.7(16)	2187.7(14)	26.2(5)
C10	-1679(2)	768.0(14)	3182.0(13)	20.6(4)
C13	-3226(3)	-220.2(16)	3641.4(16)	29.0(5)
C5	-2830(3)	2090.7(16)	507.0(14)	26.2(5)
C27	6087(2)	1827.2(16)	6967.7(15)	27.3(5)
C20	-876(3)	4575.3(16)	3444.4(14)	28.3(5)
C12	-3914(3)	359.8(16)	3031.0(15)	27.5(5)
C17	-2113(3)	4643.7(17)	4355.3(16)	31.5(6)
C1	-792(3)	2954.1(16)	849.9(15)	28.7(5)
C33	2782(3)	3977.0(18)	3241.5(18)	39.1(7)
C32	2828(4)	-55(2)	3989(2)	60.7(10)
C31	3752(3)	608(2)	3977(2)	48.6(8)
C34	3556(5)	4487(2)	3987(3)	75.3(13)
C3	-2838(3)	2996.5(18)	-462.0(15)	34.9(6)

Table 3 Anisotropic Displacement Parameters ($\text{Å}^2 \times 10^3$) for dc150. The Anisotropic displacement factor exponent takes the form: -$2\pi^2[h^2 a^{*2} U_{11} + 2hka^* b^* U_{12} + \ldots]$.

Atom	U_{11}	U_{22}	U_{33}	U_{23}	U_{13}	U_{12}
Ti1	15.38(19)	30.7(2)	12.3(2)	0.61(15)	5.97(15)	1.49(15)
O3	20.4(8)	33.7(9)	15.2(8)	3.0(6)	7.3(7)	6.4(7)
O2	19.3(8)	34.8(9)	14.0(8)	3.4(6)	6.8(7)	0.7(6)
O1	18.1(8)	37.3(9)	12.9(8)	0.4(6)	6.5(7)	-2.0(6)
O4	17.8(8)	34.8(9)	13.6(8)	1.3(6)	6.2(6)	4.7(6)
O6	20.7(8)	33.0(9)	18.7(8)	1.2(7)	8.2(7)	-1.3(7)

O5	25.4(9)	34.6(9)	23.9(9)	1.7(7)	13.4(8)	6.0(7)
C21	15.4(10)	26.1(11)	15.6(10)	−1.1(8)	2.8(8)	1.2(8)
C7	18.7(10)	26.6(11)	12.8(10)	0.1(8)	8.2(9)	3.1(8)
C26	17.7(10)	29.4(11)	17.7(11)	5.5(8)	7.2(9)	2.2(8)
C25	17.4(10)	23.6(10)	12.4(10)	2.7(8)	5.6(8)	−0.8(8)
C29	29.9(13)	35.7(13)	14.5(11)	1.5(9)	9.5(10)	−3.3(10)
C19	30.9(14)	32.7(13)	26.3(14)	5.7(10)	4.1(11)	8.3(10)
C18	25.4(13)	29.6(12)	29.5(14)	−4.5(10)	3.8(11)	8.7(10)
C6	19.1(10)	28.7(11)	13.4(10)	1.0(8)	8.7(9)	2.5(8)
C30	20.8(11)	29.7(11)	16.7(11)	2.5(8)	9.1(9)	0.2(9)
C22	15(1)	25.3(10)	16.7(10)	0.0(8)	6.1(8)	0.3(8)
C11	23.8(11)	29.1(11)	21.3(12)	2.1(9)	11(1)	1.4(9)
C14	33.3(14)	29.9(12)	26.9(13)	5.5(10)	16.1(11)	1.6(10)
C15	24.9(12)	29.3(12)	21.8(12)	3.7(9)	11.7(10)	3.3(9)
C24	15.9(10)	23.2(10)	13(1)	0.8(8)	5.6(8)	−2.5(8)
C28	25.2(12)	38.5(13)	15.8(11)	6.8(10)	2.9(10)	−0.3(10)
C9	20.7(10)	25.7(11)	15.9(10)	0.5(8)	10.6(9)	2.1(8)
C2	44.5(17)	39.4(15)	22.5(13)	5.9(11)	11.9(12)	−10.6(12)
C4	21.7(12)	46.8(15)	15.2(12)	0.3(10)	3.5(10)	1.6(10)
C16	19.4(11)	28.7(11)	22.2(12)	−0.3(9)	7.3(9)	1.3(9)
C23	19.5(11)	30.3(11)	14.1(10)	1.3(8)	7.4(9)	4.7(8)
C8	18.6(11)	40.1(13)	15.5(11)	4.7(9)	5.7(9)	−1.9(9)
C10	22.4(11)	24.2(10)	15.7(10)	−1.2(8)	10.3(9)	0.2(8)
C13	32.2(13)	28.5(12)	30.7(14)	−0.9(10)	19.3(12)	−6.2(10)
C5	20.8(11)	40.6(14)	16.0(11)	1.8(9)	8.5(10)	−1.7(9)
C27	17.3(11)	35.8(13)	22.1(12)	6(1)	5.4(10)	3.1(9)
C20	24.9(12)	34.6(13)	19.6(12)	2.8(9)	7.2(10)	3.8(10)
C12	21.3(11)	34.4(13)	26.5(13)	−0.4(10)	12.2(10)	−3.4(9)
C17	24.3(12)	36.9(13)	29.3(14)	−7.1(11)	10.9(11)	3.7(10)
C1	27.6(13)	35.4(13)	17.6(12)	1.7(9)	7.7(10)	−6.6(10)
C33	43.0(16)	38.1(15)	41.2(17)	11.3(12)	25.2(14)	4.5(12)
C32	45(2)	46.8(19)	78(3)	25.2(18)	23(2)	16.3(15)
C31	34.7(16)	51.5(18)	56(2)	22.2(16)	21.1(15)	20.5(14)
C34	106(4)	34.8(17)	72(3)	−11.3(18)	37(3)	−5(2)
C3	40.5(16)	39.1(14)	16.0(12)	7.9(10)	8.2(12)	4.1(12)

Table 4 Bond Lengths for dc150.

Atom	Atom	Length/Å	Atom	Atom	Length/Å
Ti1	O3	2.0963(17)	C19	C18	1.403(4)
Ti1	O2	2.1035(17)	C19	C20	1.413(4)
Ti1	O1	2.0197(17)	C18	C17	1.405(4)
Ti1	O4	2.0295(17)	C6	C5	1.420(3)
Ti1	O6	1.8348(17)	C6	C1	1.413(3)
Ti1	O5	1.8186(17)	C22	C23	1.430(3)
O3	C22	1.285(3)	C11	C10	1.413(3)

Atom	Atom	Length/Å	Atom	Atom	Length/Å
O2	C9	1.290(3)	C11	C12	1.408(3)
O1	C7	1.305(3)	C14	C15	1.403(3)
O4	C24	1.306(3)	C14	C13	1.408(4)
O6	C33	1.431(3)	C15	C10	1.419(3)
O5	C31	1.434(3)	C24	C23	1.414(3)
C21	C22	1.515(3)	C28	C27	1.405(4)
C21	C16	1.412(3)	C9	C8	1.425(3)
C21	C20	1.414(3)	C9	C10	1.515(3)
C7	C6	1.520(3)	C2	C1	1.412(4)
C7	C8	1.413(3)	C2	C3	1.407(4)
C26	C25	1.423(3)	C4	C5	1.403(3)
C26	C27	1.413(3)	C4	C3	1.400(4)
C25	C30	1.417(3)	C16	C17	1.407(3)
C25	C24	1.511(3)	C13	C12	1.405(4)
C29	C30	1.413(3)	C33	C34	1.521(5)
C29	C28	1.410(4)	C32	C31	1.486(5)

Table 5 Bond Angles for dc150.

Atom	Atom	Atom	Angle/°	Atom	Atom	Atom	Angle/°
O3	Ti1	O2	80.29(7)	C1	C6	C7	118.5(2)
O1	Ti1	O3	86.76(7)	C1	C6	C5	119.0(2)
O1	Ti1	O2	83.20(7)	C29	C30	C25	120.4(2)
O1	Ti1	O4	166.16(7)	O3	C22	C21	117.43(19)
O4	Ti1	O3	82.75(6)	O3	C22	C23	123.5(2)
O4	Ti1	O2	86.13(7)	C23	C22	C21	119.0(2)
O6	Ti1	O3	88.54(8)	C12	C11	C10	120.8(2)
O6	Ti1	O2	167.60(7)	C15	C14	C13	120.6(2)
O6	Ti1	O1	90.85(7)	C14	C15	C10	119.9(2)
O6	Ti1	O4	97.86(7)	O4	C24	C25	115.48(19)
O5	Ti1	O3	168.62(7)	O4	C24	C23	123.4(2)
O5	Ti1	O2	91.77(8)	C23	C24	C25	121.1(2)
O5	Ti1	O1	100.46(8)	C27	C28	C29	120.5(2)
O5	Ti1	O4	88.64(7)	O2	C9	C8	123.9(2)
O5	Ti1	O6	100.03(8)	O2	C9	C10	117.44(19)
C22	O3	Ti1	132.24(14)	C8	C9	C10	118.6(2)
C9	O2	Ti1	130.58(14)	C3	C2	C1	120.4(2)
C7	O1	Ti1	132.83(14)	C3	C4	C5	119.5(2)
C24	O4	Ti1	133.97(15)	C17	C16	C21	120.3(2)
C33	O6	Ti1	137.85(17)	C24	C23	C22	122.8(2)
C31	O5	Ti1	142.95(19)	C7	C8	C9	123.0(2)
C16	C21	C22	122.0(2)	C11	C10	C15	119.0(2)
C16	C21	C20	119.4(2)	C11	C10	C9	122.0(2)
C20	C21	C22	118.6(2)	C15	C10	C9	119.0(2)
O1	C7	C6	115.95(19)	C12	C13	C14	119.9(2)
O1	C7	C8	123.9(2)	C4	C5	C6	121.1(2)

C8	C7	C6	120.1(2)	C28	C27	C26	119.7(2)
C27	C26	C25	120.5(2)	C19	C20	C21	120.1(2)
C26	C25	C24	118.4(2)	C13	C12	C11	119.7(2)
C30	C25	C26	119.0(2)	C18	C17	C16	119.9(3)
C30	C25	C24	122.6(2)	C2	C1	C6	119.7(2)
C28	C29	C30	119.9(2)	O6	C33	C34	110.1(3)
C18	C19	C20	119.8(2)	O5	C31	C32	114.4(2)
C19	C18	C17	120.4(2)	C4	C3	C2	120.3(2)
C5	C6	C7	122.5(2)				

Table 6 Hydrogen Atom Coordinates ($Å\times10^4$) and Isotropic Displacement Parameters ($Å^2\times10^3$) for dc150.

Atom	x	y	z	U(eq)
H26	5256	1931	5790	27
H29	4295	2337	7791	33
H19	−2120	5607	2905	42
H18	−3154	5656	3665	40
H30	2582	2662	6496	27
H11	−3611	1232	2382	30
H14	−1311	−710	4426	36
H15	−11	123	4062	31
H28	6475	1808	8080	36
H2	−1018	3652	−68	46
H4	−4430	2224	−622	37
H16	−844	3633	4913	30
H13	−3743	−550	3799	35
H5	−3285	1686	647	31
H27	6973	1624	7089	33
H20	−470	4549	3132	34
H12	−4896	423	2775	33
H17	−2541	4662	4657	38
H1	121	3142	1218	34
H33A	1778	4118	2966	47
H33B	3140	4121	2898	47
H32A	2099	−191	3455	91
H32B	2398	150	4275	91
H32C	3377	−560	4242	91
H31A	4417	785	4518	58
H31B	4298	363	3765	58
H34A	3427	5088	3862	113
H34B	4550	4349	4256	113
H34C	3188	4350	4322	113
H3	−3299	3217	−974	42
H23	1360(30)	3220(20)	5371(19)	42
H8	−2450(30)	1511(19)	1829(19)	42

Experimental

Single crystals of $C_{34}H_{32}O_6Ti$ **[dc150]** were **[obtained from recrystallisation from hot ethanol]**. A suitable crystal was selected and **[mounted on a MiTeGen mesh]** on a **'Bruker APEX-II CCD'** diffractometer. The crystal was kept at 150 K during data collection. Using Olex2 [1], the structure was solved with the olex2.solve [2] structure solution program using Charge Flipping and refined with the ShelXL [3] refinement package using Least Squares minimisation.

1. Dolomanov, O.V., Bourhis, L.J., Gildea, R.J, Howard, J.A.K. & Puschmann, H. (2009), J. Appl. Cryst. 42, 339-341.
2. Bourhis, L.J., Dolomanov, O.V., Gildea, R.J., Howard, J.A.K., Puschmann, H. (2013). in preparation
3. Sheldrick, G.M. (2008). Acta Cryst. A64, 112-122

Crystal structure determination of [dc150]

Crystal Data for $C_{34}H_{32}O_6Ti$ (M =425.32): monoclinic, space group P2$_1$/c (no. 14), a = 11.2203(12) Å, b = 15.8876(16) Å, c = 20.1373(19) Å, β = 121.131(6)°, V = 3072.8(6) Å^3, Z = 4, T = 150 K, μ(MoKα) = 0.113 mm^{-1}, $Dcalc$ = 0.919 g/mm^3, 37033 reflections measured (3.486 ≤ 2Θ ≤ 60.484), 8994 unique (R_{int} = 0.0621, R$_{sigma}$ = 0.0646) which were used in all calculations. The final R_1 was 0.0612 (I > 2σ(I)) and wR_2 was 0.1908 (all data).

Refinement model description

Number of restraints - 0, number of constraints - unknown.
Details:
```
1. Fixed Uiso
 At 1.2 times of:
  All C(H) groups, {H3,H23,H8} of C3, All C(H,H) groups
 At 1.5 times of:
  {H32A,H32B,H32C} of C32, {H34A,H34B,H34C} of C34
2.a Secondary CH2 refined with riding coordinates:
 C33(H33A,H33B), C31(H31A,H31B)
2.b Aromatic/amide H refined with riding coordinates:
 C26(H26), C29(H29), C19(H19), C18(H18), C30(H30), C11(H11), C14(H14),
 C15(H15), C28(H28), C2(H2), C4(H4), C16(H16), C13(H13), C5(H5), C27(H27),
 C20(H20), C12(H12), C17(H17), C1(H1), C3(H3)
2.c Idealised Me refined as rotating group:
 C32(H32A,H32B,H32C), C34(H34A,H34B,H34C)
```

6.5. Crystallographic information for compound 8

Identification code	dc150
Empirical formula	$C_{34}H_{32}O_6Ti$
Formula weight	584.50
Temperature/K	150
Crystal system	monoclinic
Space group	$P2_1/c$
a/Å	11.2203(12)
b/Å	15.8876(16)
c/Å	20.1373(19)
α/°	90
β/°	121.131(6)
γ/°	90
Volume/Å^3	3072.8(6)
Z	4
ρ_{calc}g/cm^3	1.2634
μ/mm^{-1}	0.321
F(000)	1225.8
Crystal size/mm^3	0.085 × 0.078 × 0.011
Radiation	Mo Ka (λ = 0.71073)
2Θ range for data collection/°	4.44 to 60.48
Index ranges	$-15 \le h \le 15, -22 \le k \le 22, -28 \le l \le 24$
Reflections collected	37033
Independent reflections	8989 [R_{int} = 0.0621, R_{sigma} = 0.0646]
Data/restraints/parameters	8989/0/371

Goodness-of-fit on F^2 1.049

Final R indexes [I>=2σ (I)] R_1 = 0.0606, wR_2 = 0.1616

Final R indexes [all data] R_1 = 0.0925, wR_2 = 0.1860

Largest diff. peak/hole / e $Å^{-3}$ 1.21/-0.87

Table 6.5-1 - Crystal data and structure refinement for *bis*-(1,3-diphenylpropan-1,3-diketonate)titanium(IV) ethoxide

Atom	x	y	z	U(eq)
Ti1	6966.8(4)	7776.6(3)	8486.6(2)	20.17(12)
O2	5585.9(16)	7725.2(10)	7333.7(9)	23.6(3)
C10	3530(2)	7635.1(14)	6069.2(13)	20.5(4)
O3	5711.1(16)	6887.3(10)	8607.1(9)	24.2(3)
C26	8461(2)	7550.2(15)	11612.4(13)	22.8(4)
C22	5600(2)	6671.9(13)	9187.7(13)	20.0(4)
C9	4273(2)	7929.0(13)	6908.1(12)	19.5(4)
C25	8737(2)	7669.6(13)	11006.6(12)	18.8(4)
O6	8033.9(17)	8661.4(10)	8530.4(10)	27.8(4)
O4	7934.2(16)	7818.3(10)	9660.5(9)	23.0(3)
O5	7964.9(17)	6904.3(10)	8413.6(9)	25.2(3)
O1	5474.1(16)	8583.8(10)	8479.6(9)	23.6(3)
C27	9485(3)	7743.9(15)	12386.9(14)	27.8(5)
C6	3321(2)	9232.0(13)	8182.2(13)	20.6(4)
C11	2169(2)	7908.6(16)	5506.9(14)	26.4(5)
C23	6494(2)	6980.9(14)	9958.1(13)	22.0(4)

C21	4514(2)	6015.7(14)	9047.4(13)	21.7(4)
C30	10061(2)	7984.9(14)	11191.6(13)	22.5(4)
C28	10790(3)	8057.6(16)	12559.6(14)	30.3(5)
C20	3892(2)	5975.0(14)	9502.9(14)	25.3(5)
C8	3538(2)	8382.0(15)	7188.1(13)	26.2(5)
C24	7666(2)	7494.1(13)	10165.5(12)	18.4(4)
C7	4182(2)	8703.2(13)	7958.4(13)	20.3(4)
C12	1485(3)	7591.9(17)	4747.6(14)	30.9(5)
C29	11086(2)	8172.6(15)	11967.8(14)	27.5(5)
C5	1858(2)	9153.7(14)	7800.7(14)	25.2(5)
C1	4006(3)	9818.3(14)	8799.0(14)	25.6(5)
C15	4207(3)	7045.6(15)	5849.7(14)	28.9(5)
C2	3229(3)	10310.8(15)	9018.7(15)	30.0(5)
C3	1774(3)	10220.1(15)	8641.8(15)	29.1(5)
C4	1086(2)	9640.3(15)	8031.5(15)	27.6(5)
C16	4124(3)	5424.8(15)	8444.3(14)	28.5(5)
C13	2162(3)	7003.1(17)	4538.2(15)	35.1(6)
C18	2516(3)	4765.8(16)	8759.6(16)	33.2(6)
C14	3522(3)	6736.7(17)	5082.1(15)	38.3(6)
C19	2887(3)	5356.5(16)	9355.2(15)	31.8(5)
C17	3131(3)	4795.1(16)	8305.0(15)	35.1(6)
C31	7781(3)	6023.2(17)	8240.6(17)	39.5(6)
C33	8752(3)	9392(2)	8978(2)	49.4(8)

Atom				

| C34 | 7829(4) | 10054(2) | 8989(2) | 61.3(10) |
| C32 | 8554(5) | 5513(2) | 8986(2) | 75.0(13) |

Table 6.5-2 - Fractional Atomic Coordinates (×10^4) and Equivalent Isotropic Displacement Parameters (Å^2×10^3) for dc150. U_{eq} is defined as 1/3 of of the trace of the orthogonalised U_{IJ} tensor.

Atom	U_{11}	U_{22}	U_{33}	U_{12}	U_{13}	U_{23}
Ti1	15.53(19)	30.8(2)	12.5(2)	−1.48(14)	6.05(15)	−0.62(14)
O2	18.4(8)	37.3(9)	13.0(8)	2.0(6)	6.6(6)	−0.3(6)
C10	19.4(10)	28.8(11)	13.4(10)	−2.5(8)	8.6(9)	−1.0(8)
O3	20.8(8)	33.8(8)	15.2(8)	−6.4(6)	7.4(7)	−2.9(6)
C26	20.8(10)	29.9(11)	16.9(11)	−0.3(8)	9.2(9)	−2.6(8)
C22	15.0(9)	25.4(10)	16.8(10)	−0.2(8)	6.2(8)	0.1(8)
C9	19.2(10)	26.5(10)	12.8(10)	−3.2(8)	8.2(8)	−0.0(8)
C25	17.4(10)	23.5(10)	12.6(10)	0.8(8)	5.7(8)	−2.7(7)
O6	25.6(8)	34.7(9)	23.9(9)	−5.9(7)	13.4(7)	−1.6(7)
O4	17.8(8)	34.7(8)	13.7(7)	−4.7(6)	6.3(6)	−1.4(6)
O5	20.9(8)	32.9(8)	18.7(8)	1.3(6)	8.2(7)	−1.1(6)
O1	19.4(8)	34.8(8)	14.0(8)	−0.6(6)	6.7(6)	−3.4(6)
C27	30.0(13)	35.7(12)	14.7(11)	3.4(10)	9.6(10)	−1.4(9)
C6	22.4(11)	24.3(10)	15.8(10)	−0.3(8)	10.3(9)	1.3(8)
C11	21.0(11)	40.5(13)	16.4(11)	1.7(9)	8.8(9)	−1.8(9)
C23	19.3(10)	31.0(11)	14.3(10)	−4.7(8)	7.7(9)	−1.5(8)
C21	15.6(9)	26.2(10)	15.6(10)	−1.1(8)	2.6(8)	1.2(8)
C30	17.7(10)	29.5(11)	17.7(11)	−2.1(8)	7.2(9)	−5.5(8)
C28	25.6(12)	38.4(13)	15.9(11)	0.3(10)	2.9(10)	−6.8(9)

C20	19.7(10)	28.9(11)	22.3(12)	−1.3(8)	7.2(9)	0.2(9)
C8	18.3(10)	40.4(13)	15.5(11)	2.0(9)	5.6(9)	−4.6(9)
C24	16.1(10)	23.2(9)	13.1(10)	2.6(7)	5.6(8)	−0.8(7)
C7	20.8(10)	25.8(10)	16(1)	−2.1(8)	10.6(9)	−0.5(8)
C12	21.7(12)	46.9(14)	15.3(11)	−1.6(10)	3.4(10)	−0.2(10)
C29	17.6(11)	35.9(12)	22.3(12)	−3.2(9)	5.4(9)	−6.1(9)
C5	24.2(11)	29.1(11)	21.2(11)	−1.5(9)	11(1)	−2.0(9)
C1	24.9(11)	29.3(11)	22.1(12)	−3.2(9)	11.8(10)	−3.5(9)
C15	28.0(13)	35.2(12)	17.5(11)	6.7(9)	7.5(10)	−1.7(9)
C2	33.6(13)	30.1(12)	26.9(13)	−1.7(10)	16.1(11)	−5.4(10)
C3	32.2(13)	28.5(12)	30.8(13)	6.1(9)	19.3(11)	0.9(10)
C4	21.4(11)	34.5(12)	26.6(13)	3.4(9)	12.3(10)	0.5(10)
C16	25.0(12)	34.7(12)	19.6(12)	−3.6(9)	7.2(10)	−2.8(9)
C13	40.9(15)	39.4(13)	16.0(12)	−4.1(11)	8.3(11)	−8.1(10)
C18	25.5(12)	29.7(12)	29.7(13)	−8.8(9)	3.8(11)	4.4(10)
C14	45.1(16)	39.3(14)	22.5(13)	10.6(12)	11.9(12)	−5.9(10)
C19	24.6(12)	37.0(13)	29.6(14)	−3.6(10)	11.0(11)	7.3(10)
C17	30.9(14)	32.8(13)	26.3(13)	−8.2(10)	4.0(11)	−5.5(10)
C31	43.7(16)	38.2(14)	41.7(17)	−4.6(12)	25.6(14)	−11.5(12)
C33	35.3(16)	52.1(17)	57(2)	−20.8(13)	21.5(15)	−22.4(15)
C34	45.7(19)	47.2(18)	78(3)	−16.7(15)	22.9(19)	−25.6(18)
C32	106(4)	34.6(16)	72(3)	5.3(19)	37(3)	11.0(17)

Table 6.5-3 - Anisotropic Displacement Parameters ($\text{Å}^2 \times 10^3$) for dc150. The Anisotropic displacement factor exponent takes the form: $-2\pi^2[h^2a^{*2}U_{11}+2hka^*b^*U_{12}+...]$.

Atom	Atom	Length/Å	Atom	Atom	Length/Å
Ti1	O2	2.0194(16)	C6	C7	1.514(3)
Ti1	O3	2.0960(16)	C6	C5	1.413(3)
Ti1	O6	1.8189(16)	C6	C1	1.419(3)
Ti1	O4	2.0293(16)	C11	C12	1.402(3)
Ti1	O5	1.8349(17)	C23	C24	1.414(3)
Ti1	O1	2.1036(16)	C21	C20	1.412(3)
O2	C9	1.305(3)	C21	C16	1.414(3)
C10	C9	1.520(3)	C30	C29	1.413(3)
C10	C11	1.420(3)	C28	C29	1.404(4)
C10	C15	1.413(3)	C20	C19	1.407(3)
O3	C22	1.284(3)	C8	C7	1.425(3)
C26	C25	1.417(3)	C12	C13	1.400(4)
C26	C27	1.412(3)	C5	C4	1.407(3)
C22	C23	1.430(3)	C1	C2	1.402(3)
C22	C21	1.516(3)	C15	C14	1.412(3)
C9	C8	1.413(3)	C2	C3	1.408(3)
C25	C30	1.423(3)	C3	C4	1.405(3)
C25	C24	1.512(3)	C16	C17	1.413(3)
O6	C33	1.435(3)	C13	C14	1.407(4)
O4	C24	1.306(3)	C18	C19	1.406(4)
O5	C31	1.431(3)	C18	C17	1.403(4)
O1	C7	1.290(3)	C31	C32	1.521(5)

C27 C28   1.410(4) C33 C34   1.485(5)

Table 6.5-4 - Bond Lengths for *bis*-(1,3-diphenylpropan-1,3-diketonate)titanium(IV) ethoxide.

Atom	Atom	Atom	Angle/°	Atom	Atom	Atom	Angle/°
O3	Ti1	O2	86.77(6)	C5	C6	C7	122.01(19)
O6	Ti1	O2	100.46(7)	C1	C6	C7	119.00(19)
O6	Ti1	O3	168.62(7)	C1	C6	C5	119.0(2)
O4	Ti1	O2	166.17(7)	C12	C11	C10	121.1(2)
O4	Ti1	O3	82.75(6)	C24	C23	C22	122.8(2)
O4	Ti1	O6	88.63(7)	C20	C21	C22	122.0(2)
O5	Ti1	O2	90.84(7)	C16	C21	C22	118.6(2)
O5	Ti1	O3	88.55(7)	C16	C21	C20	119.4(2)
O5	Ti1	O6	100.01(8)	C29	C30	C25	120.4(2)
O5	Ti1	O4	97.87(7)	C29	C28	C27	120.5(2)
O1	Ti1	O2	83.22(6)	C19	C20	C21	120.4(2)
O1	Ti1	O3	80.28(7)	C7	C8	C9	123.0(2)
O1	Ti1	O6	91.78(7)	O4	C24	C25	115.47(18)
O1	Ti1	O4	86.12(6)	C23	C24	C25	121.07(19)
O1	Ti1	O5	167.61(7)	C23	C24	O4	123.4(2)
C9	O2	Ti1	132.81(14)	C6	C7	O1	117.44(18)
C11	C10	C9	122.5(2)	C8	C7	O1	123.9(2)
C15	C10	C9	118.5(2)	C8	C7	C6	118.69(19)
C15	C10	C11	118.9(2)	C13	C12	C11	119.5(2)
C22	O3	Ti1	132.23(14)	C28	C29	C30	119.8(2)
C27	C26	C25	120.4(2)	C4	C5	C6	120.8(2)

C23 C22 O3	123.52(19)	C2	C1	C6	119.9(2)
C21 C22 O3	117.43(19)	C14	C15	C10	119.8(2)
C21 C22 C23	118.94(19)	C3	C2	C1	120.6(2)
C10 C9 O2	115.96(18)	C4	C3	C2	119.9(2)
C8 C9 O2	123.9(2)	C3	C4	C5	119.7(2)
C8 C9 C10	120.1(2)	C17	C16	C21	120.2(2)
C30 C25 C26	119.0(2)	C14	C13	C12	120.4(2)
C24 C25 C26	122.62(19)	C17	C18	C19	120.4(2)
C24 C25 C30	118.39(19)	C13	C14	C15	120.4(2)
C33 O6 Ti1	142.92(18)	C18	C19	C20	119.9(2)
C24 O4 Ti1	133.97(14)	C18	C17	C16	119.8(2)
C31 O5 Ti1	137.82(16)	C32	C31	O5	110.1(2)
C7 O1 Ti1	130.59(14)	C34	C33	O6	114.4(2)
C28 C27 C26	119.9(2)				

Table 6.5-5 - Bond Angles for *bis*-(1,3-diphenylpropan-1,3-diketonate)titanium(IV) ethoxide

Atom	x	y	z	U(eq)
H26	7582(2)	7338.4(15)	11496.6(13)	27.3(5)
H27	9295(3)	7663.0(15)	12790.6(14)	33.3(6)
H11	1714(2)	8312.9(16)	5647.3(14)	31.7(6)
H23	6293(2)	6835.1(14)	10347.3(13)	26.4(5)
H30	10257(2)	8069.6(14)	10790.5(13)	27.1(5)
H28	11475(3)	8192.4(16)	13080.3(14)	36.4(6)
H20	4154(2)	6367.6(14)	9911.6(14)	30.4(6)
H8	2570(2)	8476.7(15)	6847.1(13)	31.4(6)

H12	570(3)	7775.4(17)	4378.4(14)	37.1(6)
H29	11973(2)	8375.9(15)	12089.0(14)	33.0(6)
H5	1390(2)	8767.7(14)	7383.1(14)	30.2(6)
H1	4989(3)	9877.0(14)	9062.8(14)	30.8(6)
H15	5120(3)	6857.7(15)	6217.4(14)	34.6(6)
H2	3690(3)	10709.5(15)	9425.9(15)	35.9(6)
H3	1258(3)	10550.2(15)	8799.8(15)	34.9(6)
H4	105(2)	9577.1(15)	7775.6(15)	33.1(6)
H16	4530(3)	5451.1(15)	8131.8(14)	34.2(6)
H13	1700(3)	6782.4(17)	4026.1(15)	42.2(7)
H18	1845(3)	4344.3(16)	8664.3(16)	39.9(7)
H14	3982(3)	6346.8(17)	4931.9(15)	46.0(8)
H19	2460(3)	5338.0(16)	9657.4(15)	38.1(7)
H17	2881(3)	4392.9(16)	7904.8(15)	42.1(7)
H31a	6777(3)	5882.6(17)	7965.0(17)	47.5(8)
H31b	8139(3)	5879.5(17)	7897.0(17)	47.5(8)
H33a	9418(3)	9215(2)	9518(2)	59.3(10)
H33b	9298(3)	9638(2)	8766(2)	59.3(10)
H34a	7100(18)	10191(13)	8456(2)	91.9(15)
H34b	7400(20)	9849(7)	9276(14)	91.9(15)
H34c	8377(7)	10560(6)	9243(15)	91.9(15)
H32a	9549(7)	5649(15)	9254(10)	112.5(19)
H32b	8190(20)	5651(15)	9322(8)	112.5(19)

| H32c | 8420(30) | 4912(2) | 8861(3) | 112.5(19) |

Table 6.5-6 - Hydrogen Atom Coordinates (Å×10⁴) and Isotropic Displacement Parameters (Å²×10³) for *bis*-(1,3-diphenylpropan-1,3-diketonate)titanium(IV) ethoxide.

6.5.1. Experimental

Single crystals of $C_{34}H_{32}O_6Ti$ **[dc150]** were **[Sample recrystallised from ethanol]**. A suitable crystal was selected and **[]** on a **'Bruker APEX-II CCD'** diffractometer. The crystal was kept at 150 K during data collection. Using Olex2 [1], the structure was solved with the ShelXS [2] structure solution program using Direct Methods and refined with the olex2.refine [3] refinement package using Gauss-Newton minimisation.

1. Dolomanov, O.V., Bourhis, L.J., Gildea, R.J, Howard, J.A.K. & Puschmann, H. (2009), J. Appl. Cryst. 42, 339-341.

6.5.1.1. Crystal structure determination of *bis*-(1,3-diphenylpropan-1,3-diketonate)titanium(IV) ethoxide

Crystal Data for $C_{34}H_{32}O_6Ti$ (M =584.50 g/mol): monoclinic, space group P2₁/c (no. 14), a = 11.2203(12) Å, b = 15.8876(16) Å, c = 20.1373(19) Å, β = 121.131(6)°, V = 3072.8(6) Å³, Z = 4, T = 150 K, μ(Mo Kα) = 0.321 mm⁻¹, $Dcalc$ = 1.2634 g/cm³, 37033 reflections measured (4.44° ≤ 2Θ ≤ 60.48°), 8989 unique (R_{int} = 0.0621, R_{sigma} = 0.0646) which were used in all calculations. The final R_1 was 0.0606 (I>=2u(I)) and wR_2 was 0.1860 (all data).

Refinement model description

Number of restraints - 0, number of constraints - 58.
Details:
```
1. Fixed Uiso
 At 1.2 times of:
  All C(H) groups, All C(H,H) groups
 At 1.5 times of:
  All C(H,H,H) groups
2.a Secondary CH2 refined with riding coordinates:
 C31(H31a,H31b), C33(H33a,H33b)
2.b Aromatic/amide H refined with riding coordinates:
 C26(H26), C27(H27), C11(H11), C23(H23), C30(H30), C28(H28), C20(H20),
C8(H8),
 C12(H12), C29(H29), C5(H5), C1(H1), C15(H15), C2(H2), C3(H3), C4(H4),
C16(H16),
  C13(H13), C18(H18), C14(H14), C19(H19), C17(H17)
2.c Idealised Me refined as rotating group:
 C34(H34a,H34b,H34c), C32(H32a,H32b,H32c)
```

This report has been created with Olex2, compiled on 2015.01.26 svn.r3150 for OlexSys. Please let us know if there are any errors or if you would like to have additional features.

6.6. Maple calculation methods of EC₅₀ from the logarithmic fitting of data presented in section 4.6

restart;

$$line := y = A2 + \frac{(A1 - A2)}{\left(1 + \left(\frac{x}{x0}\right)^p\right)};$$

$$y = A2 + \frac{A1 - A2}{1 + \left(\frac{x}{x0}\right)^p}$$

$x := solve(line, x);$

$$e^{\frac{\ln\left(-\frac{-y+A1}{-y+A2}\right)}{p}} \, x0$$

#150oC

$A1 := 1.89006; A2 := 95.47974; x0 := 64.63479; p := 2.07512;$

$$1.89006$$

$$95.47974$$

$$64.63479$$

$$2.07512$$

$y := 50$

$$50$$

$x;$

$$66.40989822$$

#160oC

$A1 := 1.41276; A2 := 99.141276; x0 := 35.8117; p := 166983;$

$$1.41276$$

$$99.141276$$

$$35.8117$$

$$166983$$

$x;$

$$35.81169757$$

#170oC

$A1 := 7.344; A2 := 96.38484; x0 := 28.35767; p := 2.97459;$

$$7.344$$

$$96.38484$$

$$28.35767$$

$$2.97459$$

$x;$

$$27.56988346$$

#185oC;

$A1 := 6.37499; A2 := 96.49563; x0 := 12.44093; p := 1.99357;$

$$6.46785$$

$$96.63983$$

$$9.56619$$

x;

12.04952465

#200oC;

A1 := 6.46785; *A2* := 96.63983; *x0* := 9.56619; *p* := 2.86634;

restart;

$$y := A2 + \frac{(A1 - A2)}{\left(1 + \left(\frac{x}{x0}\right)^p\right)};$$

$$A2 + \frac{A1 - A2}{1 + \left(\frac{x}{x0}\right)^p}$$

#150oC

A1 := 1.89006; A2 := 95.47974; x0 := 64.63479; p := 2.07512; x := 20; y;

1.89006

95.47974

64.63479

2.07512

20

9.43383383

#160oC

A1 := 1.41276; A2 := 99.00638; x0 := 35.8117; p := 1.66983; x := 20; y;

1.41276

99.00638

35.8117

1.66983

20

28.18594531

#170oC

A1 := 7.344; A2 := 96.38484; x0 := 28.35767; p := 2.97459; x := 20; y;

7.344

96.38484

28.35767

2.97459

20

30.62067138

#185oC;

A1 ≔ 6.37499; A2 ≔ 96.49563; x0 ≔ 12.44093; p ≔ 1.99357; x
  ≔ 15; y;

6.37499

96.49563

12.44093

1.99357

15

59.74108941

#200oC;

A1 ≔ 6.46785; *A2* ≔ 96.63983; *x0* ≔ 9.56619; *p* ≔ 2.86634; *x*
  ≔ 15; *y*

6.46785

96.63983

9.56619

2.86634

15

77.16562426